INTERNATIONAL JOURNAL

of

COMPUTERS, COMMUNICATIONS & CONTROL

With Emphasis on the Integration of Three Technologies

IJCCC

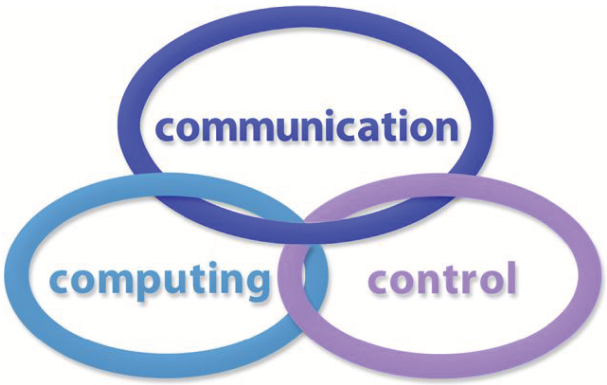

Year: 2012 Volume: 7 Number: 1 (March)

Agora University Editing House

CCC Publications

www.journal.univagora.ro

International Journal of Computers, Communications & Control

EDITORIAL ADDRESS:
R&D Agora Ltd. / S.C. Cercetare Dezvoltare Agora S.R.L.
Piaţa Tineretului 8, Oradea, jud. Bihor, Romania, Zip Code 410526
Tel./ Fax: +40 359101032
E-mail: ijccc@univagora.ro, rd.agora@univagora.ro, ccc.journal@gmail.com
Journal website: www.journal.univagora.ro

DATA FOR SUBSCRIBERS
Supplier: Cercetare Dezvoltare Agora Srl (Research & Development Agora Ltd.)
Fiscal code: RO24747462
Headquarter: Oradea, Piata Tineretului Nr.8, Bihor, Romania, Zip code 410526
Bank: MILLENNIUM BANK, Bank address: Piata Unirii, str. Primariei, 2, Oradea, Romania
IBAN Account for EURO: RO73MILB0000000000932235
SWIFT CODE (eq.BIC): MILBROBU

International Journal of Computers, Communications & Control

Mario de J. Pérez Jiménez
Dept. of CS and Artificial Intelligence
University of Seville, Sevilla,
Avda. Reina Mercedes s/n, 41012, Spain
marper@us.es

Dana Petcu
Computer Science Department
Western University of Timisoara
V.Parvan 4, 300223 Timisoara, Romania
petcu@info.uvt.ro

Radu Popescu-Zeletin
Fraunhofer Institute for Open
Communication Systems
Technical University Berlin, Germany
rpz@cs.tu-berlin.de

Imre J. Rudas
Institute of Intelligent Engineering Systems
Budapest Tech
Budapest, Bécsi út 96/B, H-1034, Hungary
rudas@bmf.hu

Yong Shi
Research Center on Fictitious Economy
& Data Science
Chinese Academy of Sciences
Beijing 100190, China
yshi@gucas.ac.cn
and
College of Information Science & Technology
University of Nebraska at Omaha
Omaha, NE 68182, USA
yshi@unomaha.edu

Athanasios D. Styliadis
Alexander Institute of Technology
Agiou Panteleimona 24, 551 33
Thessaloniki, Greece
styl@it.teithe.gr

Gheorghe Tecuci
Learning Agents Center
George Mason University, USA
University Drive 4440, Fairfax VA 22030-4444
tecuci@gmu.edu

Horia-Nicolai Teodorescu
Faculty of Electronics and Telecommunications
Technical University "Gh. Asachi" Iasi
Iasi, Bd. Carol I 11, 700506, Romania
hteodor@etc.tuiasi.ro

Dan Tufiş
Research Institute for Artificial Intelligence
of the Romanian Academy
Bucharest, "13 Septembrie" 13, 050711, Romania
tufis@racai.ro

Lotfi A. Zadeh
Professor,
Graduate School,
Director,
Berkeley Initiative in Soft Computing (BISC)
Computer Science Division
Department of Electrical Engineering
& Computer Sciences
University of California Berkeley,
Berkeley, CA 94720-1776, USA
zadeh@eecs.berkeley.edu

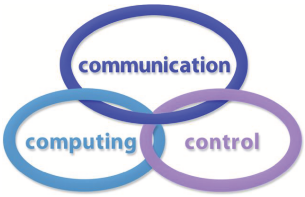

International Journal of Computers, Communications & Control

Short Description of IJCCC

Title of journal: International Journal of Computers, Communications & Control
Acronym: IJCCC
International Standard Serial Number: ISSN 1841-9836, E-ISSN 1841-9844
Publisher: CCC Publications - Agora University
Starting year of IJCCC: 2006
Founders of IJCCC: Ioan Dzitac, Florin Gheorghe Filip and Mişu-Jan Manolescu
Logo:

Number of issues/year: IJCCC has 4 issues/odd year (March, June, September, December) and 5 issues/even year (March, September, June, November, December). Every even year IJCCC will publish a supplementary issue with selected papers from the International Conference on Computers, Communications and Control.
Coverage:

- Beginning with Vol. 1 (2006), Supplementary issue: S, IJCCC is covered by Thomson Reuters - SCI Expanded and is indexed in ISI Web of Science.
- Journal Citation Reports/Science Edition 2010:
  - Impact factor = 0.650
- Beginning with Vol. 2 (2007), No.1, IJCCC is covered in EBSCO.
- Beginning with Vol. 3 (2008), No.1, IJCCC, is covered in Scopus.

Scope: IJCCC is directed to the international communities of scientific researchers in universities, research units and industry. IJCCC publishes original and recent scientific contributions in the following fields: Computing & Computational Mathematics; Information Technology & Communications; Computer-based Control.
Unique features distinguishing IJCCC: To differentiate from other similar journals, the editorial policy of IJCCC encourages especially the publishing of scientific papers that focus on the convergence of the 3 "C" (Computing, Communication, Control).
Policy: The articles submitted to IJCCC must be original and previously unpublished in other journals. The submissions will be revised independently by at least two reviewers and will be published only after completion of the editorial workflow.

Contents

Int. J. of Computers, Communications & Control, ISSN 1841-9836, E-ISSN 1841-9844
Vol. VII (2012), No. 1 (March), pp. 8-19

A Non-Fragile H_∞ Output Feedback Controller for Uncertain Fuzzy Dynamical Systems with Multiple Time-Scales

Wudhichai Assawinchaichote
Department of Electronic and Telecommnunication Engineering
King Mongkut's University of Technology Thonburi
126 Prachautits Rd., Bangkok 10140, Thailand
E-mail: wudhichai.asa@kmutt.ac.th

Abstract:
This paper determines the designing of a non-fragile H_∞ output feedback controller for a class of nonlinear uncertain dynamical systems with multiple time-scales described by a Takagi-Sugeno (TS) fuzzy model. Based on a linear matrix inequality (LMI) approach, we develop a non-fragile H_∞ output feedback controller which guarantees the $\mathcal{L}_2$-gain of the mapping from the exogenous input noise to the regulated output to be less than some prescribed value for this class of uncertain fuzzy dynamical systems with multiple time-scales. A numerical example is provided to illustrate the design developed in this paper.
Keywords: Fuzzy Control, Linear Matrix Inequality (LMI), Non-fragile $\mathcal{H}_\infty$ Output Feedback Control, Multiple Time-Scale Systems.

1 Introduction

In the last few years, the problem of control design for dynamical systems with multiple time-scale has been intensively studied by a number of researchers; see [1]- [12]. This is due not only to theoretical interest but also to the relevance of this topic in control engineering applications. Singularly perturbed systems are dynamical systems with multiple time-scales. Singularly perturbed systems often occur naturally due to the presence of small "parasitic" parameter, typically small time constants, masses, etc. Indeed multiple time-scales phenomena are almost unavoidable in "real-life" systems. Examples of such systems abound and include convection-diffusion systems, diffusion-drift motion systems, power systems, scheduling systems, economic models, telecommunication systems and bifurcations.

Presently, many researchers have studied the H_∞ control design for a general class of linear singularly perturbed systems due to a great practical importance; see [4, 5, 7]. The main purpose of the singular perturbation approach to analysis and design is the alleviation of high dimensionality and ill-conditioning resulting from the interaction of slow and fast dynamics modes. The separation of states into slow and fast ones is a nontrivial modelling task demanding insight and ingenuity on the part of the analyst. In state space, such systems are commonly modelled using the mathematical framework of singular perturbations, with a small parameter, say ε, determining the degree of separation between the "slow" and "fast" modes of the system. Although many researchers have studied linear singularly perturbed systems for many years, the H_∞ control design of nonlinear singularly perturbed systems remains as an open research area. This is because, in general, nonlinear singularly perturbed systems can not be separated into slow and fast subsystems.

Over the past two decades, there has been rapidly growing interest in application of fuzzy logic to control problem. Researches have been focused on its application to industrial processes and a number of successful results have been reported in the literature. In spite of these successes, there are many basic issues remain to be addressed. One of them is how to achieve a systematic

design that guarantees closed-loop stability and performance. Recently, a great amount of effort has been devoted to describing a nonlinear system using a Takagi-Sugeno fuzzy model; see [16]-[29]. The Takagi-sugeno (TS) fuzzy model represents a nonlinear system by a family of local linear models which smoothly blended together through fuzzy membership functions. Unlike conventional modelling techniques which uses a single model to describe the global behavior of a nonlinear system, fuzzy modelling is essentially a multi-model approach in which simple sub-models (typically linear models) are fuzzily combined to described the global behavior of a nonlinear system. Based on this fuzzy model, a number of systematic model-based fuzzy control design methodologies have been developed.

The aim of this paper is to design a non-fragile $\mathcal{H}_\infty$ output feedback controller for a uncertain nonlinear dynamical system with multuple time-scales. Based on an LMI approach, we develop the fuzzy non-fragile $\mathcal{H}_\infty$ output feedback controller that guarantees the $\mathcal{L}_2$-gain of the mapping from the exogenous input noise to the regulated output to be less than or equal to a prescribed value for this class of fuzzy dynamical systems. In order to alleviate the ill-conditioned linear matrix inequalities resulting from the interaction of slow and fast dynamic modes, the ill-conditioned LMIs are decomposed into ε-independent and ε-dependent LMIs. The ε-independent LMIs are not ill-conditioned and the ε-dependent LMIs tend to zero when ε approaches to zero. It can be shown that when ε is sufficiently small, the original ill-conditioned LMIs are solvable if and only if the ε-independent LMIs are solvable. The proposed approach does not involve the separation of states into slow and fast ones, and it can be applied not only to standard, but also to nonstandard singularly perturbed systems.

This paper is organized as follows. In Section 2, system descriptions and definition are presented. In Section 3, based on an LMI approach, we respectively develop a technique for designing a non-fragile $\mathcal{H}_\infty$ output feedback controllers such that the $\mathcal{L}_2$-gain of the mapping from the exogenous input noise to the regulated output is less than a prescribed value for the system described in Section 2. The validity of this approach is demonstrated by an example from a literature in Section 4. Finally, conclusions are given in Section 5.

2 System Descriptions and Definitions

In this section, we consider the TS fuzzy system with multiple time-scales to represent a TS fuzzy multiple time-scale system with parametric uncertainties as follows:

$$\begin{aligned} E_\varepsilon \dot{x}(t) &= \sum_{i=1}^{r} \mu_i(\nu(t)) \Big[[A_i + \Delta A_i]x(t) + [B_{1_i} + \Delta B_{1_i}]w(t) + [B_{2_i} + \Delta B_{2_i}]u(t) \Big] \\ z(t) &= \sum_{i=1}^{r} \mu_i(\nu(t)) \Big[[C_{1_i} + \Delta C_{1_i}]x(t) + [D_{12_i} + \Delta D_{12_i}]u(t) \Big] \\ y(t) &= \sum_{i=1}^{r} \mu_i(\nu(t)) \Big[[C_{2_i} + \Delta C_{2_i}]x(t) + [D_{21_i} + \Delta D_{21_i}]w(t) \Big] \end{aligned} \tag{1}$$

where $E_\varepsilon = \begin{bmatrix} I & 0 \\ 0 & \varepsilon I \end{bmatrix}$, $\nu(t) = [\nu_1(t) \ \cdots \ \nu_\vartheta(t)]$ is the premise variable vector that may depend on states in many cases, $\varepsilon > 0$ is the singular perturbation parameter, $\mu_i(\nu(t))$ denotes the normalized time-varying fuzzy weighting functions for each rule (i.e., $\mu_i(\nu(t)) \geq 0$ and $\sum_{i=1}^{r} \mu_i(\nu(t)) = 1$), ϑ is the number of fuzzy sets, $x(t) \in \Re^n$ is the state vector, $u(t) \in \Re^m$ is the input, $w(t) \in \Re^p$ is the disturbance which belongs to $\mathcal{L}_2[0, \infty)$, $y(t) \in \Re^\ell$ is the measurement, $z(t) \in \Re^s$ is the controlled output, the matrices $A_i, B_{1_i}, B_{2_i}, C_{1_i}, C_{2_i}, D_{12_i}$ and D_{21_i} are of appropriate dimensions, and r is the number of IF-THEN rules. The matrices $\Delta A_i, \Delta B_{1_i}, \Delta B_{2_i}, \Delta C_{1_i}, \Delta C_{2_i}, \Delta D_{12_i}$ and ΔD_{21_i} represent the uncertainties in the system and satisfy the following assumption.

Assumption 1.

$$\Delta A_i = F(x(t),t)H_{1_i},\ \ \Delta B_{1_i} = F(x(t),t)H_{2_i},\ \ \Delta B_{2_i} = F(x(t),t)H_{3_i},\ \ \Delta C_{1_i} = F(x(t),t)H_{4_i},$$

$$\Delta C_{2_i} = F(x(t),t)H_{5_i},\ \ \Delta D_{12_i} = F(x(t),t)H_{6_i}\ \ \textit{and}\ \ \Delta D_{21_i} = F(x(t),t)H_{7_i}$$

where H_{j_i}, $j = 1, 2, \cdots, 7$ are known matrix functions which characterize the structure of the uncertainties. Furthermore, the following inequality holds:

$$\|F(x(t),t)\| \leq \rho \tag{2}$$

for any known positive constant ρ. Next, let us recall the following definition.

Definition 1. *Suppose γ is a given positive number. A system (1) is said to have an $\mathcal{L}_2$-gain less than or equal to γ if*

$$\int_0^{T_f} z^T(t)z(t)dt \leq \gamma^2 \left[\int_0^{T_f} w^T(t)w(t)dt\right], \tag{3}$$

for all $T_f \geq 0$, $x(0) = 0$ and $w(t) \in \mathcal{L}_2[0, T_f]$.

Note that for the symmetric block matrices, we use $(*)$ as an ellipsis for terms that are induced by symmetry.

3 Non-fragile $\mathcal{H}_\infty$ Output Feedback Controller

The nature of the information of the state available to the controller has a major effect on the complexity of the designing problem and of the resulting controller. The state-feedback control design problem is an easier problem in which all information are available. However, in most real physical systems, the state is not perfectly known, and so we must estimate it. The process of estimating the system state from the measurement output that are available is called the estimator design. By utilizing the state estimator, the output feedback problem is converted to the state-feedback problem for a new problem. This new problem employs the estimated state as its own state variable and the solution of the new state-feedback problem leads to the solution of the dynamic output feedback control problem. Basically, the dynamic output feedback is a coupling of control and estimation.

This section aims at designing a full order dynamic non-fragile $\mathcal{H}_\infty$ fuzzy output feedback controller of the form

$$E_\varepsilon\dot{\hat{x}}(t) \ = \ \sum_{i=1}^r \sum_{j=1}^r \hat{\mu}_i\hat{\mu}_j\Big[\hat{A}_{ij}(\varepsilon)\hat{x}(t) + \hat{B}_i y(t)\Big], \quad u(t) = \sum_{i=1}^r \hat{\mu}_i\hat{C}_i\hat{x}(t) \tag{4}$$

where $\hat{x}(t) \in \Re^n$ is the controller's state vector, $\hat{A}_{ij}$, $\hat{B}_i$ and $\hat{C}_i$ are parameters of the controller which are to be determined, and $\hat{\mu}_i$ denotes the normalized time-varying fuzzy weighting functions for each rule (i.e., $\hat{\mu}_i \geq 0$ and $\sum_{i=1}^r \hat{\mu}_i = 1$), such that the inequality (3) holds.

Clearly, in real control problems, all of the premise variables are not necessarily measurable. Thus, in this section, we consider the designing of the non-fragile $\mathcal{H}_\infty$ output feedback control into two cases as follows. In Subsection 3.1, we consider the case where the premise variable of the fuzzy model μ_i is measurable, while in Subsection 3.2, the premise variable which is assumed to be unmeasurable is considered.

3.1 Case I–$\nu(t)$ is available for feedback

The premise variable of the fuzzy model $\nu(t)$ is available for feedback which implies that μ_i is available for feedback. Thus, we can select our controller that depends on μ_i as follows:

$$E_\varepsilon\dot{\hat{x}}(t) = \sum_{i=1}^r\sum_{j=1}^r \mu_i\mu_j\Big[\hat{A}_{ij}(\varepsilon)\hat{x}(t)+\hat{B}_i y(t)\Big], \quad u(t)=\sum_{i=1}^r \mu_i\hat{C}_i\hat{x}(t). \tag{5}$$

Before presenting our next results, the following lemma is recalled.

Lemma 1. *Consider the system (1). Given a prescribed $\mathcal{H}_\infty$ performance γ and a positive constant δ, if there exist matrices $X_\varepsilon = X_\varepsilon^T$, $Y_\varepsilon = Y_\varepsilon^T$, $\mathcal{B}_i(\varepsilon)$ and $\mathcal{C}_i(\varepsilon)$, $i=1,2,\cdots,r$, satisfying the following ε-dependent linear matrix inequalities:*

$$\begin{bmatrix} X_\varepsilon & I \\ I & Y_\varepsilon \end{bmatrix} > 0 \tag{6}$$

$$X_\varepsilon > 0 \quad and \quad Y_\varepsilon > 0 \tag{7}$$

$$\Psi_{11_{ii}}(\varepsilon) \quad and \quad \Psi_{22_{ii}}(\varepsilon) < 0, \quad i=1,2,\cdots,r \tag{8}$$

$$\Psi_{11_{ij}}(\varepsilon)+\Psi_{11_{ji}}(\varepsilon) \quad and \quad \Psi_{22_{ij}}(\varepsilon)+\Psi_{22_{ji}}(\varepsilon) < 0, \quad i<j\le r \tag{9}$$

where

$$\Psi_{11_{ij}}(\varepsilon) = \begin{pmatrix} \begin{pmatrix} E_\varepsilon^{-1}A_iY_\varepsilon + Y_\varepsilon A_i^TE_\varepsilon^{-1} + E_\varepsilon^{-1}B_{2_i}\mathcal{C}_j(\varepsilon)E_\varepsilon^{-1} \\ +E_\varepsilon^{-1}\mathcal{C}_i^T(\varepsilon)B_{2_j}^TE_\varepsilon^{-1} + \gamma^{-2}E_\varepsilon^{-1}\tilde{B}_{1_i}\tilde{B}_{1_j}^TE_\varepsilon^{-1} \end{pmatrix} & (*)^T \\ \Big[Y_\varepsilon\tilde{C}_{1_i}^T + E_\varepsilon^{-1}\mathcal{C}_i^T(\varepsilon)\tilde{D}_{12_j}^T\Big]^T & -I \end{pmatrix} \tag{10}$$

$$\Psi_{22_{ij}}(\varepsilon) = \begin{pmatrix} \begin{pmatrix} A_i^TE_\varepsilon^{-1}X_\varepsilon + X_\varepsilon E_\varepsilon^{-1}A_i \\ +\mathcal{B}_i(\varepsilon)C_{2_j} + C_{2_i}^T\mathcal{B}_j^T(\varepsilon) + \tilde{C}_{1_i}^T\tilde{C}_{1_j} \end{pmatrix} & (*)^T \\ \Big[X_\varepsilon E_\varepsilon^{-1}\tilde{B}_{1_i} + \mathcal{B}_i(\varepsilon)\tilde{D}_{21_j}\Big]^T & -\gamma^2 I \end{pmatrix} \tag{11}$$

with

$$\tilde{B}_{1_i} = \begin{bmatrix} \delta I & I & \delta I & 0 & B_{1_i} & 0 \end{bmatrix}, \ \tilde{C}_{1_i} = \begin{bmatrix} \frac{\gamma\rho}{\delta}H_{1_i}^T & 0 & \frac{\gamma\rho}{\delta}H_{5_i}^T & \sqrt{2}\lambda\rho H_{4_i}^T & \sqrt{2}\lambda C_{1_i}^T \end{bmatrix}^T,$$

$$\tilde{D}_{12_i} = \begin{bmatrix} 0 & \frac{\gamma\rho}{\delta}H_{3_i}^T & 0 & \sqrt{2}\lambda\rho H_{6_i}^T & \sqrt{2}\lambda D_{12_i}^T \end{bmatrix}^T, \ \tilde{D}_{21_i} = \begin{bmatrix} 0 & 0 & 0 & \delta I & D_{21_i} & I \end{bmatrix}$$

$$and \ \lambda = \left(1+\rho^2\sum_{i=1}^r\sum_{j=1}^r\Big[\|H_{2_i}^TH_{2_j}\|+\|H_{7_i}^TH_{7_j}\|\Big]\right)^{\frac{1}{2}},$$

then the system (1) has the prescribed $\mathcal{H}_\infty$ performance $\gamma>0$. Furthermore, a suitable controller is of the form (5) with

$$\begin{aligned} \hat{A}_{ij}(\varepsilon) &= E_\varepsilon\Big[Y_\varepsilon^{-1}-X_\varepsilon\Big]^{-1}\mathcal{M}_{ij}(\varepsilon)Y_\varepsilon^{-1} \\ \hat{B}_i &= E_\varepsilon\Big[Y_\varepsilon^{-1}-X_\varepsilon\Big]^{-1}\mathcal{B}_i(\varepsilon) \quad and \quad \hat{C}_i = \mathcal{C}_i(\varepsilon)E_\varepsilon^{-1}Y_\varepsilon^{-1} \end{aligned} \tag{12}$$

$$\begin{aligned} where \ \mathcal{M}_{ij}(\varepsilon) = &-A_i^TE_\varepsilon^{-1} - X_\varepsilon E_\varepsilon^{-1}A_iY_\varepsilon - X_\varepsilon E_\varepsilon^{-1}B_{2_i}\hat{C}_jY_\varepsilon \\ &-\big[Y_\varepsilon^{-1}-X_\varepsilon\big]E_\varepsilon^{-1}\hat{B}_iC_{2_j}Y_\varepsilon - \tilde{C}_{1_i}^T\big[\tilde{C}_{1_j}Y_\varepsilon + \tilde{D}_{12_j}\hat{C}_jY_\varepsilon\big] \\ &-\gamma^{-2}\Big\{X_\varepsilon E_\varepsilon^{-1}\tilde{B}_{1_i} + \big[Y_\varepsilon^{-1}-X_\varepsilon\big]E_\varepsilon^{-1}\hat{B}_i\tilde{D}_{21_i}\Big\}\tilde{B}_{1_j}^TE_\varepsilon^{-1}. \end{aligned} \tag{13}$$

Proof: The proof can be carried out the same technique used in Lemma 1. □

Remark 1. *The LMIs given in Lemma 3.1 may become ill-conditioned when ε is sufficiently small, which is always the case for the multiple time-scale systems. In general, these ill-conditioned LMIs are very difficult to solve. Thus, to alleviate these ill-conditioned LMIs, we have the following ε-independent well-posed LMI-based sufficient conditions for the uncertain fuzzy multiple time-scale systems to obtain the prescribed $\mathcal{H}_\infty$ performance.*

Theorem 1. *Consider the system (1). Given a prescribed $\mathcal{H}_\infty$ performance $\gamma > 0$ and a positive constant δ, if there exist matrices X_0, Y_0, $\mathcal{B}_{0_i}$ and $\mathcal{C}_{0_i}$, $i = 1, 2, \cdots, r$, satisfying the following ε-independent linear matrix inequalities:*

$$\begin{bmatrix} X_0E + DX_0 & I \\ I & Y_0E + DY_0 \end{bmatrix} > 0 \tag{14}$$

$$EX_0^T = X_0E,\ X_0^TD = DX_0,\ X_0E + DX_0 > 0 \tag{15}$$

$$EY_0^T = Y_0E,\ Y_0^TD = DY_0,\ Y_0E + DY_0 > 0 \tag{16}$$

$$\Psi_{11_{ii}} \quad and \quad \Psi_{22_{ii}} < 0, \quad i = 1, 2, \cdots, r \tag{17}$$

$$\Psi_{11_{ij}} + \Psi_{11_{ji}} \quad and \quad \Psi_{22_{ij}} + \Psi_{22_{ji}} < 0, \quad i < j \le r \tag{18}$$

where $E = \begin{pmatrix} I & 0 \\ 0 & 0 \end{pmatrix}$, $D = \begin{pmatrix} 0 & 0 \\ 0 & I \end{pmatrix}$,

$$\Psi_{11_{ij}} = \begin{pmatrix} A_iY_0^T + Y_0A_i^T + B_{2_i}\mathcal{C}_{0_j} + \mathcal{C}_{0_i}^TB_{2_j}^T + \gamma^{-2}\tilde{B}_{1_i}\tilde{B}_{1_j}^T & (*)^T \\ \left[Y_0\tilde{C}_{1_i}^T + \mathcal{C}_{0_i}^T\tilde{D}_{12_j}^T\right]^T & -I \end{pmatrix} \tag{19}$$

$$\Psi_{22_{ij}} = \begin{pmatrix} A_i^TX_0^T + X_0A_i + \mathcal{B}_{0_i}C_{2_j} + C_{2_i}^T\mathcal{B}_{0_j}^T + \tilde{C}_{1_i}^T\tilde{C}_{1_j} & (*)^T \\ \left[X_0\tilde{B}_{1_i} + \mathcal{B}_{0_i}\tilde{D}_{21_j}\right]^T & -\gamma^2I \end{pmatrix} \tag{20}$$

with

$$\tilde{B}_{1_i} = \begin{bmatrix} \delta I & I & \delta I & 0 & B_{1_i} & 0 \end{bmatrix},\ \tilde{C}_{1_i} = \begin{bmatrix} \frac{\gamma\rho}{\delta}H_{1_i}^T & 0 & \frac{\gamma\rho}{\delta}H_{5_i}^T & \sqrt{2}\lambda\rho H_{4_i}^T & \sqrt{2}\lambda C_{1_i}^T \end{bmatrix}^T$$

$$\tilde{D}_{12_i} = \begin{bmatrix} 0 & \frac{\gamma\rho}{\delta}H_{3_i}^T & 0 & \sqrt{2}\lambda\rho H_{6_i}^T & \sqrt{2}\lambda D_{12_i}^T \end{bmatrix}^T,\ \tilde{D}_{21_i} = \begin{bmatrix} 0 & 0 & 0 & \delta I & D_{21_i} & I \end{bmatrix}$$

$$and\ \lambda = \left(1 + \rho^2\sum_{i=1}^{r}\sum_{j=1}^{r}\left[\|H_{2_i}^TH_{2_j}\| + \|H_{7_i}^TH_{7_j}\|\right]\right)^{\frac{1}{2}},$$

then there exists a sufficiently small $\hat{\varepsilon} > 0$ such that for $\varepsilon \in (0, \hat{\varepsilon}]$, the prescribed $\mathcal{H}_\infty$ performance $\gamma > 0$ is guaranteed. Furthermore, a suitable controller is of the form (5) with

$$\hat{A}_{ij}(\varepsilon) = \left[Y_\varepsilon^{-1} - X_\varepsilon\right]^{-1}\mathcal{M}_{0_{ij}}(\varepsilon)Y_\varepsilon^{-1}, \quad \hat{B}_i = \left[Y_0^{-1} - X_0\right]^{-1}\mathcal{B}_{0_i}, \quad and \quad \hat{C}_i = \mathcal{C}_{0_i}Y_0^{-1} \tag{21}$$

$$\begin{aligned} where\ \ \mathcal{M}_{0_{ij}}(\varepsilon) = {} & -A_i^T - X_\varepsilon A_iY_\varepsilon - X_\varepsilon B_{2_i}\hat{C}_jY_\varepsilon - \left[Y_\varepsilon^{-1} - X_\varepsilon\right]\hat{B}_iC_{2_j}Y_\varepsilon \\ & -\tilde{C}_{1_i}^T\left[\tilde{C}_{1_j}Y_\varepsilon + \tilde{D}_{12_j}\hat{C}_jY_\varepsilon\right] - \gamma^{-2}\Big\{X_\varepsilon\tilde{B}_{1_i} + \left[Y_\varepsilon^{-1} - X_\varepsilon\right]\hat{B}_i\tilde{D}_{21_i}\Big\}\tilde{B}_{1_j}^T \end{aligned} \tag{22}$$

$$X_\varepsilon = \Big\{X_0 + \varepsilon\tilde{X}\Big\}E_\varepsilon \quad and \quad Y_\varepsilon^{-1} = \Big\{Y_0^{-1} + \varepsilon N_\varepsilon\Big\}E_\varepsilon \tag{23}$$

with $\tilde{X} = D\Big(X_0^T - X_0\Big)$ *and* $N_\varepsilon = D\Big((Y_0^{-1})^T - Y_0^{-1}\Big)$.

Proof: Suppose the inequalities (14)-(16) hold, then the matrices X_0 and Y_0 are of the following forms:

$$X_0 = \begin{pmatrix} X_1 & X_2 \\ 0 & X_3 \end{pmatrix} \text{ and } Y_0 = \begin{pmatrix} Y_1 & Y_2 \\ 0 & Y_3 \end{pmatrix}$$

with $X_1 = X_1^T > 0$, $X_3 = X_3^T > 0$, $Y_1 = Y_1^T > 0$ and $Y_3 = Y_3^T > 0$. Substituting X_0 and Y_0 into (23), respectively, we have

$$X_\varepsilon = \Big\{X_0 + \varepsilon\tilde{X}\Big\}E_\varepsilon = \begin{pmatrix} X_1 & \varepsilon X_2 \\ \varepsilon X_2^T & \varepsilon X_3 \end{pmatrix} \tag{24}$$

$$Y_\varepsilon^{-1} = \Big\{Y_0^{-1} + \varepsilon N_\varepsilon\Big\}E_\varepsilon = \begin{pmatrix} Y_1^{-1} & -\varepsilon Y^{-1}Y_2Y_3^{-1} \\ -\varepsilon(Y^{-1}Y_2Y_3^{-1})^T & \varepsilon Y_3^{-1} \end{pmatrix}. \tag{25}$$

Clearly, $X_\varepsilon = X_\varepsilon^T$, and $Y_\varepsilon^{-1} = (Y_\varepsilon^{-1})^T$. Knowing the fact that the inverse of a symmetric matrix is a symmetric matrix, we learn that Y_ε is a symmetric matrix. Using the matrix inversion lemma, we can see that

$$Y_\varepsilon = E_\varepsilon^{-1}\Big\{Y_0 + \varepsilon\tilde{Y}\Big\} \tag{26}$$

where $\tilde{Y} = Y_0N_\varepsilon(I + \varepsilon Y_0N_\varepsilon)^{-1}Y_0$. Employing the Schur complement, one can show that there exists a sufficiently small $\hat{\varepsilon}$ such that for $\varepsilon \in (0, \hat{\varepsilon}]$, (7) holds.

Now, we need to show that

$$\begin{pmatrix} X_\varepsilon & I \\ I & Y_\varepsilon \end{pmatrix} > 0. \tag{27}$$

By the Schur complement, it is equivalent to showing that

$$X_\varepsilon - Y_\varepsilon^{-1} > 0. \tag{28}$$

Substituting (24) and (25) into the left hand side of (28), we get

$$\begin{bmatrix} X_1 - Y_1^{-1} & \varepsilon(X_2 + Y_1^{-1}Y_2Y_3^{-1}) \\ \varepsilon(X_2 + Y_1^{-1}Y_2Y_3^{-1})^T & \varepsilon(X_3 - Y_3^{-1}) \end{bmatrix}. \tag{29}$$

The Schur complement of (14) is

$$\begin{bmatrix} X_1 - Y_1^{-1} & 0 \\ 0 & X_3 - Y_3^{-1} \end{bmatrix} > 0. \tag{30}$$

According to (30), we learn that

$$X_1 - Y_1^{-1} > 0 \qquad \text{and} \qquad X_3 - Y_3^{-1} > 0. \tag{31}$$

Using (31) and the Schur complement, it can be shown that there exists a sufficiently small $\hat{\varepsilon} > 0$ such that for $\varepsilon \in (0, \hat{\varepsilon}]$, (6) holds.

Next, employing (24), (25) and (26), the controller's matrices given in (12) can be re-expressed as follows:

$$\begin{aligned} \mathcal{B}_i(\varepsilon) &= \big[Y_0^{-1} - X_0\big]\hat{B}_i + \varepsilon\big[N_\varepsilon - \tilde{X}\big]\hat{B}_i\mathcal{B}_{0_i} + \varepsilon\mathcal{B}_{\varepsilon_i} \\ \mathcal{C}_i(\varepsilon) &= \hat{C}_iY_0^T + \varepsilon\hat{C}_i\tilde{Y}^T\mathcal{C}_{0_i} + \varepsilon\mathcal{C}_{\varepsilon_i}. \end{aligned} \tag{32}$$

Substituting (24), (25), (26) and (32) into (10) and (11), and pre-post multiplying (10) by $\begin{pmatrix} E_\varepsilon & 0 \\ 0 & I \end{pmatrix}$, we, respectively, obtain

$$\Psi_{11_{ij}} + \psi_{11_{ij}} \text{ and } \Psi_{22_{ij}} + \psi_{22_{ij}} \tag{33}$$

where the ε-independent linear matrices $\Psi_{11_{ij}}$ and $\Psi_{22_{ij}}$ are defined in (19) and (20), respectively and the ε-dependent linear matrices are

$$\psi_{11_{ij}} = \varepsilon \begin{pmatrix} A_i\tilde{Y}^T + \tilde{Y}A_i^T + B_{2_i}\mathcal{C}_{\varepsilon_j} + \mathcal{C}_{\varepsilon_i}^T B_{2_j}^T & (*)^T \\ \left[\tilde{Y}\tilde{C}_{1_i}^T + \mathcal{C}_{\varepsilon_i}^T \tilde{D}_{12_j}^T\right]^T & 0 \end{pmatrix} \tag{34}$$

$$\psi_{22_{ij}} = \varepsilon \begin{pmatrix} A_i^T\tilde{X} + \tilde{X}^T A_i + \mathcal{B}_{\varepsilon_i}C_{2_j} + C_{2_i}^T\mathcal{B}_{\varepsilon_j}^T & (*)^T \\ \left[\tilde{X}\tilde{B}_{1_i} + \mathcal{B}_{\varepsilon_i}\tilde{D}_{21_j}\right]^T & 0 \end{pmatrix}. \tag{35}$$

Note that the ε-dependent linear matrices tend to zero when ε approaches zero.

Employing (17)-(18) and knowing the fact that for any given negative definite matrix $\mathcal{W}$, there exists an $\varepsilon > 0$ such that $\mathcal{W} + \varepsilon I < 0$, one can show that there exists a sufficiently small $\hat{\varepsilon} > 0$ such that for $\varepsilon \in (0, \hat{\varepsilon}]$, (8)-(9) hold. Since (6)-(9) hold, using Lemma 2, the inequality (3) holds. □

3.2 Case II–$\nu(t)$ is unavailable for feedback

The output feedback fuzzy controller is assumed to be the same as the premise variables of the fuzzy system model. This actually means that the premise variables of fuzzy system model are assumed to be measurable. However, in general, it is extremely difficult to derive an accurate fuzzy system model by imposing that all premise variables are measurable. In this subsection, we do not impose that condition, we choose the premise variables of the controller to be different from the premise variables of fuzzy system model of the plant. In here, the premise variables of the controller are selected to be the estimated premise variables of the plant. In the other words, the premise variable of the fuzzy model $\nu(t)$ is unavailable for feedback which implies μ_i is unavailable for feedback. Hence, we cannot select our controller which depends on μ_i. Thus, we select our controller as (4) where $\hat{\mu}_i$ depends on the premise variable of the controller which is different from μ_i. Let us re-express the system (1) in terms of $\hat{\mu}_i$, thus the plant's premise variable becomes the same as the controller's premise variable. By doing so, the result given in the previous case can then be applied here. Note that it can be done by using the same technique as in subsection. After some manipulation, we get

$$\begin{aligned} E_\varepsilon\dot{x}(t) &= \textstyle\sum_{i=1}^r \hat{\mu}_i\Big[[A_i + \Delta\bar{A}_i]x(t) + [B_{1_i} + \Delta\bar{B}_{1_i}]w(t) + [B_{2_i} + \Delta\bar{B}_{2_i}]\Big]u(t) \\ z(t) &= \textstyle\sum_{i=1}^r \hat{\mu}_i\Big[[C_{1_i} + \Delta\bar{C}_{1_i}]x(t) + [D_{12_i} + \Delta\bar{D}_{12_i}]u(t)\Big] \\ y(t) &= \textstyle\sum_{i=1}^r \hat{\mu}_i\Big[[C_{2_i} + \Delta\bar{C}_{2_i}]x(t) + [D_{21_i} + \Delta\bar{D}_{21_i}]w(t)\Big] \end{aligned} \tag{36}$$

where

$$\Delta\bar{A}_i = \bar{F}(x(t), \hat{x}(t), t)\bar{H}_{1_i}, \quad \Delta\bar{B}_{1_i} = \bar{F}(x(t), \hat{x}(t), t)\bar{H}_{2_i}, \quad \Delta\bar{B}_{2_i} = \bar{F}(x(t), \hat{x}(t), t)\bar{H}_{3_i},$$

$$\Delta\bar{C}_{1_i} = \bar{F}(x(t), \hat{x}(t), t)\bar{H}_{4_i}, \quad \Delta\bar{C}_{2_i} = \bar{F}(x(t), \hat{x}(t), t)\bar{H}_{5_i}, \quad \Delta\bar{D}_{12_i} = \bar{F}(x(t), \hat{x}(t), t)\bar{H}_{6_i}$$

$$\text{and } \Delta\bar{D}_{21_i} = \bar{F}(x(t), \hat{x}(t), t)\bar{H}_{7_i}$$

with

$$\bar{H}_{1_i} = \left[H_{1_i}^T\ A_1^T\ \cdots A_r^T\ H_{1_1}^T \cdots H_{1_r}^T\right]^T,\ \ \bar{H}_{2_i} = \left[H_{2_i}^T\ B_{1_1}^T \cdots B_{1_r}^T\ H_{2_1}^T \cdots H_{2_r}^T\right]^T,$$
$$\bar{H}_{3_i} = \left[H_{3_i}^T\ B_{2_1}^T \cdots B_{2_r}^T\ H_{3_1}^T \cdots H_{3_r}^T\right]^T,\ \ \bar{H}_{4_i} = \left[H_{4_i}^T\ C_{1_1}^T \cdots C_{1_r}^T\ H_{4_1}^T \cdots H_{4_r}^T\right]^T,$$
$$\bar{H}_{5_i} = \left[H_{5_i}^T\ C_{2_1}^T \cdots C_{2_r}^T\ H_{5_1}^T \cdots H_{5_r}^T\right]^T,\ \ \bar{H}_{6_i} = \left[H_{6_i}^T\ D_{12_1}^T \cdots D_{12_r}^T\ H_{6_1}^T \cdots H_{6_r}^T\right]^T$$
$$\bar{H}_{7_i} = \left[H_{7_i}^T\ D_{21_1}^T \cdots\ D_{21_r}^T\ H_{7_1}^T \cdots H_{7_r}^T\right]^T \text{ and}$$

$$\bar{F}(x(t),\hat{x}(t),t) = \Big[F(x(t),t)\ (\mu_1-\hat{\mu}_1)\ \cdots\ (\mu_r-\hat{\mu}_r)\ F(x(t),t)(\mu_1-\hat{\mu}_1)\ \cdots F(x(t),t)(\mu_r-\hat{\mu}_r)\Big].$$

Note that $\|\bar{F}(x(t),\hat{x}(t),t)\| \le \bar{\rho}$ where $\bar{\rho} = \{3\rho^2+2\}^{\frac{1}{2}}$. $\bar{\rho}$ is derived by utilizing the concept of vector norm in the basic system control theory and the fact that $\mu_i \ge 0$, $\hat{\mu}_i \ge 0$, $\sum_{i=1}^r \mu_i = 1$ and $\sum_{i=1}^r \hat{\mu}_i = 1$.

Note that the above technique is basically employed in order to obtain the plant's premise variable to be the same as the controller's premise variable; e.g. [28]. Now, the premise variable of the system is the same as the premise variable of the controller, thus we can apply the result given in Case I.

Theorem 2 *Consider the system (1). Given a prescribed $\mathcal{H}_\infty$ performance $\gamma > 0$ and a positive constant δ, if there exist matrices X_0, Y_0, $\mathcal{B}_{0_i}$ and $\mathcal{C}_{0_i}$, $i = 1, 2, \cdots, r$, satisfying the following ε-independent linear matrix inequalities:*

$$\begin{bmatrix} X_0E + DX_0 & I \\ I & Y_0E + DY_0 \end{bmatrix} > 0 \tag{37}$$
$$EX_0^T = X_0E,\ X_0^TD = DX_0,\ X_0E + DX_0 > 0 \tag{38}$$
$$EY_0^T = Y_0E,\ Y_0^TD = DY_0,\ Y_0E + DY_0 > 0 \tag{39}$$
$$\Psi_{11_{ii}} \ \ and \ \ \Psi_{22_{ii}} < 0,\ i = 1, 2, \cdots, r \tag{40}$$
$$\Psi_{11_{ij}} + \Psi_{11_{ji}} \ \ and \ \ \Psi_{22_{ij}} + \Psi_{22_{ji}} < 0,\ i < j \le r \tag{41}$$

where $E = \begin{pmatrix} I & 0 \\ 0 & 0 \end{pmatrix}$, $D = \begin{pmatrix} 0 & 0 \\ 0 & I \end{pmatrix}$,

$$\Psi_{11_{ij}} = \begin{pmatrix} A_iY_0^T + Y_0A_i^T + B_{2_i}\mathcal{C}_{0_j} + \mathcal{C}_{0_i}^TB_{2_j}^T + \gamma^{-2}\tilde{\bar{B}}_{1_i}\tilde{\bar{B}}_{1_j}^T & (*)^T \\ \left[Y_0\tilde{C}_{1_i}^T + \mathcal{C}_{0_i}^T\tilde{D}_{12_j}^T\right]^T & -I \end{pmatrix} \tag{42}$$

$$\Psi_{22_{ij}} = \begin{pmatrix} A_i^TX_0^T + X_0A_i + \mathcal{B}_{0_i}C_{2_j} + C_{2_i}^T\mathcal{B}_{0_j}^T + \tilde{\bar{C}}_{1_i}^T\tilde{\bar{C}}_{1_j} & (*)^T \\ \left[X_0\tilde{\bar{B}}_{1_i} + \mathcal{B}_{0_i}\tilde{\bar{D}}_{21_j}\right]^T & -\gamma^2I \end{pmatrix} \tag{43}$$

with

$$\tilde{\bar{B}}_{1_i} = \left[\ \delta I\ \ I\ \ \delta I\ \ 0\ \ B_{1_i}\ \ 0\ \right],\ \tilde{\bar{C}}_{1_i} = \left[\ \tfrac{\gamma\bar{\rho}}{\delta}\bar{H}_{1_i}^T\ \ 0\ \ \tfrac{\gamma\bar{\rho}}{\delta}\bar{H}_{5_i}^T\ \ \sqrt{2}\bar{\lambda}\bar{\rho}\bar{H}_{4_i}^T\ \ \sqrt{2}\bar{\lambda}C_{1_i}^T\ \right]^T,$$
$$\tilde{\bar{D}}_{12_i} = \left[\ 0\ \ \tfrac{\gamma\bar{\rho}}{\delta}\bar{H}_{3_i}^T\ \ 0\ \ \sqrt{2}\bar{\lambda}\bar{\rho}\bar{H}_{6_i}^T\ \ \sqrt{2}\bar{\lambda}D_{12_i}^T\ \right]^T,\ \tilde{\bar{D}}_{21_i} = \left[\ 0\ \ 0\ \ 0\ \ \delta I\ \ D_{21_i}\ \ I\ \right]$$
$$and\ \ \bar{\lambda} = \left(1 + \bar{\rho}^2\sum_{i=1}^r\sum_{j=1}^r\left[\|\bar{H}_{2_i}^T\bar{H}_{2_j}\| + \|\bar{H}_{7_i}^T\bar{H}_{7_j}\|\right]\right)^{\frac{1}{2}},$$

then there exists a sufficiently small $\hat{\varepsilon} > 0$ such that for $\varepsilon \in (0, \hat{\varepsilon}]$, the prescribed $\mathcal{H}_\infty$ performance $\gamma > 0$ is guaranteed. Furthermore, a suitable controller is of the form (4) with

$$\hat{A}_{ij}(\varepsilon) = \left[Y_\varepsilon^{-1} - X_\varepsilon\right]^{-1}\mathcal{M}_{0_{ij}}(\varepsilon)Y_\varepsilon^{-1},\ \ \hat{B}_i = \left[Y_0^{-1} - X_0\right]^{-1}\mathcal{B}_{0_i},\ \ and\ \ \hat{C}_i = \mathcal{C}_{0_i}Y_0^{-1} \tag{44}$$

$$\begin{aligned} \textit{where}\quad \mathcal{M}_{0_{ij}}(\varepsilon) &= -A_i^T - X_\varepsilon A_i Y_\varepsilon - X_\varepsilon B_{2_i}\hat{C}_j Y_\varepsilon - \left[Y_\varepsilon^{-1} - X_\varepsilon\right]\hat{B}_i C_{2_j} Y_\varepsilon \\ &\quad -\tilde{\tilde{C}}_{1_i}^T\left[\tilde{\tilde{C}}_{1_j} Y_\varepsilon + \tilde{\tilde{D}}_{12_j}\hat{C}_j Y_\varepsilon\right] - \gamma^{-2}\Big\{X_\varepsilon \tilde{\tilde{B}}_{1_i} + \left[Y_\varepsilon^{-1} - X_\varepsilon\right]\hat{B}_i \tilde{\tilde{D}}_{21_i}\Big\}\tilde{\tilde{B}}_{1_j}^T \quad (45) \end{aligned}$$

$$X_\varepsilon = \Big\{X_0 + \varepsilon\tilde{X}\Big\}E_\varepsilon \quad \textit{and} \quad Y_\varepsilon^{-1} = \Big\{Y_0^{-1} + \varepsilon N_\varepsilon\Big\}E_\varepsilon \quad (46)$$

with $\tilde{X} = D\Big(X_0^T - X_0\Big)$ *and* $N_\varepsilon = D\Big((Y_0^{-1})^T - Y_0^{-1}\Big)$.

Proof: Since (36) is of the form of (1), it can be shown by employing the proof for Theorem 3.1. □

4 Example

Consider the tunnel diode circuit where the tunnel diode is characterized by $i_D(t) = -0.2v_D(t) - 0.01v_D^3(t)$. Assume that ε is a "parasitic" inductance in the network. Let $x_1(t) = v_C(t)$ be the capacitor voltage and $x_2(t) = i_L(t)$ be the inductor current. Then, the circuit can be modelled by the following state equations:

$$\begin{aligned} C\dot{x}_1(t) &= 0.2x_1(t) + 0.01x_1^3(t) + x_2(t) \\ \varepsilon\dot{x}_2(t) &= -x_1(t) - Rx_2(t) + u(t) + 0.1w_2(t) \\ y(t) &= Jx(t) + 0.1w_1(t), \qquad z(t) = [x_1(t) \quad x_2(t)]^T \end{aligned} \quad (47)$$

where $u(t)$ is the control input, $w_1(t)$ is the measurement noise, $w_2(t)$ are is the process noise which may represent un-modelled dynamics, y(t) is the measured output, $z(t)$ is the controlled output, J is the sensor matrix, $x(t) = [x_1^T(t) \;\; x_2^T(t)]^T$ and $w(t) = [w_1^T(t) \;\; w_2^T(t)]^T$. Note that the variables $x_1(t)$ and $x_2(t)$ are treated as the deviation variables (variables deviate from its desired trajectories). The parameters in the circuit are given by $C = 100\ mF$ and $R = 1 \pm 0.3\%\ \Omega$, with these parameters (47) can be rewritten as

$$\begin{aligned} \dot{x}_1(t) &= 2x_1(t) + (0.1x_1^2(t)) \cdot x_1(t) + 10x_2(t) \\ \varepsilon\dot{x}_2(t) &= -x_1(t) - (1 \pm \Delta R)x_2(t) + u(t) + 0.1w_2(t) \\ y(t) &= Jx(t) + 0.1w_1(t), \qquad z(t) = [x_1(t) \quad x_2(t)]^T . \end{aligned} \quad (48)$$

For the sake of simplicity, we will use as few rules as possible. Assuming that $|x_1(t)| \leq 3$, the nonlinear network system (48) can be approximated by the following TS fuzzy model:

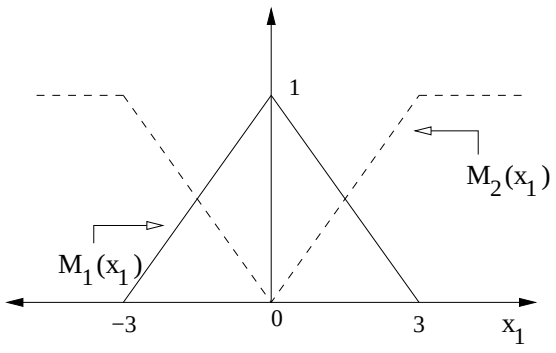

Figure 1: Membership functions for the two fuzzy set.

Plant Rule 1: IF $x_1(t)$ is $M_1(x_1(t))$ THEN

$$\begin{aligned} E_\varepsilon \dot{x}(t) &= [A_1 + \Delta A_1]x(t) + B_1 w(t) + B_{2_1} u(t), \\ z(t) &= C_1 x(t), \qquad y(t) = C_{2_1} x(t) + D_{21} w(t). \end{aligned}$$

Plant Rule 2: IF $x_1(t)$ is $M_2(x_1(t))$ THEN

$$\begin{aligned} E_\varepsilon \dot{x}(t) &= [A_2 + \Delta A_2]x(t) + B_1 w(t) + B_{2_2} u(t), \\ z(t) &= C_1 x(t), \qquad y(t) = C_{2_2} x(t) + D_{21} w(t) \end{aligned}$$

where $x(0) = 0$, $x(t) = [x_1^T(t) \;\; x_2^T(t)]^T$, $w(t) = [w_1^T(t) \;\; w_2^T(t)]^T$,

$A_1 = \begin{bmatrix} 2 & 10 \\ -1 & -1 \end{bmatrix}$, $A_2 = \begin{bmatrix} 2.9 & 10 \\ -1 & -1 \end{bmatrix}$, $B_1 = \begin{bmatrix} 0 & 0 \\ 0 & 0.1 \end{bmatrix}$, $B_{2_1} = B_{2_2} = \begin{bmatrix} 0 \\ 1 \end{bmatrix}$, $C_1 = \begin{bmatrix} 1 & 0 \\ 0 & 1 \end{bmatrix}$,

$C_{2_1} = C_{2_2} = J$, $D_{21} = \begin{bmatrix} 0.1 & 0 \end{bmatrix}$, $\Delta A_1 = F(x(t), t)H_{1_1}, ; \Delta A_2 = F(x(t), t)H_{1_2}$ and

$E_\varepsilon = \begin{bmatrix} 1 & 0 \\ 0 & \varepsilon \end{bmatrix}$. Note that, the plot of the membership functions is the same as in Figure 1. Now, by assuming that in (2), $\|F(x(t), t)\| \leq \rho = 1$ and since the values of R are uncertain but bounded within 30% of their nominal values given in (47), we have $H_{1_1} = H_{1_2} = \begin{bmatrix} 0 & 0 \\ 0 & 0.3 \end{bmatrix}$. Note that by employing the results given in Lemma 1 and the Matlab LMI solver, it is easy to realize that when $\varepsilon < 0.03$, the LMIs become ill-conditioned and the Matlab LMI solver yields the error message, "Rank Deficient". Using the LMI optimization algorithm and Theorems 3.1-3.2 with $\varepsilon = 0.01$, $\gamma = 1$ and $\delta = 1$, we obtain the following results as shown in Table 1.

Table 1: The performance index γ of the system with different values of ε.

ε	The performance index γ Output Feedback	
	Case I	Case II
0.01	0.316	0.346
0.15	0.574	0.922
0.16	0.600	> 1
0.28	0.989	> 1
0.29	> 1	> 1

Remark 2. *For a sufficiently small ε, the non-fragile output feedback controllers guarantee that the $\mathcal{L}_2$-gain, γ, is less than the prescribed value. The disturbance input signal, $w(t)$, which was used during the simulation is the rectangular signal with magnitude 0.1 and frequency 1 Hz. For an example, when ε is* 0.01*, the output feedback controller in Case I where $\gamma = 0.316$ and in Case II where $\gamma = 0.346$, all are less than the prescribed value* 1*. Thus, Table 1 shows the result of the performance index γ with different values of ε.*

5 Conclusion

This paper has considered the problem of designing a non-fragile output feedback controller for a TS fuzzy system with multiple time-scales. Sufficient conditions for the existence of non-fragile fuzzy controllers are derived in terms of a family of ε-independent linear matrix inequalities. The proposed approach does not involve the separation of states into slow and fast ones,

and it can be applied not only to standard, but also to nonstandard multiple time-scale systems. A numerical simulation example has been presented to illustrate the effectiveness of the designs.

Acknowledgment

This work is financed by Thailand National Research University Funding (NRU). The author also would like to acknowledge to the Department of Electronic and Telecommnunication Engineering, King Mongkut's University of Technology Thonburi for their supports in this research work.

Bibliography

[1] M. Suzuki, and M. Miura, "Stabilizing Feedback Controller for Singularly Perturbed Linear Constant Systems," *IEEE Trans. Automat. Control*, vol. AC-21, pp. 123–124, 1976.

[2] P.V. Kokotovic, R.E. O'Malley, Jr, and P. Sannuti, "Singular Perturbations and Order Reduction in Control Theory–An Overview," *Automatica*, vol. 12, pp. 123–132, 1976.

[3] J. O'Reilly, "Two Time-Scale Feedback Stabilization of Linear Time-Varying Singularly Perturbed Systems," *J. Franklin Inst.*, vol. 30, pp. 465–474, 1979.

[4] Z. Pan, and T. Basar, "H^∞–Optimal Control for Singularly Perturbed Systems PartI: Perfect State Measurements," *Automatica*, vol. 29, pp. 401–423, 1993.

[5] Z. Pan, and T. Basar, "H^∞–Optimal Control for Singularly Perturbed Systems PartII: Imperfect State Measurements," *IEEE Trans. Automat. Control*, vol. 39, pp. 280–299, 1994.

[6] E. Fridman, "State-Feedback H^∞ Control of Nonlinear Singularly Perturbed Systems," *Int. J. Robust Nonlinear Control*, (in press), 2001.

[7] P. Shi, and V. Dragan, "Asymptotic H_∞ Control of Singularly Perturbed System with Parametric Uncertainties," *IEEE Trans. Automat. Control*, vol. 44, pp. 1738–1742, 1999.

[8] P.Z.H. Shao, and M.E. Sawan, "Robust Stability of Singularly Perturbed Systems," *Int. J. Control*, vol. 58, pp. 1469–1476, 1993.

[9] W.C. Su, Z. Gajic, and X.M. Shen, "The Exact Slow-Fast Decomposition of the Algebraic Riccati Equation of Singularly Perturbed Systems," *IEEE Trans. Automat. Control*, vol. 37, pp. 1456–1459, 1992.

[10] W.C. Su, "Sliding surface design for singularly perturbed systems," *Int. J. Control*, vol. 72, pp. 990–995, 1999.

[11] T. Grodt, and Z. Gajic, "The Recursive Reduced-Order Numerical Solution of the Singularly Perturbed Matrix Differential Riccati Equation," *IEEE Trans. Automat. Control*, vol. 33, pp. 751–754, 1998.

[12] P.V. Kokotovic, H.K. Khalil, and J. O'Reilly, *Singular Perturbation Methods in Control: Analysis and Design*, Academic Press, London, 1986.

[13] K. Gu, "H_∞ Control of Systems under Norm Bounded Uncertainties in All Systems Matrices," *IEEE Trans. Automat. Contol*, vol. 39, pp. 1320–1322, 1994.

[14] H. Mukaidani, and H. Xu, "Robust H_∞ Control Problem for Nonstandard Singularly Perturbed Systems and Applications," *Proc. ACC*, Arlington, pp. 3920–3925, June 2001.

[15] B.D.O. Anderson, and J.B. Moore, *Optimal Control: Linear Quadratic Methods*, Prentice-Hall, New Jersey, 1990.

[16] L. A. Zadeh, "Fuzzy set," *Information and Contr.*, vol. 8, pp. 338–353, 1965.

[17] L. A. Zadeh, "Outline of a new approach to the analysis of complex systems and decision processes," *IEEE Trans. Syst. Man, Cybern.*, vol. 3, pp. 28–44, 1973.

[18] E. H. Mamdani and S. Assilian, "An experiment in linquistic synthesis with a fuzzy logic controller," *Int. J. Man-Machine-Studies.*, vol. 7, pp. 1–13, 1975.

[19] L. X. Wang, *A course in fuzzy systems and control.* Englewood Cliffs, NJ: Prentice-Hall, Inc., 1997.

[20] J. Yoneyama, M. Nishikawa, H. Katayama, and A. Ichikawa, "Output stabilization of Takagi-Sugeno fuzzy system," *Fuzzy Sets Systs.*, vol. 111, pp. 253–266, 2000.

[21] K. Tanaka and M. Sugeno, "Stability analysis and design of fuzzy control systems", *Fuzzy Sets Systs.*, vol. 45, pp. 135–156, 1992.

[22] K. Tanaka, "Stability and stabiliability of fuzzy neural linear control systems", *IEEE Trans. Fuzzy Syst.*, vol. 3, pp. 438–447, 1995.

[23] C. L. Chen, P. C. Chen, and C. K. Chen, "Analysis and design of fuzzy control system", *Fuzzy Sets Systs.*, vol. 57, pp. 125–140, 1995.

[24] X. J. Ma, Z. Q Sun, and Y. Y He, "Analysis and design of fuzzy controller and fuzzy observer", *IEEE Trans. Fuzzy Syst.*, vol. 6, pp. 41–51, 1998.

[25] W.Assawinchaichote and S. K. Nguang, "$\mathcal{H}^\infty$ filtering for nonlinear singularly perturbed systems with pole placement constraints: An LMI approach", *IEEE Trans. Signal Processing*, vol. 52, pp. 579–588, 2004.

[26] W. Assawinchaichote and S. K. Nguang, "$\mathcal{H}_\infty$ fuzzy control design for nonlinear singularly perturbed systems with pole placement constraints: An LMI approach," *IEEE Trans. Syst., Man, Cybern. B*, vol. 34, pp. 579–588, 2004.

[27] L. X. Wang, "Design and analysis of fuzzy identifiers of nonlinear dynamic systems," *IEEE Trans. Automat. Contr.*, vol. 40, pp. 11–23, 1995.

[28] S. K. Nguang and P. Shi, "$\mathcal{H}^\infty$ fuzzy output feedback control design for nonlinear systems: An LMI approach ," *IEEE Trans. Fuzzy Syst.*, vol. 11, pp. 331–340, 2003.

[29] H. J. Lee, J. B. Park, and G. Chen, "Robust fuzzy control of nonlinear system with parametric uncertainties," *IEEE. Trans. Fuzzy Syst.*, vol. 9, pp. 369–379, 2001.

Int. J. of Computers, Communications & Control, ISSN 1841-9836, E-ISSN 1841-9844
Vol. VII (2012), No. 1 (March), pp. 20-38

Controlling the Double Rotary Inverted Pendulum with Multiple Feedback Delays

V. Casanova, J. Salt, R. Piza, A. Cuenca

V. Casanova, J. Salt, R. Piza, A. Cuenca
Departamento de Ingeniería de Sistemas y Automática
Instituto Universitario de Automática e Informática Industrial
Universitat Politécnica de Valencia
Camino de Vera s/n 46022 Valencia (Spain)
E-mail: {vcasanov, julian, rpiza, acuenca}@isa.upv.es

Abstract:
The aim of this work is the development and implementation of a control structure for the double rotary inverted pendulum, suitable to be used in a Networked Control System environment. Delays are quite common in this kind of systems and, when controlling multivariable plants, it is possible that different delays are applied to the multiple inputs and outputs of them. A control structure that allows compensating individually each one of the multiple loop delays would be useful when one of these delays changes. Inverted pendulums are quite sensitive to delays and for this reason are appropriated plants to be used in these conditions. The control structure is developed modifying the control in no-delay conditions with a generalized predictor able to deal with unstable and non-minimum plants as the chosen one is. The proposed structure has been simulated and implemented to control a real double rotary inverted pendulum.
Keywords: Control applications, delay compensation, distributed control, multi-loop control, multi-variable feedback control, transport delay.

1 Introduction

The main goal of this paper is to propose a control structure that deals with multivariable plants when different delays are applied to the feedback signals. Consider the scenario in figure 1. A multivariable (MIMO) plant is going to be controlled by a MIMO controller. The plant outputs are feedback into the controller and the control actions are calculated by it, following some predesigned control law. These actions are applied to the plant. If the communication links between controller and plant is ideal, no delays are present. When a real link is used at least one sample time delay must be considered in each communication link. The influence of these delays must be removed to reach the desired behavior: the one in ideal (no-delay) conditions.

In the proposed scenario sensors and actuators (i.e. AD and DA conversions) are supposed to be separated by long distances among them and from the controller. The communication follows different paths for output signals and control actions, suffering different transport delays. The controller used in ideal conditions must be modified to compensate these delays. This is a common situation in networked control systems (NCS) when a shared medium is used to communicate a number of sensors and actuators with the main control. The longer the distance is, the greater the delay must be removed. The delay compensator becomes a MIMO structure to deal with the delay in each pair action/signal.

In wide-area NCS it is usual to have a great number of AD and DA conversions involved in the same control structure. The communication is performed through a shared medium instead of using point-to-point links. This allows to reduce costs (wiring, maintenance...) and

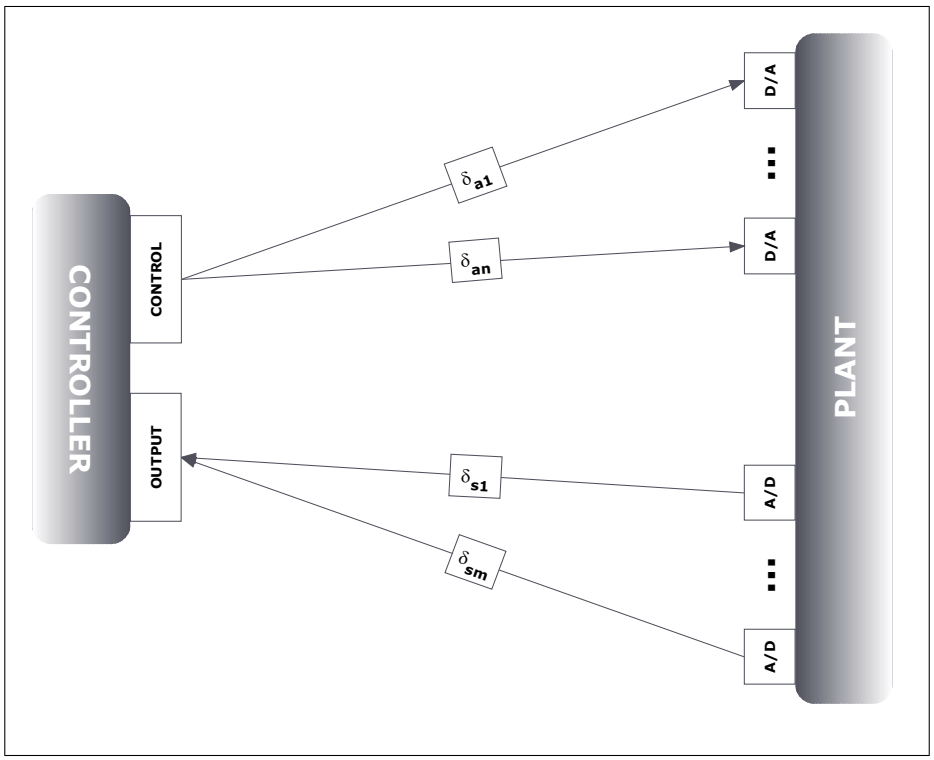

Figure 1: Problem scenario

to increase flexibility of the control system. The main drawbacks are the delay uncertainty and the bandwidth limitation. If there are different distances between sensors/actuators and the controller and/or the priority of the devices attached to the network is different, multiple delays can arise in the control structure.

In the most general case different number of sample time delays are applied to each one of the signals towards the actuators (δ_{an} being n the n^{th} control action) and to the signals from the sensors (δ_{sm} being m the m^{th} measured variable). The control structure becomes a collection of nxm loops each one of them includes a δ_{an}+δ_{sm} sample time delay, from the point of view of the controller (loop delay). This is the delay to be compensated in the controller of each one of these loops in the control structure. By removing the influence of the delays, the ideal behavior is intended to be reached. The goal of this work is to use the same controller, designed without considering the delays, to deal with the problem when they are present.

The presence of multiple delays in a NCS environment has been considered in many descriptions of this kind of systems ([1], [2], [3], [4], [5], [6], [7]) and several previous works have dealt with this problem. In [8] and [9] there is a description of the problem of multiple delays in NCS when they are smaller than one sampling period. In [10], [11] and [12] a NCS with multiple distributed delays is modeled and an optimal control is proposed. [13] proposes a model of an NCS with multiple successive delay components in the state. [14] deals with the problem of observability and optimal control in these control systems. [15] analyses the maximum allowable delay bound in control loops with network induced delays. [16] considers the problem of multiple delays in NCS from the point of view of fault diagnosis. Some works ([17], [18]) have considered the problem as a multivariable control design in which multiple input-output delays are included in the plant model. [19] uses an observer to provide state information, comparing the system behaviour with the Smith predictor.

The proposed solution is going to be applied to a classical control problem: the double rotary

inverted pendulum (also known as double Furuta pendulum, see figure 2). This is a classical textbook example of non-linear, non-minimum phase plant. The plant to be controlled has one input (the control action to the motor) and three outputs (the angular position of the motor shaft, the angular position of the first rod of the inverted pendulum and the angular position of the second rod). The goal of this control problem is to keep the pendulum angles as close to zero as possible, avoiding disturbances and to follow a certain reference with the shaft angle. So, four signals are involved between control and plant and four different time delays are going to be considered. As it is well known, this plant is quite sensitive to delays between controller and plant becoming unstable even with small delays. This sensitivity makes the Furuta pendulum quite appropriated to the proposed environment. The controller used in ideal conditions (i.e. no delays) must be properly modified to remove the delay influence in the feedback loop. In addition, the plant is an unstable and non-minimum phase one which makes more difficult the delay compensation. The single and double inverted pendulums have been widely used as a test-bed for different control strategies ([20], [21], [22]).

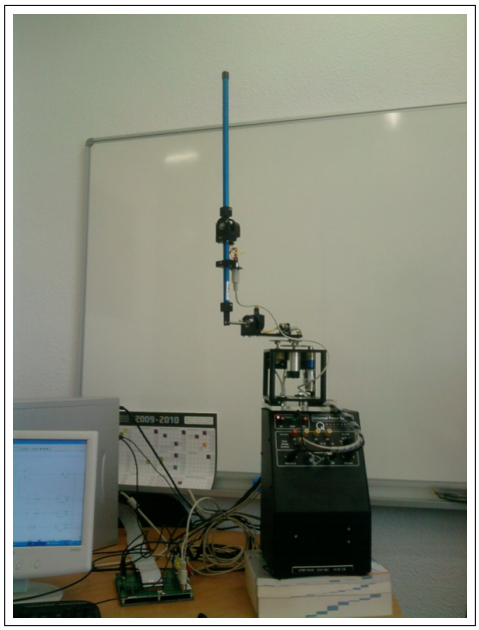

Figure 2: The double rotary inverted pendulum

The paper begins with a description of the plant to be controlled (section 2), followed by the controller used in ideal conditions (section 3). In section 4 the controller is modified to remove the influence of the delays, considering different control-plant delays for each one of the signals involved. Simulated results are presented in these sections to compare the behavior in ideal conditions, the nearly-unstable behavior when delays are included and the behavior when delay influence is removed from the loops. Results from a real plant are presented in section 5 showing how the proposed structure works when real disturbances and noise are present in the system. Finally, in section 6 conclusions and future work are presented.

2 Double Rotary Inverted Pendulum Model

The plant that has been chosen to implement the proposed control structure is the double rotary inverted pendulum (double Furuta pendulum) due to its sensitivity to feedback delays. The theoretical model of this plant is described in this section and it is particularized to model

a real one, the double rotary inverted pendulum developed by *Quanser Consulting Inc.* (shown in figure 2 in its upwards position).

The equations describing the behavior of the double inverted pendulum can be derived, using the Euler-Lagrange method. A complete development of this model can be found in [23] and [24]. By applying the Euler-Lagrange equation to the Lagrangian (i.e. the difference between kinetic and potential energy) the development of the mathematical model is greatly simplified. Figure 3 shows a schematic representation (top and front view) of the plant. The variables considered in the model are:

- θ, $\dot{\theta}$, $\ddot{\theta}$: Angular position, velocity and acceleration of the motor shaft, around the vertical axis.
- α, $\dot{\alpha}$, $\ddot{\alpha}$: Angular position, velocity and acceleration of the first rod, around the motor shaft axis.
- γ, $\dot{\gamma}$, $\ddot{\gamma}$: Angular position, velocity and acceleration of the second rod, around the motor shaft axis.
- τ: Torque applied to the motor shaft.
- u: Control action applied to the DC motor (voltage).

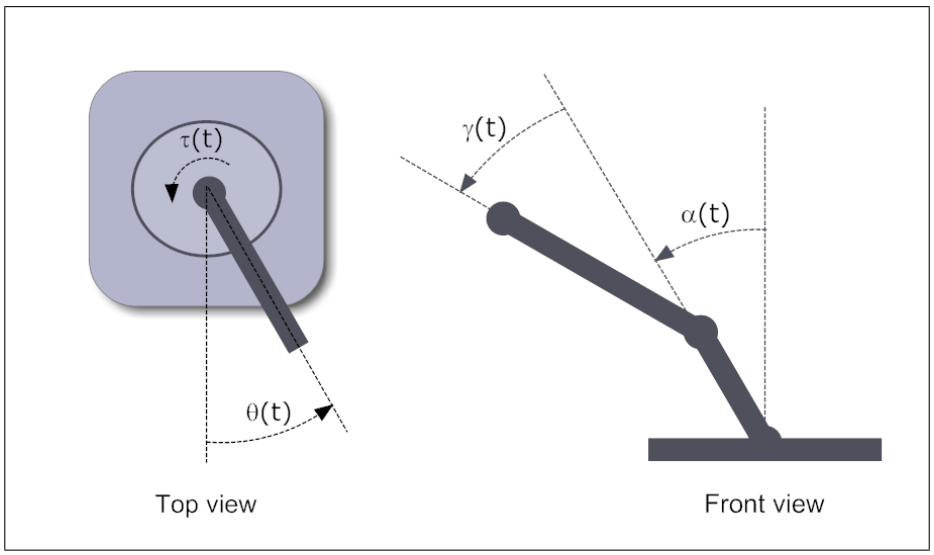

Figure 3: Significant variables.

First, the torque applied by the motor must be related with the angular positions. The three equations defining the non-linear dynamics of the mechanical part of the pendulum can be expressed as follows:

$$\tau(t) = [J_1 L_1^2 (m_2 + m_3)]\ddot{\theta}(t) - [L_1(m_2 l_2 + m_3 L_2)\cos\alpha(t)]\ddot{\alpha}(t) + [m_3 l_3 L_1 \cos\gamma(t)]\ddot{\gamma}(t) + \quad (1)$$
$$+b_1\dot{\theta}(t) + [L_1(m_2 l_2 + m_3 L_2)\sin\alpha(t)]\dot{\alpha}(t)^2 + [m_3 l_3 L_1 \sin\gamma(t)]\dot{\gamma}(t)^2$$
$$0 = -[L_1(m_2 l_2 + m_3 L_2)\cos\alpha(t)]\ddot{\theta}(t) + [J_2 + m_2 l_2^2 + m_3 L_2^2]\ddot{\alpha}(t) + \quad (2)$$
$$+[m_3 l_3 L_2 \cos(\gamma(t) - \alpha(t))]\ddot{\gamma}(t) + b_2\dot{\alpha}(t) -$$
$$-[m_3 l_3 L_2 \sin(\gamma(t) - \alpha(t))]\dot{\gamma}(t)^2 - [g(m_2 l_2 + m_3 L_2)\sin\alpha(t)]$$
$$0 = -[m_3 l_3 L_1 \cos\gamma(t)]\ddot{\theta}(t) + [m_3 l_3 L_2 \cos(\gamma(t) - \alpha(t)]\ddot{\alpha}(t) + [J_3 + m_3 l_3^2]\ddot{\gamma}(t) + \quad (3)$$
$$+[m_3 l_3 L_2 \sin(\gamma(t) - \alpha(t))]\dot{\alpha}(t)^2 + b_3\dot{\gamma}(t) - [g m_3 l_3 \sin\gamma(t)]$$

The parameters (whose values are provided by the manufacturer) in these equations are the lengths, masses, moments of inertia and friction coefficients of the elements in the pendulum.

- J_1: Moment of inertia around the center of rotation of the motor arm.
- J_2: Moment of inertia around the center of rotation of the first rod of the pendulum.
- J_3: Moment of inertia around the center of of the second rod of the pendulum.
- L_1: Length of the motor arm.
- L_2: Length of the first rod of the pendulum.
- l_2: Length between the centers of rotation and gravity of the first rod of the pendulum.
- l_3: Length between the centers of rotation and gravity of the second rod of the pendulum.
- m_2: Mass of the first rod of the pendulum.
- m_3: Mass of the second rod of the pendulum.
- b_1: Viscous friction in the joint of the motor arm.
- b_2: Viscous friction in the joint of the first rod of the pendulum.
- b_3: Viscous friction in the joint of the second rod of the pendulum.
- g: Acceleration of the gravity.

The non-linear model must be linearized to reach a MIMO linear model to be used in the design of the linear controller. The setting point for the linearization will be around $\alpha = 0$ and $\gamma = 0$, , corresponding this values to the upwards position, in which the pendulum is desired to remain stable. The signal derivatives must be zero at the settling point to keep the pendulum stable. In these conditions, the three linear (linearized) equations are:

$$\tau(t) = [J_1 L_1^2 (m_2 + m_3)]\ddot{\theta}(t) - [L_1(m_2 l_2 + m_3 L_2)\ddot{\alpha}(t) + [m_3 l_3 L_1]\ddot{\gamma}(t) + b_1\dot{\theta}(t) \quad (4)$$
$$0 = -[L_1(m_2 l_2 + m_3 L_2)]\ddot{\theta}(t) + [J_2 + m_2 l_2^2 + m_3 L_2^2]\ddot{\alpha}(t) + [m_3 l_3 L_2]\ddot{\gamma}(t) + \quad (5)$$
$$+b_2\dot{\alpha}(t) - [g(m_2 l_2 + m_3 L_2)\alpha(t)]$$
$$0 = -[m_3 l_3 L_1]\ddot{\theta}(t) + [m_3 l_3 L_2]\ddot{\alpha}(t) + [J_3 + m_3 l_3^2]\ddot{\gamma}(t) + b_3\dot{\gamma}(t) - [g m_3 l_3]\gamma(t)] \quad (6)$$

To implement the controller the input must be the voltage applied to the motor that moves the arm that carries the pendulum rods. The relationship between the voltage applied and the torque can be stated from the typical DC motor:

$$\tau(t) = \frac{\eta_g \eta_m K_g K_t}{R_m}(u(t) - K_g K_m \dot{\theta}(t)) \tag{7}$$

The mechanical parameters in this fourth equation are:

- η_g: Gearbox efficiency.
- η_m: Motor efficiency.
- K_g: Total gear ratio.
- K_t: Motor torque constant.
- K_m: Motor back-EMF constant.
- R_m: Motor armature resistance.

Solving the system of four equations, the linear continuous state-space model of the plant to be controlled can be obtained. The model must have the motor voltage as input signal and the three angular positions as output signals. The three angular velocities are not included as outputs because they are not going to be measured in the real plant. The development is omitted here for space reasons. As the goal is to control a real pendulum, the model has to be particularized with the real parameters (dimensions, masses, inertias, frictions, motor constants...). These parameters have been provided by the manufacturer. This information can be reached from the Quanser documentation [25].

As the control is going to be designed and implemented in discrete time, the continuous model must be discretized. The sample time is going to be 10 ms, small enough to control the plant and large enough to become unstable with a couple of sample time delays.

This model is the one to be used when designing, first, the controller in ideal conditions and, after that, the predictor to remove the influence of the loop delays. The behavior, with and without the delays, must be similar in both, simulated and real systems. The delay compensation is going to be different (because the delays are different) for the three controlled variables. The MIMO system can be divided into three SISO systems one for each of the output signals, (θ, α and γ as described before):

$$G_\theta(z) = \frac{\theta(s)}{U(s)} = \frac{0.0015763(z+0.9446)(z-0.9432)(z-0.8953)(z-1.061)(z-1.145)}{(z-1)(z-0.9716)(z-0.9077)(z-1.084)(z-1.18)(z-0.7665)} \tag{8}$$

$$G_\alpha(z) = \frac{\alpha(s)}{U(s)} = \frac{0.0018286(z+0.9477)(z-0.912)(z-1)(z-1.114)}{(z-0.7665)(z-0.9077)(z-0.9716)(z-1.084)(z-1.18)} \tag{9}$$

$$G_\gamma(z) = \frac{\gamma(s)}{U(s)} = \frac{-0.0019976(z+0.9538)(z-0.9968)(z-1)^2}{(z-0.7665)(z-0.9077)(z-0.9716)(z-1.084)(z-1.18)} \tag{10}$$

As can be seen these transfer functions describe the dynamical behaviour of unstable and non-minimum phase systems. The MIMO model will be used in the following section to design the controller in ideal conditions. The three SISO models will be used in section 4 to design the predictors for delay compensation purposes.

3 Control Structure in No Delay Conditions

To reach the desired behavior, a Linear-Quadratic Regulator (LQR) controller is going to be used control the plant *in absebtia* of delays. The controller must keep the angles of the two rods as close to zero as possible (unstable equilibrium upwards position), canceling the unavoidable disturbances. In addition the system must follow a certain reference for the motor shaft angle. The control structure is not robust enough to cope with delays, becoming unstable, even though they are very small. This ideal control will be appropriately modified to remove loop delays in the following section. In order to improve the steady-state error of the shaft position and the robustness of the controller, the six-state model is increased including an integration term. With this term the motor shaft can follow step references with zero error, even with the small dead zone present in the real plant. The integral of $\theta(t)$ will be computed in the controller from the measured angle. This augmented state is now:

$$\tilde{X} = \begin{pmatrix} \theta(t) & \alpha(t) & \gamma(t) & \dot{\theta}(t) & \dot{\alpha}(t) & \dot{\gamma}(t) & \int \theta(t)dt \end{pmatrix}^T \tag{11}$$

The six-state MIMO model obtained in the previous section is modified, including this new state:

$$\dot{X} = AX + Bu \quad \longrightarrow \quad \dot{\tilde{X}} = \begin{pmatrix} A & 0 \\ 0 & 0 \end{pmatrix} \tilde{X} + \begin{pmatrix} B \\ 0 \end{pmatrix} u \tag{12}$$

Using Matlab *lqr* command, the seven feedback control gains for the seven states from the augmented plant model are:

$$K = \begin{pmatrix} 1.2824 & -42.4077 & -101.7583 & 1.8735 & -11.8712 & -11.5716 & 0.3162 \end{pmatrix} \tag{13}$$

Although is not included in the model and, so, not considered when designing the controller, the real control action saturated ± 10 volts. This saturation has been included in the simulation model. However, in ideal conditions and when the delay is compensated, the control action always remains in this range and the saturation can be ignored.

This controller needs the seven states as inputs to generate the control action to be applied to the plant. In the real plant only the first three of them will be available, by means of sensors measuring the angular positions. There will not be sensors to measure the other states (angular velocities and integral error). These states are going to be computed in the control structure using a filtered discrete derivative and a discrete integrator. So, the controller becomes a three inputs-one output discrete system to be implemented in the control device.

As it has been described in the introduction, the three inputs of the controller are arriving through different paths and different delays are applied to them. To compensate the delays independently it will be useful to decompose the controller into three sub-controllers, each one of them concerned for one of the three measured angles. The transfer functions of these individual controllers are as follows:

$$C_\theta(z) = \frac{U_\theta(z)}{\theta(z)} = K(1) + K(4)Drv(z) + K(7)Int(z) = K(1) + K(4)\frac{50z - 50}{z - 0.6065} + K(7)\frac{0.01}{z - 1} \tag{14}$$

$$C_\alpha(z) = \frac{U_\alpha(z)}{\alpha(z)} = K(2) + K(5)Drv(z) = K(2) + K(5)\frac{50z - 50}{z - 0.6065} \tag{15}$$

$$C_\gamma(z) = \frac{U_\gamma(z)}{\gamma(z)} = K(3) + K(6)Drv(z) = K(3) + K(6)\frac{50z - 50}{z - 0.6065} \tag{16}$$

Using $Drv(z)$ and $Int(z)$ as discrete derivator and integrator respectively, all the states can be considered measurable. The control structure with these three sub-controllers is shown in figure 4.

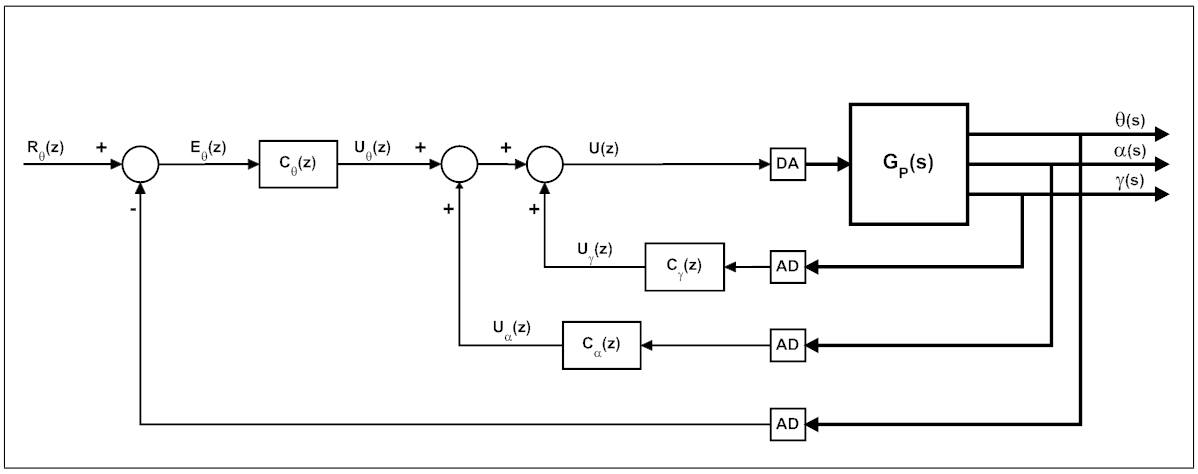

Figure 4: Control structure without delay compensation.

The inner loop tries to keep γ angle as close to zero as possible, avoiding disturbances. The middle loop does the same with α angle. The combination of these two loops keep the pendulum in the upwards position as desired. The outer loop tries to follow the desired reference with θ angle and drives the integral of the error to zero. As the three plant-to-control signals and the control-to-plant signal are separated, different delays will be applied to the four communication links to study its influence in the system performance. With the described control structure, three sub-control actions are generated and the addition of them is the control action to be sent and then applied to the plant.

Closing the loop with the model from the previous section and the gain matrix from the LQR, the simulated results are shown in figures 5 and 6. A ± 45 degrees step reference has been applied to be tracked by the shaft angle (θ) and a small random noise has been added to the measured pendulum angles (α and γ). No loop delay is present. Figure 5 depicts the output variables (θ, α and γ angles in degrees). As can be seen, the reference is followed properly (with zero steady-state error) by the shaft angle and the pendulum angles are kept close to zero, despite the noise and the changes in the main reference. Figure 6 shows the control actions of the three sub-controllers and the addition, which is the final control action to be applied to the plant. Note that α and γ control actions are clearly influenced by the noise, added to the measured angles.

4 Control Structure with Delay Compensation

Delays in the communication between controller and plant are a well-known source of instability. This is critical when controlling processes as unstable as the Furuta pendulum is. The influence of the delay in the control loop must be removed to assure that the system remains stable. Figure 7 shows the behavior of the three controlled angles when a single sample time delay is included in the control action (with ± 10 volts saturation in the control action as in the real plant). Another sample time delay in one of the feedback signals makes the system completely unstable. The sensitivity of the plant to loop delays makes this plant the ideal one for the work in this paper. The proposal is to modify the original delay-free controller to handle with delays even when they are different in the signals transmitted to and from the plant.

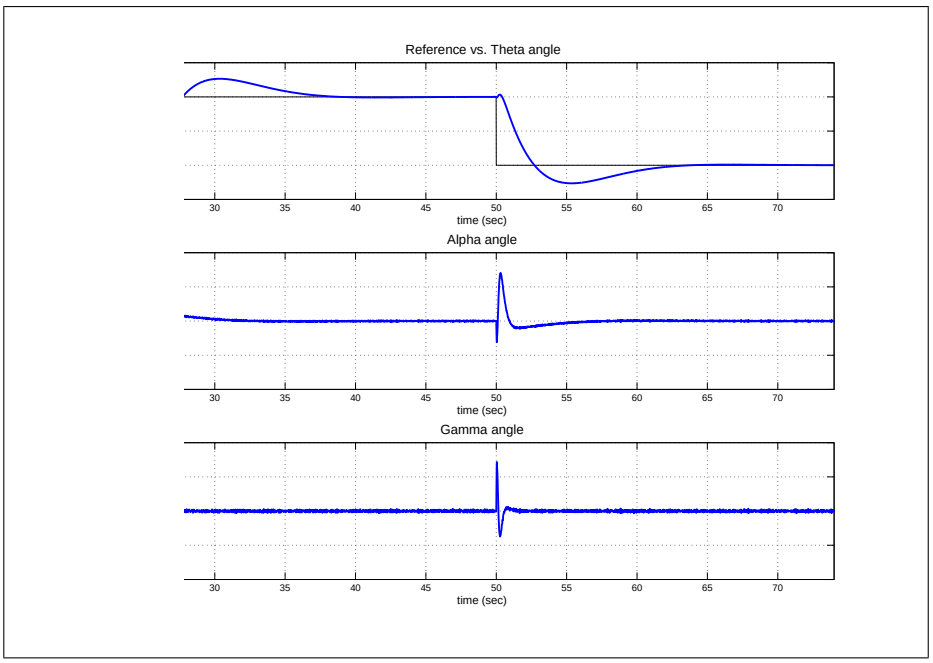

Figure 5: Theta, alpha and gamma angles: ideal conditions.

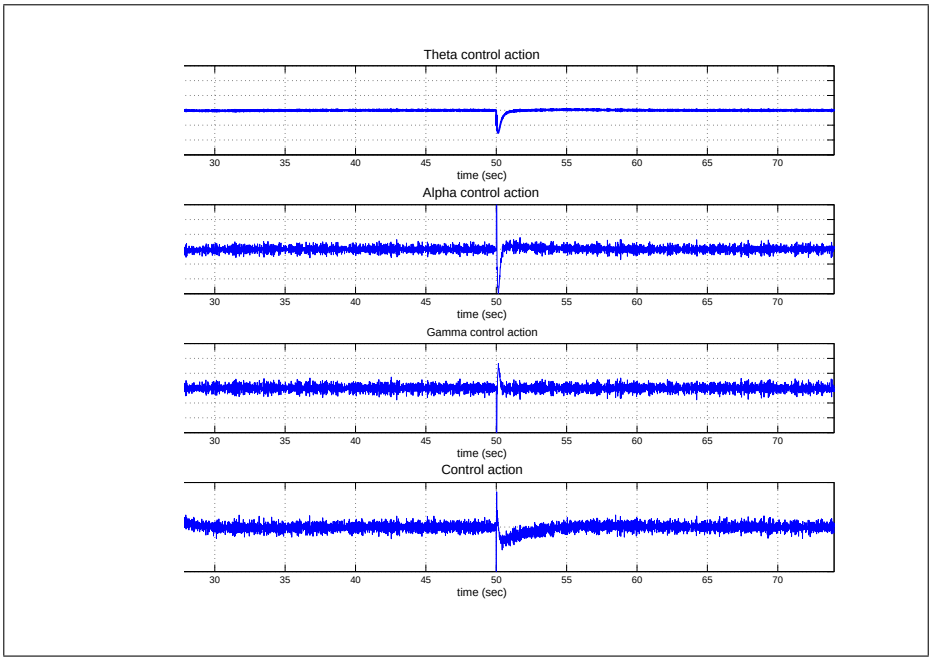

Figure 6: Control actions: ideal conditions.

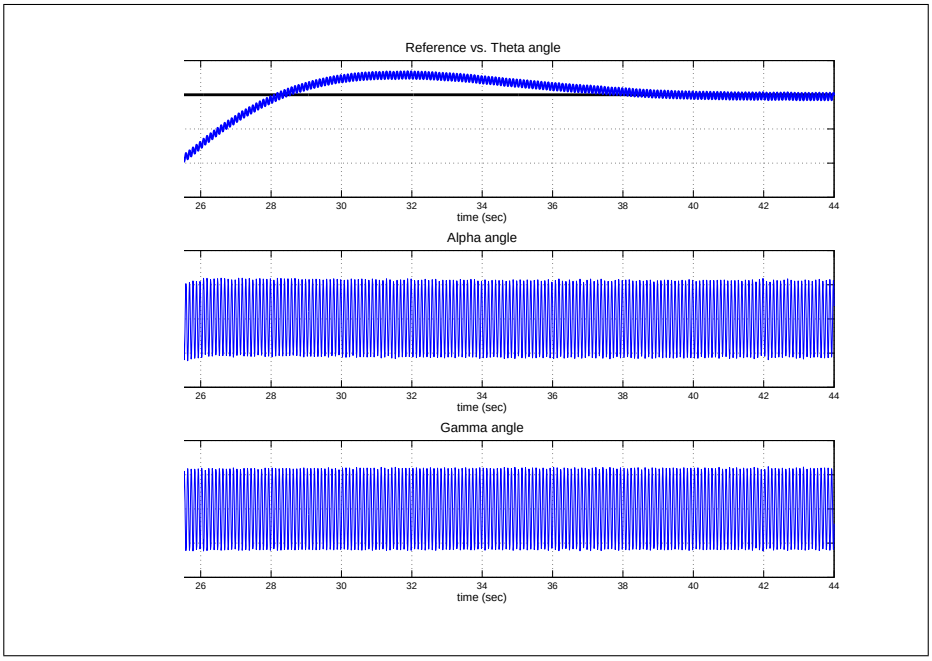

Figure 7: Theta, alpha and gamma angles: delayed.

Smith predictor has been traditionally used to overcome delays for stable plants without integral behavior. Several modifications ([26], [27], [28]) of the original idea have been proposed to be used for multivariable plants, with different input-output delays. The limitation is that they usually cannot be used with non-minimum phase, unstable plants with integral behavior. The classical Smith predictor has been modified ([29], [30], [31]) to deal with unstable plants. If all the controlled variables (i.e. all the loops in the control system) have the same delay, one of these modified predictors could be used.

The plant to be controlled in this paper is an unstable and non-minimum MIMO (one input and three outputs) plant but it can be easily decomposed into three SISO plants. In addition, in the scenario considered in this work, each one of the SISO plants is influenced by a different loop delay to be compensated. Parameter δ_u is the number of sample time delays for the control action (controller-to-plant signal). Parameters δ_θ, δ_α and δ_γ are the delays for the shaft and pendulum angles (plant-to-controller signals). The most general case is given when the four delays are different, as shown in figure 4, there are three loops in the systems. The loop delay (from the output to the input of the controller) for each one of the loops is given by the addition of the control action delay and the corresponding output signal delay. These are the delays to be compensated in each one of the sub-controller. Only constant and integer multiple of the sample time delays are considered in this work but the idea can be extended to fractional and variable delays.

In [32] and [33] a delay compensation is proposed, suitable to be used with unstable and non-minimum phase SISO plants. The predictor proposed and described in these references (Generalized predictor, GP, figure 8) is stable for unstable/stable, minimum/non-minimum plants.

The inputs of the GP are the plant input (control action) and output (controlled variable). The output of the GP is the predicted signal. Depending on the quality of the plant model used to design the predictor, the predicted signal will be equal to the controlled variable without the delay. It is the same behavior than with the classical Smith predictor but, in this case, it can be used with the transfer functions of the inverted pendulum. From the (unstable non-minimum phase) transfer function and the known loop delay the GP can be designed. This GP

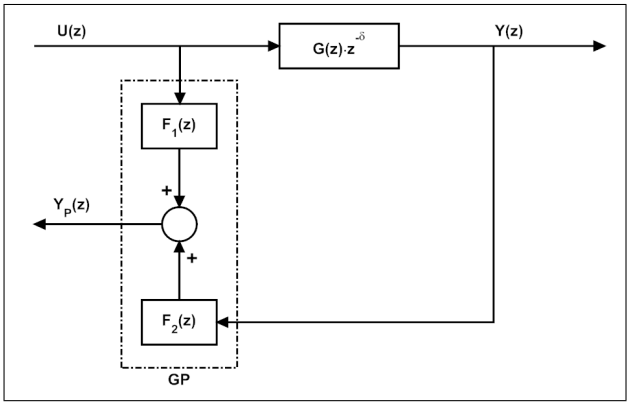

Figure 8: Generalized predictor.

will provide the information to be used by the controller, removing the influence of the delay in the feedback. The predicted (undelayed) output will be used instead of the measured one, by the same controller designed in ideal (no-delay) conditions. As usual, the system behavior depends on the uncertainty of the model and the presence of significant disturbances.

To generate this predicted signal, transfer functions $F_1(z)$ and $F_2(z)$ must be calculated. Being $G(z)$ the plant to be controlled, this transfer function can be divided in two parts:

$$G(z) = G_{MP}(z)G_{NMP}(z) \tag{17}$$

$G_{MP}(z)$ is a transfer function including al the poles (stable and unstable) and the minimum phase zeros. $G_{NMP}(z)$ is a polynomial including the non-minimum phase zeros. $G_{MP}(z)$ can be expressed as a polynomial quotient or as a minimum order state space model:

$$G_{MP}(z) = \frac{N_{MP}(z)}{D_{MP}(z)} = C_{MP}(zI - A_{MP})^{-1}B_{MP} \tag{18}$$

A new transfer function can be defined, including the delay (δ) in the minimum phase one:

$$G^*_{MP}(z) = \frac{N^*_{MP}(z)}{D_{MP}(z)} = C_{MP}(zI - A_{MP})^{-1}A^{\delta}_{MP}B_{MP} \tag{19}$$

From these definitions the two transfer functions of the GP can be calculated as follows:

$$F_1(z) = \left(C_{MP} \sum_{i=1}^{\delta} A^{\delta}_{MP} B_{MP} z^{-i} \right) G_{NMP}(z) \tag{20}$$

$$F_2(z) = \frac{N^*_{MP}(z)}{N_{MP}(z)} \tag{21}$$

The predicted output (i.e. the estimation of the plant output without delay) is calculated by the GP as follows:

$$Y_P(z) = U(z)F_1(z) + Y(z)F_2(z) \tag{22}$$

In the proposed scenario, three nested loops are present in the system. Three different loop delays are considered and had to be compensated. Three different predictors must be designed and included in the control structure. Figure 9 shows the control structure including the three

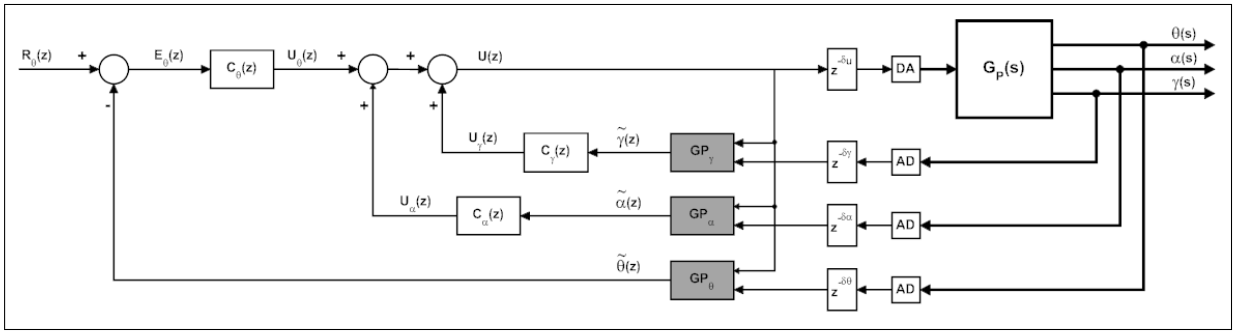

Figure 9: Control structure with delay compensation.

predictors to provide undelayed information for the controllers. Note that the controllers in this structure are the same used in figure 3, when no delay was present in the system.

To compare the information provided by the plant (measured) and by the GP's (predicted), figure 10 shows a detail of the measured angles (in radians) compared with the predicted ones. Measured (red) and predicted (blue) signals can be easily distinguished as the measured is delayed signal respect to the predicted one. Undelayed signals are not equal to the plant outputs due to the noised included in the simulation. It can be seen that the delay compensated by the predictors are different for θ, α and γ angles. In the simulation one sample period delay has been included in the control action, two sample delays in the γ angle, three sample delays in the α angle and four sample delays in the θ angle. So, the loop delay for the GP_γ predictor is $\delta_u + \delta_\alpha = 3$ and for GP_α $\delta_u + \delta_\theta = 4$. These delays can be seen in the time between predicted and measured signals.

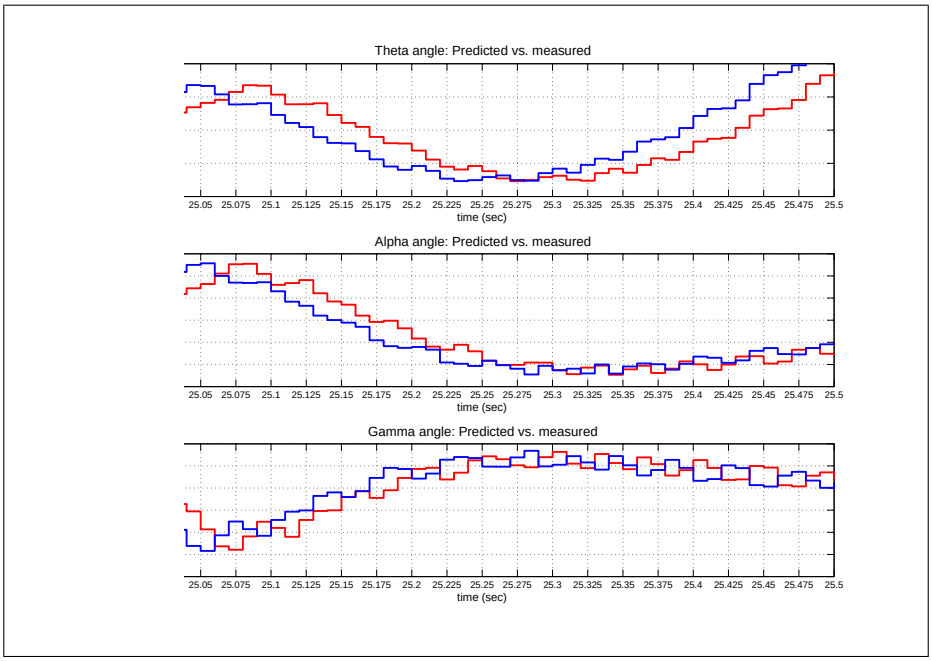

Figure 10: Measured and predicted angles.

The delay-free predicted signals are used as inputs for the three independent controllers to generate the control action to be applied to the plant. Figures 11 and 12, show simulation results in these conditions. Comparing these results with the ones in figures 5 and 6, it can be seen that the system recovers the ideal conditions behavior, even with different loop delays in the signals

between controller and plant. Real results are presented in the following section.

5 Experimental Results

The results presented in the previous section have been obtained from a simulation model. It is easier to see how the control structure works in simulated results without (unbounded) noise and/or uncertainty. Nevertheless, the work would remain uncompleted if not implemented over a real plant to reach real results.

The proposed structure has been implemented to control a real plant, the Quanser double rotary inverted pendulum (figure 2). The plant is endowed with a potentiometer to measure the shaft angle (θ) and a couple of incremental encoders to measure the angles of the two rods of the pendulum (α and γ). It has also a tachometer to measure the shaft angular velocity but it has not been used in the implementation.

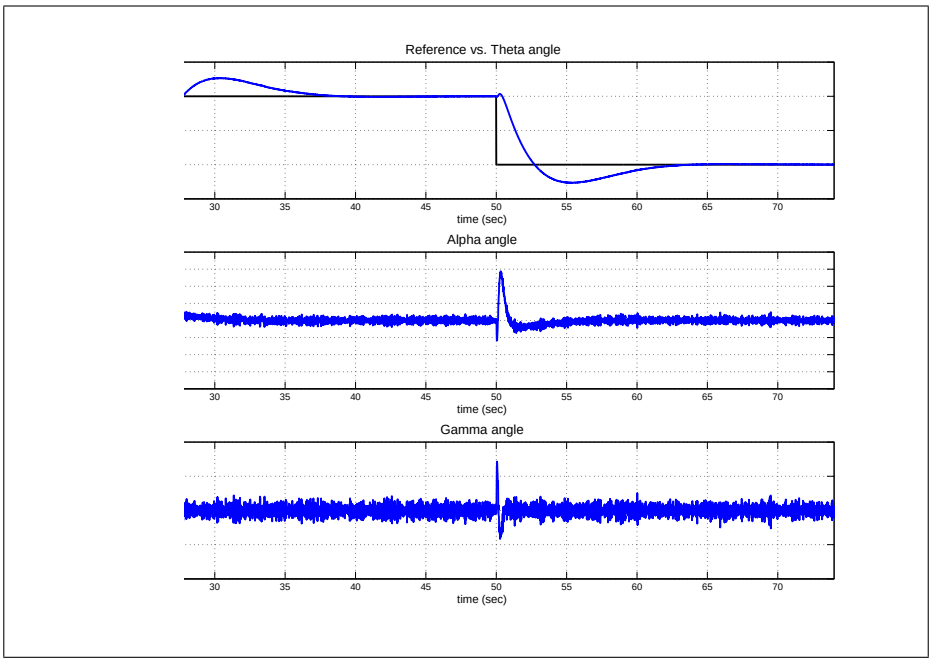

Figure 11: Measured angles: delayed+compensated.

The signal applied to the plant saturates at ± 10 volts but the action calculated by the controller is almost always inside this range. The aim is to consider a plant in which the different (and long enough) distance between each one the three sensors and the device implementing the control introduces non-negligible delays. However, with the dimensions of the used prototype, the multiple delays between controller and plant had to be simulated and included in the control structure.

Matlab/Simulink Real-Time Windows Target has been used to implement the control structure, using Quanser Q4 board for the A/D and D/A conversions. As noted in section 2, a sample time $T = 10ms$ has been used, being large enough for real-time requirements. With this sample time, two sample time delays in the inner loop of the proposed structure are enough to make the system unstable. Figure 13 shows the real measured angles when the delays appear, being the pendulum in its upwards stable position. The conventional control cannot bear this delay and the pendulum falls.

To overcome this delay influence, three GP's has been included in the control structure, as

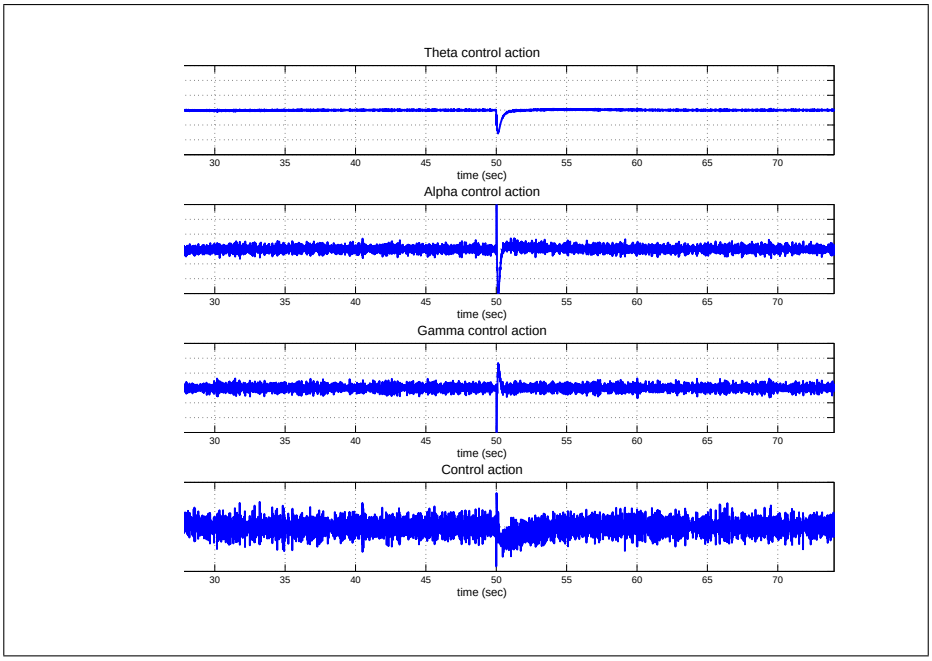

Figure 12: Control actions: delayed+compensated.

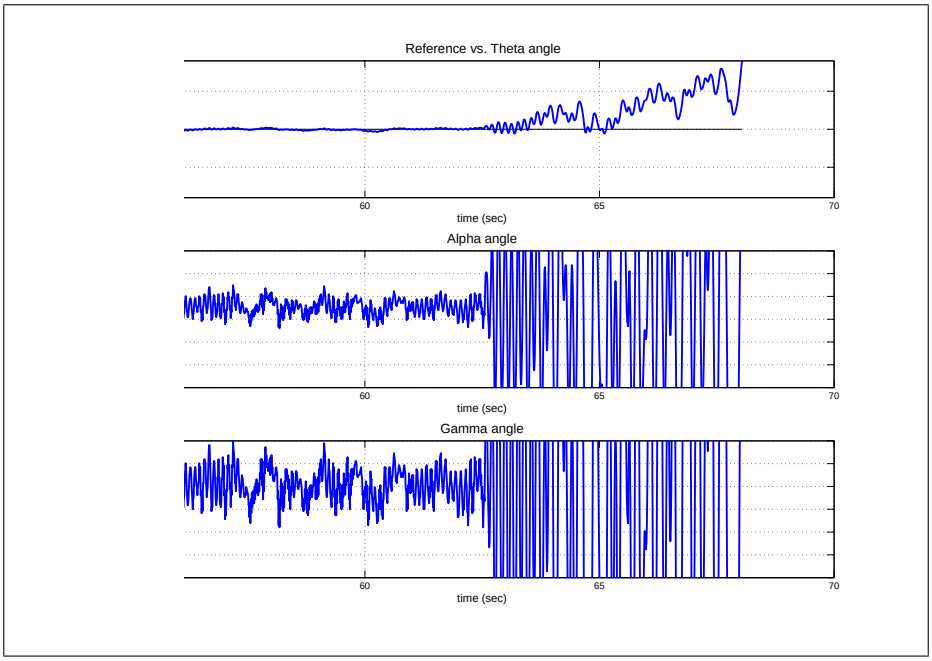

Figure 13: Real results: unstable behavior.

shown in figure 9.As in the simulation results, the GP's have been calculated to compensate delays $\delta_u = 1$, $\delta_\theta = 3$, $\delta_\alpha = 2$ and $\delta_\gamma = 1$. The predictor in the inner loop, GP_γ offers a prediction for the γ angle with a z^{-2} delay. In the middle loop, GP_α has been designed for a z^{-3} delay. Finally, in the outer loop GP_θ predicts the shaft angle removing a z^{-4} delay. With these delays in the loops, the control is absolutely unstable if the measured angles are used. Figure 14 shows the results in these conditions, using the predicted signals instead of the measured ones.

As can be seen, the shaft angle is following a ± 45 degrees reference and keeps the rods angles close to zero, to hold the pendulum in its upwards position, despite noises and disturbances. It is quite difficult to see differences between these results and the ones in ideal conditions (without delays) because the behavior depends deeply on the initial setup to put the plant in its working point. Figure 15 shows the behavior with some mechanical disturbances in the second rod angle. The control structure keeps the pendulum in its upwards position despite the multiple delays in the plant-control communications.

Due to the noise in the measured angles it is difficult to compare the real with the predicted signals. To see the operation of the predictors, both measured and predicted signals, have been low-pass filtered to remove the noise. These filtered signals are shown in figure 16 for θ, α and γ angles in radians. Although it is not easy to measure because the signals are slightly different, the time between predicted and measured signals is 40, 30 and 20 ms, respectively. These are the loop delays between the plant ant the three sub-controllers in the control structure. As the predictors remove the delay influence from the feedbacks, the system behaves as in ideal conditions.

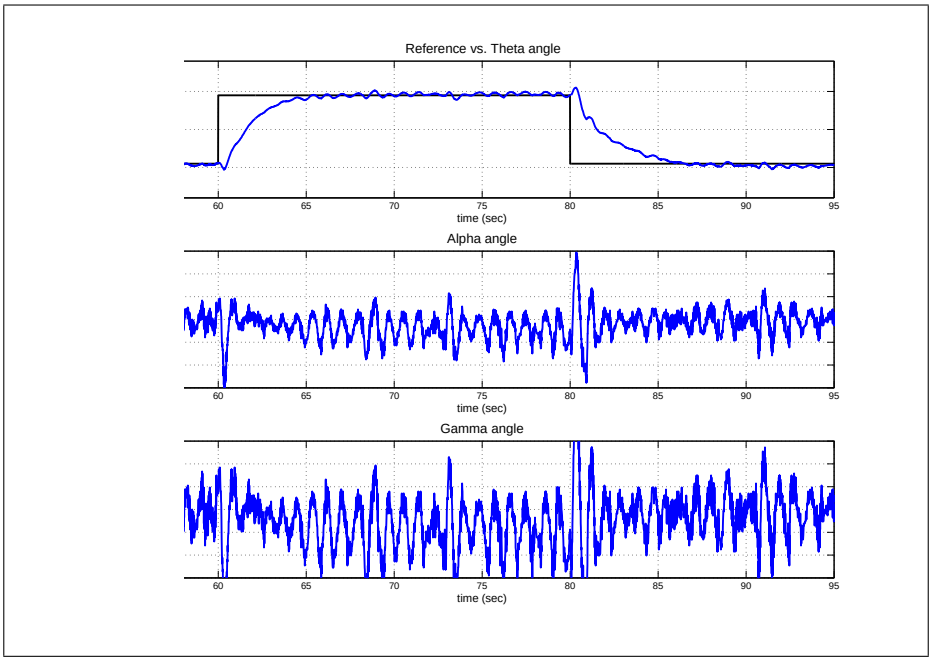

Figure 14: Real results: delayed+compensated.

6 Conclusions and Future Works

The aim of this work was to propose a multiloop control structure for a multivariable plant with different delays in each one of the signals between controller and plant. The double inverted rotary pendulum has been chosen for a practical implementation of the proposed control. This

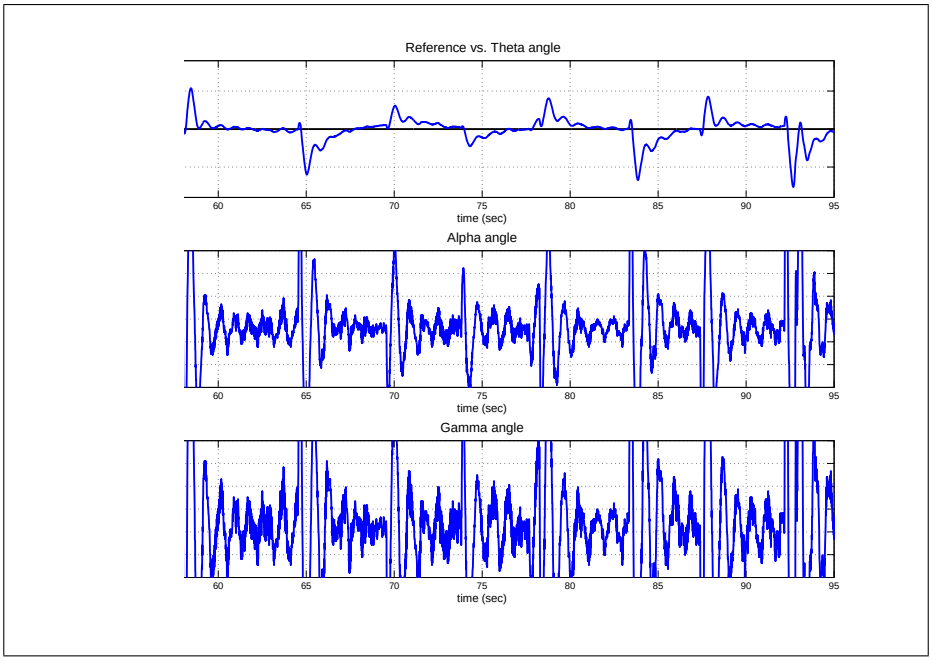

Figure 15: Real results: disturbances.

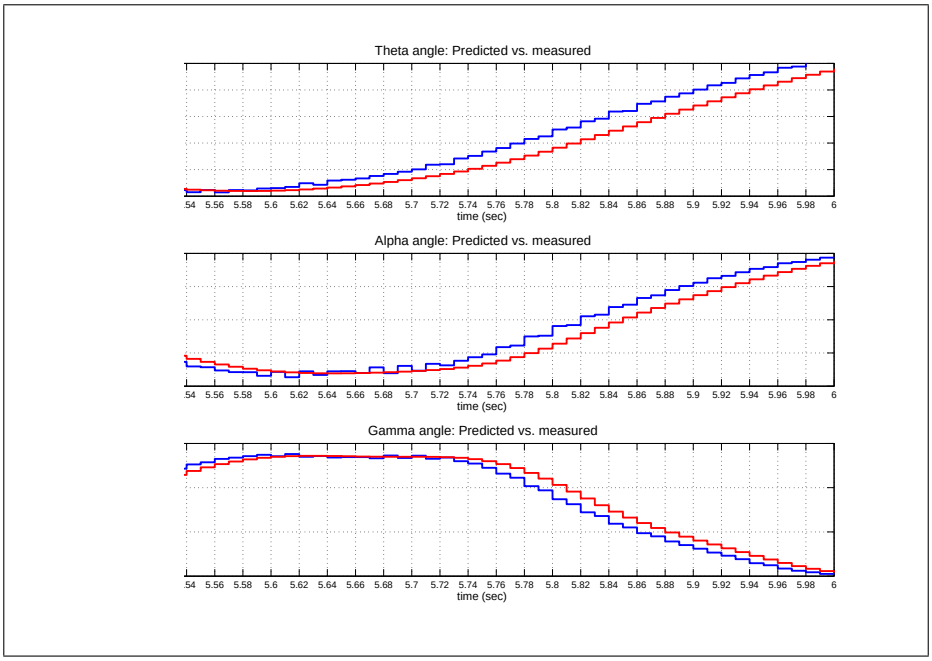

Figure 16: Real results: measured and predicted angles.

is a classic example of multivariable plant whose stability is seriously worsened even with small delays. There are four links in the system: one control-plant link (actuator) and three plant-control ones (sensors). The scenario assumes that this four links are a submitted to different communication delays which increases the difficulty to remove its influence on the stability.

A generalized predictor has been used to provide delay-free information for each one of the three loops in the control structure. Each one has been designed attending to each loop delay. Depending on the quality of the model used in the predictor, the system behaves as in ideal conditions, even with one different delay in each of the links. The validity of the proposed control structure has been shown by means of simulated results. The real implementation using the Quanser double rotary inverted pendulum shows how the proposed structure works when a certain degree of uncertainty, non-negligible noises and disturbances are present.

The delays in this work have been included in the control structure but they should be caused by the communication between sensors/actuators and the device in which the control algorithm is implemented. The goal is to close the loops through a shared communication medium (fieldbus, wireless network...), following different paths for each one of the links. This will cause different transport delays in each loop that may be solved with the proposed structure. In this more realistic implementation an additional problem will arise. The unavoidable lack of synchronization between the devices (sensors, controllers and actuators) will make the delay variable and, probably unknown. Some kind of delay identification must be performed or the control structure must be modified to be adaptive to compensate variable (maybe random) delays.

Another improvement of this proposal is to use a plant with more than one input. This will increase the number of communication links and the number of feedback loops. The 2D inverted pendulum is a good choice to be used in this improvement. This plant increases the degrees of freedom allowing movement in the XY plane. It has two inputs for a planar movement of the cart carrying the pendulum. Two measurements of the cart position must be used in the controller. The rod can bend in two directions giving two angular measurements. So, the plant offers a multivariable model (two inputs, four outputs) and, as is also quite sensitive to delays, is an appropriated plant to extend the work in this paper.

Acknowledgement

This work was supported by the Spanish Ministerio de Ciencia y Tecnologa Project DPI2009-14744-C03-03, by Generalitat Valenciana Project GV/2010/018, and by Universidad Polit´ecnica de Valencia Project PAID06-08.

Bibliography

[1] Y. Halevi, A. Ray, Integrated communication and control systems: Part I-Analysis, *Journal of Dynamic Systems, Measurement and Control*, vol. 110, pp. 367-373, 1988.

[2] A. Ray, Y. Halevi, Integrated communication and control systems: Part II-Design considerations, *Journal of Dynamic Systems, Measurement and Control*, vol. 110, pp. 374-381, 1988.

[3] L.G. Bushnell, Networks and control, *IEEE Control Systems Magazine*, vol. 21, no. 1, pp. 22-23, 2001.

[4] Y. Tipsuwan, M-Y. Chow, Control methodologies in networked control systems, *Control Engineering Practice*, vol. 11, no. 10, pp. 1099-1111, 2001.

[5] P.F. Hokayem, C.T. Abdallah, Inherent issues in networked control systems: A survey, *Proceedings of the 23rd American Control Conference, Boston (USA)*, vol.6, pp. 4897-4902, 2004.

[6] T.C. Yang, Networked control systems: A brief survey, *IEE Proceedings on Control Theory and Applications*, vol. 153, no. 4, pp. 403-412, 2006.

[7] V. Casanova, J. Salt, Multirate control implementation for an integrated communication and control system, *Control Engineering Practice*, vol. 11, no. 11, pp. 1335-1348, 2003.

[8] J. Nilsson, Real-time control systems with delays. *PhD thesis*, Lund Institute of Technology, Lund, Sweden, 1998.

[9] J. Nilsson, B. Bernhardsson, B. Wittenmark, Stochastic analysis and control of real-time systems with random time delays, *Automatica*, vol. 34, no. 1, pp. 57-64, 1998.

[10] F.L. Lian, J.R. Moyne, D.M. Tilbury, Performance evaluation of control networks: Ethernet, ControlNet, and DeviceNet, *IEEE Control Systems Magazine*, vol. 21, pp. 66-83, 2001.

[11] F.L. Lian, J.R. Moyne, D.M. Tilbury, Network design consideration for distributed control systems, *IEEE Transactions on Control Systems Technology*, vol. 10, pp. 297-307, 2002.

[12] F.L. Lian, J.R. Moyne, D.M. Tilbury, Modelling and optimal controller design of networked control systems with multiple delays, *International Journal of Control*, vol. 76, no. 6, pp. 591-606, 2003.

[13] H. Gaoa, T. Chenb, J. Lamc, A new delay system approach to network-based control, *Automatica*, vol. 44, no. 1, pp. 39-52, 2008.

[14] A.V. Savkin, Analysis and synthesis of networked control systems: Topological entropy, observability, robustness and optimal control, *Automatica*, vol. 42, no. 1, pp. 51-62, 2006.

[15] D.S. Kim et al, Maximum allowable delay bounds of networked control systems, *Control Engineering Practice*, vol.11, no. 11, pp.1301-1313, 2003.

[16] H. Fanga, H. Yeb, M. Zhong, Fault diagnosis of networked control systems, *Annual Reviews in Control*, vol.31, no. 1, pp. 55-68, 2007.

[17] O.E. Agamennoni, A.C. Desages, J.A. Romagnoli, A multivariable delay compensator scheme, *Chemical Engineering Science*, vol. 47, no. 5, pp. 1173-1185, 1992.

[18] B.A. Ogunnaike, W.H. Ray, Multivariable controller design for linear systems having multiple time delays, *AIChE Journal*, vol. 25, no. 6, pp. 1043-1057, 1979.

[19] K. Watanabe, M. Ito, An observer for linear feedback control laws of multivariable systems with multiple delays in controls and outputs, *Systems & Control Letters*, vol. 1, no. 1, pp. 54-59, 1981.

[20] S. Mori, H. Nishihara, K. Furuta, Control of unstable mechanical system: Control of pendulum, *International Journal of Control*, vol. 23 no. 5, pp. 673-692, 1976.

[21] K. Furuta, M. Yamakita, S. Kobayashi, M. Nishimura, A new inverted pendulum apparatus for education, *IFAC Advances in Control Education Conference*, pp. 191-196, 1991.

[22] S. Yurkovich, M. Widjaja, Fuzzy controller synthesis for an inverted pendulum, *Control Engineering Practice*, vol. 4, no. 4, pp. 455-469, 1996.

[23] W. Zhong, H. Röck, Energy and passivity based control of the double inverted pendulum on cart, *IEEE Conference on Control Applications*, pp. 896-901, 2001.

[24] J. Driver, D. Thorpe, Design, build and control of a single/double rotational inverted pendulum, *The University of Adelaide*, School of Mechanical Engineering, Australia, 2004.

[25] Quanser Consulting Inc, Rotary experiment #8: Double Inverted Pendulum (DBPEN), 2006.

[26] G. Alevisakis, D.E. Seborg, An extension of the Smith predictor method to multivariable linear systems containing time delays, *International Journal of Control*, vol. 17, no. 3, pp. 541- 551, 1973.

[27] K. Watanabe, Y. Ishiyama, M. Ito, Modified Smith predictor control for multivariable systems with delays and unmeasurable step disturbances, *International Journal of Control*, vol. 37, no. 5, pp. 959-973, 1983.

[28] J.M. Maciejowski, Robustness of multivariable Smith predictors, *Journal of Process Control*, vol. 4, no. 1, pp. 29-32, 1994.

[29] A.M. De Paor, A modified Smith predictor and controller for unstable processes with time delay, *International Journal of Control*, vol. 41, no. 4, pp. 1025-1036, 1985.

[30] H.J. Kwak, S.W. Sung, I.B. Lee, A modified Smith predictor with a new structure for unstable processes, *Industrial & Engineering Chemistry Research*, vol. 38, no. 2, pp. 405-411, 1999.

[31] T. Liu, Y.Z. Cai, D.Y. Gu, W.D. Zhang, New modified Smith predictor scheme for integrating and unstable processes with time delay, *IEE Proceedings on Control Theory and Applications*, vol. 152, no. 2, pp. 238-246, 2005.

[32] P. García, P. Albertos, T. Hägglund, Control of unstable non-minimum-phase delayed systems, *Journal of Process Control*, vol. 16, no. 10, pp. 1099-1111, 2006

[33] P. Albertos, P. García, Robust control design for long time-delay systems, *Journal of Process Control*, vol. 19, no. 10, pp. 1640-1648, 2009.

Int. J. of Computers, Communications & Control, ISSN 1841-9836, E-ISSN 1841-9844
Vol. VII (2012), No. 1 (March), pp. 39-52

A Data Fusion Methodology for Wireless Sensor Systems

J.I.-Z. Chen, Y.-N. Chung

Joy Iong-Zong Chen
Department of Electrical Engineering
Dayeh University
Changhua 51505,Taiwan (ROC)
E-mail: jchen@mail.dyu.edu.tw

Yi-Nung Chung
Department of Electrical Engineering
National Chunghua University of Education
Changhua 51505, Taiwan (ROC)
E-mail: yichung@ncue.dyu.edu.tw

Abstract: An efficient DFA (data fusion algorithm) plays an important role in tracking for moving objects over WSS (wireless sensor system) deployments in order to track the objects accurately. Accuracy in object tracking is mainly dominated by the prediction for those moving targets by filtering and refining the results from wireless mobile sensors deployed in WSS environment. A DFA based on CHHN (competitive Hopfield neural network) technique for obtaining the relationship between measurements results from wireless mobile sensors and estimation of existing tracks over WSS (wireless sensor system) is proposed in this paper. Embedded within the CHNN is also a competitive learning mechanism which creatively removes the dilemma of occasional irrational solutions in traditional HNN (Hopfield neural networks). In this research, except the proposed approach is established with CHNN, the methodology of data fusion over WSS is guaranteed to converge into a stable state when performing a data association. In words, the CHNN-based DFA is combined with wireless mobile sensors in a WSS environment to demonstrate the target tracking capabilities. Computer simulation results illustrate that the new methodology of data fusion based on CHNN is not only successfully able to solve the data association problems addressed over WSS environments, but the specified simulated targets can also be tracked without large scale missing.
Keywords: CHNN (competitive Hopfield neural network), DFA (data fusion algorithm), mobile sensors, WSN (wireless sensor network).

1 Introduction

Mobile-sensor data association tracking is generally an essential technique for WSS (wireless sensor system) surveillance systems employing one or more sensors, which may be deployed as stationary or maneuverable, together with computer subsystems. The main objective of a data association tracking algorithm is to partition sensor data into sets of observations produced by the same target; the other object to avoid the coupling effect existing between the mobile sensors for the same target. Once tracks are formed and confirmed, it not merely the number of mobile sensors that can be estimated and quantified; rather, the information gathered by the tracking algorithm can also be associated and fused. It is known that the role of multi-sensor data association in WSS environments involves acquiring, processing and combining data [1, 2] coming from different sources, including sensors and databases, into a more precise set of data. Thus,

data association consists of the three aforementioned steps. A DFA (data fusion algorithm) is the most important technique for maintaining tracking procedures. Mobile-sensor tracking with a DFA is a prerequisite step for mobile-sensor surveillance systems in WSS deployments. Once tracks are formed and confirmed, the number of targets can be estimated and information, such as the target position and velocity, computed for each track [3]. In the literature, several DFAs for MTT (multiple target tracking) have been proposed and discussed. It is well known that the JPDA (joint probabilistic data association) DFA technique, discussed in References [4–8] focusing mainly on MTT deployment, is appropriate for a high false-target density environment. However, these techniques for solving MTT problems may cause some unreliability (latency) because in a nearest-neighbor or all-neighbors-based environment, the relationships between sensor measurements and existing target tracks are usually considered independently [9]. Thus, currently a traditional HNN (Hopfield neural network), which incorporates weighted objective costs and constraints into an overall energy function, is employed to combine with the neural network approaches for achieving good tracking results. [10] Then, through minimizing the overall energy function, superior performance results can be obtained. [11] The CHNN (competitive Hopfield neural network) algorithm has been applied in image processing. [12] Moreover, Soujeri and Bilgekul [13] adopted a conventional HNN to solve the problems of multiuser reception for asynchronous MC-CDMA (multi-carrier coded-division multiple-access) systems in multipath fading channels. Since this approach is defective in that the weighting values are very difficult to properly determine, frequently the solution obtains an irrational result, as reported by Zhou. [14] Thereafter, conventional HNN schemes for tracking maneuvering or non-maneuvering targets with mobile sensors over WSS deployments are very sparse. However, Wang et al. [15], recently, combined an HNN with a genetic algorithm, designated as HNN-GA, for proposing a mobile agent-based strategy utilizing a low network load and cooperation of mobile agents, to dynamically optimize the combination of nodes and deploy tasks among nodes. Based on HNN, the selection method investigated by Liang et al. [16], in which the sensor node having the lowest cost and satisfying the distance requirement of a MIMO (multi-input multi-output) system, is selected to function as the best transmitting and receiving antenna in WSN environments. By extending the idea expressed in [17], Wang et al. [18] proposed a new dynamic sensor node selection strategy to implement global searching to reduce the search space of a GA and ensure the validity of each chromosome in WSN applications. Deploying with mobile sensors in WSS environment is increasingly becoming integral to targets tracking, mainly due to its convenient deployment, small size, real-time characteristic, and flexibility to support integrated applications. The technique of WSS is applied to the traffic monitoring and control in [19] by the authors Semertzidis et al. The information is fused and used to provide real-time analytical. However, it is necessary for the important issue of energy supply to the operation of sensor nodes over WSS. Yen et al. in [20] proposed CLD (controlled layer deployment) protocol to guarantee coverage and energy efficiency for sensor nodes deployed in a WSS. In order to promote the operation efficiency of the data fusion for the sensor nodes deployed in WSS environment. Multi-layer clustering routing algorithm is presented by Liu et al. in [21] where the WSS techniques is developed to track the moving vehicles, and the new scheme efficiently overcomes the hot spot problem in WSS environment. Furthermore, the authors, Shi et al., propose a structure that represents the sensor communications with the fusion centre, obtain the optimal estimation algorithm at the fusion centre, and provide a theoretical closed-form for the steady-state error covariance matrix which has low energy consumption and guarantees a desired level of estimation quality at the fusion centre. [22] However, to apply the advantages of the HNN technique in this research the improved CHNN method, which can by artfully arranging the updating function and the cost measurement properly eliminate the aforementioned dilemma, is adopted for solving target tracking with mobile sensors in WSS deployments. The CHNN is an improved HNN wherein a

cooperative decision is made on the basis of the simultaneous input of a community of neurons. Each neuron receives information from other neurons and also conveys information to others [11, 14]. With this collective information, each neuron moves to a stable stage with the lowest value of a predefined energy function. With such a result, the operation of association between mobile sensor measurements and existing tracks can be obtained under global optimal consideration, which in turn can increase the accuracy of mobile sensor tracking systems. Furthermore, due to the embedded competitive updating scheme, the CHNN concept has the capability of removing the burden of weight setting. It has also been demonstrated that the network is guaranteed to converge into a stable and rational stage during evolution. [13] Thus, the dilemma of lapsing into irrational solutions such as those in traditional HNNs can be eliminated.

To the best of the author knowledge, the proposed mean is an innovative idea for discussion when exploring the field of WSNs. The aim of this study is to enhance system performance by means of a DFA for WSS environments, the focus being on a CHNN to obtain global matching between mobile sensor measurements and existing tracks. As illustrated in Fig.1, moving targets tracked by sensor nodes are considered for improving the tracking deployment for mobile-sensor data association with assumed targets. Moreover, in an environment where the dense targets are spread out randomly, some targets can be very close to each other. The measurements produced by these close targets can confuse the data association computation algorithm and result in inaccurate relations hips. Consequently, the approach for solving the data association problem should be considered globally. The reminder of this report is organized as follows. In Section II the problem formulation includes the gating technique, and the basic concept of the HNN is illustrated; developing a DFA based on the CHNN scheme is presented in Section III; the maneuvering compensator algorithm is explicated in Section IV; Section V reports the simulation results for the proposed algorithm; and Section VI both concludes the report and offers recommendations for further research.

2 Problem Formulation

In this sub-section to obtain the information from the mobile sensor belonging to all of the sensors, without loss of generality, the type of sensing methods is considered to be completely established. It is also assumed that the synchronization between various sensor levels under circumstances of multiple levels of data association is finished. Several synchronization methods can be adopted for this procedure [18]. Moreover, since this study focuses on data association for tracking targets within WSN environments, several issues are reasonably ignored, e.g., the impact of sensing accuracy on the sensing range and node densities of a sensor, as well as the data fusion overhead and sensing lifetime of a network. Thus, a dynamic model with a discrete model set for a multi-sensor tracking algorithm for a mobile sensor can be formulated.

2.1 Gating Technique

According to the mobile sensor tracking situation, the model of a moving target can be defined in variable state equations, given as [23]

$$X(k+1) = F(k)X(k) + G(k)W(k) + U(k) \tag{1}$$

and

$$Y(k) = H(k)X(k) + V(k) \tag{2}$$

where $X(k)$ denotes the state vector of the target, $Y(k)$, the measurement vector of the target, $F(k)$ and $G(k)$, the transition matrix and the noise-gain matrix of the target, respectively; $W(k)$,

is the system noise associated with the target, assumed to be normally distributed with a zero mean and variance $Q(k)$. Moreover, $U(k)$ represents the forced input; $V(k)$, the measurement error associated with the target, assumed to be normally distributed with zero mean and variance, $R(k)$, uncorrelated with $W(k)$; and $H(k)$ the measurement matrix of the target. The initial state of the target is considered to be a Gaussian pdf (probability density function) with a known mean vector, $\widehat{X}(0 \mid 0)$, and a covariance matrix, $P(0 \mid 0)$. A large number of close measurements observed from the mobile sensors in an actual tracking situation are provided to determine the trajectory estimates for any target that might be presented. It is difficult to precisely determine which target corresponds to which in such closely spaced measurements. i.e., the data association problem in mobile sensor tracking or associating the measurement vector $Y(k)$ to the existing track model for each step, k, must first be solved. Additionally, consider an environment wherein a dense target is completely deployed. Here, determining the gating size is the obligatory first step in solving the problem of associating observations with tracks. Additional logic is required when an observation or multiple observations fall within the gates of multiple target tracks or a single track. A typical situation for a gate diagram consisting of three target tracks $T1$, $T2$ and $T3$ is illustrated in Fig. 2. In this figure there are three targets, but eight measurements are assumed to have been obtained. First, the gating technique is applied to eliminate the less probable measurements such as M_6 to M_8. A CHNN algorithm is applied to complete the associative relationship between the remaining measurements and the tracked targets. Then, the association of the measurements of the remaining $M_1, M_2, \cdots, M_5$, with the respective targets should be determined.

2.2 Two-dimensional Binary Neural Network-HNN

Consider that a network consists of $n \times m$ mutually interconnected neurons. In this research, the HNN specifically adopted to search for the algorithm belongs to a two-dimensional binary neural network wherein the total input-to-neuron, indexed by (g, i) , i.e., $\Lambda_{g,i}$, at time k, can be calculated as [15]

$$\Lambda_{g,i} = \sum_{h=1}^{n} \sum_{j=1}^{m} T_{g,j;h,j} \cdot V_{h,j} + I_{g,i} \tag{3}$$

where $I_{g,i}$ denotes a bias input, $T_{g,j;h,j}$, the interconnection intensity between neuron (g, i) and neuron (h, j); $V_{g,i}$, a binary state of the (g, i)th neuron. Moreover, the state of $V_{g,i}$ is determined by the signum function

$$V_{g,i} = \begin{cases} 1, & \Lambda > 0 \\ 0, & otherwise \end{cases} \tag{4}$$

Thus, the expression in 1 explicitly describing the HNN dynamics operating in this network receives weighted inputs $T_{g,j;h,j} \cdot V_{h,j}$ from each neuron, e.g., (h, j), and a bias input (g, i) from outside. Therefore, one neuron at a time is updated while the rest remain stationary after a random initialization of each neuron with binary values. This method for neuron updating has been shown to decrease the Lyapunov function of a two-dimensional Hopfield network given by

$$E = -\sum_{g=1}^{n} \sum_{h=1}^{n} \sum_{i=1}^{m} \sum_{j=1}^{m} T_{g,j;h,j} V_{g,i} V_{h,j} - 2 \sum_{g=1}^{n} \sum_{i=1}^{m} I_{g,i} V_{g,i} \tag{5}$$

where $V_{g,i}$ has the constraint defined in (4).

3 Joint Data Association in a Competitive Neural Network

In this subsection the CHNN algorithm is applied to the potential-target measurements to formulate a solution for data association problems. The CHNN concept is applied to the data association technique presented here. By means of a network for joint data association, the state of $V_{g,i}$ indicates an associative status between the $g-th$ mobile sensor measurement and the $i-th$ target, expressed as

$$V_{g,i} = \begin{cases} 0, & \text{data noassociated} \\ 1, & \text{data associated} \end{cases} \tag{6}$$

Then the objective function used for obtaining measurements and mobile sensor targets association with the best decision is given by

$$E = \alpha \sum_{g=1}^{n}\sum_{i=1}^{m} d_{g,i}V_{g,i} + \beta \sum_{g=1}^{n}\sum_{h=1}^{n}\sum_{i=1}^{m}\sum_{j=1}^{m} V_{g,i}V_{h,j}\delta_{g,h} + \gamma \sum_{i=1}^{m}\left(\sum_{g=1}^{n} V_{g,i} - 1\right)^2 \tag{7}$$

where $d_{g,i}$ is the distance between the $i-th$ true target and the $g-th$ measurement. The factor $d_{g,i}$ here needs a special design for achieving the task of data association as described subsequently. In Eq. 7 the first term is the sum of the distances between the associated measurements and the mobile sensor targets. A situation wherein none of the newly obtained measurements is appropriate for certain specific targets in the processing of data association is unavoidably vexing. Concurrently, the previous target information should be kept and chosen as the next item of information in such cases. To achieve this end, the m target data is included as part of the measurement. Assume that there are m targets and $n-m$ newly obtained mobile sensor measurements and that the m targets are arranged in front of the $n-m$ measurements to obtain a total of m measurements. Where $g=i$, the distance $d_{g,i}$ is defined as $d_{g,i}=r$ where r is the radius of the gate, according to the aforementioned arrangements. Hence, if measurements are distributed inside the gate, then one should be chosen. However, if no measurements are there, then the target itself should be chosen. Another constraint is that if $g \neq i$ and $1 \leq g \leq m$, then $d_{g,i}=\infty$. This constraint prevents one target from choosing another as its measurement. Thus, after the aforementioned calculations, the distance $d_{g,i}$ can be determined as

$$d_{g,i} = \begin{cases} r, & g = i \\ \infty, & g \neq i \text{and} 1 \leq g \leq m \\ \sqrt{[\tau^T(k)S(k)^{-1}\tau(k)]}, & g \neq i \text{and} g > m \end{cases} \tag{8}$$

where $S(k)$ is the covariance matrix of the innovation $\tau(k)$, the superscript denotes the transportation of a matrix, and $\tau(k) = Y(k) - H\widehat{X}\,(k \mid k-1)$. Moreover, in 5 the second term attempts to guarantee that each measurement can be associated with only one target. Moreover, the third term forces the condition wherein each target has one, and only one, associated measurement and the three terms α, β, and γ specify important constant factors. Since these factors are highly dependent on the number of targets, the target-measurement distances and the radius of the gate, it is very difficult to determine the appropriate values for them. For this reason, irrational solutions have periodically been reported for the use of traditional Hopfield approaches [10, 14] when the weighting factors have not been properly determined. However, to reduce the difficulty in determining the values of the weighting factors, a CWTA (competitive winner-take-all) updating is proposed and adopted as

$$V_{g,i} = \begin{cases} 1, & \Lambda_{g,i} = \max\{U_{1,i} \cdots\cdots U_{n,i}\} \\ 0, & otherwise \end{cases} \tag{9}$$

With this modified updating rule, the rigid constraint that each target should be associated with one and only one measurement is automatically embedded inside the network evolution results. As such, the third term can naturally be removed from the objective function. Thus, the objective function is simplified and obtained as

$$E = \alpha \sum_{g=1}^{n} \sum_{i=1}^{m} d_{g,i} V_{g,i} + \beta \sum_{g=1}^{n} \sum_{h=1}^{n} \sum_{i=1}^{m} \sum_{j=1}^{m} V_{g,i} V_{h,j} \delta_{g,h} \tag{10}$$

To avoid being bounded by irrational solutions, a reasonable method for the network described below is adopted. *I.e.*, once the CWTA updating has been applied, it is noteworthy that if α is set as a unit, β can be easily considered greater than the radius of gate r, a relatively constant value. By comparing the resultant objective function with the Lyapunov function of the two-dimensional Hopfield network in 5, the parameters of the interconnection intensity and the bias input can be obtained as

$$I_{g,i} = -\frac{\alpha \cdot d_{g,i}}{2} \tag{11}$$

and

$$T_{g,i;h,j} = -\beta \delta_{g,h} \tag{12}$$

respectively. It can be clearly to seen that the CHNN is not fully interconnected from, 11 and 12. However, the CHNN is locally connected instead of the neurons in the same column. Hence, the total input to neuron (g, i) can be applied to these two equations and obtained as

$$\Lambda_{g,i} = -\beta \sum_{j=1}^{m} V_{g,j} - \frac{\alpha}{2} d_{g,j} \tag{13}$$

The proposed algorithm was found to be convergent during network evolutions.

4 Estimation of Maneuvering Targets with an Adaptive Filter

In real-world applications, either maneuvering or non-maneuvering targets must be tracked simultaneously with mobile sensor data association tracking techniques. On the basis of the concept of wireless sensor network equipped with different sensing hardware for distinctly specified applications, a viable method for human interfacing with the environment can be provided. Therefore, if target maneuvers occur, then the maneuver-detection and acceleration-estimation algorithm should be applied to modify the parameters of the tracking filter. The developed methods allow the maneuvers to be tracked without diverging or severely distorting the estimate. To complete such an adaptive procedure, the Kalman filter equations are modified in this subsection. Specifically, certain parameters must be changed for fitting the data association and matching the CHNN algorithm. Now, the measurement innovation, $\rho(k)$, and the innovative covariance matrix, $S(k)$, of the Kalman filter should be modified as

$$\rho(k) = Y(k) - H(k)\widehat{X}\left(k \mid k-1\right) \tag{14}$$

and

$$S(k) = \delta(k) - R(k) \tag{15}$$

, respectively, where $\delta(k) = H(k)P\left(k \mid k-1\right)H^T(k)$. Furthermore, two hypotheses, H_0 and H_1, corresponding to the assumptions that the system behavior is normal and the target is moving

with the maneuvers, are assumed as generating events. The detection criterion can be defined as

$$f(k) = \sum_{j=k-n+1}^{k} \rho^T(j) S^{-1}(j) \rho(j) \underset{H_0}{\overset{H_1}{\gtrless}} \zeta \tag{16}$$

where $f(k)$ is a Chi-squared random variable with $n \times m$ degrees of freedom, where n is the residual window size and m denotes the dimension of the measurement vector, since the noises $V(k)$ and $W(k)$ are assumed to be zero mean Gaussian white noises. In (16) the criterion ζ can be chosen from standard Chi-squared tables [24]. Moreover, now consider a situation wherein the target initiates and suffers from a severe maneuvering condition. In this case the proposed algorithm will implement the detection and the estimation for the situation on the basis of certain statistical calculations. In this situation, another important algorithm is also applied to increase the estimation accuracy. In such an algorithm, for the $i-th$ component of a vector, on the basis of the detection results, the testing condition with the components which have jumps are expressed as

$$|\rho_i(k)| \leq \left| D\sqrt{S_{ii}(k)} \right| \tag{17}$$

where D represents the rejected innovation, being a constant related to the Gaussian pdf. The variance of the rejected innovation can be calculated as

$$\mathrm{var}(D^2) = \rho_i^2(k) \left\{ a_i(k)\delta_{ii}(k) + R_{ii}(k) \right\}^{-1} \tag{18}$$

where var$(\cdot)$ is variance operator; the parameter $a_i(k)$ can be computed as

$$a_i(k) = \frac{[\rho_{ii}(k)/D]^2 - R_{ii}(k)}{R_{ii}(k)} \tag{19}$$

Once the parameters have been modified and determined by Eq. 18 and 19, the innovative values $\rho(k)$ at time k can exist on the boundaries of the acceptable region defined by 17. Thus, to keep the target on track, the covariance of the prediction error $P(k \mid k-1)$ is modified to $[a_m(k) \cdot P(k \mid k-1)]$, where $a_m(k)$ is the largest value of all the $a_i(k)$ shown in 19. By virtue of the data association algorithm, not only is a better performance obtained, but the tracking filter also has faster responses in server-maneuvering situations. However, under such a procedure, i.e., after the approach is adopted, the Kalman gain increases gradually, after which the tracking performance of the WSS will become more stable and efficient.

5 Simulation Results and Discussion

Developing simulation programs (using Matlab) by virtue of the proposed DFA is implemented in this subsection. The developed DFA associating with CHNN technique is first validated in an environment wherein three targets are tracked in WSN deployments. Next the DFA is also applied to track five targets, including two non-maneuvering and three maneuvering ones. The initial conditions for simulating the tracking of two targets are listed in Table I, mentioned here mainly for demonstrating the accuracy and efficiency of the proposed algorithms. The transition matrix $F(k)$ and the noise gain matrix $G(k)$ corresponding to the target for the sampling interval T, which is assumed in the simulation to be two seconds, are given by

$F(k) = \begin{bmatrix} 1 & T & 0 & 0 \\ 0 & 1 & 0 & 0 \\ 0 & 0 & 1 & T \\ 0 & 0 & 0 & 1 \end{bmatrix}$ and $G(k) = \begin{bmatrix} T^2/2 & 0 \\ T & 0 \\ 0 & T^2/2 \\ 0 & T \end{bmatrix}$, respectively. The initial value of the state error covariance is assumed to default as $P(0 \mid 0) = \begin{bmatrix} 10000 & 100 & 0 & 0 \\ 0 & 100 & 100 & 0 \\ 0 & 0 & 10000 & 100 \\ 0 & 0 & 100 & 100 \end{bmatrix}$. After the assignment of initial conditions is completed, the procedure of simulation for the DFA algorithm is following the steps illustrated in Fig. 3. The results from tracking three targets without and with the DFA calculation are graphed in Fig. 4 and Fig. 5, respectively. In these simulations eighty steps Monte Carlo are implemented; moreover, 10 estimated tracking (measurements) with data-association calculation are sampled for reciprocal comparison for accuracy. It is easy to see that the many more matching situations occur in Fig. 5. I.e., all of the tracking paths tightly parallel the true path marked with circles. It should be emphasized that a little difference does exist the paths of the true targets and the results presented in Fig. 4 and Fig. 5, since the tracking is generated with a random function of the software program. Usage of random-number generators for the measurement of noise and clutter points is illustrated in the simulation. Furthermore, a Kalman filter is utilized to recursively estimate the state vector $\widehat{X}(k|k)$. On the basis of each hypothesis formulated from the measurement data received, the corresponding correlations can be promptly calculated. Hence, the position errors caused by the use and non-use of DFA calculation and without DFA calculation are plotted in Fig. 6, and Fig. 7, respectively. It is reasonable to state that the larger position error, with an order of ten thousands, is generated by the results obtained prior to DFA calculation; whereas, a smaller position error, in an approximate order of hundreds, occurs in the case after DFA calculation. A case with all the noise uncorrelated is assumed in the simulation. Thus the values $\alpha = 1$ and $\beta = r + 1$ are chosen in the simulation for five targets and ten to thirty measurements, where r is the radians of the gate. After eighty Monte Carlo iterations the simulation results from tracking the five targets, two non-maneuvering (Target 1 and Target 2) and three maneuvering (Target 3 to Target 5), are graphed in Fig. 8. The results of the tracking position errors after DFA calculation are plotted in Fig. 9. According to the simulation results based on several different situations, we know that the performance of the proposed algorithm, DFA on CHNN-based, is quite well. The proposed CHNN-based DFA algorithm might have a hardware complexity (number of neurons) in direct linear proportion to the number of tracked targets and the deployed mobile sensors in WSSs. Moreover, tracking for targets with mobile sensors by using the DFA algorithm in WSNs is constrained by the requirement for training the CHNN. However, this CHNN can be thoroughly implemented in analog VLSI technology with currently existing methods. Therefore, the authors believe that, overall, since a CHNN is more appropriate for a neural network based in multi-mobile sensor tracking environments, one may expect to see many such applications in WSS constructions in the near future. Furthermore, although in this type of environment the size of the optimization problem requiring much attention is considerably larger, the proposed DFA algorithm performs quite well, as in the simulation illustration. This is probably due to a sparse assumption of fewer tracked targets. However, the scale of the CHNN that would be required for the implementation of a practical mobile sensor might become a problem when the number of sensors and the measurements become very large. A current issue for development is reduction of the scale of the quadratic optimization problem that the CHNN must solve, so that available analog CHNN IC (integrated circuit) implementation can be used to build practical mobile sensors. Besides, the trends for implementing the WSS in large scale network are

generally to distribute the fused-data in some small area networks separately. The DFA based on CHNN proposed in this paper, thus, can be implemented in the various mobile environments both in large scale and small scale networks. Finally, since the amount of energy consumed by a mobile sensor during the processing of the DFA is large, such consumption is another important issue. Recently, several methods have been proposed for investigating energy-awareness problems in the mobile sensors in WSS [25]. The authors are currently working on developing a method for decreasing energy consumption by a mobile sensor so that the lifetime of sensors in WSS can be increased.

Table 1: Initial conditions of two targets

	$x(m)$	$\dot{x}(m/s)$	$y(m)$	$\dot{y}(m/s)$
Target 1	1500	400	3500	560
Target 2	1000	600	4000	440

Table 2: Initial conditions of five targets

	$x(m)$	$\dot{x}(m/s)$	$y(m)$	$\dot{y}(m/s)$
Target 1	100	400	3500	560
Target 2	1000	600	400	440
Target 3	0	550	8000	80
Target 4	20	540	9400	-100
Target 5	0	0	12500	-70

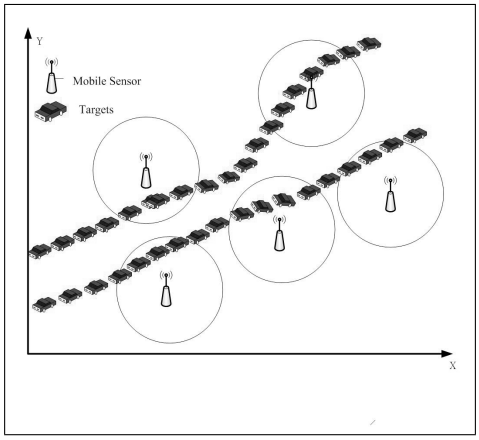

Figure 1: Deployment with two targets and five mobile sensor nodes, with sensing areas covered in circles.

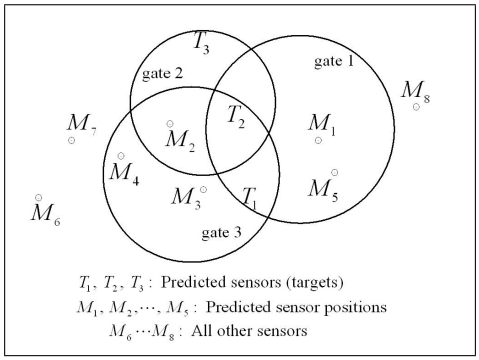

Figure 2: Relationships between measurements and predicted targets, based on gating technique.

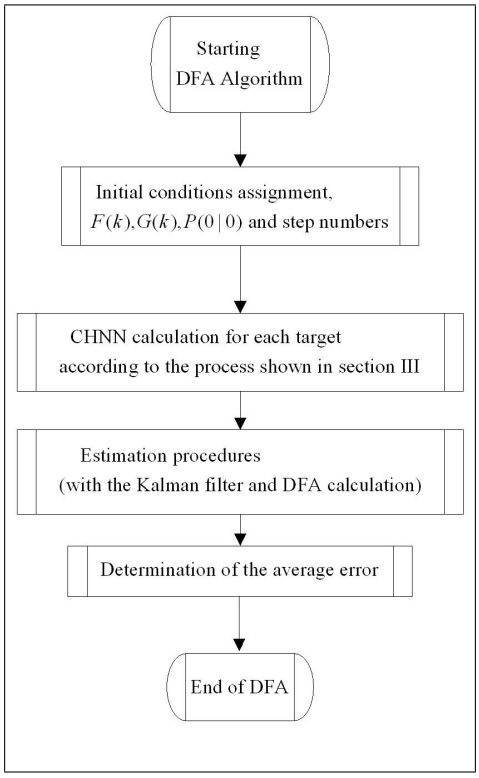

Figure 3: The procedure of simulation for the DFA algorithm.

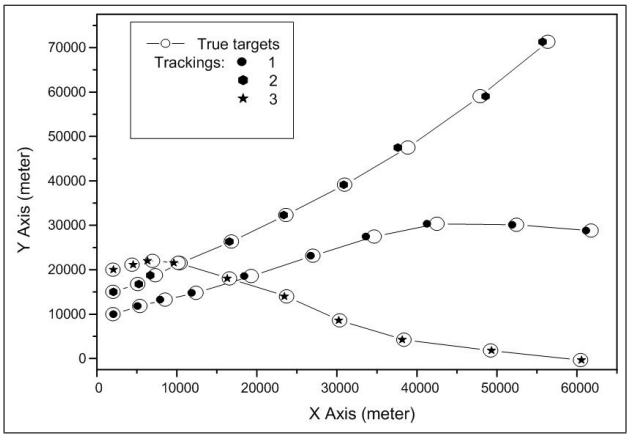

Figure 4: Data association results for tracking three targets prior to DFA calculation.

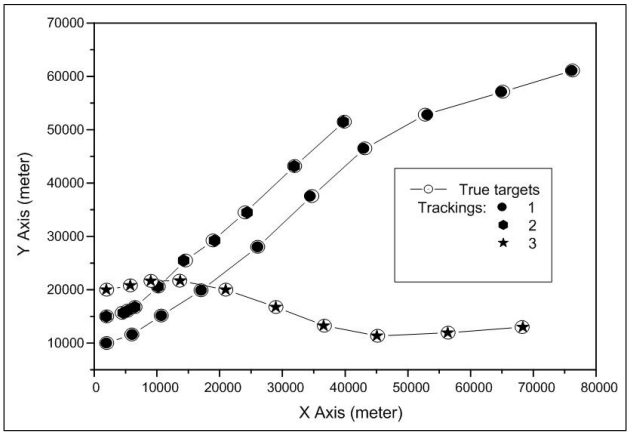

Figure 5: Data association results for tracking three targets after DFA calculation

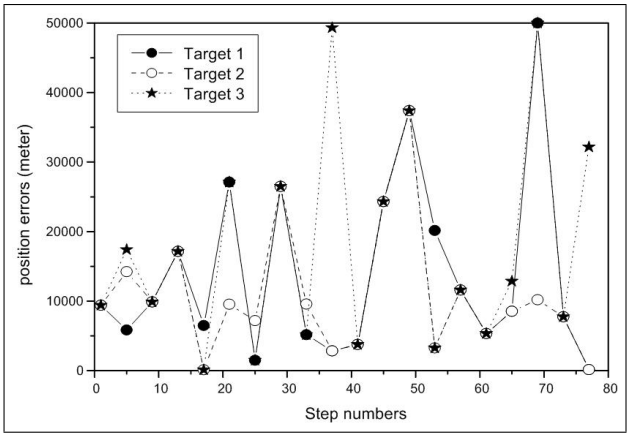

Figure 6: Position errors in tracking three targets prior to DFA calculation.

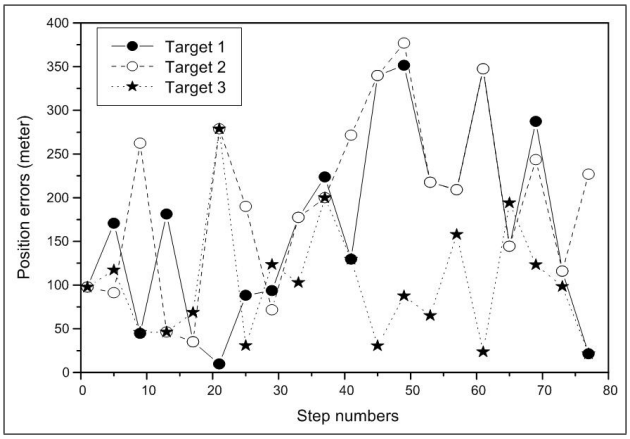

Figure 7: Position errors in tracking three targets after DFA calculation.

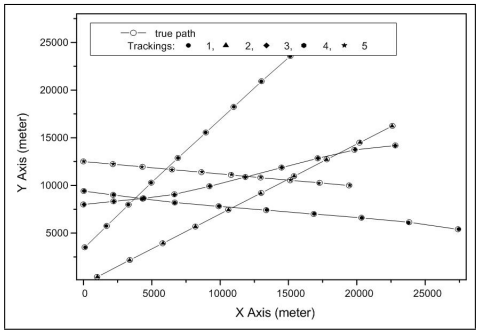

Figure 8: Simulations of tracking of five targets (using CHNN algorithm).

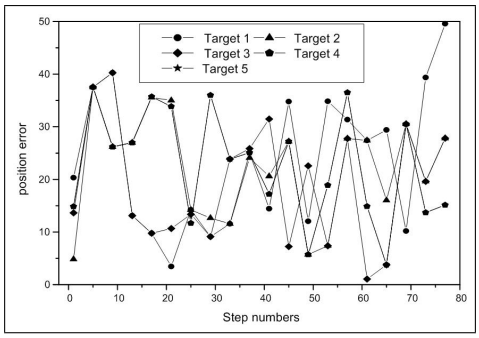

Figure 9: Position errors in tracking six targets after DFA calculation (using CHNN technique).

6 Conclusions

An innovative DFA algorithm based on CHNN techniques for tracking multiple targets with mobile sensors over WSS environments has been proposed in this report. This tracking technique has been investigated for its advantages in choosing an optimal correlation between mobile sensor measurements and existing target tracks. Because of the application of the CHNN technique, it was discovered that the system is relieved of the burden of determining the proper weighting factors as in a traditional HNN; therefore, the network can always achieve a rational solution. Moreover, an adaptive procedure for tracking maneuvering targets is also employed in this algorithm via stochastic process obtained by the DFA. On the basis of the simulation results obtained in this study, it can be claimed that this DFA algorithm is capable of obtaining the optimal correlations between true targets and mobile sensor measurements in WSS scenarios. Finally, the approach developed in this research has demonstrated not only stable performance for tracking procedures but definitely also excellent efficiency when tracking both constant velocity and maneuvering targets.

Acknowledgement

The author expresses appreciation to Dr. C. Rutledge, Department of English, Dayeh University, for her editorial assistance. The authors also would like to thank the anonymous reviewers for many useful comments which help to improve the quality and readability of this paper.

Bibliography

[1] F. Zhao, L. Guibas, Wireless Sensor Networks: An Information Processing Approach. *Elsevier Pte. Ltd., Singapore*, 2004.

[2] M. Cetin, Lei Chen, Fisher, J. W., III, Ihler, A. T., Moses, R. L., Wainwright, M. J. Willsky, A. S., Distributed Fusion in Sensor Networks. *IEEE Signal Processing Magazine*, vol. 23, issue 4, pp. 42-55, 2006.

[3] J. Miguez, A. Artes-Rodriguez, Monte Carlo Algorithms for Tracking a Maneuvering Target Using a Network of Mobile Sensors. *Proc. 1st IEEE Int. Workshop Computational Advances in Multi-Sensor Adaptive Processing, Puerto Vallarta, Mexico*, vol. 1, pp. 89-92, 2005.

[4] K. C. Chang, C. Y. Chong, Y. Bar-Shalom, Joint Probabilistic Data and Association Distributed Sensor Networks. *IEEE Transactions on Automatic Control*, vol. AC-31, pp. 889-897, 1986.

[5] N. Okello, B. Ristic, Maximum Likelihood Registration for Multiple Dissimilar Sensors. *IEEE Transactions on Aerospace Electronic Systems*, vol. 39, issue 3, pp. 1074-1083, 2003.

[6] Y. Bar-Shalom, T. E. Fortmann, Tracking and Data Association. *Academic Press, Inc.*, 1989.

[7] S.S. Blackman, Multiple Hypothesis Tracking for Multiple Target Tracking. *IEEE Aerospace Electronic Systems*, vol. 19, issue 1, pp. 5-18, 2004.

[8] Y.N. Chung, J. I. -Z. Chen, Applying Both Kinematic and Attribute Information for a Target Tracking Algorithm. *Journal of Control Systems and Technology*, pp. 203-209, 1997.

[9] C. Hue, Le Cadre., J. -P., P. Perez, Sequential Monte Carlo Methods for Multiple Target Tracking and Data Fusion. *IEEE Transactions on Signal Processing*, vol. 50, issue 2, pp. 309-325, 2002.

[10] D. Sengupta, R.A. Iltis, Neural Solution to the Multitarget Tracking Data Association Problem. *IEEE Aerospace Electronic Systems*, vol. 25, issue 1, pp. 96-108, 1989.

[11] L. Chin, Application of Neural Networks in Target Tracking Data Fusion. *IEEE Aerospace Electronic Systems*, vol. 30, issue 1, pp. 281-287, 1994.

[12] C. Y. Chang, P. C. Chung, Medical Image Segmentation Using a Contextual-constraint Based Hopfield Neural Cube. *Image and Vision Computing*, pp. 669-678, 2001.

[13] E. Soujeri, H. Bilgekul, Hopfield Multiuser Detection of Asynchronous MC-CDMA Signals in Multipath Fading Channels. *IEEE Communications Letters*, vol. 6, issue 4, pp. 147-149, 2002.

[14] B. Zhou, N. K. Bose, A Comprehensive Analysis of Neural Solution to the Multitarget Tracking Data Association Problem. *IEEE Aerospace Electronic Systems*, vol. 29, issue 1, pp.260-263, 1993.

[15] X. Wang, A. Jiang, S. Wang, Mobile Agent Based Moving Target Methods in Wireless Sensor Networks. *Proc. IEEE Int. Symp. Commun. and Info. Tech., Beijing, China*, vol. 1, pp. 22-26, 2005.

[16] Q. Liang, D. F. Yuan, Y. Wang, R. H. Zhang, A New Sensor Antenna-array Selecting Method in Wireless Sensor Networks. *In Proceeding Int. Conf. on Communications, Circuits and Systems, Guilin, China*, vol. 3, pp. 1523-1526, 2006.

[17] S. Y. Kung, Digital Neural Networks. *PTR Prentice Hall, Englewood Cliffs, New Jersey*, 1993.

[18] X. Wang, S. Wang, D. Bi, Dynamic Sensor Node Selection Strategy for Wireless Sensor Networks. *In Proceeding IEEE Int. Symp. Commun. and Info. Tech., Darling Harbour, Sydney, Australia*, vol. 1, pp. 1137-1142, 2007.

[19] T. Semertzidis, K. Dimitropoulos , A. Koutsia, N. Grammalidis, Video Sensor Network for Real-time Traffic Monitoring and Surveillance. *IET Intelligent Transport Systems*, vol. 4, Issue 2, pp. 103-112, 2010.

[20] Y. -S. Yen, S. Hong, R. -S. Chang, H. -C. Chao, Controlled Deployments for Wireless Sensor Networks. *IET Communications*, vol. 3, Issue 5, pp. 820-829, 2009.

[21] Y. Liu, N. Xiong, Y. Zhao, A.V. Vasilakos, J. Gao, Y. Jia, Multi-layer Clustering Routing Algorithm for Wireless Vehicular Sensor Networks. *IET Communications*, vol. 4, Issue 7, pp. 810-816, 2010.

[22] L. Shi, A. Capponi, K. H. Johansson, R. M. Murray, Resource Optimization in a Wireless Sensor Network with Guaranteed Estimator Performance. *IET Control Theory Applications*, vol. 4, Issue 5, pp. 710-723, 2010.

[23] M. S. Grewal, A. P. Andrew, Kalman Filtering, Theory and Practice-using MATLAB, 2nd ed. *John Wiley & Sons, Inc., New York*, 2001

[24] A. Papoulis, S. U. Pillai, Probability, Random Variables, and Stochastic Processes. 4th ed. *McGraw-Hill, Comp., Inc., New York*, 2002

[25] X. Wang, D. Wang, Y. Wang, Agrawal, D. P., A. Mishra, On Data Fusion and Lifetime Constrains in Wireless Sensor Networks. *In Proceeding IEEE Int. Communication. Conf., Glasgow, Scotland*, vol. 9, pp. 3942-3947, 2007.

Int. J. of Computers, Communications & Control, ISSN 1841-9836, E-ISSN 1841-9844
Vol. VII (2012), No. 1 (March), pp. 53-60

Adaptation Mechanism based on Service-Context Distance for Ubiquitous Computing

M. Cremene, M. Riveill, A. Rarau, C. Miron, B. Iulian, V. Todica

Marcel Cremene, Anca Rarau, Costin Miron,
Benta Iulian, Valeriu Todica
Technical University of Cluj-Napoca Romania,
Cluj-Napoca, Memorandumului nr. 28, 400114
E-mail(s): cremene@com.utcluj.ro, anca.rarau@cs.utcluj.ro,
miron@bel.utcluj.ro, iulian.benta@com.utcluj.ro,
todicav23@yahoo.com

Michel Riveill
University of Nice, Sophia-Antipolis
I3S, Route de Colles, BP 145 - F-06903,
Sophia Antipolis CEDEX
E-mail: riveil@unice.fr

Abstract: Service adaptation is one of the main research subjects in Ubiquitous Computing. Dynamic service adaptation, at runtime, is necessary for services that cannot be stopped (banking, airport, etc.). The classical approaches for dynamic adaptation require predicting all service and context states in order to specify service and context-specific adaptation policies. This prediction may lead to a combinatorial explosion. The aim of this research is to create a service and context-independent adaptation mechanism. Our proposal is based on a service-context model that is causally connected with the service and context, in a *model@run.time* paradigm. A closed-loop control principle is used for the adaptation mechanism. We introduce an equivalent for the *error* that is expressed by the notion of *service-context distance*. This distance represents a measure of how *adequate* is a service to its context. This distance is computed by some generic, reusable components. The adaptation algorithm that minimizes this distance is also service and context-independent.
Keywords: Services, Dynamic Adaptation, Context, Autonomic computing, Adaptation Control

1 Introduction

Background and motivation. Service adaptation to the context (physical infrastructure/resources, user needs, and environment) is one of the main research subjects in high interest domains such as Ubiquitous/Pervasive/Mobile Computing. Adapting a service is to reconfigure that service in order to maximize its QoS (Quality of Service) and also the efficiency of the resource utilization. We use a component-oriented approach for services, thus the reconfiguration concerns the service architecture: parameterize, add/remove, connect/disconnect or migrate components.

Numerous situations require a dynamic service adaptation [1,2], at runtime, because there are an important number of services that cannot be stopped (modified and recompiled). Examples are: banking services, airport services, spatial services, corporate services, groupware services and others. Even for services that may be stopped, the human intervention means important time and costs.

Issues about dynamic adaptation control mechanism. The adaptation mechanism, that encapsulates the system "intelligence", is the most important part of an adaptive system. It main function is to decide *when* a service should be adapted and *how* to adapt it.

After studying several different approaches for dynamic service adaptation, some of them presented in [3], we observed that the large majority of these solutions are based on the prediction about all possible service and context states. This prediction is an essential condition for specifying adaptation policies. Usually these policies are service and context-specific, they are not reusable and they do not evolve as the context evolves, without human intervention. A service can be adapted only inside the limits fixed a priori by these services and context-specific polices. For instance, in the case of "Event-Condition-Action" adaptation mechanism, which is one of the most used, a service cannot be adapted if the events, the conditions and the actions have not been predicted/specified priori by a human expert. But these events, conditions and actions are service and context-specific. This means that the human expert decides a priori *when* and *how* to adapt a service.

The problem is that, the prediction of all possible service and context states, may lead to a combinatory explosion. For instance, a state machine specification MDE (Model Driven Engineering) approach leads to a extremely high number of possible artefacts, as it is shown in [2]. Another problem of the classical state machine approach is that it does not deal with adding/removing/changing dynamically new states and transitions. Thus, such an approach is impossible to be used in practice for complex services and contexts.

Objective and approach. The aim of this research is to build a service and context-independent (generic) adaptation mechanism. Our proposal is based on a *model@run.time* approach. According to this approach, we propose a service-context model describing the service and the context as a whole system. This model is causally connected with the service and the context. The service-context model is represented as a directed graph having as nodes the service components and the context elements. Each node has attributes related to the entities (services' components, context elements) and to the interactions between these entities.

A closed-loop control principle is used for the adaptation mechanism, as suggested by the *Autonomic Computing* paradigm [4]. We introduce an equivalent for the notion of *error* that is expressed in our model by the notion of *service-context distance*. This distance represents a measure of how *adequate* is a service to its context in terms of user needs satisfaction and resources utilisation. The adaptation algorithm is also service and context-independent.

Paper outline. This paper is organized as it follows: the next section is an overview about the dynamic service adaptation issues and the models@run.time approach. Section three presents the proposed solution that is based on the service-context model, service-context distance and a generic adaptation algorithm. Section four present presents the conclusions.

2 Dynamic service adaptation in a models@run.time approach

2.1 Dynamic service adaptation

For defining more precisely what *service adaptation* means for us, we consider a mixture between the categories defined by the *Autonomic Computing* [4] and the adaptation types proposed in [1]:

a. Self-healing/Corrective adaptation. The system automatically detects, diagnoses, and repairs localized software (and hardware) problems. For example, if a system component responds too slow it will be replaced by another component, with the same functions, that responds on time (or the component will be moved on another physical machine). Self-healing/corrective adaptation deals usually with failure cases, when a component must be replaced/moved.

b. Self-adaptation. The adaptation is necessary when the context state changes. We may have two cases of self-adaptation:*Adaptive adaptation* concerns the situations when the context change and the service should change also in order to keep its functions. This type of adaptation is usually transparent to the user.*Extending adaptation* concerns the situations when some new user needs are discovered a posteriori and the service should be extended in order to satisfy these new needs.

c. Self-optimization/Perfective adaptation. The system continuously searches for opportunities to improve its own performance. The performance is maximal when the QoS parameter are maximized (for instance the response time) and when the resource utilization is minimal and well balanced. Self-optimization/Perfective adaptation deals with a service that is working correctly but it may be tuned in order to increase its efficiency/quality.

The adaptation is *dynamic* when the service reconfiguration happens at runtime. In the last years, numerous researchers have concentrated on developing middleware that enables dynamic adaptation. For instance, the *WComp* middleware [5, 6] offers a support for composing and adapting services at runtime. The design and the execution phases are simultaneous. An event-based communication model is used. It offers the possibility to use services installed on various devices and also web services from Internet. WComp manages also the dynamic service apparition/extinction.

Fractal [7] proposes a middleware and a component model enabling hierarchical composition. The middleware offers support for reflection and dynamic reconfiguration. A particularity of Fractal is the possibility to share a component between two other composite components.

OpenCCM (Open CORBA Component Model) [8] is the first public available and open source implementation of CCM (CORBA Component Model).

OSGi propose a platform based on dynamic modules/components that may be assembled at runtime, it provides a service-oriented, component-based environment. A service-oriented middleware allowing spontaneous distributed service composition at runtime, based on OSGi, is proposed in [9]. Facing with a high number of existent middleware, our intention is to propose an independent solution that may be adapted to different middleware.

2.2 The *models@run.time* approach

Models@run.time [10] represents a novel approach that aim is to extend the usage of software models (MDE - Model Driven Engineering) to runtime. The need of such models is motivated by the dynamic adaptation of mission-critical software issues. This is also related with *Autonomic Computing* paradigm because the adaptation should be autonomous (without human intervention).

This approach is also strongly related with the *reflection* paradigm and has a similar principle: a *model@run.time* is an abstraction of a system that is causally connected with that system and may be used for dynamic system adaptation. The difference comparing to reflection is that in model@run.time we look for high-level models while in reflection paradigm the (meta)model is strongly related to the low-level software aspects [10]. Such a model@run.time describes aspects as: structure, behaviour and goals of the system, from a problem space perspective.

One of the advantages of the *model@run.time* approach is the possibility to treat independently two main issues:

I. Propose a model that will be used at runtime for discovering the service-context adequacy problems and for adapting the service by solving these problems. Our proposal is based on a *service-context* model, a service-context distance that reflects the service-context adequacy and an adaptation algorithm that aim is to minimize this distance (and to increase the adequacy).

II. Create a middleware that will causally connect the two parts: a) the proposed service-context model with b)the adapted system (a modification of one part will be reflected on the other part). If we want to offer a general solution, a part of this middleware will make the adaptation with a specific adaptation support-middleware (see the examples presented in the section 2.1).

The second issue is more a technical issue than a scientific one because today many middleware and context monitoring tools offers a large number of solutions that may be reused. That is why; in this paper we are concentrated only on the first issue which is the most important and difficult.

3 The service-context model, the service-context distance and the adaptation algorithm

3.1 Service-context model

We have introduced the *service-context model* concept in [3, 11] as a possible approach for autonomic computing. In this paper we re-interpret this model from a *models@run.time* perspective, we extend it with the service-context distance.

Service-context graph. The service-context model (figure 1) aim is to describe the service and the context as a whole system that may be analyzed from the service to context adequacy point of view. This model is based on a directed graph composed by the following elements:

a. The nodes correspond to service and context entities. The service′ entities (S in fig. 1) are the software components that constitute the service. In order to simplify the model, a complex component is described by decomposing it in a sum of basic components having only three types: source (1 output), sink (1 input) or filter (1 input, 1 output). The context entities are context components: users (U in fig. 1), infrastructure elements (I in fig. 1) such as devices, networks and environment elements (E in fig. 1).

b. The vertex corresponds to the relations and interactions existent between these entities. We define three types of vertex corresponding to two types of possible relations/interactions:

   - *Informational flows* interactions. The service components are communicating by exchanging information. Also, the user exchange information with the service. This information has some *attributes* that describes it.
   - *Resource utilization* interactions. The service components consume resources provided by the hardware infrastructure (memory, cpu, bandwidth, etc).
   - *Environment influence* interactions. The environment may influence the user needs (ex. location) or the infrastructure (ex. the rain effect on a radio network).

For simplifying the model, we will discuss in this paper only the most important interactions which are the first two: information flows and resource utilization.

Attributes. The graph is annotated with some attributes. Each node has attributes related to the node itself or to the node ports (input and output vertex). These attributes are making a semantic connection between the service nodes and the context nodes. For instance, the 'language' attribute means the user U language but also the service S language, the 'memory' attribute means the memory consumed by a component and the memory provided by a device.

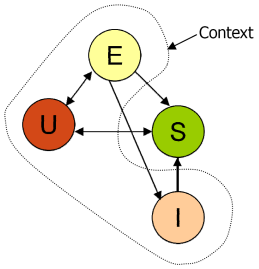

Figure 1: Service-Context general model

A common attribute vocabulary for service and context components should be respected by the component developers/providers.

For each attribute a input and output domain are specified. For filter-type components, a *transfer function* (input-output) should be specified. For instance, a translation component change the language between the input and the output, a compression component change the compression rate, etc.

The attributes, their input/output domains and the transfer functions should be specified for each component by the component developer/provider, in a form of a *profile* (i.e. an XML-based descriptor of the component). This is a necessary condition for enabling the machine to understand what a component does. Same thing for the context elements, each one has a *profile*.

Composition. One of the most important property of the service-context model is the *composition*. By composition we understand here to assimilate a graph to a node. This is a necessary condition for describing the service behaviour and properties using only the service's internal components behaviour and properties. We propose a composition mechanism based on the attributes specified by the profiles. The elementary composition cases are described in figure 2. The composition means to determine the equivalent node for a graph composed by two nodes.

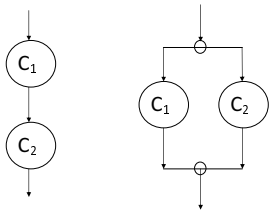

Figure 2: Serial and parallel composition

The composition operation depends on the attribute nature. The composition is different for information flows interactions and for resource utilization interactions. These operators are described in the figure 3.

3.2 Service-context distance

The first idea for describing the service-context adequacy, used in [11], was to use a binary approach: a service is adequate or not to its context. In order to have a more general approach, we introduce in this paper the concept of *service-context distance*. The distance is minimal when the service to context adequacy is maximal. This distance has two components: the *S-U distance* measures the distance from the information flow point of view and the *S-I distance* measures the distance from the resource utilization point of view.

Information flow composition		
Atribute name	**Serial composition**	**Parallel composition**
response_time	*Sum, +*	*Max function*
security_level	*Min function*	*Min function*
language	*language of the output component*	*Intersection*
type_hmi	*type_hmi of the output component*	*Reunion*

Resource utilization composition			
Atribute name	**Paralel composition**	**Serial composition**	**Shared composition**
memory	*Sum, +*	*Max function*	$m_1 + m_2 - m_{shared}$
cpu_time	*Sum, +*	*Max function*	$t_1 + t_2 - t_{shared}$
screen_surface	*Reunion*	*Max function*	*Reunion*

Figure 3: Composition operators for different attributes

Each distance is represented as a vector having as components the distances corresponding to each attribute. For each attribute we define a specific distance that will be computed by some dedicated components/services. In some cases the distance is expressed by a simple formula or set of rules. Some examples are described in figure 4.

Information flow distance evaluation		
Attribute name	**Domain**	**Distance**
response_time	*0..inf*	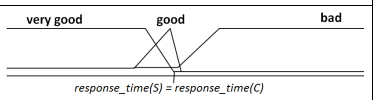
security_level	*{none, low, medium, high, very high}*	*d = 0 if security_level(S) >= security_level(U) and ∞ else*
language	*{RO, FR, DE, ES……..}*	*d = 0 if language(S) == language(U) and ∞ else*

Resource utilization distance evaluation		
Attribute name	**Domain**	**Distance**
memory	*0…100%*	*d = memory(S) / memory(I) * 100*
cpu_time	*0..100%*	*d = cpu_time(S) / cpu_time(I) * 100*
network_capacity	*0..100%*	*d = network_capacity(S) / network_capacity(I) * 100*

Figure 4: Distance expressions for different attributes

A more complex distance is the distance between the user requests expressed in natural language and the service features. For such complex distances we cannot present a simple formula but we use dedicated component/services that implement the algorithm for computing the distance. Such an algorithm is proposed in [12].

The model may be extended by adding new attributes definitions and new distances measuring components.

3.3 Adaptation algorithm

The adaptation algorithm goal is to minimize the service-context distance. For doing that, the adaptation algorithm dynamically transforms the service-context graph from a less adequate one toward a more adequate one.

The primitive operations used by the adaptation algorithm are the following: changing a node parameter, connecting/disconnecting a node, inserting a new node, removing a node, replacing a node. In order to minimize the service-context distance, the adaptation algorithm should find a list of primitive operations that transforms the graph from the current state into the desired state (for the desired state the service-context distance is minimal). Several alternative solutions may exists. In order to make a difference between these possible solutions, we associate an *adaptation cost* to each primitive operation. For instance, the parameterization has a cost equal to 1 while the insertion cost is 5. This is because it is faster and easier to apply a parameterization than an insertion.

We have implemented an algorithm, described in [11], that uses one attribute and one adaptation strategy: the insertion of a new component. This algorithm starts from a mismatch between the desired value *V2* for an attribute *A* and the current value *V1* and search for a new component that transforms the value of the attribute from *V1* to *V2*. The place where the new component may be inserted is searched based on the syntactic interface compatibility. The user is confirmation is asked before transforming the service.

We are working in present on a general adaptation algorithm, able to apply a succession of different primitive operations and deal with several attributes simultaneously. We have done some tests with genetic algorithms which seem promising but are not very fast.

3.4 Implementation

As a proof of concept, in [11] we have implemented a simple forum service that is adapted dynamically to the user language. The components are developed in Java, using the CCM (Corba Component Model) specifications. The adaptation consists in inserting a translation component, at runtime. We have used a mechanism based on ISL (Interaction Specification Language) that is used also in WComp middleware [6].

In present we are developing a general service-context simulator, based on the open source JGraphX API that should allow us to test the adaptation at the model level by simulating various service and context states.

4 Conclusions

The issue discussed in this paper was to propose a service and context-independent adaptation mechanism for dynamic service adaptation. We have proposed a solution, based on the service-context model and service-context distance concepts, that fits into the very recent *model@run.time* approach. The generality of the proposed model is given by its following properties: the service attributes/behaviour are determined automatically by composing the attributes/behaviour of its internal components, the service-context distance depends only on the model attributes nature and are not dependent to a particular service/context and the adaptation algorithm is also service/context independent. As future work we intend to generalize the adaptation algorithm.

Acknowledgments

This work was supported by CNCSIS-UEFISCSU, PNII-IDEI, project number 1062/2007. Thanks to members of the Rainbow team, I3S laboratory, Sophia-Antipolis.

Bibliography

[1] A. Ketfi, N. Belkhatir, and P.-Y. Cunin, "Automatic adaptation of component-based software: Issues and experiences," in *PDPTA '02: Proceedings of the International Conference on Parallel and Distributed Processing Techniques and Applications*, pp. 1365–1371, CSREA Press, 2002.

[2] B. Morin, O. Barais, J. M. Jezequel, F. Fleurey, and A. Solberg, "Models@ run.time to support dynamic adaptation," vol. 42, pp. 44–51, October 2009.

[3] M. Cremene, *Adaptation Dynamique de Services.* PhD thesis, Double coordination between University of Savoie, France and Technical University of Cluj-Napoca, Romania, 2005.

[4] J. O. Kephart and D. M. Chess, "The vision of autonomic computing," *Computer*, vol. 36, no. 1, pp. 41–50, 2003.

[5] D. Cheung-Foo-Wo, J.-Y. Tigli, S. Lavirotte, and M. Riveill, "Self-adaptation of event-driven component-oriented middleware using aspects of assembly," in *MPAC '07: Proceedings of the 5th international workshop on Middleware for pervasive and ad-hoc computing*, (New York, NY, USA), pp. 31–36, ACM, 2007.

[6] J.-Y. Tigli, S. Lavirotte, G. Rey, V. Hourdin, D. Cheung-Foo-Wo, E. Callegari, and M. Riveill, "WComp Middleware for Ubiquitous Computing: Aspects and Composite Event-based Web Services," *Annals of Telecommunications (AoT)*, vol. 64, Apr. 2009.

[7] E. Bruneton, T. Coupaye, M. Leclercq, V. Quéma, and J.-B. Stefani, "The fractal component model and its support in java: Experiences with auto-adaptive and reconfigurable systems," *Softw. Pract. Exper.*, vol. 36, no. 11-12, pp. 1257–1284, 2006.

[8] S. Gorappa and R. Klefstad, "Empirical evaluation of openccm for java-based distributed, real-time, and embedded systems," in *SAC '05: Proceedings of the 2005 ACM symposium on Applied computing*, (New York, NY, USA), pp. 1288–1292, ACM, 2005.

[9] A. Bottaro, A. Gerodolle, and P. Lalanda, "Pervasive service composition in the home network," in *AINA '07: Proceedings of the 21st International Conference on Advanced Networking and Applications*, (Washington, DC, USA), pp. 596–603, IEEE Computer Society, 2007.

[10] G. Blair, N. Bencomo, and R. B. France, "Models@ run.time," *Computer*, vol. 42, no. 10, pp. 22–27, 2009.

[11] M. Cremene, M. Riveill, and C. Martel, "Autonomic adaptation solution based on service-context adequacy determination," *Electron. Notes Theor. Comput. Sci.*, vol. 189, pp. 35–50, 2007.

[12] M. Cremene, J.-Y. Tigli, S. Lavirotte, F.-C. Pop, M. Riveill, and G. Rey, "Service composition based on natural language requests," in *IEEE SCC*, pp. 486–489, 2009.

Int. J. of Computers, Communications & Control, ISSN 1841-9836, E-ISSN 1841-9844
Vol. VII (2012), No. 1 (March), pp. 61-72

A New Approach to Nonlinear Tracking Control Based on Fuzzy Approximation

Z. Du, T.-C. Lin, V.E. Balas

Zhenbin Du
Yantai University,
Yantai, Shandong 264005, China
E-mail: zhenbindu@yahoo.com.cn

Tsung-Chih Lin
Feng-Chia University
Taichung, 40724, Taiwan
E-mail: tclin@fcu.edu.tw

Valentina E. Balas
Aurel Vlaicu University
B-dul Revolutiei 77
310130 Arad, Romania
E-mail: balas@drbalas.ro

Abstract: The problem of tracking control is addressed for a class of nonlinear systems with uncertainties. The original nonlinear systems are approximated by a fuzzy T-S model based on which a state-feedback controller is constructed by using the linear matrix inequalities. The approximating error is eliminated by an adaptive compensator based on fuzzy logic systems. The effectiveness of the proposed control scheme is demonstrated by a simulation example. The main advantage is that the designer makes milder constraint assumption for the approximation error and the uncertainties in nonlinear systems.
Keywords: fuzzy T-S model; fuzzy logic systems; nonlinear systems; uncertainties; tracking control.

1 Introduction

The problem of controller design for the nonlinear systems with uncertainties is a challenging work. One of effective tools used to solve the problem is fuzzy method. There are two frequently used fuzzy models: fuzzy T-S model [1-13] and fuzzy logic systems [16-17]. Fuzzy T-S model is usually used to approximate nonlinear systems, and it has been widely applied to analyze the stability of nonlinear systems [1-4]. The contributions of these works are very important, but these works could be further improved by a simpler and more practical control scheme. The approximating error is neglected in [1-4], which impacts the stability of the system. Therefore, the designed controller can't always guarantee the stability of the original system. To overcome the effect of the approximating error, some relaxed stability methods are developed in [5-8]. These methods improve the approximation accuracy for nonlinear system. However, the original nonlinear system is still neglected in [5-8]. In order to further relax the effect of the approximating error, it is assumed to satisfy the matching condition in [9-11] and have a upper bound in [12-13]. However, the matching condition and the upper bound are not easy to be found in practice, which adds some difficulties to the controller design. The uncertainties in nonlinear systems are assumed to satisfy the constraint of the upper bound in [14-15]. However, the upper bound may be too large or doesn't exist. On the other hand, fuzzy logic systems have been proved to have

the universal approximation property. By constructing a set of fuzzy "IF-THEN" rules, fuzzy logic system is used to model uncertain nonlinear systems [16-17].

There exist some conservatism of pure fuzzy T-S model in dealing with the approximating error. The pure adaptive fuzzy control also has some shortages of excessively depending on the chosen membership functions. Therefore, it is more interesting to combine both fuzzy models to overcome their shortages each other.

Based on the above discussions, fuzzy T-S model and fuzzy logic systems are combined to design a new tracking-control scheme for a class of nonlinear systems with uncertainties in this paper. A fuzzy T-S model is used to approximate the nonlinear system based on which a state-feedback controller is constructed by use of the linear matrix inequalities. The approximating error and the uncertain nonlinear parts are eliminated by a compensator based on fuzzy logic systems. The main advantages are summarized as follows:

Firstly, fuzzy T-S model and fuzzy logic systems are combined to develop a controller. Compared with the existing works based on fuzzy T-S model [1-13], the proposed method in this paper makes milder constraint assumptions for the approximating error. Secondly, the dimension of the matrix inequalities is reduced, thus, the difficulty of solving the matrix equalities is relaxed. Thirdly, the existing works based on fuzzy logic systems [16-17] excessively depend on the chosen membership functions which are improved in the proposed method of this paper. Finally, the developed controller makes full use of the advantages of two fuzzy models. As a result, it is more convenient to implement the controller in practice.

The rest of the paper is organized as follows. Section 2 provides preliminaries and the formulation of the problem. Section3 develops a procedure of the controller design. Section 4 presents a simulation example of 2-link manipulator to illustrate the effectiveness of the proposed method. These are followed by conclusions in Section 5.

2 Problem formulation

Consider the following nonlinear systems with uncertainties

$$\begin{aligned}
&\dot{x}_1 = x_2,\\
&...\\
&\dot{x}_{(\beta_1-1)} = x_{\beta_1},\\
&\dot{x}_{\beta_1} = f_1(x,u) + \tilde{f}_1(x,u) + d_1,\\
&\dot{x}_{(\beta_1+1)} = x_{(\beta_1+2)},\\
&...\\
&\dot{x}_n = f_m(x,u) + \tilde{f}_m(x,u) + d_m,
\end{aligned} \tag{1}$$

where x,u are the system state vector, control input vector, respectively;
$x = [x_1, ..., x_1^{(\beta_1-1)}, ..., x_{(n-\beta_m+1)}, ..., x_{(n-\beta_m+1)}^{(\beta_m-1)}]^T \in R^n$, $\beta_1 + \beta_2 + ... + \beta_m = n$, $u = [u_1, ..., u_m]^T \in R^m$, $f_i(i = 1, ..., m)$ are known smooth nonlinear functions, $\tilde{f}_i(i = 1, ..., m)$ are unknown uncertain nonlinearities of the system, and d_i(i=1,2,...,m) denote the external disturbances.

Remark 1: There are many practical physical systems which can be described by the model (1), for example, the mass-spring-damper [18], the rotated inverted pendulum [19] and the n-link manipulator [20].

A reference model is as follows:

$$\dot{x}_r(t) = A_r x_r(t) + r(t), \tag{2}$$

where $x_r(t)$ is a reference state, r(t) is a bounded reference input, and A_r is an asymptotically stable matrix.

Control objective: Design a controller to guarantee that the nonlinear system (1) is stable and the state can track the reference state $x_r(t)$.

The known part of the system (1) can be approximated by a fuzzy T-S model composed of L rules. For convenience of research, fuzzy T-S model includes the external disturbance d. The *ith* rule of the fuzzy model is as follows:

IF $z_1(t)$ is F_1^i and,...,and $z_s(t)$ is F_s^i, THEN

$$\dot{x}(t) = A_i x(t) + B_i u(t) + d, \quad i = 1, 2, ..., L, \tag{3}$$

where $z_1(t), ..., z_s(t)$ are the premise variables, F_j^i(j=1,2,...,s) are the fuzzy sets, L is the number of IF-THEN rules, A_i and B_i are some constant matrices with compatible dimensions, $B_i = [0, ..., b_{i1}^T, ..., 0, ..., b_{im}^T]^T \in R^{n\times m}$ with $b_{i1} \in R^m, ..., b_{im} \in R^m$, and $d = [0, ..., d_1, ..., 0, ..., d_m]^T$. The final output of the fuzzy system is inferred as follows:

$$\dot{x}(t) = \sum_{i=1}^{L} \mu_i A_i x(t) + \sum_{i=1}^{L} \mu_i B_i u(t) + d, \tag{4}$$

where

$$\mu_i = \nu_i(z(t)) \Big/ \sum_{i=1}^{L} \nu_i(z(t)), \ \nu_i(z(t)) = \prod_{j=1}^{S} F_j^i(z_j(t)), \tag{5}$$

and $F_j^i(z_j(t))$ is the grade of membership of $z_j(t)$ in F_j^i. Therefore, the approximating error for the nonlinear system (1) and the uncertainties of the nonlinear system (1) can be expressed as $B\Delta(x)$, where $B = diag[B^1, ..., B^m], B^i = [0, ..., 0, 1]^T \in R^{\beta_i}$ and $\Delta(x) = [\Delta_1, ..., \Delta_m]^T$.

Therefore, the nonlinear system (1) could be rearranged as

$$\dot{x}(t) = \sum_{i=1}^{L} \mu_i A_i x(t) + \sum_{i=1}^{L} \mu_i B_i u(t) + B\Delta(x) + d. \tag{6}$$

3 Design of controller and stability analysis

3.1 Design of controller

The controller is chosen as

$$u(t) = u_l(t) - u_f(t), \tag{7}$$

where $u_l(t)$ denotes the state-feedback controller based on fuzzy T-S model, $u_f(t)$ is the adaptive compensator based on fuzzy logic systems.

The state-feedback controller $u_l(t)$ based on fuzzy T-S model is designed as

$$u_l(t) = \sum_{i=1}^{L} \mu_i K_i(x(t) - x_r(t)), \tag{8}$$

where $u_l(t)$ is used to stabilize the linear part of the system (1), and K_i(i=1,2,...,L) are matrices with proper dimensions and satisfy

$$\overline{A}_{ij}^T + P\overline{A}_{ij} + \frac{1}{\rho^2} PP + \overline{Q} < 0, \ i, j = 1, 2, ..., L, \tag{9}$$

where $\overline{A}_{ij} = \begin{bmatrix} A_i + B_i K_j & -B_i K_j \\ 0 & A_r \end{bmatrix}$, $\overline{Q} = diag\{2Q, 2Q\}$, P and Q are some symmetric and positive definite matrices, and ρ is a positive constant.

The adaptive compensator based on fuzzy logic systems is given by

$$u_f(t) = \begin{cases} E^{-1}\hat{u}(x|\Theta), & \text{if } E \text{ is nonsingular} \\ E^T(I + EE^T)^{-1}\hat{u}(x|\Theta) & \text{if } E \text{ is singular,} \end{cases} \tag{10}$$

which is used to compensate the approximating error and the uncertainties. In(10),

$$E_i = [b_{i1}^T, ..., b_{im}^T]^T \in R^{m\times m}, E = \sum_{i=1}^{L} \mu_i E_i,$$

and $\hat{u}(x|\Theta)$ is constructed by fuzzy logic systems. The updating law of Θ is as follows:

$$\dot{\Theta} = \eta_1 \Psi^T(x)\overline{B}^T P x, \tag{11}$$

where η_1 is a positive constant, $\Psi(x)$ is a fuzzy basis-function matrix, and the definition of $\Psi(x)$ is given in (16).

3.2 Stability analysis

Note that

$$\sum_{i=1}^{L} \mu_i B_i u_f(t) - B\Delta(x, x(t-\tau)) = B(Eu_f(t) - \Delta(x)) \tag{12}$$

$$= \begin{cases} B(\hat{u}(x|\Theta) - \Delta(x)) \\ B(\hat{u}(x|\Theta) - (I + EE^T)^{-1}\hat{u}(x|\Theta) - \Delta(x)) \end{cases}$$

$$\underline{\underline{\Delta}} B(\hat{u}(x|\Theta) - \Delta(x)). \tag{13}$$

Substituting (7) into (6) yields

$$\dot{x}(t) = \sum_{i=1}^{L} \mu_i A_i x(t) + \sum_{i=1}^{L}\sum_{j=1}^{L} \mu_i\mu_j B_i K_j (x(t) - x_r(t)) - B(\hat{u}(x|\Theta) - \Delta(x)) + d. \tag{14}$$

Denote $\tilde{x}(t) = [x^T(t), x_r^T(t)]^T$, and $\overline{B} = [B^T \quad 0]^T$. From (2) and (14), a new extended closed-loop system is as follows:

$$\dot{\tilde{x}}(t) = \sum_{i=1}^{L}\sum_{j=1}^{L} \mu_i\mu_j \overline{A}_{ij}\tilde{x}(t) + \overline{B}(-(\hat{u}(x|\Theta) - \Delta(x))) + d\prime, \tag{15}$$

where $d\prime = [d^T, r^T(t)]^T$. When fuzzy logic systems $\hat{u}(x|\Theta)$ eliminate $\Delta(x)$, then the closed-loop system (15) is stable. Thus, fuzzy logic systems are constructed to approximate the vector function $\Delta(x)$ as follows:

$$\hat{\Delta}(x|\Theta) = \Psi(x)\Theta, \tag{16}$$

where

$$\Psi(x) = diag[\xi_1^T(x), ..., \xi_m^T(x)], \Theta = [\theta_1^T, \theta_2^T, ..., \theta_m^T]^T$$

in which θ_i(i=1,2,...,m) are the column vectors, and the weight Θ is an adaptive parameter. Define the optimal parameter estimation Θ^* as follows:

$$\Theta^* \triangleq \arg\min_{\Theta\in\Omega}[\sup_{x\in U}||\hat{\Delta}(x|\Theta) - \Delta(x)||], \tag{17}$$

where $U = \{x \in R^n\}, \Omega = \{\Theta \in R^{pm\times 1}\}$. U,$\Omega$ denote the sets of suitable bounds on x, Θ, respectively. Then the estimation error for the vector function $\Delta(x)$ can be expressed as

$$\hat{\Delta}(x|\Theta) - \Delta(x) = \Psi(x)\tilde{\Theta} + w, \tag{18}$$

where $w = [w_1, ..., w_m]^T$ is a residual term, $\tilde{\Theta} = \Theta - \Theta^* = [(\theta_1 - \theta_1^*)^T, ..., (\theta_m - \theta_m^*)^T]^T$.

Denote $w\prime = [\overline{w}^T, r^T(t)]^t$, and $\overline{w} = [0, ..., d_1 - w_1, ..., 0, ..., d_m - w_m]^T$. Substituting (18) into (15), (15) is rearranged as

$$\dot{\tilde{x}}(t) = \sum_{i=1}^{L}\sum_{j=1}^{L}\mu_i\mu_j\overline{A}_{ij}\tilde{x}(t) + \overline{B}(-\Psi(x)\tilde{\Theta}) + w\prime. \tag{19}$$

Theorem 1. For the nonlinear system (1), if the controller is chosen as (7) composed of the fuzzy state-feedback controller (8) and the adaptive compensator(10), and the updating law for the weight is chosen as (11), then the closed-loop system (15) is uniformly ultimately bounded (UUB) and the following tracking performance is achieved as

$$\int_0^T (x(t) - x_r(t))^T Q(x(t) - x_r(t))dt \le \tilde{x}^T(0)P\tilde{x}(0) + \frac{1}{\eta_1}\tilde{\Theta}^T(0)\tilde{\Theta}(0) + \rho^2\int_0^T (w\prime^T w\prime)dt, \tag{20}$$

where $\rho > 0$, P, Q are some symmetric and positive definite matrices.

Proof. Consider the following functional

$$V = \frac{1}{2}\tilde{x}^T P\tilde{x} + \frac{1}{2\eta_1}\tilde{\Theta}^T\tilde{\Theta} \tag{21}$$

whose derivative can be computed as follows:

$$\dot{V} = \frac{1}{2}\dot{\tilde{x}}^T(t)P\tilde{x}(t) + \frac{1}{2}\tilde{x}^T(t)P\dot{\tilde{x}}(t) + \frac{1}{\eta_1}\tilde{\Theta}^T\dot{\tilde{\Theta}} = \dot{V}_1 + \dot{V}_2, \tag{22}$$

where

$$\dot{V}_1 = (\sum_{i=1}^{L}\sum_{j=1}^{L}\mu_i\mu_j\overline{A}_{ij}\tilde{x}(t))^T P\tilde{x}(t) + \tilde{x}^T(t)P(\sum_{i=1}^{L}\sum_{j=1}^{L}\mu_i\mu_j\overline{A}_{ij}\tilde{x}(t)) + \frac{1}{2}w\prime^T Px(t) + \frac{1}{2}x^T(t)Pw\prime \tag{23}$$

$$V_2 = [\tilde{x}^T P\overline{B}(-(\Psi(x)\tilde{\Theta}) + \frac{1}{\eta_1}\tilde{\Theta}^T\dot{\tilde{\Theta}}. \tag{24}$$

$$\dot{V}_1 \le \frac{1}{2}\sum_{i=1}^{L}\sum_{j=1}^{L}\mu_i\mu_j\tilde{x}^T(t)(\overline{A}_{ij}^T P + P\overline{A}_{ij} + \frac{1}{\rho^2}PP)\tilde{x}(t) + \frac{1}{2}\rho^2 w\prime^T w\prime \tag{25}$$

Substituting (9) into (25) yields

$$\dot{V}_1 \leq -\frac{1}{2}\tilde{x}^T(t)\overline{Q}\tilde{x}(t) + \frac{1}{2}\rho^2 w\prime^T w\prime. \tag{26}$$

From (11),(24)

$$V_2 = [\tilde{x}^t P\overline{B}(-(\Psi(x)\tilde{\Theta}) + \frac{1}{\eta_1}\tilde{\Theta}^T\dot{\tilde{\Theta}}] = 0. \tag{27}$$

Thus

$$\dot{V} = \dot{V}_1 + \dot{V}_2 \leq -\frac{1}{2}\tilde{x}^T(t)\overline{Q}\tilde{x}(t) + \frac{1}{2}\rho^2 w\prime^T w\prime. \tag{28}$$

When $||e|| > \frac{\rho}{\lambda_{min}(\overline{Q})}||\overline{w}||, \dot{V} < 0$.Thus, the closed-loop system (15) is UUB.

Note that

$$\int_0^T (x(t) - x_r(t))^T Q(x(t) - x_r(t))dt = \int_0^T [x^T(t)\ x_r^T(t)] \begin{bmatrix} Q & -Q \\ -Q & Q \end{bmatrix} [x^T(t)\ x_r^T(t)]^T dt$$

$$\leq \int_0^T [x^T(t)\ x_r^T(t)] diag\{2Q, 2Q\} [x^T(t)\ x_r^T(t)]^T dt = \int_0^T \tilde{x}^T(t)\overline{Q}\tilde{x}(t)dt \tag{29}$$

Integrating the above inequality (28) from t=0 to T yields (20).

By Schur complements, the inequalities (9) are transformed into the linear matrix inequalities. Therefore, the common solution P and K_j(j=1,2,...,L) are required to be found. P is chosen as the form $P = diag\{P_1, P_2\}$, where P_1, P_2 are some symmetric and positive definite matrices. The inequalities (9) are equivalent to the following matrix inequalities

$$\begin{bmatrix} S_{11} & -P_1 B_i K_j & 0 \\ -(B_i K_j)^T P_1 & S_{22} & P_2 \\ 0 & P_2 & -\rho^2 I \end{bmatrix} < 0,\ i, j = 1, 2, ..., L, \tag{30}$$

where $S_{11} = P_1(A_i + B_i K_j) + (A_i + B_i K_j)^T P_1 + \frac{1}{\rho^2} P_1 P_1 + 2Q$, and $S_{22} = P_2 A_r + A_r^T P_2 + 2Q$.

The matrix inequalities (30) imply $S_{11} < 0$. Denote W=P_1^{-1} and $Y_j = K_j W$. $S_{11} < 0$ is equivalent to the linear matrix inequalities

$$\begin{bmatrix} S & W \\ W & -(2Q)^{-1} \end{bmatrix} < 0,\ i, j = 1, 2, ..., L, \tag{31}$$

where $S = A_i W + W A_i^T + B_i Y_j + (B_i Y_j)^T + (\rho^2)^{-1} I$.

P_1 and $K_j (j = 1, 2, ..., L)$ are obtained by (31).And then, substituting P_1 and $K_j (j = 1, 2, ..., L)$ into (30), P_2 is obtained.

Remark 2: If a controlled system is fourth-order, the dimension of the matrix inequalities (30) is 12. By use of the method in [12], the dimension of the matrix inequalities (58) is 20. By use of the method in [9], the dimension of matrix inequalities in Theorem 1 is no less than 20. Thus, the dimension of matrix inequalities is reduced.

4 Simulation example

Consider a 2-link manipulator system in [20]

$$M(q)\ddot{q}(t) + C(q,\dot{q})\dot{q}(t) + G(q) = \tau(t). \tag{32}$$

Consider the existence of the uncertainties and external disturbances in system (32). Thus, the plant is modified as follows:

$$\ddot{q}(t) + C(q,\dot{q})\dot{q}(t) + g(q) = B(q)u(t) + \sum_{i=1}^{r}\xi_i(t)q(t) + d\prime, \tag{33}$$

where $C(q,\dot{q}) = H^{-1}(q)C\prime(q,\dot{q}), g(q) = H^{-1}(q)g\prime(q), B(q) = H^{-1}(q), d\prime = H^{-1}(q)d, q = [q_1,q_2]^T$ and $u(t) = [u_1,u_2]^T = \tau(t)$. $\xi_i(t)(i = 1,2,...,r)$ are uncertain and bounded. d is random noise with zero mean and variance 0.05, and d is bounded.

The reference model is as follows:

$$\dot{x}_r(t) = A_r x_r(t) + r(t),$$

where

$$A_r = diag\{A_{r1},A_{r2}\}, A_{r1} = A_{r2} = \begin{bmatrix} 0 & 1 \\ -6 & -5 \end{bmatrix}, r(t) = [0,r_1(t),0,r_2(t)]^T.$$

Denote $x_1 = q_1, x_2 = \dot{q}_1, x_3 = q_2, x_4 = \dot{q}_2$. Fuzzy T-S model is used to approximate the nonlinear system at $x_1 = -\frac{\pi}{2}, 0, \frac{\pi}{2}$ and $x_3 = -\frac{\pi}{2}, 0, \frac{\pi}{2}$. The membership functions are adopted as triangle type. Fuzzy T-S model with Nine rules in the form (3) is given, where

$$A_1 = \begin{bmatrix} 0 & 1 & 0 & 0 \\ 5.927 & -0.001 & -0.315 & -0.0000084 \\ 0 & 0 & 0 & 1 \\ -6.859 & 0.002 & 3.155 & 0.0000062 \end{bmatrix}, A_2 = \begin{bmatrix} 0 & 1 & 0 & 0 \\ 3.0428 & -0.0011 & -0.1791 & -0.0002 \\ 0 & 0 & 0 & 1 \\ -3.5436 & 0.0313 & 2.5611 & 0.0000114 \end{bmatrix},$$

$$A_3 = \begin{bmatrix} 0 & 1 & 0 & 0 \\ 6.2728 & 0.003 & 0.4339 & -0.0001 \\ 0 & 0 & 0 & 1 \\ -9.1041 & 0.0158 & -1.0574 & -0.000032 \end{bmatrix}, A_4 = \begin{bmatrix} 0 & 1 & 0 & 0 \\ 6.5434 & 0.0017 & 1.2427 & -0.0002 \\ 0 & 0 & 0 & 1 \\ -3.1873 & 0.0306 & -5.1911 & -0.000018 \end{bmatrix},$$

$$A_5 = \begin{bmatrix} 0 & 1 & 0 & 0 \\ 11.1336 & 0 & -1.8145 & 0 \\ 0 & 0 & 0 & 1 \\ -9.0918 & 0 & 9.1638 & 0 \end{bmatrix}, A_6 = \begin{bmatrix} 0 & 1 & 0 & 0 \\ 6.1702 & -0.001 & 1.687 & -0.0002 \\ 0 & 0 & 0 & 1 \\ -2.3559 & 0.0314 & 4.5298 & -0.000011 \end{bmatrix},$$

$$A_7 = \begin{bmatrix} 0 & 1 & 0 & 0 \\ 6.1206 & 0.0041 & 0.6205 & 0.0001 \\ 0 & 0 & 0 & 1 \\ 8.8794 & 0.0193 & -1.0119 & 0.000044 \end{bmatrix}, A_8 = \begin{bmatrix} 0 & 1 & 0 & 0 \\ 3.6421 & -0.0018 & 0.0721 & 0.0002 \\ 0 & 0 & 0 & 1 \\ 2.429 & -0.0305 & 2.9832 & -0.000019 \end{bmatrix},$$

$$A_9 = \begin{bmatrix} 0 & 1 & 0 & 0 \\ 6.2933 & -0.0009 & 0.2188 & -0.000012 \\ 0 & 0 & 0 & 1 \\ -7.4649 & 0.0024 & 3.2693 & -0.0000092 \end{bmatrix}, B_1 = \begin{bmatrix} 0 & 1 & 0 & -1 \\ 0 & -1 & 0 & 2 \end{bmatrix}^T, B_2 = \begin{bmatrix} 0 & 0.5 & 0 & 0 \\ 0 & 0 & 0 & 1 \end{bmatrix}^T$$

$$B_3 = \begin{bmatrix} 0 & 1 & 0 & 1 \\ 0 & 1 & 0 & 2 \end{bmatrix}^T, B_4 = \begin{bmatrix} 0 & 0.5 & 0 & 0 \\ 0 & 0 & 0 & 1 \end{bmatrix}^T \; B_5 = \begin{bmatrix} 0 & 1 & 0 & -1 \\ 0 & -1 & 0 & 2 \end{bmatrix}^T, B_6 = \begin{bmatrix} 0 & 0.5 & 0 & 0 \\ 0 & 0 & 0 & 1 \end{bmatrix}^T$$

$$B_7 = \begin{bmatrix} 0 & 1 & 0 & 1 \\ 0 & 1 & 0 & 2 \end{bmatrix}^T, B_8 = \begin{bmatrix} 0 & 0.5 & 0 & 0 \\ 0 & 0 & 0 & 1 \end{bmatrix}^T \; B_9 = \begin{bmatrix} 0 & 1 & 0 & -1 \\ 0 & -1 & 0 & 2 \end{bmatrix}^T.$$

Using the LMI box in Matlab, $K_j (j = 1, 2, ..., L)$ are obtained

$$K_1 = \begin{bmatrix} -75.5707 & -41.2895 & -19.7728 & -8.9886 \\ 4.5163 & -0.5944 & -49.7511 & -24.5727 \end{bmatrix}, K_2 = \begin{bmatrix} -76.4364 & -41.3132 & -13.7595 & -5.9976 \\ 7.1834 & 1.0290 & -49.0587 & -24.2578 \end{bmatrix},$$

$$K_3 = \begin{bmatrix} -75.4503 & -41.2461 & -19.8614 & -9.0371 \\ 4.3907 & -0.6474 & -49.6965 & -24.54837 \end{bmatrix}, K_4 = \begin{bmatrix} -76.4364 & -41.3132 & -13.7595 & -5.9976 \\ 7.1834 & 1.0290 & -49.0587 & -24.2578 \end{bmatrix},$$

$$K_5 = \begin{bmatrix} -76.4364 & -41.3132 & -13.7595 & -5.9976 \\ 7.1834 & 1.0290 & -49.0587 & -24.2578 \end{bmatrix}, K_6 = \begin{bmatrix} -76.4364 & -41.3132 & -13.7595 & -5.9976 \\ 7.1834 & 1.0290 & -49.0587 & -24.2578 \end{bmatrix},$$

$$K_7 = \begin{bmatrix} -76.4364 & -41.9511 & -6.2666 & -2.2808 \\ 11.1565 & 3.4005 & -48.7116 & -24.1209 \end{bmatrix}, K_8 = \begin{bmatrix} -76.4364 & -41.3132 & -13.7595 & -5.9976 \\ 7.1834 & 1.0290 & -49.0587 & -24.2578 \end{bmatrix},$$

$$K_9 = \begin{bmatrix} lcl - 76.7763 & -42.0400 & -6.0715 & -2.1821 \\ -11.3875 & 3.4986 & -48.8204 & -24.1694 \end{bmatrix},$$

Then, the controller is given by

$$u(t) = u_l(t) - u_f(t),$$

where

$$u_l(t) = \sum_{i=1}^{9} \mu_i K_i (x(t) - x_r(t)) \; and \; u_f = (\sum_{i=1}^{9} \mu_i E_i)^{-1} \hat{u}(x|\Theta)$$

with the updating law (11). In (11), the symmetric and positive definite matrix

$$P = \begin{bmatrix} 0.0070 & 0.0035 & -0.0004 & -0.0002 \\ 0.0035 & 0.0021 & 0.0004 & 0.0001 \\ -0.0004 & 0.0004 & 0.0073 & 0.0032 \\ -0.0002 & 0.0001 & 0.0032 & 0.0017 \end{bmatrix}.$$

Seven fuzzy rules are defined in adaptive fuzzy logic systems.
$R^{(j)}$: if x_1 is F_1^j,..., x_4 is F_4^j, then y is G^j (j=1,2,...,7),

$$\mu_{F_i^1}(x_i) = \frac{1}{1+\exp[5(x_i+0.8)]}(i=1,2,...,4), \quad \mu_{F_i^1}(x_i) = \exp[-(x_i+0.6)^2](i=1,2,...,4),$$

$$\mu_{F_i^3}(x_i) = \exp[-(x_i+0.4)^2](i=1,2,...,4), \quad \mu_{F_i^4}(x_i) = \exp[-(x_i)^2](i=1,2,...,4),$$

$$\mu_{F_i^5}(x_i) = \exp[-(x_i-0.4)^2](i=1,2,...,4), \quad \mu_{F_i^6}(x_i) = \exp[-(x_i-0.6)^2](i=1,2,...,4),$$

$$\mu_{F_i^7}(x_i) = \frac{1}{1+\exp[5(x_i-0.8)]}(i=1,2,...,4).$$

$$\textbf{Denote } S_1 = \sum_{j=1}^{7}\sum_{i=1}^{4}\mu_{F_i^j}(x_i), \textbf{ then}$$

$$\xi(x) = \left[\prod_{i=1}^{4}\mu_{F_i^1}(x_i)/S_1, ..., \prod_{i=1}^{4}\mu_{F_i^7}(x_i)/S_1\right] = [\xi_1, ..., \xi_7], \Psi(x) = diag[\xi^T(x), \xi^T(x)].$$

The initial condition is set to be

$$(x_1(0), x_2(0), x_3(0), x_4(0), x_{r1}(0), x_{r2}(0), x_{r3}(0), x_{r4}(0)) = (0.4, 0, -0.4, 0, 0, 0, 0, 0).$$

Choose $r_1(t) = r_2(t) = 4sin(t), r = 2, \xi_1(t) = 1 + 20$ sin(t),ξ_2(t)=2(1-exp(-t))/(1+exp(-t)) and the parameter $\eta_1 = 20$. Simulation results are shown in Fig.1- Fig.3.

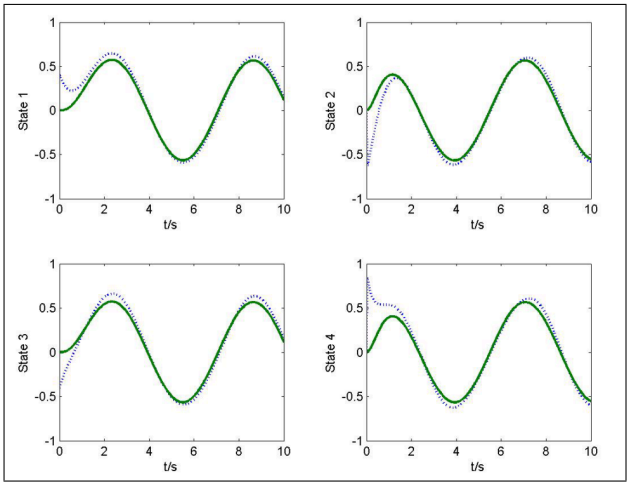

Figure 1: State responses of x_1, x_2, x_3 and x_4 (dotted line), x_{r1}, x_{r2}, x_{r3} and x_{r4} (solid line)

By only using the fuzzy controller based on T-S model [20], simulation result is shown in Fig.4 and the tracking performance comparison between proposed method and approach in [20] is given in table 1.

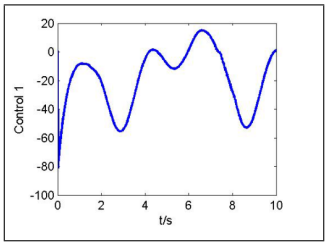

Figure 2: The control input u_1

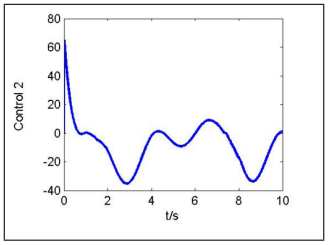

Figure 3: The control input u_2

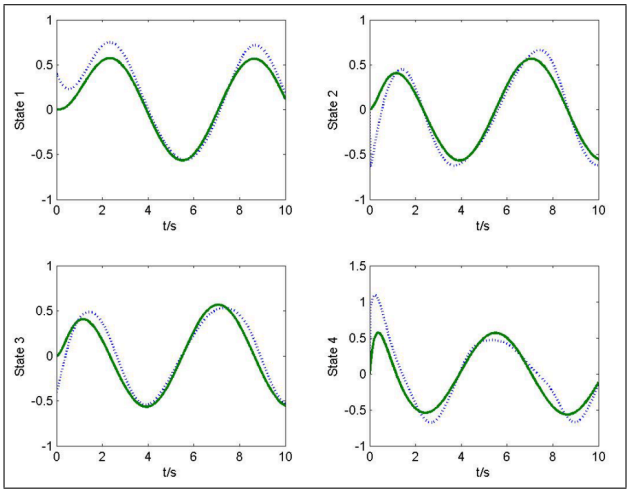

Figure 4: State responses of x_1, x_2, x_3 and x_4 (dotted line), x_{r1}, x_{r2}, x_{r3} and x_{r4} (solid line)

Table 1: The tracking performance comparison between proposed method and approach in [20].

$E_i = \int_0^t (x_i - x_{ri})^2 dt$	E_1	E_2	E_3	E_4
The proposed method	0.0677	0.1338	0.0587	0.2177
The method in [20]	0.1380	0.1760	0.1244	0.3343

5 Conclusion

The developed controller makes full use of the advantages of two fuzzy models. Theory analysis verifies the feasibility of the proposed control scheme and simulation results demonstrate the effectiveness of the proposed control scheme.

Acknowledgements
This work is supported by the National Natural Science Foundation of China (60974028).

Bibliography

[1] K.Tanaka, M.Sugeno. *Stability analysis and design of fuzzy control systems.* Fuzzy Sets and Systems,1992,45(2):135-156.

[2] Bong-Jae Rhee, Sangchul Won.*A new fuzzy Lyapunov function approach for a Takagi -Sugeno fuzzy control system design.* Fuzzy Sets and Systems, 2006, 157(9): 1211 - 1228.

[3] H. K. Lam, Lakmal D. Seneviratne. *Stability Analysis of Interval Type-2 Fuzzy-Model- Based Control Systems.* IEEE Transactions on Systems, Man, and Cybernetics-Part B: Cybernetics,2008,38(3): 617-628.

[4] Sung Hyun Kim ,Poo Gyeon Park.*Observer-Based Relaxed H∞ Control for Fuzzy Systems Using a Multiple Lyapunov Function.* IEEE Transactions on Fuzzy Systems, 2009,17(2):476-484.

[5] Antonio Sala, Carlos Ariño.*Relaxed Stability and Performance LMI Conditions for Takagi-Sugeno Fuzzy Systems With Polynomial Constraints on Membership Function Shapes.* IEEE Transactions on Fuzzy Systems,2008,16(5):1328-1336.

[6] Miguel Bernal, Thierry Marie Guerra,Alexandre Kruszewski.*A membership-function- dependent approach for stability analysis and controller synthesis of Takagi-Sugeno models.* Fuzzy Sets and Systems,2009,160(19):2776-2795.

[7] Yan-Wu Wang,Zhi-Hong Guan,Hua O.Wang.*Impulsive synchronization for Takagi-Sugeno fuzzy model and its application to continuous chaotic system.*Physics Letters A, 2005,339(3-5):325-332.

[8] Shinn-Horng Chen, Wen-Hsien Ho, Jyh-Horng Chou.*Robust Controllability of T-S Fuzzy-Model-Based Control Systems With Parametric Uncertainties.* IEEE Transactions on Fuzzy Systems,2009,17(6):1324-1335.

[9] J.C.Lo, M.L.Lin. *Robust nonlinear modeling and control via uncertain fuzzy systems.* Fuzzy Sets and Systems,2004,143(2):189-209.

[10] JunYoneyama.*Robust H∞ control analysis and synthesis for Takagi-Sugeno general uncertain fuzzy systems.* Fuzzy Sets and Systems 2006,157(16):2205- 2223.

[11] Fuwen Yang,Yongmin Li,*Set-Membership Fuzzy Filtering for Nonlinear Discrete- Time Systems.* IEEE Transactions on Fuzzy Systems,2010,40(1):116-123.

[12] B.S.Chen, C.S.Tseng, H.J.Uang. *Mixed fuzzy output feedback control design for nonlinear dynamic systems: an LMI approach.* IEEE Transactions on Fuzzy Systems,2000,8(3): 249-265.

[13] C.M.Park.*LMI-based robust stability analysis for fuzzy feedback linearization regulators with its application.*Information Sciences,2003,152:287-301.

[14] Changchun Hua, Qing-Guo Wang , Xinping Guan.*Robust Adaptive Controller Design for Nonlinear Time-Delay Systems via T-S Fuzzy Approach.* IEEE Transactions on Fuzzy Systems,2009,17(4):901-910.

[15] Guoliang Wei, Gang Feng, Zidong Wang . *Robust H∞ Control for Discrete-Time Fuzzy Systems With Infinite-Distributed Delays.*IEEE Transactions on Fuzzy Systems,2009,17(1) 224-232.

[16] Li-Xin Wang. *Stable adaptive fuzzy control of nonlinear systems.* IEEE Transactions on Fuzzy Systems, 1993,1(3): 146-155.

[17] Weisheng Chen, Zhengqiang Zhang. *Globally stable adaptive backstepping fuzzy control for output-feedback systems with unknown high-frequency gain sign.* Fuzzy Sets and Systems, 2010, 161(6): 821-836.

[18] Huai-Ning Wu, Kai-Yuan Cai.*H2 guaranteed cost fuzzy control for uncertain nonlinear systems via linear matrix inequalities.* Fuzzy Sets and Systems, 2004,148(3):411-429.

[19] Y. Liu, S.S. Hu. *Fuzzy Robust Tracking Control for Uncertain Nonlinear Systems.* Acta Automatica Sinica. 2004,30(6):949-953.

[20] C. S. Tseng, B. S. Chen, H.J. Uang. *Fuzzy tracking control design for nonlinear dynamic systems via T-S fuzzy model.* IEEE Transactions on Fuzzy Systems,2001,9(3): 381-392.

Int. J. of Computers, Communications & Control, ISSN 1841-9836, E-ISSN 1841-9844
Vol. VII (2012), No. 1 (March), pp. 73-89

A WPAN Platform Design in Mobile Phone Considering Application Development and Usability

I.-H. Kim, G.-M. Jeong, E.-C. Park, K.-D. Chung

In-Hwan Kim
Mobile Device Development Team
SK Telecom, Seoul, Korea
E-mail: inhwan.kim@sk.com

Gu-Min Jeong
School of Electrical Engineering
Kookmin University, Seoul, Korea
E-mail: gm1004@kookmin.ac.kr

Eun-Chan Park
Department of Information and
Communication Engineering
Dongguk University-Seoul, Korea
E-mail: ecpark@dongguk.edu

Ki-Dong Chung
School of Computer Science and Engineering
Pusan National University, Pusan, Korea
E-mail: kdchung@pusan.ac.kr

Abstract: In this paper, we propose a WPAN (Wireless Personal Area Network) platform for converged network services integrating a cellular network and a WPAN. We mainly focus on an easy-to-develop and easy-to-use WPAN platform for wireless communication services using both networks. The proposed WPAN platform consists of a WPAN handset platform, a WPAN connection scheme, and a WPAN server platform. The WPAN handset platform provides abstract WPAN API (Application Programming Interface) set and application management module. Using the WPAN connection scheme, the user can enjoy converged network services in a convenient way. The WPAN server platform manages the overall services and digital devices that are connected to the handset. Compared to the existing WPAN related platform, we consider the need for the integrated service components allowing for the development of WPAN applications in the handset and their convenience for the user. Also, illustrative services and devices are implemented using the proposed method, which show the applicability of the proposed WPAN platform.
Keywords: WPAN, Converged Network, Platform, API Abstraction, Connection Scheme, Server Structure, Mobile Game

1 Introduction

Mobile phones are becoming essential devices thanks to their portability and mobility. Numerous new technologies are being merged into mobile handsets and various new services are provided based on cellular networks, leading to the development of ubiquitous services [1].

Recently, wireless network technologies such as Mobile WiMAX (Worldwide Interoperability for Microwave Access), WPAN, and WLAN (Wireless Local Area Network) have become alternatives to high rate data services. Although each technology has its own benefits, enhanced

services cannot be developed without a cellular network. With this in mind, various studies have been conducted on the interoperability and integration for the heterogeneous networks [2]-[9].

Among these, WLAN and WPAN are generally adopted in mobile phones. Although 3G and WLAN interworking makes WLAN popular in smart phones, WPAN [10]-[12], which is widely used in mobile phones, also has its own advantages such as convenient device connection and reduced power consumption for mobile phones. Especially, Bluetooth [10] is used in mobile phone for the headset and data transmission. However, since the main objective of the WPAN is to connect devices without cables, the usage of WPAN in mobile phone is somewhat restrictive when it comes to providing ubiquitous network services [2], [13]. For example, Bluetooth is used only for the headset, the connection to a PC, or the connection to other handsets. Likewise, the use of the WPAN in mobile phone appears to be independent of the cellular network. This has been a major drawback of the application of WPAN to mobile phones.

Up to now, there have been many studies on the integration of WPAN and cellular networks and the convenience of such integration for the user. With JSR (Java Specification Request)-82 [14], Bluetooth APIs are provided in the J2ME (Java 2 Platform, Micro Edition) environment, which makes it possible to utilize both Bluetooth and a cellular network. The Gaia platform [15] supports a middleware for ad-hoc pervasive computing. Also, CTIA (Cellular Telephone Industries Association) provides a certification and test rules for the interoperability of Bluetooth devices in order to enhance their usability [16]-[17].

Considering these points discussed herein, we can think that for the converged network services, there must be consideration for the APIs in mobile phone, the user scenario, server structure and application management.

In this paper, we propose a WPAN platform that integrates a cellular network and a WPAN, in order to provide ubiquitous network services and implement converged network services. We primarily consider the development of services which utilize both networks fully. Compared to the existing WPAN integrations, we focus on the platform environment and user applicability of the wireless communication services being developed. We summarize the concept of the converged network service and propose a WPAN handset platform, a WPAN connection scheme, and a WPAN server platform in this paper. For the design of the WPAN handset platform, we investigate various use cases of service scenarios and integrate the cellular network and the WPAN in mobile handsets. The WPAN server platform takes control of the services and devices connected to the handset. Also, for the convenience of the user, a WPAN connection scheme is presented.

Although the platform is implemented with Bluetooth at present, the overall architecture is designed to take into consideration its extension to other WPAN technologies, and the implementation of ZigBee and UWB (Ultra-Wide Band) is currently underway.

To show the validity of the proposed platform, we present various illustrative implementation and service examples such as a PC to phone application, phone to phone game, Voice Terminal, PMP (Portable Media Player) and LBS (Location Based Service).

The remainder of this paper is organized as follows. In Section II, related work is briefly introduced. In Section III, we summarize the basic concept of the converged network services and the proposed WPAN platform. In Sections IV, V and VI, we present the WPAN handset platform, the WPAN connection scheme, and the WPAN server platform, respectively. In Section VII, performance evaluation is presented considering number of API calls. In Section IIX, service implementations are described and the conclusion follows in Section IX.

2 Related Works

Since WPAN is widely used in mobile phones, many studies have been conducted on integration of WPAN and various standards have been established. Also, many researches have been performed on the implementation of ubiquitous services.

Until now, the integration of WPAN in mobile phones has generally focused on the WPAN functions in the mobile phone. However, little consideration has been given to the development of converged network services and the convenience of the user.

JSR-82 (JavaTM APIs for Bluetooth) [14] is a standard of JCP (Java Community Process), which provides Bluetooth APIs for the J2ME environment. There are standard APIs for the various Bluetooth profiles. Using JSR-82, WPAN functions can be supported in handsets. JSR-82 supports only Bluetooth APIs and there still remain other platform components for converged network services.

Recently, CTIA makes a certification program for Bluetooth, viz. the BCCP (Bluetooth Compatibility Certification Program). Bluetooth devices made by different companies provide different user scenarios and this may cause inconvenience to the user. Considering these points, CTIA presents the BCCP with consideration given to the end-user perspective [16]-[17].

To provide ubiquitous services, many platform structures have been suggested [18]. Among them, Gaia [15] provides a middleware for ad-hoc pervasive computing. The structure of Mobile Gaia supports various mediums such as Bluetooth, IrDA, Wi-Fi, Ethernet, etc. and provides core services such as discovery and cluster management services, event services, location services, context services and security services.

Also, PNM (Personal Network Management) [19]-[20] deals with the composition of private networks for UMTS or GSM networks and the control of the UE (User Equipment). PNM is a home network-based application provides for the home network-based management of Personal Networks (PN) consisting of multiple devices belonging to a single user, as described in 3GPP TS 22.259. Basically, PNM describes the protocols required for the composition of private networks and user equipment.

As described in related works, in order to provide WPAN services and ubiquitous services efficiently in mobile phones, we should consider the easy development and the easy use of WPAN applications. Considering these points and related works, a WPAN platform is designed and implemented in this study.

3 Basic Concept of Converged Network Services

In this section, we present a basic concept of the proposed WPAN platform and the WPAN platform-based services.

WPAN technologies are mainly used for the connection between the mobile handset and other devices. They are adopted only for data transmission among devices or for headset functions. However, if we integrate the cellular network and the WPAN effectively, various converged network services can be developed easily.

Table 1 shows service examples of the integration of WPAN and the cellular network. As shown in Table 1, handsets can connect to handsets, application devices, and access points. Various ubiquitous services can be provided using the cellular network and the WPAN.

This paper proposes a WPAN platform which enables the service providers to develop the services listed in Table 1 more easily. Considering the service development of services, we aim to design a WPAN platform that integrates the cellular network and the WPAN effectively.

In fact, the services in Table 1 could be developed without the proposed WPAN platform. However, they can be developed more easily if the proposed WPAN platform is applied and the

Table 1: The classification of WPAN services

Service Type	Example
Handset to Handset Services	Community Service, Contents Distribution, Handset to Handset game, etc.
Handset to Application Device Services	Dial-Up Networking, SMS Forwarding, Phonebook Sync, Contents Download for Application Device
Handset to Access Point Services	Zone Based Services such as Location-based Service, Personalized Service, D-Home, Home Security, etc.

service scenario can be more practical.

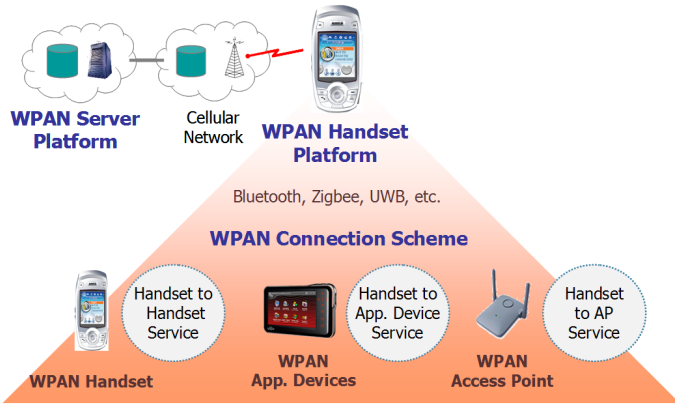

Figure 1: Overview of various converged network services

Figure 1 shows the basic concept of the proposed WPAN platform and the service flow. The proposed platform consists of the WPAN handset platform, the WPAN server platform, and the WPAN connection scheme. The WPAN handset platform provides abstract WPAN APIs and an application management module that enables service developers to create WPAN services more easily. The WPAN connection scheme offers a convenient user scenario for WPAN services. The converged network services and service scenarios may be unfamiliar to the user. Using this scheme, we can make the service scenario easy to use. The WPAN server platform manages the devices connected to the handset provides the handset with appropriate services. Also, provisioning and downloads are handled in this platform.

4 WPAN HANDSET PLATFORM

This section deals with the WPAN handset platform. We design abstract APIs and an application management module in this platform.

4.1 Basic structure of the WPAN handset platform

For the developers who are not familiar with WPAN technology, we aim to provide an easy development environment using this platform. Considering this objective, the major characteristics of the proposed platform are as follows:

- We provide both cellular network APIs and WPAN APIs for the developers.
- The WPAN APIs are abstracted for the easy development of WPAN applications.
- Though the current implementation is for Bluetooth, the platform design considers its extension to ZigBee and UWB.
- Different from other applications, WPAN applications should be executed without any user input. We provide the application management module and PAN Agent for this purpose.

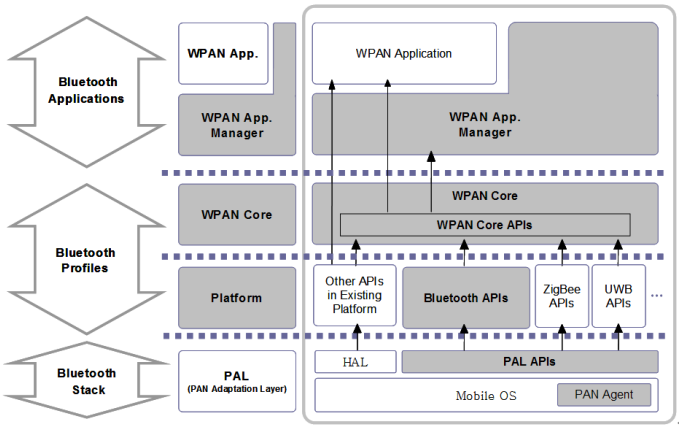

Figure 2: WPAN handset platform architecture

Figure 2 shows the WPAN handset platform architecture. In order to implement abstract APIs, we design a layered structure. The gray areas in Figure 2 are the platform components of the WPAN handset platform. The WPAN APIs have three layers, which are the PAL Layer, Platform Layer, and WPAN Core Layer. Also, for the management of WPAN applications and their connections, the WPAN Application Manager (WAM) and the PAN Agent are provided. The detailed descriptions of the each abstraction layer are as follows:

- PAL (PAN Adaptation Layer) is a HAL (Hardware Adaptation Layer) related to WPAN technologies and implemented by the manufacturer.
- In the Platform Layer, APIs for each WPAN technology (e.g., Bluetooth, ZigBee, UWB, etc.) are implemented using the PAL Layer. In order to use the APIs in the Platform Layer, developers must know each WPAN technology in detail. Besides the WPAN APIs, the Platform Layer supports numerous API sets such as UI, memory, and process.
- The WPAN Core Layer provides the encapsulated WPAN Core APIs, which are independent of the WPAN technologies. Using WPAN Core APIs, services can be implemented without any specific knowledge of each WPAN technology. Also, the applications are independent of the WPAN physical layer.

For the management of the WPAN applications and connections, the WPAN platform provides the WAM (WPAN Application Manager) and the PAN Agent.

- The WAM handles the WPAN applications, user interface, and WPAN events that are sent to the handset. The WAM can be implemented using the Platform Layer and the WPAN Core API.

- The PAN Agent is a kind of daemon process and always runs in background mode. Regardless of the state of the handset, the PAN agent receives WPAN events and delivers them to the WAM. Therefore, though the handset is in an idle state, it can receive and send WPAN events to the WAM.

For developers who are familiar with each WPAN technology, PAL APIs can be used directly. In this case, it is possible to access each profile directly.

4.2 Design of Abstract WPAN APIs

Table 2: Abstraction Example from the PAL to the WPAN Core APIfor the Connection Function

Layer	Description	Prototype
WPAN Core API	Connect to device	M_Int32 WPAN_Connect(M_Int32 fd, Callback cb);
WPAN API	Get fd for BT SPP connection	M_Int32 BT_Connect(M_Int32 spp_fd,MC_BluetoothSDPInfo *btSDPInfo, SVCCONNECTCB cnncb);
PAL API	Get fd for BT SPP connection	Typedef M_Int32(*DEVCONTROLFUN) (M_UInt16 devnum, M_char *cmd, void *param1, void *param2);

Table 2 shows the abstraction step of APIs for Bluetooth, where the WPAN_connect() API is presented. The PAL Layer is an implementation of a device driver level. In the Platform Layer, there is a Bluetooth-level API. Finally, in the WPAN Core Layer, WPAN_Connect() is provided. Developers can get the fd (file descriptor) for the communication and then use the WPAN_Connect() API. Therefore, without specific knowledge of the Bluetooth SDP and SPP, one can develop WPAN applications easily.

Table 3: WPAN Core APIs

APIs	Descriptions
WPAN_ONOFF()	Turn on/off the hardware module for the WPAN (Bluetooth, ZigBee, UWB, etc.) in the WPAN handset.
WPAN_Create()	In the server mode of WPAN handset, get the fd after making a serial port channel, and then remain in the listen state.
WPAN_GetPairedList()	Get the list of devices that were connected before.
WPAN_Connect()	In the client mode of the WPAN handset, connect to the server and get the fd for the connected serial port channel.
WPAN_Disconnect()	Disconnect the serial port connection between the server and the client.
WPAN_Remove()	In the server mode of the WPAN handset, release the listen state of the serial port channel
WPAN_spClose()	Close the connected serial port channel.
WPAN_SendData()	Send data to the connected serial port channel.
WPAN_ecvData()	Receive data from the connected serial port channel.
WPAN_GetLocalInfo()	Get the information such as device name, BD_ADDR of the WPAN handset.
WPAN_GetLibVersion()	Get the version information of the WPAN Core Library.

Table 3 shows the list of WPAN Core APIs. As shown in Table 3, WPAN Core APIs are independent of WPAN technologies.3 The proposed WPAN handset platform is implemented

only for Bluetooth. However, the applications developed with the proposed platform can be easily adapted for other WPAN technologies, as shown in Figure 3. Figure 3 shows an example of a game application. Since the application is independent of the physical layer, it is possible to re-use the source code of the applications and run them regardless of the WPAN physical layer.

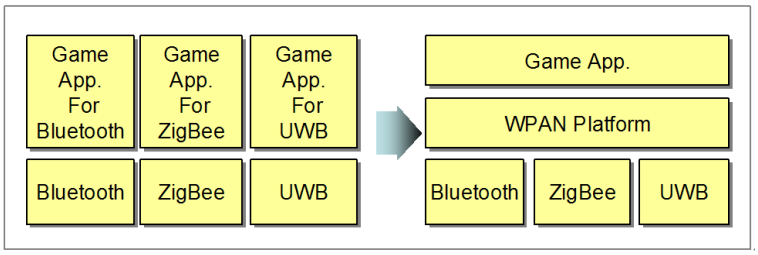

Figure 3: Platform that is independent of WPAN physical layer

In fact, the characteristics of each WPAN technology must be considered. We are currently developing a Platform Layer for ZigBee and UWB. Also, the development of an API set design for the differences between the various WPAN technologies remains future work.

5 WPAN Connection Scheme considering user scenario

In this section, we introduce various issues concerning the WPAN services in the handset and the WPAN connection scheme. WPAN services need a usage scenario that is different from cellular network services. This can be inconvenient for the user. The WPAN connection scheme considers these points and makes it easier for the user to enjoy the services.

5.1 Easy-to-use WPAN connection scheme

To make a connection between devices in the WPAN, one of the devices must be in the standby mode. However, it is inconvenient for the user to set the WPAN handset to the standby mode manually to receive the WPAN service. For example, if the user enters a zone providing for LBS (location based service) and sets the handset to the standby mode manually to receive LBS messages through the WPAN, he or she may feel that the process is complicated. This can be a drawback for such services. Hence, the user should be able to receive any WPAN event without needing to type any input into the handset.

To overcome this problem, we present a scheme which enables the new connection to be conveniently set up. Figure 4 shows the processes of the WPAN platform for the serial port channel connection.

The detailed scenario is as follows:

- The WPAN handset always opens one serial port channel to receive a WPAN event. If other devices try to connect to this WPAN handset, they must try to connect to this serial port channel.
- The connection request to the serial port arrives from the sending device to the handset.
- When receiving a WPAN event (sp_connected_event) for the connection to the open serial port channel, the PAN agent executes the WAM and sends information including the BD_ADDR of the sending device and event (sp_connected_event) to the WAM.

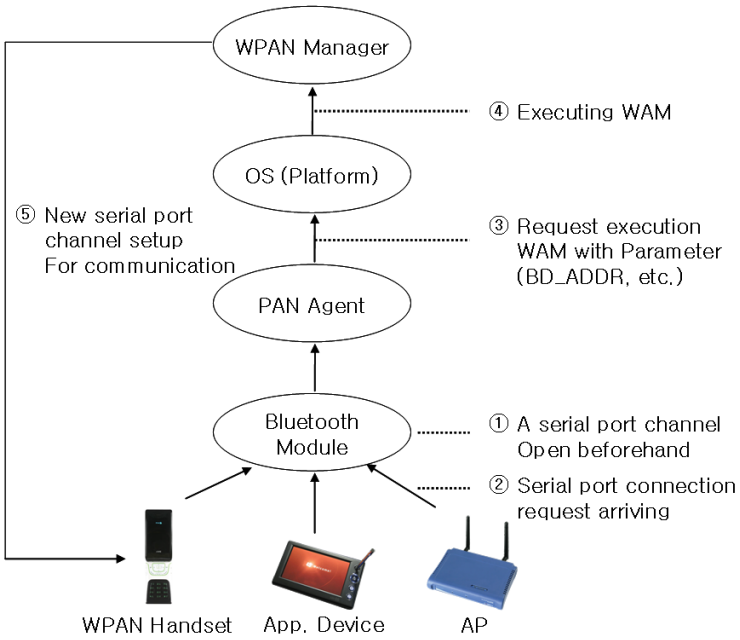

Figure 4: The process used to make a new WPAN connection

- The WAM is executed.

- The WAM creates a new SPP channel, connects to the sending device, and closes the existing connection. Then all events are processed using the new serial port channel. Also, connection requests from other more devices are handled using the conventional serial port channel.

If the event is managed at a lower level, rather than the platform level, additional services cannot be provided. Using the proposed method, however, the event is handled at the platform level and the user can be provided with additional services.

5.2 Authentication between Devices

The WPAN has its own authentication process according to the security level. In Bluetooth, almost all of the devices use Security Level 2 and the user must input a PIN code to the device. This can be a drawback for WPAN services.

To overcome these problems, in this paper, a pre-defined number is used as the PIN code for the connection. To compensate for the resulting lack of security, the WPAN platform authentication process is performed after the serial port channel connection is opened. We adopt the Blowfish encryption algorithm. After the connection is established, the authentication procedure using the Blowfish algorithm is performed at the serial port level and is independent of the Bluetooth encryption. After the successful authentication, the serial port channel remains open. Otherwise, it is closed. This can block anonymous connections from external devices. Figure 5 shows the authentication and execution procedures used in the proposed WPAN platform. Devices which are successfully authenticated can execute all WPAN applications of the WPAN handset.

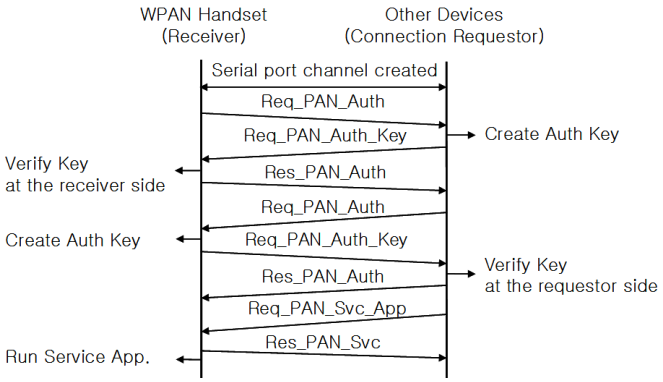

Figure 5: Authentication and application execution flow

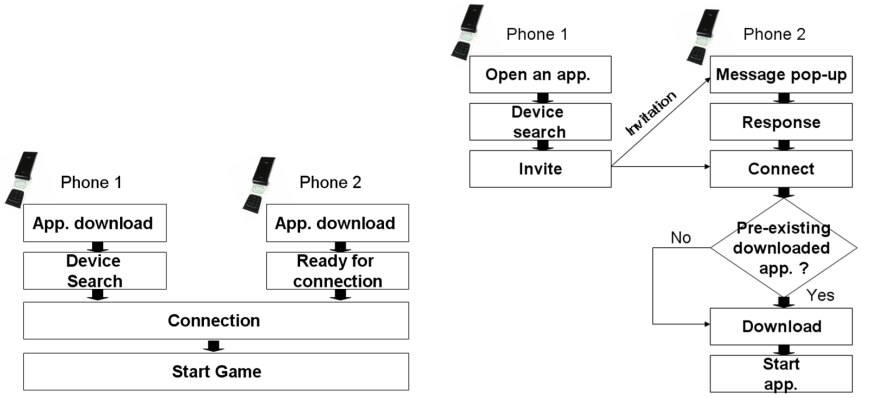

(a) Conventional WPAN user scenario (b) The proposed user scenario for WPAN applications

Figure 6: WPAN application scenario for usability

5.3 User scenario for the WPAN applications between users

One of the major drawbacks of WPAN applications is the user scenario. Because there is no standard of user scenario for WPAN applications in mobile phones, the usage of applications depends on the manufacturers of the mobile phone and other WPAN devices.

In the conventional method, for phone to phone applications using WPAN, user 1 executes a WPAN application and waits for the response, as shown in Figure 6(a). Then, user 2 executes the application and connects to user 1. The connection is established only when the users have downloaded the application. If the application has not yet been downloaded, the user must do so manually. This is inconvenient for the user and makes the usage complicated.

In the proposed method, as shown in Figure 6(b), the connection is set up even if user 2 does not have the application. In this case, user 2 can download the application through the cellular network after the connection is made.

6 WPAN Server Platform

To provide the user with various converged network services, the server should manage the information of the devices that are connected to the WPAN handset and handle the contents and

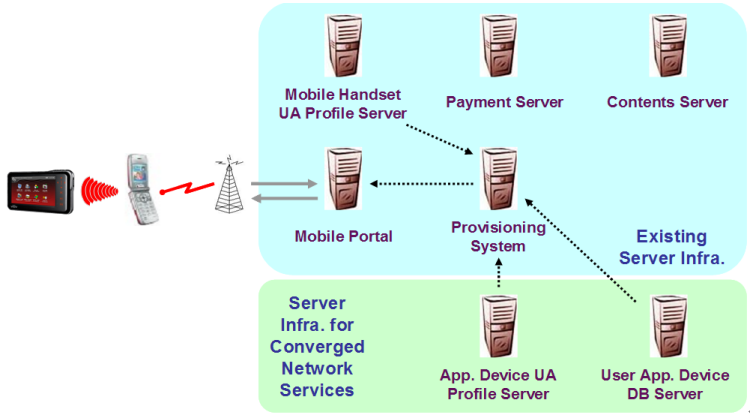

Figure 7: Server infrastructures for converged network services

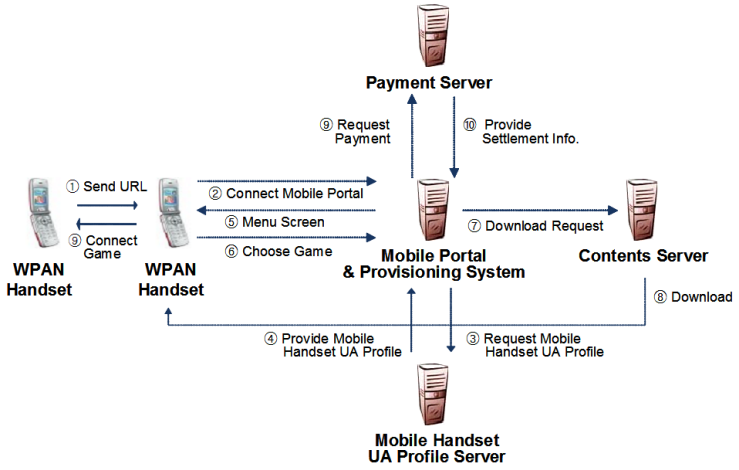

Figure 8: Server infrastructures and service flow for a converged network game

services according to the devices. We present a WPAN server architecture for WPAN applications and services, as shown in Figure 7.

Service providers keep the DB (Data Base) information of the subscriber's mobile handset in a UA (User-Agent) Profile Server. This enables the user to receive appropriate services for the user's mobile handset. Likewise, in the proposed converged network service, the service provider must keep the information of the application devices and match them to the user's mobile handset. For this purpose, the App. Device UA Profile Server and the User App. Device DB Server are required.

- The App. Device UA Profile Server provides the information required for the services according to the App. Device for the provisioning system. It manages properties such as the information of the App. Device and the service categories.
- The User App. Device DB Server handles the list of all of the App. Devices that the subscriber owns.
- When a WPAN handset connects to a Mobile Portal, the Provisioning System provides the information about mobile handset connected to the Mobile Portal using the Mobile

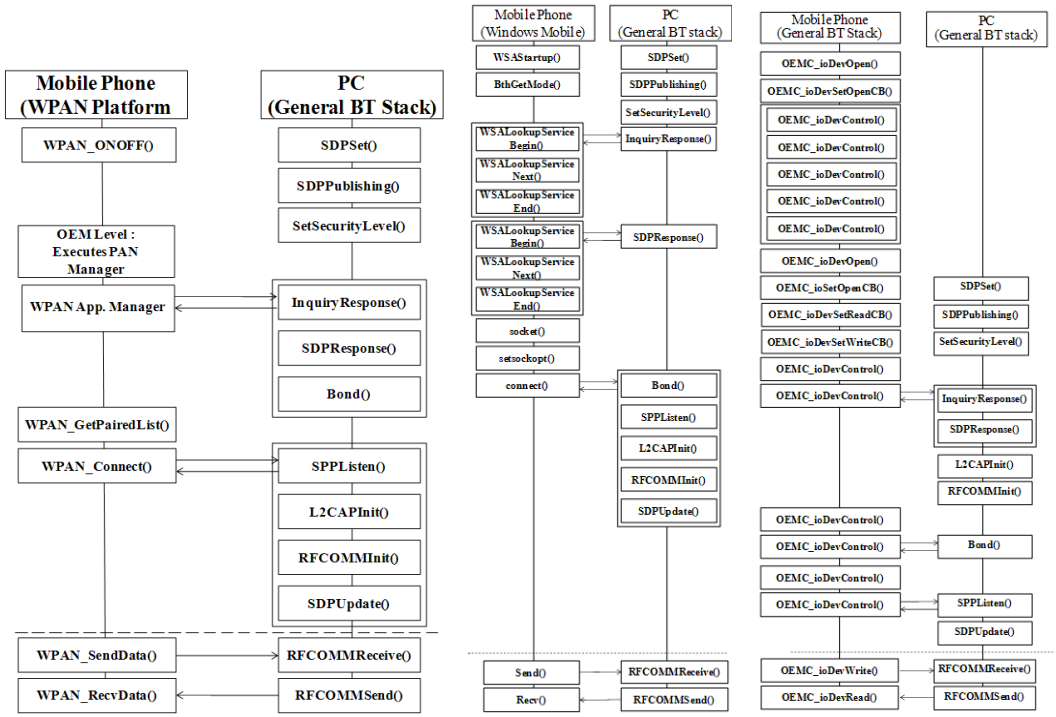

(a) WPAN platform (b) MS stack (c) General BT stack

Figure 9: API flows and number of API calls for connection using WPAN platform, general BT stack and MS stack

Handset UA Profile Server, the App. Device UA Profile Server and the User App. Device DB Server. Afterwards, the Mobile Portal can provide the user with proper contents and services. There must be an additional interface between the conventional provisioning system and the additional servers.

Figure 8 shows an example of the server infrastructure and service flows for mobile game contents. One can request to play a WPAN game with another user by transmitting the game ID and the URL location of the game. If the game does not exist in the handset, its contents can be downloaded using the URL information. In this case, the mobile portal decides whether the game is appropriate for the handset through the Mobile Handset UA Profile System. If so, the game is downloaded to the handset using both the contents server and the payment server.

For the connection of application devices such as PMP, PDA, and MP3P, we must use the App. Device UA Profile System and the User App. Device DB Server to download the contents.

7 Performance Evaluation of the presented WPAN platform

In this section, we present a performance evaluation of the proposed WPAN platform considering API calls for application development. In fact, performance evaluation of a platform depends on applications and performance indices. In this section, we focus on the number of API calls for an application development using WPAN core APIs in Table 3.

Although the comparison depends on applications and programming language, we make evaluation based on C/C++ APIs. We design PC to phone connection application for the different API sets, which are the presented APIs in Table 3, Windows Mobile Bluetooth stack and general BT stack.

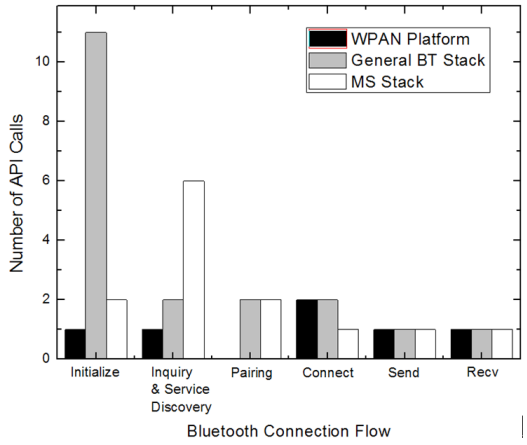

Figure 10: Number of API calls for different API sets

Table 4: Number of API calls

	WPAN Platform	MS Stack	General BT Stack
Initialize	1	2	11
Inquiry and Discovery	1	6	2
Pairing	0	2	2
Connect	2	1	2
Send	1	1	1
Receive	1	1	1
Total	6	13	19

Using the WPAN platform, the connection is processed as the following sequences.

- Turn on the Bluetooth module. (WPAN_ONOFF())
- Invoke the WPAN manager and search for WPAN devices. Then, exchange the PIN code and perform authentication. (WPAN Manager)
- Get the list of the searched devices. (WPAN_GetPairedList())
- Request connection and make the connection. (WPAN_Connection())
- Exchange data between PC and handset. (WPAN_SendData(), WPAN_RecvData())

Figure 9 shows the API flows for the PC to phone connection using WPAN platform, MS stack and general BT stack, respectively. As shown in Figure 9, the connection procedure can be made easily using WPAN platform.

Figure 10 and Table 4 show the number of API calls for the process of application. The total number of API calls is about 6, 13 and 19 for WPAN platform, MS stack and general Bluetooth stack respectively, in a sample application. As shown in Figure 9, Figure 10 and Table 4, we can develop the WPAN applications easily using WPAN Platform APIs.

8 Illustrative Services

To show the validity of the proposed WPAN platform, we present illustrative service examples adopting the proposed WPAN platform. As examples of converged network services, a PC to phone connection, handset to handset game, Voice Terminal, PMP, and LBS are introduced. For example, aside from the existing Bluetooth handset to handset games, the proposed game design considers a full connection between the cellular network and the WPAN.

8.1 PC to phone connection

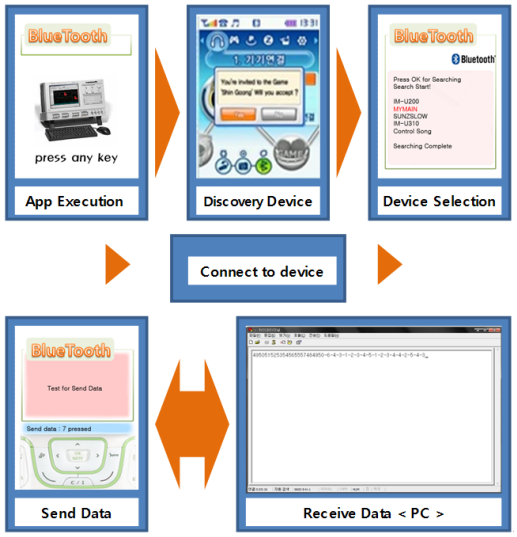

Figure 11: Example of data transmission between PC and mobile phone

Figure 12: Converged network service using PC to phone connection

Although PC to phone connections are widely used already, we present an implementation of a PC to phone connection using the proposed platform in order to validate the proposed WPAN APIs for the connection to general Bluetooth devices. Using a PC, the user can download various multimedia contents, as well as phone books, pictures, etc. In Section 7, overall connection procedure is briefly introduced already. Figure 11 shows an example of data transmission between the PC and mobile phone.

Also, as seen in Figure 12, various services can be made through the converged networks, i.e., Bluetooth connection between PC and mobile phone, internet and 3G network.

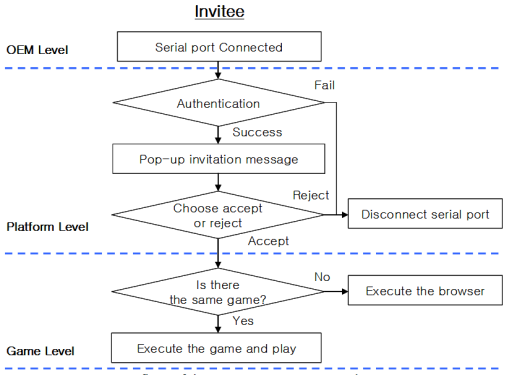

Figure 13: A flow of the WPAN game setup and termination

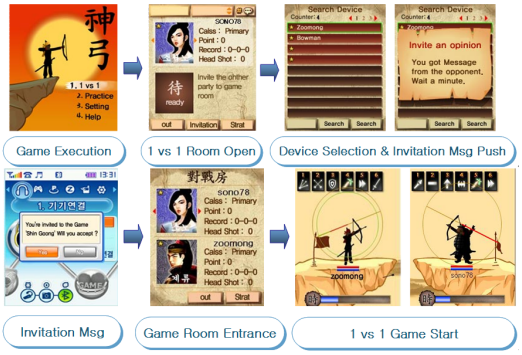

Figure 14: A WPAN game scenario with screen shots

8.2 Mobile Game using WPAN Platform

In a conventional mobile game in a mobile phone, people play locally after downloading the game using a cellular network. Otherwise, they can enjoy online games through a cellular network. In a converged network environment, we can provide various service models for mobile games by using both the cellular network and WPAN. First, we can apply new items or characters to the existing game through the cellular network and it is possible to download charged items with the connection of the mobile payment service. In addition, we can download the scenarios of the game itself. Second, it is possible to play the game among WPAN game groups. This can be used in a large scale game such as a role playing game.

Using the platforms and schemes presented in this paper, a new mobile game model can be derived. As shown in Figure 6 and Figure 13, we can have a new user scenario model for mobile games. A game user can invite any new user or registered user to play a WPAN game. A counterpart who receives a WPAN event for the game request can choose to accept or reject the invitation. If the game does not exist on the receiver side, the WPAN platform (WPAN App. Manager, to be exact) invokes the WAP (Wireless Application Protocol) browser in order to download the game application to the mobile handset through the cellular network. Figure 13 shows the flow of the WPAN game setup and termination in terms of the invitee and Figure 14 shows an example of the WPAN game scenario with screen shots. Likewise, the WPAN platform must identify the existence of the game according to the request message. If the game is not present on the handset, it should be downloaded and the connection setup should be processed.

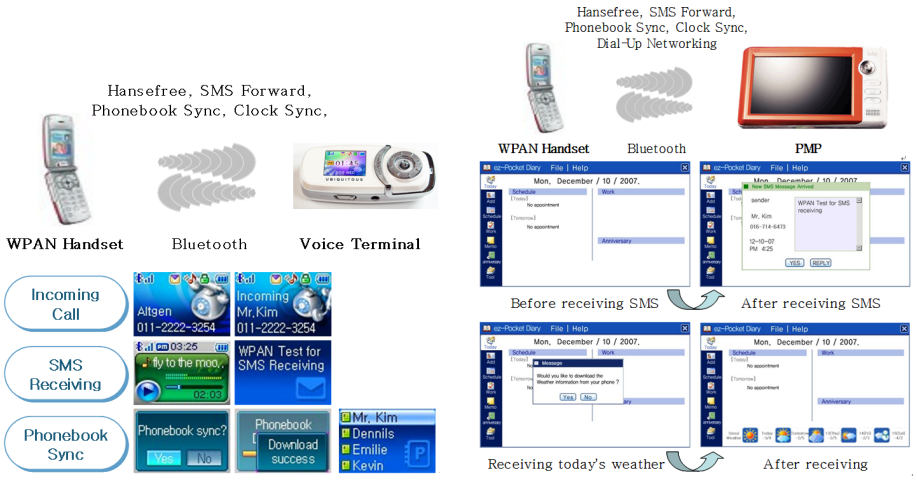

(a) Voice Terminal and its functions

(b) PMP interacting with a WPAN handset and its functions

Figure 15: Voice Terminal and PMP

8.3 Voice Terminal

A Voice Terminal is a digital device using the WPAN platform functioning as both an MP3 Player and a headset. In addition, users can receive SMS messages and make calls by selecting one of the phone numbers from the downloaded phone book.

By directly using the Handsfree profile of Bluetooth in PAL APIs, one audio link (SCO Link) and one data link (ACL Link) are established between the handset and Voice Terminal. The SCO link is used for the Handsfree function and PCM data is transmitted using the SCO link. The ACL link is used for control commands (AT commands). After the Handsfree profile connection is established, another data link (ACL Link) is connected to the Voice Terminal. Through this data link, the SMS or phonebook can be downloaded from the handset. Users can see the SMS and make calls with the Voice Terminal. Likewise, new functions can be added using new data links and new protocols.

Figure 15(a) shows the appearance of the Voice Terminal and its functions.

8.4 Portable Media Player

A PMP can be connected to the handset and various applications can be provided. First, SMS forwarding, phonebook, clock sync, and Handsfree functions can be adapted for the PMP. Second, The PMP can be connected to the internet through the WPAN and the cellular network using dial-up networking.

Figure 15(b) shows an overview of the implemented PMP and some of its functions.

8.5 LBS using Bluetooth AP

We can develop Location Based Services using WPAN platform in mobile phone. In the BT based service, the location estimation can be more precise than those of GPS and cellular network for indoor applications. Figure 16 shows a basic concept of LBS using Bluetooth.

Figure 16: . Location Based Service using BT access point

9 Conclusion

In this paper, we proposed a WPAN platform architecture that integrates a cellular network and a WPAN, presenting illustrative service implementations of the platform. For the development of wireless communication services, we introduced the WPAN handset platform, WPAN server platform, and WPAN connection scheme.

The WPAN handset platform supplies WPAN APIs and cellular network APIs in order to integrate both networks. The WPAN APIs are abstracted for the easy development of WPAN services. Considering the various user scenarios, a WPAN connection scheme, which consists of easy-to-use WPAN connections, a WPAN authentication scheme and user scenario for WPAN applications was proposed. The WPAN server platform manages the connected devices and content related functions.

To demonstrate the applicability of the proposed platform, a PC to phone connection, mobile game, Voice Terminal, PMP and LBS implementation were discussed. The proposed architecture was implemented based on Bluetooth and has since been commercialized.

Also, as part of this study, the basic concept of converged network services was proposed and adopted as work item under the name of CPNS (Converged Personal Network Service) in OMA (Open Mobile Alliance) and AD (Architecture Document) process is in progress.

The development of an API set design for the differences between the various WPAN technologies remains future work.

Acknowledgments

This work was supported in part by the research program 2009 of SK Telecom, Korea and also supported in part by the Ministry of Knowledge Economy (MKE), Korea, under the Information Technology Research Center (ITRC) support program supervised by the National IT Industry Promotion Agency (NIPA) (NIPA-2011-C1090-1121-0005). K.-D. Chung is the corresponding author.

Bibliography

[1] Mark Weiser, The Computer for 21st Century, *Scientific American*, pp. 94-104, Sep., 1991.

[2] H. Kanna, N. Wakabayashi, R. Kanazawa, and H. Ito, Home appliance control system over Bluetooth with a cellular phone, *ICCE 2003*, pp. 380 - 381, 2003.

[3] A. K. Salkintzis, Interworking Techniques and Architecturees for WLAN/3G Integration toward 4G Mobile Data Networks, *IEEE Transactions on Wireless Communications*, vol. 11, no. 3, pp. 50-61, June 2004.

[4] D. I. Axiotis, T. Al-Gizawi, K. Peppas, E. N. Protonotarios, F. I. Lazarakis, C. Papadias, and P. I. Philippopoulos, Services in interworking 3G and WLAN environments, *IEEE Transactions on Wireless Communications*, vol. 11, no. 5, pp. 14-20, Oct., 2004 .

[5] M. Buddhikot, G. Chandranmenon, S. J. Han, Y. W. Lee, S. Miller, and L. Salgarelli, Integration of 802.11 and third generation wirelesss data networks,*Proceedings of IEEE Infocom*, 2003.

[6] M. Buddhikot, G. Chandranmenon, S. J. Han, Y. W. Lee, S. Miller, and L. Salgarelli, Design and implementation of a WLAN/cdma2000 interworking architecture, *IEEE Communications Magazine*, vol. 41, no. 11, pp. 90-100, Nov. 2003.

[7] B. Ahlgren, L. Eggert, B. Ohlman, and A. Schielder, Ambient networks : bridging heterogeneous network domains, *PIMRC 2005*, pp. 937-941, Sept. 2005.

[8] I.-H. Kim, H.-J. Kim, and G.-M. Jeong, WPAN platform design in handset integrating cellular network and its application to the mobile game, *Lecture Notes in Computer Science*, vol. 4097, pp.103-111, 2006.

[9] J. H. Hwang, N. P. Kim, T. S. Jeong, and J. S. Koh A Framework for IM Interworking with Heterogeneous Networks, *Fifth International Conference on Networking and Services*, Valencia, Spain, April, pp.426-431, 2009.

[10] Specification of the Bluetooth System: Volume1, Core, Version 2.1, Bluetooth SIG, 2007

[11] ZigBee Document 053474r06 Version 1.0, ZigBee Alliance Std., 2004.

[12] WiMedia UWB PHY Layer Specification, Version 1.1, WiMedia Alliance, 2005.

[13] P. D. Garner, Mobile Bluetooth networking: technical considerations and applications, *4th International Conference on 3G Mobile Communication Technologies*, pp. 274-276, 2003.

[14] JSR-82, JavaTM APIs for Bluetooth, June, 2006.

[15] S. Chetan, J. Al-Muhtadi, R. Campbell, and M. D. Mickunas, A middeleware for enabling personal ubiquitous spaces, *CCNC 2005*, pp. 223-228, 2005.

[16] Bluetooth Compatibility Certification program Management Document Revision 2.1, CTIA, 2009

[17] CTIA Bluetooth Compatibility Test Plan Revision 2.1, CTIA, 2009.

[18] P. Bellavista and A. Corradi, The Handbook of Mobile Middleware, Boston: Auerbach publications, 2006.

[19] 3GPP TS 22.259 V8.3.0, Technical Specification Group Service and System Aspects ; Service requirements for Personal Network Management (PNM); Stage 1, June, 2006.

[20] 3GPP TS 23.259 V1.0.0, Technical Specification Group Services and System Aspects; Personal Network Management (PNM); Procedures and Information Flows, Aug, 2007

Int. J. of Computers, Communications & Control, ISSN 1841-9836, E-ISSN 1841-9844
Vol. VII (2012), No. 1 (March), pp. 90-100

Quantized Feedback Control for Networked Control Systems Under Communication Constraints

Q.Q. Liu, G.H. Yang

Qing-Quan Liu
School of Information Science and Engineering
Shenyang Ligong University
No. 6, Nan Ping Zhong Road, Hun Nan Xin
District, Shenyang, 110159, China
E-mail: lqqneu@163.com

Guang-Hong Yang
College of Information Science and Engineering
Northeastern University
Shenyang, 110004, China

Abstract: This paper investigates the feedback stabilization problem for networked control systems (NCSs) with unbound process noise, where sensors and controllers are connected via noiseless digital channels carrying a finite number of bits per unit time. A sufficient condition for stabilization of NCSs, which relies on a variable-rate digital link used to transmit state measurements, is derived. A lower bound of data rates, above which there exists a quantization, coding and control scheme to guarantee both stabilization and a prescribed control performance of the unstable discrete-time plant, is presented. An illustrative example is given to demonstrate the effectiveness of the proposed method.

Keywords: networked control systems (NCSs), quantized feedback control, communication constraints, feedback stabilization.

1 Introduction

As is well known, in recent emerging applications (e.g., industrial automation, sensor networks, vehicle systems, aerospace industry and etc), the main aim is to control one or more dynamical systems employing multiple sensors and actuators transmitting and receiving information via a digital communication network. However, the limitations in the communication links often affect control performances significantly.

Our focus in this paper is on control under communication constraints. The research on the interplay among coding, estimation, and control was initiated by [1]. A high-water mark in the study of quantized feedback using data-rate limited feedback channels is known as the data-rate theorem that states the larger the magnitude of the unstable poles, the larger the required data rate through the feedback loop. The intuitively appealing result was proved (see [2]- [5]), indicating that it quantifies a fundamental relationship between unstable physical systems and the rate at which information must be processed in order to stably control them. When the feedback channel capacity is near the data-rate limit, control designs typically exhibit chaotic instabilities. This result was generalized to different notions of stabilization and system models, and was also extended to multi-dimensional systems (see [6]- [8]). The research on Gaussian linear systems was addressed in [9]- [11]. Information theory was employed in control systems as a powerful conceptual aid, which extended existing fundamental limitations of feedback systems, and was used to derive necessary and sufficient conditions for robust stabilization of uncertain

linear systems, Markov jump linear systems and unstructured uncertain systems (see [12]- [16]). The decentralized control schemes were addressed in [17]. The result on continuous-time linear Gaussian systems was derived in [18]. The result on time-varying communication channel was derived in [19]. Control under communication constraints inevitably suffers signal transmission delay, date packet dropout and measurement quantization which might be potential sources of instability and poor performance of control systems (see [22] and [23]). The survey papers [20] and [21] gave a historical and technical account of the various formulations.

The data-rate inequality is now well known and provides good intuition into the connection between achievable bit-rate and stability of linear time-invariant systems. It states that for a linear time-invariant system which is open-loop unstable, a controller can be designed to stabilize it if and only if the data rate R around the closed feedback loop satisfies the data rate inequality: $R > \log|\det(A)|$ (bits/sample) where A denotes the system matrix composed by only unstable modes. However, as the data rate R is reduced to the critical value $\log|\det(A)|$, the plant states must always become unbounded. In engineering systems, It is of importance to present a lower bound of data rates above which there exists a quantization, coding and control scheme to guarantee both the stabilization and control performances of plants.

In this paper, we address quantized feedback control problem for stochastic linear systems with limited data rates. The aim is to present a lower bound of data rates above which there exists a coder-controller to guarantee both the stabilization and a prescribed control performance.

The following notation is adopted throughout this paper.

- Upper case variables, like X, represent random vectors.
- We write $\log_2(\cdot)$ simply as $\log(\cdot)$.
- Let $p(X)$ denote the probability density function of X and $p(X|Y)$ denote the conditional probability density function of X given Y.
- $\|\cdot\|$ represents either the Euclidean norm on a real vector space or the matrix norm induced by it.
- $E_X[\cdot]$ denotes expectation on X.

The remainder of this paper is organized as follows: Section II introduces problem formulation. Section III deals with quantized feedback control problem for NCSs with limited data rates. The results of numerical simulation are presented in Section IV. Conclusions are stated in Section V.

2 Problem Formulation

2.1 Preliminaries

We start this section by summarizing the main definitions of Information Theory and adopt [24], as a primary reference. The definitions listed in this section hold under general assumptions.

- Let x and y denote two random variables. The differential entropy $h(x)$ is defined as

$$h(x) := E_x[\log \frac{1}{p(x)}].$$

The conditional differential entropy of x given y is defined as

$$h(x|y) := E_{x,y}[\log \frac{1}{p(x|y)}].$$

- The mutual information between x and y is defined as

$$I(x;y) := h(x) - h(x|y) = E_{x,y}[\log \frac{p(x|y)}{p(x)}].$$

- The information rate distortion function between x and y is defined as

$$R(D) := \inf_{p(y|x)\in\Xi}\{I(x;y)\}$$

  with $\Xi = \{p(y|x) : E_{x,y}[d(x,y)] \leq D\}$. Therein, $d(x,y)$ denotes a distortion function or distortion measure, which is a mapping $d : x \times y \to \mathbb{R}^+$ and D is a given constant.

- Over communication channels, there are two different methods to define data rates. One is the code element rate $R_c(t)$ that denotes the number of code element transmitted in unit time, and the other is the information transmission rate $R_e(t)$ that denotes the amount of information transmitted in unit time. $R_e(t)$ may or may not be time-varying. We write $R_e(t)$ simply as $R(t)$. Therefore $R(t)$ is given by

$$R(t) = \tfrac{1}{h} I(x;y)(\text{bits/s})$$

  where h is the transmission time for $I(x;y)$.

In NCSs, after completing sample quantization procedure in state observation, we generally encode state values and transmit the information of plant states over digital channels. Therein, quantization precision and sampling period are determined by conditions for the stabilization of control systems and demands for control performances. Based on quantization precision and sampling period given, we may calculate the amount of information to be transmitted, which determine the value of the data rate $R(t)$. It means that the data rate $R(t)$ must satisfy requirements of the stabilization of control systems and control performances.

Example 1. Assume $p(x) = \frac{1}{\sqrt{2\pi\sigma_1^2}} e^{\frac{-x^2}{2\sigma_1^2}}$ and $p(x|y) = \frac{1}{\sqrt{2\pi\sigma_2^2}} e^{\frac{-x^2}{2\sigma_2^2}}$. Let $h = 1s$. Then, we obtain

$$h(x) = \tfrac{1}{2}\log 2\pi e\sigma_1^2 \text{ (bits)},$$
$$h(x|y) = \tfrac{1}{2}\log 2\pi e\sigma_2^2 \text{ (bits)},$$
$$I(x;y) = \tfrac{1}{2}\log \tfrac{\sigma_1^2}{\sigma_2^2} \text{ (bits)}.$$

Then, we quantity, encode the value x and obtain the estimate y of x. Here, $D = \sigma_2^2$. Thus, we have

$$R(D) = \begin{cases} \frac{1}{2}\log \frac{\sigma_1^2}{\sigma_2^2} \text{ (bits)}, & 0 \leq \sigma_2^2 \leq \sigma_1^2, \\ 0 \text{ (bit)}, & \sigma_2^2 > \sigma_1^2. \end{cases}$$

Finally, we transmit y, and the information transmission rate $R(t)$ must satisfy the following inequality:

$$R(t) \geq \frac{1}{h}R(D) = \begin{cases} \frac{1}{2}\log \frac{\sigma_1^2}{\sigma_2^2} \text{ (bits/s)}, & 0 \leq \sigma_2^2 \leq \sigma_1^2, \\ 0 \text{ (bit/s)}, & \sigma_2^2 > \sigma_1^2. \end{cases}$$

2.2 System Model

Consider a stochastic linear system described by

$$\begin{aligned} X(t+1) &= AX(t) + BU(t) + FW(t), \\ Y(t) &= CX(t) \end{aligned} \tag{1}$$

where $X(t) \in \mathbb{R}^n$ is the state process, $U(t) \in \mathbb{R}^m$ is the control input, $Y(t) \in \mathbb{R}^p$ is the observation output, and $W(t) \in \mathbb{R}^l$ is the process disturbance. A, B, C and F are known constant matrices with appropriate dimensions (see Fig. 1).

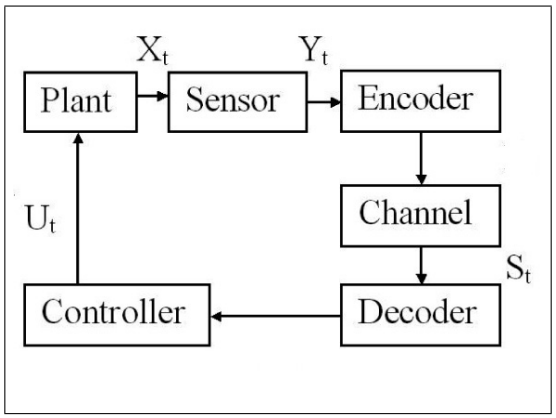

Figure 1: A networked control system with a communication channel.

The following is assumed to hold.

A_0. Without loss of generality, suppose that the pair (A, B) is controllable, and the pair (A, C) is observable.

A_1. The matrix A is uniquely composed by unstable modes (having magnitude greater than or equal to unity).

A_2. The initial condition $X(0)$ and disturbance $W(0), \cdots, W(t)$ are mutually independent random variables with zero mean, satisfying $E\|X(0)\|_2^2 < \Phi_0 < \infty$ and $E\|W(t)\|_2^2 < \Phi_W < \infty$, respectively.

A_3. The sensors and the controller are geographically separated and connected by errorless digital channels.

2.3 Problem Statement

We consider the system (1) under assumptions $A_0 - A_3$ above. We quantify the performance of a coder-controller as a prescribed control performance by the asymptotic state norm

$$J := \lim_{t \to \infty} E\|X(t)\|^2. \tag{2}$$

Here we are concerned with how small the plant states can be made as $t \to \infty$.

If the system (1) is controllable in the unstable modes, then there exists a matrix K such that all eigenvalues of $A - BK$ have magnitude smaller than unity. In this case it seems logical to try to implement a quantized state feedback control law of the form $U(t) = -K\hat{X}(t)$ where $\hat{X}(t)$ denotes the estimate of $X(t)$.

The main problem is to construct an encoder-decoder pair and to design a controller which guarantee both the stabilization and the control performance (2) of the system (1) in the mean square sense

$$\lim_{t\to\infty}\sup E\|X(t)\|^2 < \infty \tag{3}$$

using the finite data rate provided by the digital feedback link.

3 Feedback Control Under Data-Rate Constraints

This section deals with the quantized feedback stabilization problem for the system (1). The purpose here is to present a quantization, coding and control scheme to stabilize the closed-loop system (1) with the performance (2) in the mean square sense (3). Assume that the encoder has access to the full state vector for practical plants. First we give a preliminary lemma.

Lemma 1[24]. *Let $x \in \mathbb{R}$ denote a random variable and $\hat{x}$ denote an estimate of x. The expected distortion constraint is defined as $D \in \mathbb{R}^+$. For a given $D \geq E_x(x-\hat{x})^2$, there must exist a quantization and coding scheme if $R(t)$ satisfies*

$$R(t) > R(D) \geq \tfrac{1}{2}\log\tfrac{\sigma^2(x)}{D}(\textit{bits/sample})$$

where $\sigma^2(x) = E_x(x-Ex)^2$.

Proof. See [24].

Remark 1.

- $R(D)$ denotes the lower bound of the amount of information which is needed to reconstruct the initial condition to some distortion fidelity which satisfies conditions for the stabilization. It means that more information available at the decoder will lead to better control performance.
- Since Lemma 1 gives a lower bound of data rate for all quantization and coding scheme, for a given D, $\hat{X}_t$ can be obtained by many quantization and coding schemes. However, $R(D)$ can not approach the fundamental lower limit if the scheme used is not optimal.

The following theorem is our main result in this paper.

Theorem 1. *Consider the fully-observed system (1). Under assumptions $A_0 - A_3$, given a state feedback control law of the form $U(t) = -K\hat{X}(t)$, satisfying that all eigenvalues of A-BK have magnitudes smaller than 1, $\forall\varepsilon \in (0,1)$, the system (1) is mean-square stabilizable with*

$$J = \lim_{t\to\infty} E\|X(t)\|^2 < \frac{1}{1-\varepsilon}\|F\|^2\Phi_W$$

if the data rate $R(t)$ satisfies the following inequality:

$$R(t) > \tfrac{1}{2}\log\tfrac{|\det[A^TA-(A-BK)^T(A-BK)]|}{|\det[\varepsilon I-(A-BK)^T(A-BK)]|}\ (\textit{bits/sample}).$$

Proof:

Consider the closed-loop system

$$X(t+1) = AX(t) - BK\hat{X}(t) + FW(t)$$

which we can also write as

$$X(t+1) = A(X(t)-\hat{X}(t)) + (A-BK)\hat{X}(t) + FW(t).$$

Then, we have

$$\begin{aligned}
&E\|X(t+1)\|^2\\
&=\text{trace}[EX(t+1)X^T(t+1)]\\
&=\text{trace}[AE(X(t)-\hat{X}(t))(X(t)-\hat{X}(t))^TA^T]+\text{trace}[FEW(t)W^T(t)F^T])\\
&+\text{trace}[(A-BK)E\hat{X}(t)\hat{X}^T(t)(A-BK)^T]+2\text{trace}[(A-BK)E\hat{X}(t)W^T(t)F^T]\\
&+2\text{trace}[AE(X(t)-\hat{X}(t))W^T(t)F^T]+2\text{trace}[AE(X(t)-\hat{X}(t))\hat{X}^T(t)(A-BK)^T].
\end{aligned} \tag{4}$$

Notice that X(t) and W(t) are mutually independent. This implies

$$\begin{aligned}
E\hat{X}(t)W^T(t)=0,\\
E(X(t)-\hat{X}(t))W^T(t)=0
\end{aligned} \tag{5}$$

following from assumption A_2. Furthermore, $E[X(t)-\hat{X}(t)]\hat{X}^T(t)=EV(t)\hat{X}^T(t)=0$ where $V(t)$ denotes the quantization error with zero mean. Substituting it and (5) into (4), we obtain

$$E\|X(t+1)\|^2=\text{trace}A\Sigma_{X(t)|\hat{X}(t)}A^T+\text{trace}(A-BK)\Sigma_{\hat{X}(t)}(A-BK)^T+E\|FW(t)\|^2$$

where we define $\Sigma_{X(t)|\hat{X}(t)}:=E(X(t)-\hat{X}(t))(X(t)-\hat{X}(t))^T$ and $\Sigma_{\hat{X}(t)}:=E\hat{X}(t)\hat{X}^T(t)$.

If assume that

$$E\|X(t)\|^2>\text{trace}A\Sigma_{X(t)|\hat{X}(t)}A^T+\text{trace}(A-BK)\Sigma_{\hat{X}(t)}(A-BK)^T$$

which is equivalent to

$$\varepsilon E\|X(t)\|^2=\text{trace}[A\Sigma_{X(t)|\hat{X}(t)}A^T]+\text{trace}[(A-BK)\Sigma_{\hat{X}(t)}(A-BK)^T] \tag{6}$$

with $\varepsilon\in(0,1)$, we see that

$$E\|X(t+1)\|^2=\varepsilon E\|X(t)\|^2+E\|FW(t)\|^2.$$

Then, we obtain

$$\begin{aligned}
E\|X(t)\|^2 &= \varepsilon^tE\|X(0)\|^2+\textstyle\sum_{i=0}^{t-1}\varepsilon^{t-i-1}E\|FW(i)\|^2\\
&< \varepsilon^t\Phi_0+\tfrac{1-\varepsilon^t}{1-\varepsilon}\|F\|^2\Phi_W
\end{aligned}$$

following from assumption A_2. Thus,

$$J=\lim_{t\to\infty}E\|X(t)\|^2<\tfrac{1}{1-\varepsilon}\|F\|^2\Phi_W.$$

It means that if we can design a quantization and coding scheme such that (6) holds, the system (1) is mean square stabilizable.

Next, we further argue that there exists a lower bound of the data rate $R(t)$ based on the quantization and coding scheme to stabilize the system (1) with

$$J=\lim_{t\to\infty}E\|X(t)\|^2<\tfrac{1}{1-\varepsilon}\|F\|^2\Phi_W.$$

Observe that

$$\varepsilon E\|X(t)\|^2=\varepsilon\text{trace}\Sigma_{X(t)}$$

and

$$\begin{aligned}\Sigma_{\hat{X}(t)} &= E\hat{X}(t)\hat{X}^T(t) - EX(t)X^T(t) + EX(t)X^T(t)\\ &= \Sigma_{X(t)} - E(X(t)X^T(t) - \hat{X}(t)\hat{X}^T(t))\\ &= \Sigma_{X(t)} - E(X(t) - \hat{X}(t))(X(t) - \hat{X}(t))^T\\ &= \Sigma_{X(t)} - \Sigma_{X(t)|\hat{X}(t)}\end{aligned}$$

where we define $\Sigma_{X(t)} := EX(t)X^T(t)$. Substituting the equations above into (6), we have

$$\begin{aligned}\varepsilon\text{trace}\Sigma_{X(t)} =&\text{trace}[A\Sigma_{X(t)|\hat{X}(t)}A^T]+\text{trace}[(A-BK)\Sigma_{\hat{X}(t)}(A-BK)^T]\\ =&\text{trace}[A^TA\Sigma_{X(t)|\hat{X}(t)}]+\text{trace}[(A-BK)^T(A-BK)\Sigma_{\hat{X}(t)}]\\ =&\text{trace}[A^TA\Sigma_{X(t)|\hat{X}(t)}]+\text{trace}[(A-BK)^T(A-BK)(\Sigma_{X(t)}-\Sigma_{X(t)|\hat{X}(t)})]\\ =&\text{trace}[(A^TA-(A-BK)^T(A-BK))\Sigma_{X(t)|\hat{X}(t)}]\\ &+\text{trace}[(A-BK)^T(A-BK)\Sigma_{X(t)}]\end{aligned}$$

which we can also write as

$$\text{trace}(\Theta_1\Sigma_{X(t)}) =\text{trace}(\Theta_2\Sigma_{X(t)|\hat{X}(t)}) \tag{7}$$

where we define $\Theta_1 := \varepsilon I - (A-BK)^T(A-BK)$ and $\Theta_2 := A^TA - (A-BK)^T(A-BK)$. Notice that there exist unitary matrices P, Q, H that diagonalize the symmetric matrices Θ_1, Θ_2, $\Sigma_{X(t)}$ and $\Sigma_{X(t)|\hat{X}(t)}$, respectively. Namely, $\Theta_1 = P^T\bar{\Theta}_1P$, $\Theta_2 = Q^T\bar{\Theta}_2Q$, $\Sigma_{X(t)} = H^T\Sigma_{\bar{X}(t)}H$ and $\Sigma_{X(t)|\hat{X}(t)} = H^T\Sigma_{\bar{X}(t)|\tilde{X}(t)}H$ where we define $\bar{X}(t) := HX(t)$, $\tilde{X}(t) := H\hat{X}(t)$, $\bar{\Theta}_1 :=\text{diag}[\alpha_1,\cdots,\alpha_n]$ and $\bar{\Theta}_2 :=\text{diag}[\beta_1,\cdots,\beta_n]$. Then, (7) is equivalent to the following equations:

$$\text{trace}(P^T\Theta_1\Sigma_{X(t)}H) =\text{trace}(Q^T\Theta_2\Sigma_{X(t)|\hat{X}(t)}H).$$

Since traceMN=traceNM with matrices $M \in R^{n\times m}$ and $N \in R^{m\times n}$ holds , thus the equality above is equivalent to

$$\text{trace}(\Sigma_{X(t)}HP^T\Theta_1) =\text{trace}(\Sigma_{X(t)|\hat{X}(t)}HQ^T\Theta_2).$$

Then, we have

$$\text{trace}(H^T\Sigma_{X(t)}HP^T\Theta_1P) =\text{trace}(H^T\Sigma_{X(t)|\hat{X}(t)}HQ^T\Theta_2Q).$$

Namely

$$\text{trace}(\Sigma_{\bar{X}(t)}\bar{\Theta}_1) =\text{trace}(\Sigma_{\bar{X}(t)|\tilde{X}(t)}\bar{\Theta}_2).$$

Thus, we obtain

$$\text{trace}(\bar{\Theta}_1\Sigma_{\bar{X}(t)}) =\text{trace}(\bar{\Theta}_2\Sigma_{\bar{X}(t)|\tilde{X}(t)})$$

which we can also write as

$$\Sigma_{i=1}^n\alpha_iE\bar{x}_i^2(t) = \Sigma_{i=1}^n\beta_iE(\bar{x}_i(t)-\tilde{x}_i(t))^2 \tag{8}$$

where define $\bar{X}(t) := [\bar{x}_1(t),\cdots,\bar{x}_n(t)]^T$ and $\tilde{X}(t) := [\tilde{x}_1(t),\cdots,\tilde{x}_n(t)]^T$. (8) can be viewed as a quantization and coding criterion. Then, based on the criterion (8), we can design a quantization and coding scheme to stabilize the system (1) in the mean square sense (3).

However, the analyses on the quantization and coding scheme rely heavily on the assumption of the boundability of the initial condition X(0) and the disturbance input $W(t)$. Similar to

Shannon source coding, there exists a lower bound of the data rate $R(t)$, satisfying the criterion (8). We quantize each $\bar{x}_i(t)$ and obtain the estimate $\tilde{x}_i(t)$ of $\bar{x}_i(t)(i = 1, \cdots, n)$, and encode it into a symbol s_{ti} which is transmitted over an errorless digital channel. Then, the symbol S_t=$[s_{t1}$ $\cdots$ $s_{tn}]$ is decoded and converted into a control input $U_t = -BK\hat{X}_t = -BKH^T\tilde{X}_t$. Namely, we get $\hat{X}(t) = H^T\tilde{X}(t)$. Notice that $\sigma^2(\bar{x}) \leq E\bar{x}_i^2(t)$. Define $D := [\ D_1 \cdots D_n]$. Thus, if let $D_i \leq \frac{\alpha_i}{\beta_i}\sigma^2(\bar{x}_i(t))$, the criterion (8) must be satisfied. Following from Lemma 3.1, the following inequality can be obtained:

$$\begin{aligned} R_i(t) &> R_i(D_i) \\ &\geq \tfrac{1}{2}\log\tfrac{\sigma^2(\bar{x}_i(t))}{D_i} \\ &\geq \tfrac{1}{2}\log\tfrac{\sigma^2(\bar{x}_i(t))}{\frac{\alpha_i}{\beta_i}\sigma^2(\bar{x}_i(t))} \\ &\geq \tfrac{1}{2}\log\tfrac{\beta_i}{\alpha_i}\ \text{(bits/sample)}. \end{aligned}$$

Thus, it follows that

$$\begin{aligned} R(t) &= \textstyle\sum_{i=1}^n R_i(t) \\ &> \tfrac{1}{2}\log\textstyle\prod_{i=1}^n \tfrac{\beta_i}{\alpha_i} \\ &= \tfrac{1}{2}\log\tfrac{|\det(\bar{\Theta}_2)|}{|\det(\bar{\Theta}_1)|} \\ &= \tfrac{1}{2}\log\tfrac{|\det(\Theta_2)|}{|\det(\Theta_1)|} \\ &= \tfrac{1}{2}\log\tfrac{|\det(A^TA-(A-BK)^T(A-BK))|}{|\det(\varepsilon I-(A-BK)^T(A-BK))|}\ \text{(bits/sample)}. \end{aligned}$$

Thus, if $R(t)$ satisfies the inequality above, there exists a coder-controller to stabilize the system (1) with

$$J = \lim_{t\to\infty} E\|X(t)\|^2 < \frac{1}{1-\varepsilon}\|F\|^2\Phi_W.$$

□

Remark 2.

- Theorem 1 states how fundamental tradeoffs between the data rate and the prescribed control performance. Clearly, the better performance can be achieve when the greater data rate is employed.
- Observe that corresponding to the classical situation without communication constraints, the performance becomes

  $$J = \lim_{t\to\infty} E\|X(t)\|^2 \to \|F\|^2\Phi_W$$

  as the limit $R(t) \to \infty$.

4 Numerical example

To illustrate the effectiveness of communication constraints for stabilization of stochastic linear systems, we present an open loop unstable system as follows,

$$X(t+1) = \begin{bmatrix} 1.61 & 0.52 & 0.25 \\ 0.52 & 1.61 & 0.36 \\ -0.21 & 0.61 & 4.31 \end{bmatrix} X(t) + \begin{bmatrix} 1 \\ 1 \\ 2 \end{bmatrix} U(t) + 0.3W(t).$$

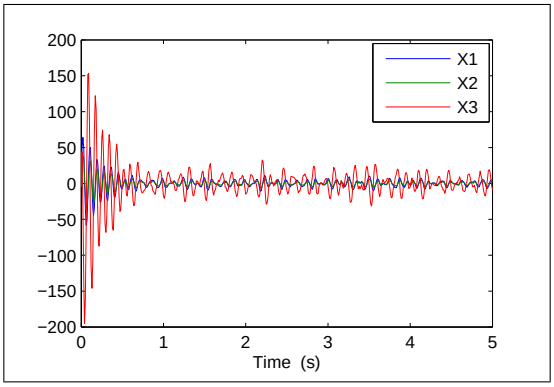

Figure 2: The system state responses with limited data rates.

Let $\varepsilon = 0.4$, X(0)=[50 -20 -50]^T, and $\Phi_W = 10$. Here we give a controller gain $K = [-0.6738 \quad -0.0681 \quad 2.9360]$. A simulation is shown in Fig.2.

Remark 3. The obtained state responses are shown in Fig.2. It states that the encoding-control scheme based on Theorem 1 can stabilize the system above.

5 Conclusion

This paper addressed the feedback control problem for stochastic linear systems with limited data rates. The approach taken here was based on the hypothesis that sensors and controllers are connected by a rate-limited, time-varying communication channel. Based on the presented lower bound of data rates, there exists a coder-controller to guarantee both stabilization and a prescribed control performance. The simulation results have illustrated the effectiveness of the quantization, coding and control scheme.

Acknowledgment

This work was supported in part by the Funds for Creative Research Groups of China (No. 60821063), National 973 Program of China (Grant No. 2009CB320604), the Funds of National Science of China (Grant No. 60974043), the 111 Project (B08015), and the Funds of Doctoral Program of Ministry of Education, China (20100042110027).

Bibliography

[1] W. S. Wong and R. W. Brockett, Systems with finite communication bandwidth constraints II: Stabilization with limited information feedback, *IEEE Trans. Automat. Control*, 44(5):1049-1053, May 1999.

[2] J. Baillieul, Feedback designs for controlling device arrays with communication channel bandwidth constraints, in *ARO Workshop on Smart Structures*, Pennsylvania State Univ, Aug. 1999.

[3] J. Baillieul, Feedback designs in information based control, in *Stochastic Theory and Control Proceedings of a Workshop Held in Lawrence, Kansas*, B. Pasik-Duncan, Ed. New York: Springer-Verlag, 2001, pp. 35-57.

[4] J. Baillieul, Data-rate requirements for nonlinear feedback control, in *Proc. 6th IFAC Symp. Nonlinear Control Syst.*, Stuttgart, Germany, 2004, pp. 1277-1282.

[5] K. Li and J. Baillieul, Robust quantization for digital finite communication bandwidth (DFCB) control, *IEEE Trans. Automat. Control*, 49(9):1573-1584, Sep. 2004.

[6] G. N. Nair and R. J. Evans, Stabilizability of stochastic linear systems with finite feedback data rates, *SIAM J. Control Optim.*, 43(2):413-436, Jul. 2004.

[7] N. Elia and S. K. Mitter , Stabilization of linear systems with limited information, *IEEE Trans. Automat. Control*, 46(9):1384-1400, Sep. 2001.

[8] N. Elia, When Bode meets Shannon: Control-oriented feedback communication schemes, *IEEE Trans. Automat. Control*, 49(9):1477-1488, Sep. 2004.

[9] S. Tatikonda and S. K. Mitter, Control under communication constraints, *IEEE Trans. Automat. Control*, 49(7):1056-1068, Jul. 2004.

[10] S. Tatikonda and S. K. Mitter, Control over noisy channels, *IEEE Trans. Automat. Control*, 49(7):1196-1201, Jul. 2004.

[11] S. Tatikonda, A. Sahai and S. K. Mitter, Stochastic linear control over a communication channel, *IEEE Trans. Automat. Control*, 49(9):1549-1561, Sep. 2004.

[12] N. C. Martins, M. A. Dahleh, and N. Elia, Feedback stabilization of uncertain systems in the presence of a direct link, *IEEE Trans. Automat. Control*, 51(3):438-447, Mar. 2006.

[13] N. C. Martins and M. A. Dahleh, Feedback control in the presence of noisy channels: 'Bode-like' fundamental limitations of performance, *IEEE Trans. Automat. Control*, 53(7):1604-1615, Jul. 2008.

[14] G. N. Nair, S. Dey, and R. J. Evans, Infimum data rates for stabilizing Markov jump linear systems, in *Proc. IEEE Conf. Decision and Control*, 2003, pp. 1176-1181.

[15] A. Sahai and S. Mitter, The necessity and sufficiency of anytime capacity for stabilization of a linear system over a noisy communication link Part I: Scalar systems, *IEEE Trans. Automat. Control*, 52(8):3369-3395, Aug. 2006.

[16] J. Q. Sun and S. M. Djouadi, Robust stabilization over communication channels in the presence of unstructured uncertainty, *IEEE Trans. Automat. Control*, 54(4):830-834, Apr. 2009.

[17] S. Yüksel and T. Basar, Communication constraints for decentralized stabilizability with time-invariant policies, *IEEE Trans. Automat. Control*, 52(6):1060-1066, Jun. 2007.

[18] C.D. Charalambous, A. Farhadi, and S.Z. Denic, Control of continuous-time linear Gaussian systems over additive Gaussian wireless fading channels: A separation principle, *IEEE Trans. Automat. Control*, 53(4):1013-1019, Apr. 2008.

[19] P. Minero, M. Franceschetti, S. Dey, and G. N. Nair, Data rate theorem for stabilization over time-varying feedback channels, *IEEE Trans. Automat. Control*, 54(2):243-255, Feb. 2009.

[20] J. Baillieul and P. Antsaklis, Control and communication challanges in networked real time systems, in *Proceedings of IEEE Special Iss. Emerg. Technol. Netw. Control Syst*, USA: IEEE, 2007, pp. 9-28.

[21] G. N. Nair, F. Fagnani, S. Zampieri, and R. J. Evans, Feedback control under data rate constraints: An overview, in *Proceedings of IEEE Special Iss. Emerg. Technol. Netw. Control Syst*, USA: IEEE, 2007, pp. 108-137.

[22] Y. L. Wang and G. H. Yang, H_∞ control of networked control systems with time delay and packet disordering, *IET Control Theory & Applications*, 1(5):1344-1354, May. 2007.

[23] Y. L. Wang and G. H. Yang, Multiple communication channels-based packet dropout compensation for networked control system, *IET Control Theory & Applications*, 2(8):717-727, Aug. 2008.

[24] T. Cover and J. Thomas, *Elements of Information Theory*. New York: Wiley, 2006.

Int. J. of Computers, Communications & Control, ISSN 1841-9836, E-ISSN 1841-9844
Vol. VII (2012), No. 1 (March), pp. 101-114

Optimal Tuning of PID Controller using Adaptive Hybrid Particle Swarm Optimization Algorithm

S. Morkos, H. Kamal

Sawsan Morkos Gharghory
Electronics Research Institute
Dokki, Cairo, Egypt
E-mail: sawsan@eri.sci.eg

Hanan Ahmed Kamal
Faculty of Engineering, Cairo University
Giza, Egypt
E-mail: Hanan_ak2003@yahoo.com

Abstract:
Particle swarm optimization (PSO) has proved its ability as an efficient search tool in many optimization problems. However, PSO is easy to be trapped into local minima due to its mechanism in information sharing. Under this circumstance, all the particles could quickly converge to a position by the attraction of the best particle; all particles could hardly be improved. To overcome premature convergence of the standard PSO algorithm, this paper presents an adaptive hybrid PSO, namely (AHPSO) by employing an adaptive mutation operator for local best particles instead of applying the mutation operator to the global best particle as has been done in previous work. The developed algorithm is a new approach which allows the swarm to be more diverse by making better exploration of the local search space instead of global search space investigated by previous researchers. The proposed algorithm holds on the properties of simple structure, fast convergence, and at the same time enhances the variety of the population, and extends the search space. It is applied to self-tuning of proportional-integral-derivative-(PID) controller in the ball and hoop system which represents a system of complex industrial processes. The results are compared with those obtained by applying standard PSO, and adaptive hybrid PSO based on global best particles. It has been shown that the developed AHPSO local best algorithm is faster in convergence and the obtained results are proved to have higher fitness than the other two algorithms.
Keywords:PSO, Adaptive mutation, PID Controller, and ball and hoop system.

1 Introduction

The PID controller was the most popular controller of this century because of its remarkable effectiveness, simplicity of implementation and broad applicability. In practice, it is hard to obtain optimal tuning for PID controller. Most of PID tuning is done manually which is difficult and time consuming. In order to use PID controller better, the optimal tuning of its parameters have become an important research field [1]. People have made lots of research, and proposed some advanced PID control methods, such as expert PID control based on knowledge inference[2], self-learning PID control based on regulation, neural network PID control based on connection mechanism[3], and intelligent PID control based on fuzzy logic[4,5]. Genetic algorithm (GA) has

been applied to self-tuning of PID parameters, too [6]. However, GA has the disadvantages of premature and slow convergence rate, and the need to set up many parameters. Recently, the computational intelligence has proposed particle swarm optimization (PSO) [7, 8] as opened paths to a new generation of advanced process control. The PSO algorithm, proposed by Kennedy and Eberhart [7] in 1995, was an evolution computation technology based on population intelligent methods. In comparison with genetic algorithm, PSO is simple, easy to realize and has very deep intelligent background. It is not only suitable for scientific research, but also suitable for engineering applications in particular. Thus, PSO received widely attentions from evolution computation field and other fields. Now the PSO has become a hotspot of research.

Many efforts on the enhancement of traditional PSO have been proposed, by combining the PSO with other techniques, especially evolutionary computation techniques. The research effort in [9] has developed a hybrid method combining two heuristic optimization techniques, GA and PSO, for the global optimization of multimodal functions. The work in [10], obtained better results by applying PSO first followed by applying GA in their profiled corrugated horn antenna optimization problem. The effort in [11] has introduced a new integrated genetic swarm optimization algorithm (IGSA), combining the strengths of PSO with GA. It is applied in the tuning of PID controllers for the ball and hoop system. A genetic programming based adaptable evolutionary hybrid particle swarm optimization algorithm, have presented in [12], for avoiding premature convergence to local minima by the introduction of diversity in the swarm.

In addition to incorporate evolutionary algorithms into PSO, another research trend is to merge evolutionary operators like selection, crossover and mutation to the PSO. By applying selection operation in PSO, the particles with the best performance are copied into the next generation; therefore, PSO can always keep the best performed particles [13]. By applying crossover operation, information can be swapped between two individuals to have the ability to "fly" to the new search area as that in evolutionary programming and GA [14]. Among the three evolutionary operators, the mutation operators are the most commonly applied evolutionary operators in PSO. The purpose of applying mutation to PSO is to increase the diversity of the population and the ability to have the PSO to escape from the local minima. One approach is to mutate PSO parameters such as the position of the best neighborhood, as well as the inertia weight [15]. Another approach is to prevent particles from moving too close to each other so that the diversity could be maintained and therefore escape from being trapped into local minima. In [16], the particles are relocated when they are too close to each other. In [17], collision- avoiding mechanisms are designed to prevent particle from colliding with each other and therefore increase the diversity of the population. In [18], deflection and stretching techniques as well as a repulsion technique are incorporated into the original PSO to avoid particles to move toward the already found global minima, so that the PSO can have more chances to find as many global minima as possible. Chen [19] presented a Gaussian mutation operator with adaptive mutation probability. Wang [20] proposed an adaptive mutation on the basis of average velocity of swarm. Pant [21] used an adaptive Cauchy mutation operator in PSO, which was based on beta distribution. Tang [22] proposed Local Search PSO, namely LSPSO by applying an adaptive mutation operator which dynamically adjusts the step size of local search in terms of the size of current search space in order to improve the global search ability of PSO. He introduced one technique for mutating the global best particle by a value which based on the difference between the maximum and minimum value for each dimension of the search space. However, the results given by LSPSO as well as the standard PSO, PSO with both Gaussian and Cauchy mutation fall into local optima for some types of test functions.

In the present work, a new adaptive hybrid PSO, called AHPSO local best is proposed by applying an adaptive mutation operator, which differs from the above mutation techniques by using three types of mutation operators instead of using one technique. The main idea

of AHPSO local best is to generate an operator that can adaptively select the most suitable mutation method in each generation according to each stage of the problem. Three types of mutation operators are used in this work, Gaussian, Cauchy, and Levy mutation operators. In the proposed algorithm, the local best particles are to be mutated by the selected mutation operator instead of applying the mutation operator to the global best particle as in the previous literatures. This can be accomplished by searching the neighborhood of the global best particles in each generation, resulting in more exploration of the search space and increasing the diversity of the population and the ability to have the PSO to avoid the local optima. The new developed algorithm is carried out for the optimal tuning of PID controller to the ball and hoop system. The performance of the system is compared with the standard PSO and adaptive PSO using the global best particle. Experimental studies on tuning the parameters of PID controller for the ball and hoop problem show that AHPSO local best performs better than the standard PSO and adaptive PSO based on global best particle search technique. The obtained results have higher fitness and faster convergence.

The rest of the paper is organized as follows. Section 2 describes the standard PSO. In Section 3, PSO with adaptive mutation operator is described and the proposed AHPSO local best algorithm is presented in detail. An overview of the control problem which will be solved is provided in Section 4. Experimental results and discussions are presented in Section 5. Finally, Section 6 concludes the whole work.

2 Particle Swarm Optimization

PSO is a stochastic optimization technique [7] which operates on the principle of social behavior like bird flocking or fish schooling. Like other evolutionary algorithms, PSO is also a population-based search algorithm and stats with an initial population of randomly generated solutions called particles which fly through the search space. Each particle represents a candidate solution to the optimization problem, and has a velocity and a position. The position of a particle is influenced by the best position visited by itself i.e. its own experience and the position of the best particle in its neighborhood i.e. the experience of neighboring particles. The best particle in the population is denoted by (global best), while the best position that has been visited by the current particle is denoted by (local best). Consequentially, each particle is influenced by the best performance of any member in the entire population due to the sharing information between them. The performance of each particle is measured using a fitness function that varies depending on the optimization problem. Each particle in the swarm is represented by the following characteristics:
X_i : The current position of the particle i.
V_i: The current velocity of the particle i.
P_i : The best position of particle i so far,and P_g is the best position found in the whole swarm so far. Equations (1) and (2) are used for updating both of the velocity and the position of each particle.

$$V_i = w_i.V_i + c_1.r_1.(P_i - X_i) + c_2.r_2.(P_g - X_i) \tag{1}$$

$$X_i = X_i + V_i \tag{2}$$

Where: c_1 and c_2 are the cognitive coefficients and r_1, and r_2 are random real numbers drawn from U (0, 1), ω is the inertia weight which is used to achieve a balance in the exploration and exploitation of the search space and plays very important role in PSO convergence behavior. The

inertia dynamically reduces during a run from 1.0 to near 0 in each generation which facilitates a balance in the exploration and exploitation of the search space, it is determined as follows:

$$w_i = w_{max} - \frac{w_{max} - w_{min}}{iter_{max}}.iter \tag{3}$$

Where iter_max, is the maximum number of iterations, and iter is the current number of iteration. Several topologies exist in literature for the particles to communicate with one another. The topologies are ring, star, pyramid and master-slave topologies [23]. Among the topologies, the star is the best topology.

3 Adaptive particle swarm optimization

Different types of mutation operators can be used to increase the diversity of the population and to help PSO jump out of local minima. The type of mutation operator may be more effective or worse depending on the stage of optimization process. In the present work, three types of mutation operators are applied at different stages of the problem for more exploration of search space. An adaptive method for selecting the mutation operator that is suitable for each stage of the problem was proposed in this paper. Also, the developed approach search for the best neighborhood of the global best particle to be mutated by the selected mutation operator. The proposed mutation operators are presented in the following section as follow:

-Cauchy Mutation operator

$$V_g = V_g \exp(\delta) \tag{4}$$

$$X_g = X_g + V_g \delta_g \tag{5}$$

Where:
X_g and V_g represent position and velocity of the global best particle.
δ and δ_g denote Cauchy random numbers with the scale parameter of 1.

-Gaussian Mutation operator

$$V_g = V_g \exp(N) \tag{6}$$

$$X_g = X_g + V_g N_g \tag{7}$$

Where:
X_g and V_g represent position and velocity of the global best particle.
N and N_g are Gaussian distribution numbers with the mean equals 0 and the variance equals 1.

-Levy Mutation operator

$$V_g = V_g \exp(L(\alpha)) \tag{8}$$

$$X_g = X_g + V_g L_g(\alpha) \tag{9}$$

$L(\alpha)$ and $L_g(\alpha)$ are random numbers generated from Levy distribution with a parameter α which is set to 1.3 [24].

3.1 The Adaptive mutation operator

The method proposed for adaptive mutation uses the three mutation operators described above. Initially, the selection ratio is set equal to 1/3 for the three mutation operators, by this ratio; the number of particles mutated by each operator is calculated. Then, each mutation operator is applied to the swarm particles according to its selection ratio and finally, the resulting offspring fitness is evaluated. The mutation operators that result in higher fitness values of offspring have the most chance to be selected than the other one with lower fitness values of offspring. Gradually the most suitable mutation operator will be chosen automatically and control all the mutation behavior in the whole swarm. The steps for selecting the best mutation operators are described as follows [24]:

1- The progress value for each operator at each generation is evaluated as:

$$prog_i(t) = \sum_{j=1}^{M_i} f(P_j^i(t)) - min(f(P_j^i(t)), f(c_j^i(t))) \tag{10}$$

Where:
$P_j^i(t)$, and $c_j^i(t)$ denote the fitness of a parent and its child produced by mutation operator i at generation t, and M_i is the number of particles that select mutation operator i to mutate.

2- The reward value for each operator is calculated as:

$$reward_i(t) = \exp(\frac{prog_i(t)}{\sum_{j=1}^{N} prog_j(t)}\alpha + \frac{S_i}{M_i}(1-\alpha)) + c_i P_i(t) - 1 \tag{11}$$

Where:
S_i is the number of particles whose children have a better fitness than themselves after the mutation by operator i, $P_i(t)$ is the selection ratio of mutation operator i at generation t, α is a random weight between (0,1), N is the number of mutation operator, and c_i is a penalty factor for mutation operator i, and is defined as:

$$c_i = \begin{cases} 0.9 & \text{if } S_i = 0 \text{ and } P_i(t) = max_{j=1}^{N}(P_j(t)) \\ 1, & \text{otherwise} \end{cases} \tag{12}$$

The mutation operator with maximum reward has the best chance to mutate the best local particles selected during each generation.

3- The selection ratio to the next generation for the mutation operator is updated as follows:

$$P_i(t+1) = \frac{reward_i(t)}{\sum_{j=1}^{N} reward_j(t)}(1 - N - \gamma) + \gamma \tag{13}$$

Where, γ is the minimum selection ratio for each mutation operator and is set equal to 0.01 in our problem. The selection ratio for the next generation depends on four factors: the progress value, the minimum selection ratio, the previous selection ratio, and the ratio of successful mutation operator. The selection of each mutation operator may be updated each generation or after a fixed number of generations, in this paper we update the selection ratio after each generation.

3.2 The proposed AHPSO local best particles algorithm

The standard *PSO* was inspired by the social and cognitive behavior of swarm. According to the analysis given in [25], particles are largely influenced by its previous best particles and the global best particle. Once the best particle has no change in a local optimum, all the rest particles will quickly converge to the position of the best particle. The present work proposes searching neighbors of the global best particle to be mutated in each generation, rather than selecting the global best particle for mutating. As a result, it would be helpful for the best particles to jump out the local minima, and the whole swarm would move to better position. This can be accomplished by applying the adaptive mutation operator described above to the neighborhood of the global best particle in each generation. The framework of PSO algorithm with one of the three mutations operators according to its selection ratio to mutate the best neighborhood particles of the global best particle is given as follows:
1- Generate the initial position and velocity for each particle in the swarm randomly.
2- Evaluate the fitness of each particle, and determine the local and the global best fitness for each particle in the swarm.
3- Set the initial selection ratio equal 1/3.
4- Update each particle according to equation (1) and (2)
5- For each particle i, if its fitness is smaller than the fitness of its previous best position (P_i) update P_i .
6- Update the fitness of the best position (P_g) of all particle if there is a particle with fitness smaller than the current best fitness P_g .
7- Apply each one of mutation operator to number of particles according to its selection ratio.
8- Evaluate the progress and the reward values to select the best one from the three above mutation operators, and then update the selection ratio of each operator for the next generation.
9- Mutate the best neighborhood particles of the global best particle with the best mutation operator (with maximum reward), and select the best one from the mutated best neighborhood to produce ($P_g^\star$).
10- Compare $P_g^\star$ and P_g to select the better to reproduce in the next generation.
11- Stop if the stop criterion is satisfied otherwise, go to step 4.

4 Plant System

The Ball and Hoop system illustrates the dynamics of a steel ball that is free to roll on the inside of a rotating circular hoop. There is a groove on the inside edge of the hoop so that a steel ball can roll freely inside the hoop. This introduces the complexity of the rolling radius of the ball being different to the actual radius of the ball as illustrated in Figure 1where angle θ is the hoop angular position. The position of the ball is given by:
1- γ is the position of the ball on the hoop periphery with respect to a datum point.
2-Ψ is the slosh angle which measures the deviation of the ball from its rest position.
A fourth order system for the Ball and Hoop system with the following transfer function[26] is:

$$G(s) = \frac{1}{S^4 + 6S^3 + 11S^2 + 6S} \tag{14}$$

The ball and hoop apparatus is difficult to control optimally using a PID controller because the system parameters are constantly changing. The parameters of PID controller will be tuned offline separately, using PSO, AHPSO global best, and AHPSO local best algorithms as shown in figure 2.

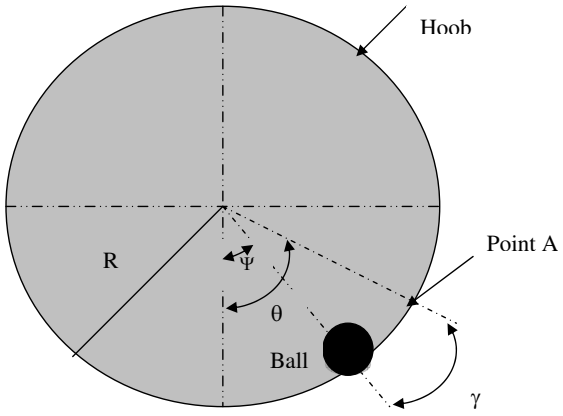

Figure 1: The ball and hoop system

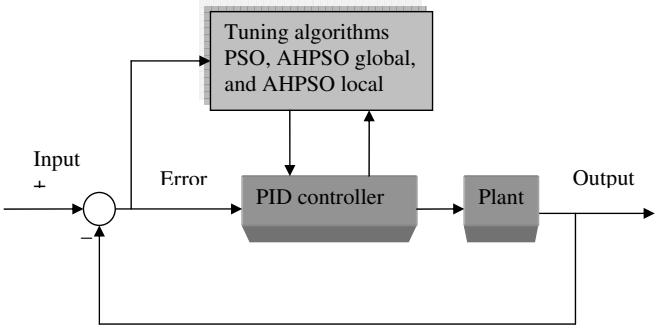

Figure 2: The structure of the proposed algorithms in tuning PID controller for the plant system

Various objective functions based on error performance criterion are used to evaluate the performance of the above algorithms. Each objective function is fundamentally the same except for the section of code that defines the specific error performance criterion being implemented to optimize the performance of a PID controlled system. The Performance index is calculated over a time interval T. Performance indices used to estimate the best parameters of PID controller are given by:

- Integral of the Square of the Error (ISE)

$$I_{ISE} = \int_0^T e^2(t)dt \tag{15}$$

- Mean of the Square of the Error (MSE)

$$I_{MSE} = \frac{1}{n}\sum_{i=1}^{n}(e(t))^2 \tag{16}$$

- Integral of Absolute Magnitude of the Error (IAE)

$$I_{IAE} = \int_0^T |e(t)|dt \tag{17}$$

Where: e is the error calculated over a time interval T. The effectiveness of the proposed AHPSO local best algorithm in comparison with the other two algorithms is tested using the above three performance indices.

5 Simulation Result

To evaluate the performance of AHPSO based on local best particles, experiments have been carried out for optimal tuning of PID controller to the ball and hoop system. The performance results of PID controller tuned by AHPSO local best search in comparison with PSO, and AHPSO global best particle in the swarm is analyzed using IAE, ISE, and MSE performance indices. Cost functions achieved by each algorithm are averaged over 10 runs for 30 generations. The resulted time response and cost function for the three algorithms using three performance indices are shown in Figures 3-8 respectively. Tables 1-3 give comparison of cost function values and the transient response characteristics for PSO, AHPSO global best, and AHPSO local best algorithms using IAE, ISE and MSE performance indices.

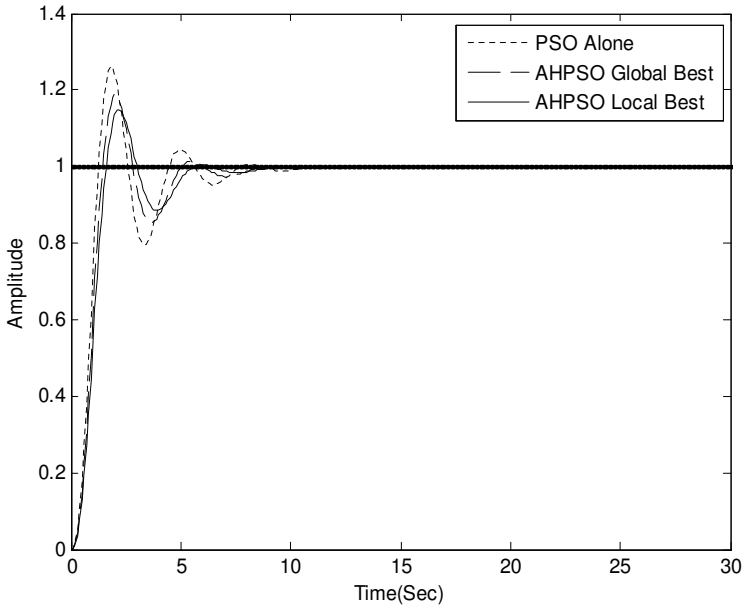

Figure 3: System response using IAE for PSO, AHPSO global particle, and AHPSO local particle

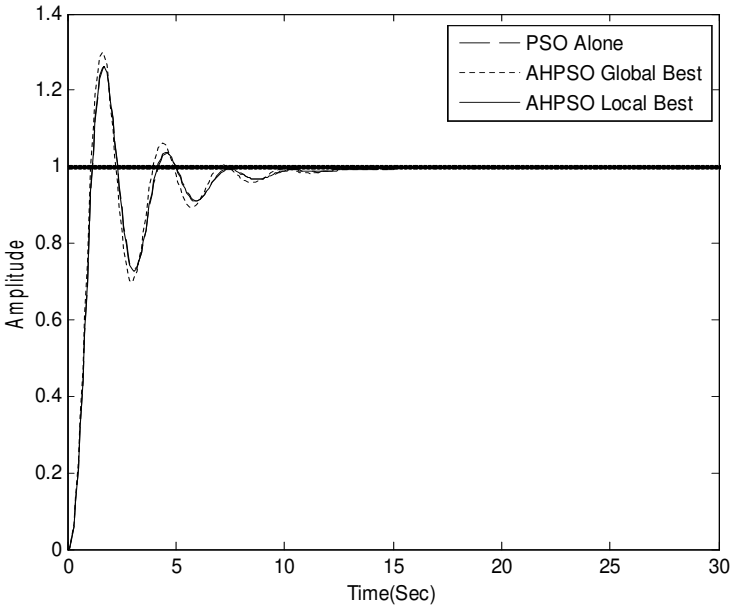

Figure 4: System response using ISE for PSO, AHPSO global particle, and AHPSO local particle

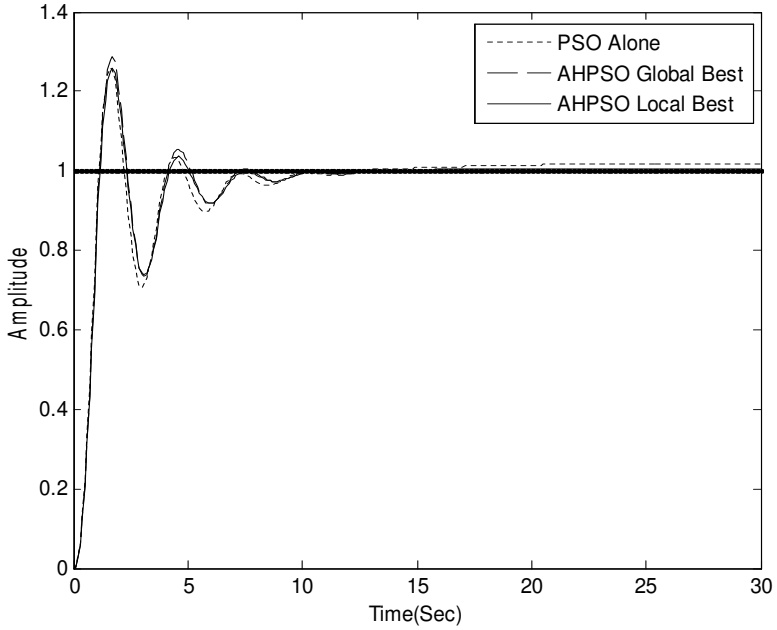

Figure 5: System response using MSE forPSO, AHPSO global particle and AHPSO local particle

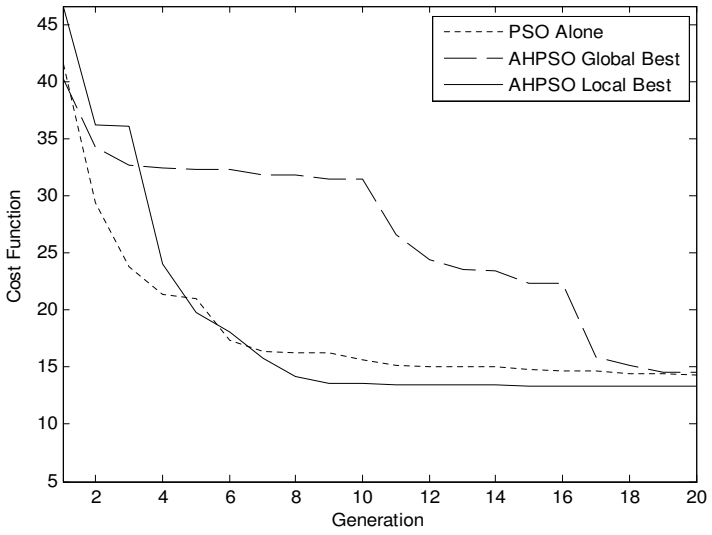

Figure 6: Cost function using IAE for PSO, AHPSO global particle, and AHPSO local particles

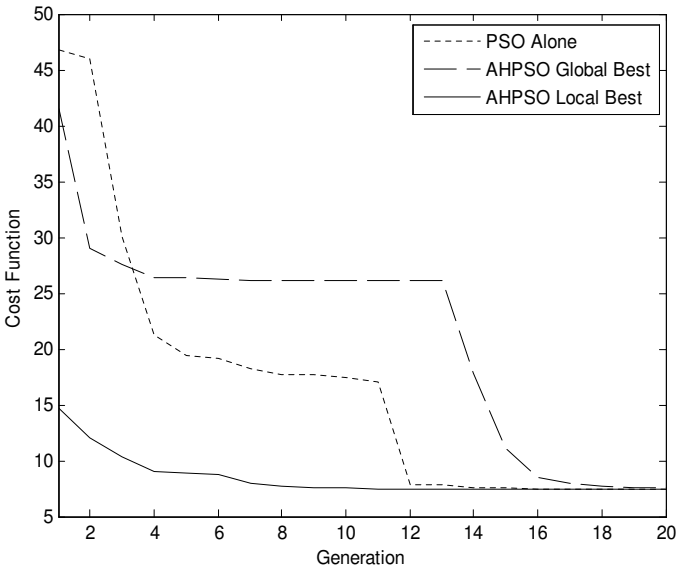

Figure 7: Cost function using ISE for PSO, AHPSO global particle, and AHPSO local particles

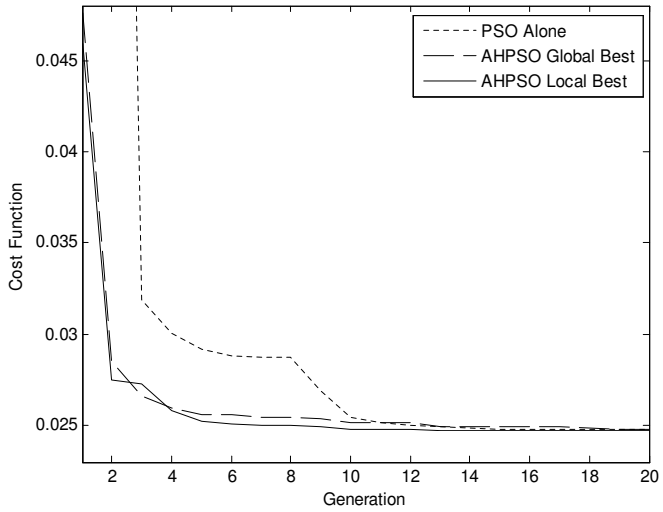

Figure 8: Cost function using MSE for PSO, AHPSO global particle, and AHPSO local particles

Table 1: Transient response charteristics using IAE criteria

Criteria IAE	Standard PSO	AHPSO Global	AHPSO Local
Rise Time T_r	1.12	1.29	1.17
Peak Value M_p	25%	15.5%	14%
Settling Time T_s	7.2	7.58	5.1
Peak Time T_p	1.27	2.30	2.25
Cost Function	13.39	13.38	13.36

Table 2: Transient response charteristics using ISE criteria

Criteria ISE	Standard PSO	AHPSO Global	AHPSO Local
Rise Time T_r	1.02	0.97	0.83
Peak Value M_p	25.95%	28%	25.89%
Settling Time T_s	9.54	9.29	9.14
Peak Time T_p	1.72	1.72	1.67
Cost Function	7.46	7.49	7.43

Table 3: Transient response charteristics using MSE criteria

Criteria MSE	Standard PSO	AHPSO Global	AHPSO Local
Rise Time T_r	1.012	1.01	0.84
Peak Value M_p	25.9%	29%	25.6%
Settling Time T_s	9.59	9.4	9.32
Peak Time T_p	1.72	1.72	1.69
Cost Function	0.0248	0.0248	0.0247

Simulation results demonstrate the superiority of AHPSO based on local search comparing to the other algorithms. In terms of overshoot (peak value), AHPSO local search has a lower overshoot by 1.3% than AHPSO global search and 8.8% than PSO for IAE performance index. In ISE performance index, the improvement is about 1.6% over AHPSO global search and has 0.047 over PSO. For MSE, the improvement is about 0.23% over PSO, and about 2.6% over AHPSO global search using MSE performance index.

For cost function the results are as follows: the improvement is about 0.22% over PSO, and 0.149% over AHPSO global search using IAE performance index. For ISE performance index it is about 0.4% over PSO, and 0.8% over AHPSO global search. The improvement using MSE performance index is about 0.68% over PSO, and 0.4% over AHPSO global search.

As for settling time, AHPSO local search has minimum settling time to reach the final minimum cost function. The improvement is about 29% over PSO, and 32.7% over AHPSO global search using IAE. It equals 4.2% over PSO, and is 1.6% over AHPSO global search for ISE. Also, it is about 2.8% over PSO, and is 0.85% over AHPSO global search using MSE metric.

6 Conclusion

This paper is concerned with developing adaptive operator for the selection of best mutation technique of three investigated mutation techniques: Cauchy, Gaussian, and Levy techniques. Instead of applying single mutation operator, several mutation operators are applied at different stages for best performance. A new particle swarm algorithm based on adaptive mutation operator to local best particles namely AHPSO local best is proposed in this paper. Instead of applying the best mutation operators to the global particle, it is applied to the neighbors' of global best particle. Besides, the paper investigates the use of AHPSO based on local best particles for tuning PID controller parameters for the ball and hoop system and compares the system performance with the standard PSO and AHPSO based on global best particles. The performance of the three algorithms is analyzed based on three performance indices; IAE, ISE, and MSE. Experimental results show the superiority of the AHPSO local search over the other techniques for the optimal tuning of PID controller to the ball and hoop system. Also, it has been shown that the developed algorithm is faster in convergence and gives higher fitness value than the other algorithms, at the same time enhances the variety of the population, and extends the search space. Also, the time response characteristics of the proposed algorithm are better than other techniques. In future research, we intend to apply the technique to different set of practical constrained problems to show the robustness of the technique. Also, comparison of the effectiveness of different mutation operators on particles velocity for different types of problems will be studied.

Bibliography

[1] Astroöm K., and Hagglund T., "The future of PID control". Control Engineering Practice, 9, pp. 1163-1175, 2001.

[2] Conradie A., Miikkulainen R., and Aldrich C., "Adaptive Control Utilizing Neural Swarming", In Proceedings of the Genetic and Evolutionary Computation Conferences, USA, 2002.

[3] Hossein Shayeghi, Heidar Ali Shayanfar and Aref Jalili," Multi Stage Fuzzy PID Load Frequency Controller in a Restructured Power System", Journal of Electrical Engineering, Vol. 58, No.. 2, pp. 61-70, 2007.

[4] Saban Cetin, and Ozgür Demir," Fuzzy PID Controller with Coupled Rules for a Nonlinear Quarter Car Model", World Academy of Science, Engineering and Technology Vol. 41, pp.238-241, 2008.

[5] Aye Aye Mon," Fuzzy Logic PID Control of Automatic Voltage Regulator System", Proceedings of PWASET, Vol. 38, Feb., 2009.

[6] Cipperfield A. Flemming P., and Fonscea C., "Genetic Algorithms for Control System Engineering", in Proceedings Adaptive Computing in Engineering Design Control, pp- 128-133, 1994.

[7] Kennedy J. and Eberhart C., "Particle Swarm Optimization", Proceedings of the IEEE International Conference on Neural Networks, Australia, pp. 1942-1948, 1995.

[8] Oliveira, P. M., Cunha, J. B., and Coelho, J. o. P., "Design of PID controllers using the Particle Swarm Algorithm.", Twenty-First IASTED International Conference: Modeling, Identification, and Control (MIC 2002), Innsbruck, Austria. 2002.

[9] Yi-Tung Kao and Erwie Zahara," A hybrid genetic algorithm and particle swarm optimization for multimodal functions", Applied Soft Computing Vol. 8, pp 849-857, 2008.

[10] Robinson, J., Sinton, S., and Rahmat-Samii, Y., " Particle swarm, genetic algorithm, and their hybrids: optimization of a profiled corrugated horn antenna", IEEE International Symposium on Antennas & Propagation. San Antonio, Texas. June, 2002.

[11] H. A. Kamal, " A new integrated GA/PSO Algorithm for Optimal tuning of PID Controller", the Mediterranean Journal of Measurement and Control, Vol. 6, No. 1, pp.18-24, January 2010.

[12] M. Rashid and A. Rauf Baig, " A genetic programming based adaptable evolutionary hybrid particle swarm optimization algorithm", International Journal of Innovative Computing, Information and Control (ICIC), Vol. 6, Nu. 1, January 2010.

[13] Angeline, P. J., "Using selection to improve particle swarm optimization", Proceedings of the IEEE Congress on Evolutionary Computation (CEC 1998), Anchorage, Alaska, USA. 1998.

[14] Lvbjerg, M., Rasmussen, T., and Krink, T, "Hybrid particle swarm optimizer with breeding and subpopulations", Proceedings of the third Genetic and Evolutionary Computation Conference (GECCO), Vol. 1, pp. 469-476, 2001.

[15] Miranda, V., and Fonseca, N.," New evolutionary particle swarm algorithm (EPSO) applied to voltage/VAR control", The 14th Power Systems Computation Conference (PSCC'02), Seville, Spain, June, 2002.

[16] Lvbjerg, M., and Krink, T., "Extending particle swarms with self-organized criticality", Proceedings of the Fourth Congress on Evolutionary Computation (CEC-2002).

[17] Blackwell, T., and Bentley, P. J., (2002). "Don't push me ! Collision-avoiding swarms". IEEE Congress on Evolutionary Computation, Honolulu, Hawaii USA, 2002.

[18] Parsopoulos, K. E., and Vrahatis, M., "On the computation of all global minimizers through particle swarm optimization", IEEE Transactions on Evolutionary Computation, (accepted for special issue on PSO, 2004.

[19] J. Chen, Z. Ren and X. Fan, "Particle swarm optimization with adaptive mutation and its application research in tuning of PID parameters," in Proc. 1st International Symposium on Systems and Control in Aerospace and Astronautics, pp. 990-994, 2006.

[20] H. Wang, Y. Liu C. H. Li, and S. Y. Zeng, "A Hybrid Particle swarm algorithm with Cauchy Mutation," IEEE Swarm Intelligence Symposium, Honolulu, Hawaii, pp. 356-360, 2007.

[21] Pant, M. Thangaraj, R. Abraham, A. , "Particle swarm optimization using adaptive mutation," in Proc. 19th International Conference on Database and Expert Systems Application, pp. 519-523, 2008.

[22] Jun Tang, and, X. Zhao, "A Hybrid Particle Swarm Optimization with Adaptive Local Search", journal of networks, Vol. 5, No.4, April 2010.

[23] Fatih Ta?getiren M and Yun-Chia Liang, "A Binary Particle Swarm Optimization Algorithm for Lot Sizing Problem", Journal of Economic and Social Research, Vol.5 No.2, pp. 1-20, 2004.

[24] C. Li, S. Yang and I. A. Korejo. "An Adaptive Mutation operator for Particle Swarm". Proceedings of the 2008 UK Workshop on Computational Intelligence, pp. 165-170, 2008.

[25] H. Wang, Y. Liu C. H. Li, and S. Y. Zeng, "A hybrid particle swarm algorithm with Cauchy mutation," IEEE Swarm Intelligence Symposium, Honolulu, Hawaii, pp. 356-360, 2007.

[26] I. Griffin, "On-line PID Controller Tuning using Genetic Algorithms", MSc. Thesis School of Electronic Engineering Dublin City University, 2003.

Int. J. of Computers, Communications & Control, ISSN 1841-9836, E-ISSN 1841-9844
Vol. VII (2012), No. 1 (March), pp. 115-122

Switched Nonuniform and Piecewise Uniform Scalar Quantization of Laplacian Source

A.V. Mosic, Z.H. Peric, S.R. Panic

Aleksandar V. Mosić
Faculty of Electronic Engineering, University of Niš
Aleksandra Medvedeva 14, 18000 Niš, Serbia
E-mail: mosicaca@yahoo.com

Zoran H. Perić
Faculty of Electronic Engineering, University of Niš
Aleksandra Medvedeva 14, 18000 Niš, Serbia
E-mail: zoran.peric@elfak.ni.ac.rs

Stefan R. Panić
Faculty of Natural Science and Mathematics,
University of Priština
Lole Ribara 29, 38200 Kosovska Mitrovica, Serbia
E-mail: stefanpnc@yahoo.com

Abstract:
In this paper switched nonuniform and piecewise uniform scalar quantization of Laplacian source are analyzed. This scalar quantization techniques are used in order to obtain higher signal quality by increasing signal-to-quantization noise ratio ($SNRQ$) with respect to it's necessary robustness over a broad range of input variances in a wide range of signal volumes. We observe μ-law compandor implementation to achieve compromise between high-rate digitalization and variance adaptation. The main contribution of this model is kipping almost the same quality as the nonuniform compandor model, with simpler realization structure and the possibility of it's applying for digitalization of wide range continuous signals.
Keywords: switching quantization, μ-law companding, variance adaptation, Laplacian source.

1 Introduction

Quantization denotes the heart of analog to digital (A/D) conversion and efficient technique of data compression. Quantizers play an important role in the theory and practice of modern day signal processing. They are applied for the purpose of storage and transmission of continual signals. In a number of papers like this one the quantization of Laplacian source was analyzed since the probability density function (PDF) of the instantaneous speech signal values for higher number of digitalization samples is better represented by Laplacian then the Gaussian function [1], [2], [4], [7], [10]. Analysis of nonlinear quantization optimization in wide volume range [5], [6], for Gaussian source is given in [8], [9]. In this paper we analyze robust and switched nonuniform and piecewise uniform scalar quantization of Laplacian source to achieve compromise between high-rate digitalization and variance adaptation. The aim of our research is to find a simple way to realize a quantizer system having high quality performance but maintaining robustness in wide range of input signal. The goal of the paper is designing piecewise uniform scalar quantizer based on the μ-law compandor which satisfy $G.712$ standard. In this purpose, we must to find optimal values for parameter μ and number of quantizers. Proposed solution

has the same complexity as the $G.711$ standard, because we use 8 bits, but it satisfy $G.712$ standard with 7 bits/sample. Important issues from the engineer's point of view are the design and implementation of quantizers to meet performance objectives. When the required hardware solution it is better to use piecewise uniform scalar quantizers, because they can be realized using linear electronic circuits. But if the required software solution it is better to use nonuniform scalar quantizers.

This paper is organized as follows. In chapter 2. we have developed expressions for granular and overload distortion of nonuniform scalar quantization, using Bennett's integral on Laplacian distribution. Then in chapter 3. a switching nonuniform model and numerical results for μ-logarithmic compandor are presented. In chapter 4. our switching piecewise uniform model and numerical results for μ-logarithmic compandor are presented. Last two chapters show how the increase of number of quantizers, in switching scheme, affects the $SQNR$ dependence of input power. Also we have discussed how constant μ should be chosen in order for total distortion to be as minimum as possible in the wide volume range of input signal. Finally, in conclusion we have discussed obtained results, and on these bases, we derived conclusions about the possibilities of this switched quantization application in speech processing.

2 Distortion for nonuniform μ-logarithmic compandor

Scalar quantizers are the only types of quantizers considered in this paper, so we just briefly recall their properties. An N-point fixed rate scalar quantizer is characterized by the set of real numbers $t_1, t_2, \ldots, t_N$, called *decision thresholds*, which satisfy $-\infty = t_0 < t_1 < \cdots < t_{N-1} < t_N = +\infty$, and set $y_1, y_2, \ldots, y_N$, called *representation levels*, which satisfy $y_j \in \alpha_j = (t_{j-1}, t_j]$, for $j = 1, \ldots, N$. Sets $\alpha_1, \alpha_2, \ldots, \alpha_N$ form the partition of the set of real numbers R and are called *quantization cells*. The quantizer is defined as many-to-one mapping $Q : R \to R$, $Q(x) = y_j$ where $x \in \alpha_j$. In practice, input signal value x is quantized to the value y_j. Cells $\alpha_2, \alpha_3, \ldots, \alpha_{N-1}$ are *inner cells* (or *granular cells*) while α_1 and α_N are *outer cells* (or *overload cells*). In such way, cells $\alpha_2, \alpha_3, \ldots, \alpha_{N-1}$ form granular while cells α_1 and α_N form an overload region.

Let input signal is characterized by continuous random variable X with PDF $p(x)$. The first approximation to the long-time-averaged PDF of amplitudes is provided by a two-sided exponential or Laplacian model. Waveforms are sometimes represented in terms of adjacent-sample differences. The PDF of the difference signal for an image waveform follows the Laplacian function [4]. Laplacian source can be also used for modelling of the speech signal. In the rest of the paper we assume that information source is Laplacian source with memoryless property and zero mean value. The PDF of that source is given by:

$$p(x) = \frac{1}{\sqrt{2\sigma^2}}\, e^{-\frac{|x|\sqrt{2}}{\sigma}}, \tag{1}$$

where x is zero-mean statistically independent Laplacian random variable of variance σ^2.

The quality of the quantizer is measured by distortion of resulting reproduction in comparison to the original one. Mostly used measure of distortion is mean-squared error. It is defined by:

$$D(Q) = E(X - Q(X))^2 = \sum_{i=1}^{N} \int_{t_{i-1}}^{t_i} (x - y_i)^2 p(x) dx. \tag{2}$$

The N-point quantizer Q is *optimal* for the source X if there is no other N-point quantizer Q_1 such that $D(Q_1) < D(Q)$. We also define granular distortion $D_g(Q)$ and overload $D_{ol}(Q)$

distortion by:

$$D_g(Q) = \sum_{j=2}^{N-1} \int_{t_{j-1}}^{t_j} (x - y_j)^2 p(x) dx, \tag{3}$$

$$D_{ol}(Q) = \int_{-\infty}^{t_1} (x - y_1)^2 p(x) dx + \int_{t_{N-1}}^{+\infty} (x - y_N)^2 p(x) dx. \tag{4}$$

Obviously follows that $D(Q) = D_g(Q) + D_{ol}(Q)$.

The companding technique is one of the commonly used techniques for the construction of nearly optimal quantizers for large number of quantization levels. It forms the core of the ITU-T G.711 standard [3]. It is a nonuniform PCM standard recommended for encoding speech signals. The recommendation is based on digitally linearizable companding, which permits a precise control of quantization characteristics. The compression and expansion characteristics are piecewise linear approximations to μ-law , where $\mu = 255$, with 8 bits/sample are adopted, leading to a bit-rate of 64 kbps at 8 kHz of sampling frequency. Companding procedure consists of following steps: i) compressing the input signal x by applying the compressor function $c(x)$. ii) applying the uniform quantizer Q_u on the compressed signal. iii) expanding the quantized version of the compressed signal using an inverse compressor function $c^{-1}(x)$. As explained the corresponding non-uniform quantizer consisting of a compressor, a uniform quantizer, and an expander in cascade is called *companding quantizer* (*compandor*). Hence, the companding quantizer can be represented as $Q(x) = c^{-1}(Q_u(c(x)))$, where $Q_u(x)$ is uniform quantizer in the interval $[-1, 1]$. Let us denote by $t_{u,i}$ and $y_{u,i}$ decision thresholds and representation levels of the uniform quantizer $Q_u(x)$. Corresponding values t_i and y_i of the companding quantizer $Q(x)$ could be determined as the solutions of the following equations:

$$c(t_i) = t_{u,i} = -1 + \frac{2i}{N}, \quad c(y_i) = y_{u,i} = -1 + \frac{2i-1}{N}. \tag{5}$$

There are several ways how to choose the compressor function $c(x)$ for compression law. In practice, a piecewise linear approximation of the logarithmic compression characteristic is used. There are two different ways. In North America, a μ-law compression characteristic is used, which is defined as follows:

$$c(x) = \begin{cases} \frac{x_{max}}{\ln(1+\mu)} \ln\left(1 + \mu \frac{x}{x_{max}}\right), & 0 \le x \le x_{max} \\ -\frac{x_{max}}{\ln(1+\mu)} \ln\left(1 - \mu \frac{x}{x_{max}}\right), & -x_{max} \le x \le 0 \end{cases}. \tag{6}$$

Substituting (1), (5) and (6) in (3) and (4), and considering that y_N can be approximated with x_{max}, granular and overload distortions are defined as:

$$D_g(Q) = \frac{\sigma^2 \ln^2(1+\mu)}{3N^2} \left[\frac{1}{\mu^2} \frac{x_{max}^2}{\sigma^2} + \frac{x_{max}}{\sigma} \frac{\sqrt{2}}{\mu} + 1\right], \tag{7}$$

$$D_{ol}(Q) = \sigma^2 e^{-\frac{\sqrt{2} x_{max}}{\sigma}}. \tag{8}$$

Since we now know how to calculate total distortion for quantization of a Laplacian source that has variable average power in a wide range:

$$D(Q) = \frac{\sigma^2 \ln^2(1+\mu)}{3N^2} \left[\frac{1}{\mu^2} \frac{x_{max}^2}{\sigma^2} + \frac{x_{max}}{\sigma} \frac{\sqrt{2}}{\mu} + 1\right] + \sigma^2 e^{-\frac{\sqrt{2} x_{max}}{\sigma}}, \tag{9}$$

we can find the signal power-to-total-distortion ratio (dB), which is denoted as $SQNR$:

$$\begin{aligned} SQNR &= 10\lg\frac{\sigma^2}{D(Q)} \\ &= 10\lg\frac{1}{\frac{\ln^2(1+\mu)}{3N^2}\left[\frac{1}{\mu^2}\frac{x_{max}^2}{\sigma^2}+\frac{x_{max}}{\sigma}\frac{\sqrt{2}}{\mu}+1\right]+e^{-\frac{\sqrt{2}x_{max}}{\sigma}}}. \end{aligned} \tag{10}$$

On the basis of this expression we will design the desired model below.

3 Switching nonuniform scalar quantization and numerical results for μ-logarithmic compandor

Classical quantizer with μ-law compression characteristic (see Fig. 1, $\mu = 255$) has limited range of input variances. We will solve that problem with switching quantization application. One simple technique is switched codebook adaptive scalar quantization. The basic scheme of robust and switched codebook adaptation is shown in [8]. This technique uses a classifier that looks at the contents of the input frame buffer and decides that the next block of samples belongs to a particular statistical class of samples from a finite set of K possible classes. Namely, the index specifying the class is used to select a particular codebook from a redesigned set of K codebooks. In addition, this index is transmitted as side information to the receiver. Then, each sample in the block is encoded by the scalar quantizer, which performs a search through the selected codebook. One frame has length of M. The index to identify the class is sent on the end of block. If each of the K codebooks has size N, the bit rate per sample is:

$$R = \log_2 N + \frac{\log_2 K}{M}. \tag{11}$$

Codebook size N depends on number of bits that are used for the encoding n. The relation between N and n is $N = 2^n$, where n is the number of bits per sample.

We will use this switching technique for our problem solving. We have K codebooks, i.e., K nonuniform scalar quantizers designed for particular values σ_{0j} to cover input power range $\sigma_{0j}^2/\sigma_0^2 \in [\sigma_{1j}^2/\sigma_0^2, \sigma_{2j}^2/\sigma_0^2)$,where σ_0 denotes referent value of input power and $\cup_{j=1}^{K}[\sigma_{1j}^2/\sigma_0^2[dB]$, $\sigma_{2j}^2/\sigma_{0j}^2[dB]) = [-20, 20)$. Maximal amplitude for each quantizer x_{maxj} (each codebook j) is chosen in a way, that for each input power range $\sigma_{0j}^2/\sigma_0^2 \in [\sigma_{1j}^2/\sigma_0^2, \sigma_{2j}^2/\sigma_0^2)$ the total distortion has a minimum. The procedure is as follows: We optimize total distortion (9) to have a minimum. The optimization is going over parameter c, witch denotes ratio x_{max}/σ. After finding c_{opt}, for corresponding μ, which satisfies the following term:

$$\frac{\partial D(Q)}{\partial c} = 0 \Rightarrow c = c_{opt}. \tag{12}$$

We can easily evaluate x_{maxj} for each input power range $\sigma_{0j}^2/\sigma_0^2 \in [\sigma_{1j}^2/\sigma_0^2\sigma_{2j}^2/\sigma_0^2)$, from the expression $x_{maxj} = c_{opt}\sigma_{0j}$. Each particular value σ_{0j} can be represented as $\sigma_{0j} = k_j\sigma_0$, where k_j is called adaptation factor. During the switched quantizer design, a particular type of memory is needed. Each input class $j = 1, 2, \ldots, K$ requires one quantizer, for which we know adaptation factor k_j and input power range $[\sigma_{1j}^2/\sigma_0^2, \sigma_{2j}^2/\sigma_0^2)$ for which the quantizer is designed. Also we have to store in memory the corresponding μ and c_{opt}.

First, let us examine switched codebook adaptive scalar quantization model with only one quantizer present. Here, only parameter that can be optimized, for achieving high quality of transmission by increasing $SNRQ$, in a wide range of signal volumes (variances) with respect to

it's necessary robustness over a broad range of input variances is the l' parameter in expression for $SNRQ$. Parameter μ can be optimized, for the case when expression for $SNRQ$ has his maximum, which means that expression (9) for total distortion should have his minimum. Optimization of total distortion is derived in two steps. First, we accomplish adaptation on maximal amplitude of input signal, or the optimization for parameter c in corespondents to μ, which is described as:

$$\frac{\partial D(Q)}{\partial c} = 0 \Rightarrow c = c_{opt}(\mu). \tag{13}$$

Then in the second step, we find required μ_{opt}, for witch total distortion should have his minimum, which is described as

$$\left.\frac{\partial D(Q)}{\partial \mu}\right|_{c=c_{opt}(\mu)} = 0 \Rightarrow \mu = \mu_{opt}, \quad D(Q)(\mu_{opt}) = D_{min}(Q). \tag{14}$$

These two steps can be represented as the following equation system:

$$\frac{\partial D(Q)}{\partial c} = \sigma^2 \left(-\sqrt{2}e^{-\sqrt{2}c} + \frac{\left(\frac{2c}{\mu^2} + \frac{\sqrt{2}}{\mu}\right)\ln^2(1+\mu)}{3N^2} \right) = 0 \tag{15}$$

$$\begin{aligned} \left.\frac{\partial D(Q)}{\partial \mu}\right|_{c=c_{opt}(\mu)} &= \sigma^2 \left(\frac{2\left(1 + \frac{c_{opt}^2(\mu)}{\mu^2} + \frac{\sqrt{2}c_{opt}(\mu)}{\mu}\right)\ln(1+\mu)}{3N^2(1+\mu)} \right. \\ &- \left. \frac{\left(\frac{2c_{opt}^2(\mu)}{\mu^3} + \frac{\sqrt{2}c_{opt}(\mu)}{\mu^2}\right)\ln^2(1+\mu)}{3N^2} \right) = 0. \end{aligned} \tag{16}$$

For $N_1 = 128$ and $N_2 = 256$, numerical solutions for presented systems are $c_{opt1} = 8.8$, $\mu_{opt1} = 15$ and $c_{opt2} = 9.9$ and $\mu_{opt2} = 17$, respectively. If there are not restrictive limitations about memory size and sample bit rate for the transmission system, then there is a possibility to choose optimal number of quantizers in our model, for which we can achieve high quality measured by $SQNR$, in a wide range of signal volumes (variances) with respect to it's necessary robustness over a broad range of input. If we increase number of quantizers K, there is a way to flatten the $SQNR$ dependence of input power in such a way that, if the memory size isn't the limiting factor, with data compression being disregarded, we will achieve a signal-to-noise ratio that does not have a large variation during input power changes which is shown in Figs 1 and 2. In Fig 2, we can see that $SQNR$ varies from it's peak value, for maximum 0.282 dB and 0.313 dB for each input power range $[\sigma_{1j}^2/\sigma_0^2, \sigma_{2j}^2/\sigma_0^2)$, $\cup_{j=1}^{K}[\sigma_{1j}^2/\sigma_0^2[dB], \sigma_{2j}^2/\sigma_{0j}^2[dB]) = [-20, 20)$, for which the quantizer is designed, in case of codebook size of 128 and 256, with 16 codebooks. There is a conclusion, that if we want to satisfy the same standard for varying of $SQNR$ in twice larger input power range of [-40dB,40dB], we will have to use same codebook size for 32 codebooks. If we want to satisfy less restrictive standards of $SQNR$ variance for each input power range $[\sigma_{1j}^2/\sigma_0^2, \sigma_{2j}^2/\sigma_0^2)$, we can use smaller number of codebooks, and if we want to achieve smaller peak value of $SQNR$, we can use smaller size of each codebook, for each input power range. If we analyze bit sample rate in function of frame length with respect to number of quantizers K, we can se that for relatively small frame length of 80 samples, bit sample rate rapidly convergates to the value of bit sample rate of transmission without side information. So we can derive conclusion that memory size is much more restrictive limitation for multi-quantizer implementation, than sample rate is.

From Fig. 2, we can see that presented nonuniform switched quantizer with optimized μ outperform classical $\mu = 255$ switched quantizer characteristic for 3 dB and 2.7 dB in the cases of $N = 128$ and $N = 256$, respectively.

4 Switched piecewise uniform scalar quantization and numerical results for μ-logarithmic compandor

This paper utilizes the basic concept of the Jayant quantizer model in order to provide the development of the adaptive piecewise uniform scalar quantizer [4]. Particularly, the model avails the Jayant manner of maximum amplitude adaptation, which means according to the one word memory. Finally, since one of the main goals when designing quantizers is to provide as high as possible quality, i.e. as low as possible distortion, an analysis will be conducted in order to provide optimal values of μ. In this section, it is showed that segmental μ-law better than method presented in Section 3, when the required hardware solution because they can be realized using linear electronic circuits, and provide almost the same results for quality. Switched piecewise uniform scalar quantization of memoryless Laplacian source is asymptotically analyzed for the case where the power of input signal varies in a wide range. One possible solution for encoder design is given for the same quantizer. Switched quantization is used in order to give a higher quality in a wide range of signal volumes (variances). These systems, although not optimal, may have asymptotic performance arbitrarily close to the optimum. Furthermore, their analysis and implementation can be simpler than those of optimal systems. We also define granular distortion $D_g(Q)$ and overload $D_{ol}(Q)$ distortion by:

$$D_g(Q) = 2\sum_{i=1}^{L} \frac{\Delta_i^2}{12} P_i(\sigma) \tag{17}$$

$$D_{ol}(Q) = 2\int_{x_{max}}^{+\infty} (x - y_{L,n_{unif}})^2 p(x)dx. \tag{18}$$

where are amplitudes quant in the i-th segment defines es:

$$\Delta_i = \frac{x_i - x_{i-1}}{\frac{N}{2L}} \tag{19}$$

and $y_{L,nunif}$ is representation layer in the last cell of L-th segment:

$$y_{L,nunif} = x_{max} - \frac{\Delta_L}{2} \approx x_{max} \tag{20}$$

Finally $p(x)$ is the PDF of inner signal on quantizer, which define probability $P_i(\sigma)$ that quantum of signal belong the i-th segment:

$$P_i(\sigma) = \int_{x_{i-1}}^{x_i} p(x,\sigma)dx. \tag{21}$$

As we know $D(Q) = D_g(Q) + D_{ol}(Q)$. After sam basic mathematical operations we can get that:

$$\begin{aligned} D(Q) &= \frac{x_{max}^2}{12(N/2L)^2\mu^2} \sum_{i=1}^{L} (1+\mu)^{\frac{2(i-1)}{L}} ((1+\mu)^{\frac{1}{L}} - 1)^2 e^{-\frac{\sqrt{2}x_{max}}{\mu\sigma}((1+\mu)^{\frac{i-1}{L}}-1)} \\ &\times \left(1 - e^{-\frac{\sqrt{2}x_{max}}{\mu\sigma}((1+\mu)^{\frac{i}{L}} - (1+\mu)^{\frac{i-1}{L}})}\right) + \sigma^2 e^{-\frac{\sqrt{2}x_{max}}{\sigma}}. \end{aligned} \tag{22}$$

Optimizing the previous expression in the same manner as in Section 3, we get the results given in the Table 1 and Figure 2. In Figure 2 we can observe that our $L = 4$ switching piecewise uniform method with $N_1 = 128$ and $N_2 = 256$ outperforms the classical $\mu = 255$ law method for 2.5 dB and 2.2dB, respectively. Comparatione is also made with G.711 standard, and it is also shown that our model satisfy the G.712 standard with 1 bit compression obtained. Our switching piecewise uniform model, with $L = 8$ segments and $L = 16$ segments (see table 1), gives almost same results as switching nonuniform method, with much more simpler realization structure of hardware.

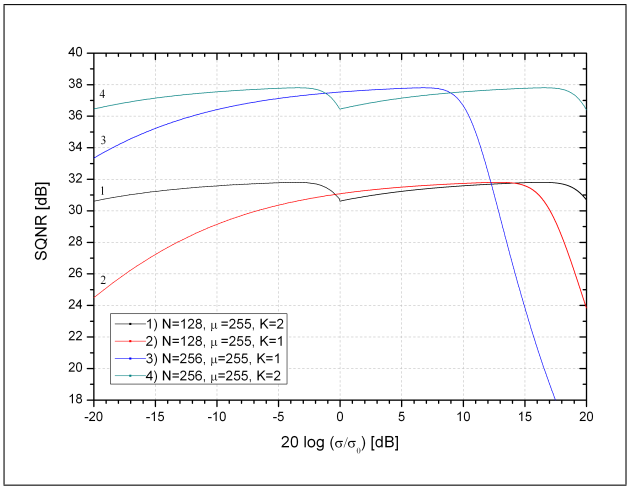

Figure 1: Improvement of quality of transmission ($SNRQ$), for model implementations with two quantizers over robust quantization.

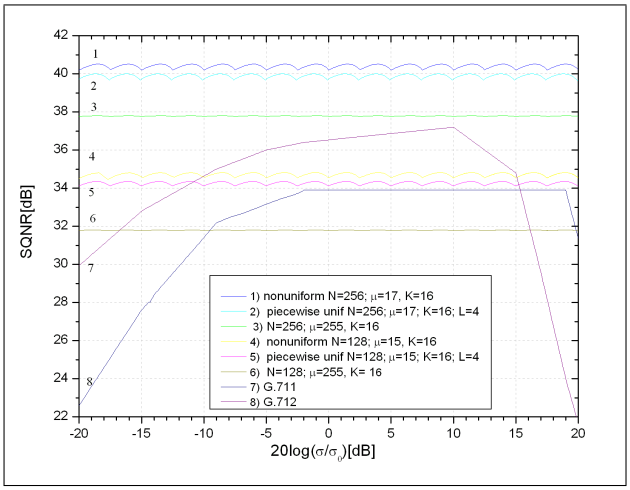

Figure 2: Comparatione of quality of transmission ($SQNR$), for model implementations with sixteen quantizers for standard and optimized value of parameter μ.

5 Conclusions and Future Works

We have suggested switched nonuniform and piecewise uniform scalar quantzation of Laplacian source that solve the problem of variable input power in a wide range. We also have presented

L	$SQNR_{N=128}$	$SQNR_{N=256}$
2	32.76	38.21
4	34.35	39.96
8	34.73	40.37
16	34.82	40.48
64	34.85	40.51
128	34.85	40.52

Table 1: Comparison between values of $SQNR$ of piecewise uniform scalar quantizers for different values of bitrate R, i.e. $N_1 = 128$, $\mu_1 = 15$ and $N_2 = 256$, $\mu_2 = 17$.

how they can accomplish high quality of $SNRQ$ by optimization on maximal amplitude of input signal, by optimization on parameter μ, and by adaptation on input variance range length. They can be applied for coding of speech signals and other continuous signals. The dependence of quality and robustness of quantized signals is analyzed over the broad range of input variances and corresponding number of codebooks with respect to system memory and sample bit rate. Presented switching piecewise uniform model gives almost same results as switching nonuniform method, with much more simpler realization structure of hardware.

Bibliography

[1] R. Gray, Quantization and Data Compression, *Lecture Notes*, Stanford University, 2004.

[2] D. Hankerson, G. A. Harris, P. D. Jr. Johnson, Introduction information theory and data compression, 2nd Ed., *CHAPMAN & HALL/CRC*, 2004.

[3] ITU-T, Recommendation G.711, Pulse Code Modulation (PCM) of Voice Frequencies, *International Telecommunication Union*, 1972.

[4] N. S.Jayant, P. Noll, Digital Coding of Waveforms, *Prentice-Hall*, New Jersey, 1984.

[5] Z. H. Perić, I. Djordjević , M. Stefanović, S. Bogosavljević, Combined Source and Channel Coding of Speech Signal in Wide Volume Range, *Proceedings of the IASTED*, Las Vegas, Nevada, USA, 1998.

[6] Z. H. Perić, Quantization Optimizations of Speech Signal in Wide Volume Range, *Electroniccs and Electrical Engineering*, Vol.45, pp.41-48, 2003.

[7] Z. H. Perić, J. Nikolić, An effective method for initialization of Lloyd-Max's algorithm of optimal scalar quantization for Laplacian source, *Informatica*, Vol.18, pp.1-10, 2007.

[8] Z. H. Perić, A. V. Mosić , S. R. Panić, Robust and switched nonuniform scalar quantization of Gaussian source in a wide dynamic range of power, *Journal of Communications Technology and Electronics*, AVT Journal, Vol.6, pp.74-84, 2008.

[9] Z. H. Perić, A. V. Mosić , S. R. Panić, Coding Algorithm Based on Loss Compression using Scalar Quantization Switching Technique and Logarithmic Companding, *Journal of Information Science and Engineering*, Vol.26, pp.967-976, 2010.

[10] K. Sayood, Introduction to data Compression, 3rd Ed., *Elsevier Inc*, 2006.

Int. J. of Computers, Communications & Control, ISSN 1841-9836, E-ISSN 1841-9844
Vol. VII (2012), No. 1 (March), pp. 123-134

An IMS Architecture and Algorithm Proposal with QoS Parameters for Flexible Convergent Services with Dynamic Requirements

M. Navarro, Y. Donoso

Miguel Navarro
Universidad de los Andes
Bogotá, Colombia
E-mail: mignavarro@egresados.uniandes.edu.co

Yezid Donoso
Universidad de los Andes
Bogotá, Colombia
E-mail: ydonoso@uniandes.edu.co

Abstract:
Quality of Service (QoS) provisioning is one of the main requirements in the 3GPP IP Multimedia Subsystem (IMS) and it has been addressed in different works since the beginning of the IMS standardization process. As a result of the fixed and mobile networks evolution, the parameters standardized in IMS have changed constantly until the specification of the Policy and Charging Control (PCC) architecture that integrates IMS QoS and charging functionalities. However, current IMS QoS specifications still have some limitations to handle service flexibility that is required to provide Internet services over IMS. In this work, we propose an enhanced IMS QoS architecture to support efficient QoS providing for flexible services with dynamic requirements. This proposal is compared against different approaches to evaluate their behavior under network saturation conditions. Simulations results show that the architecture we propose achieves efficiency and flexibility, maintaining the number of blocked and active sessions, and increasing the number of high priority sessions activated in a saturated network.
Keywords: Convergent services, IP Multimedia Subsystem, Quality of Service

1 Introduction

Networks for convergent services are the result of an evolution process followed by fixed and mobile networks. As a result of different trends of evolution, the IP Multimedia Subsystem (IMS) was introduced as the accepted network architecture for convergent services with guaranteed requirements, such as QoS, security, charging, and roaming. QoS provision on IMS networks is a problem that has been studied since the first IMS standardization given by the 3rd Generation Partnership Project (3GPP) in Release 5 [1]. IMS was first introduced as the subsystem in charge of session control for IP services in 3G networks, and for this reason, its evolution process towards IP in mobile networks could be compared to the Next Generation Network´s(NGN) evolution process in fixed networks. However, since IMS was already considering session control features, it was accepted as the unifying standard Core Network (CN) for IP convergent services, increasing its initial scope to include fixed networks as an additional access network [2] [3]. Currently, with the specification of the fourth generation (4G) in mobile networks, 3GPP introduced the program named Evolved Packet System (EPS), which combines the Long Term Evolution (LTE) program,

and the Evolved Packet Core (EPC) program. IMS objectives continued having a leading role in EPS, since LTE is considered as a new access network that may be integrated to the network architecture, and the core in EPS integrates IMS architecture. At this point, networks working with these programs are referred as Next Generation Mobile Networks (NGMN) [4] [5].

In IMS, the problem regarding QoS provision at the IP Media Transport layer is the same as it is defined for the Internet. Several authors have already covered this problem and the models of Integrated Services (IntServ) and Differentiated Services (DiffServ) have been studied under different contexts. Both models apply for IMS networks; nevertheless, DiffServ model's ability to keep minimal information about the network state makes it more scalable compared to IntServ. As a result, 3GPP defined DiffServ as the QoS model for the IP Media Transport layer [1] [6]. For upper layers, 3GPP has also specified the mechanisms for providing QoS. Since IMS Release 7 specification, 3GPP introduced the Policy and Charging Control (PCC) architecture, which continued until Release 9 as the mechanism for determining QoS and charging for convergent services. Although, the PCC architecture specification gives the definition of the entities involved and their basic functions, there is still much work to do in order to cover all possible scenarios and to guarantee QoS requirements. In [7], 3GPP standardized the QoS parameters applied in the service level, and also introduced the concepts of service priority and pre-emption capability and vulnerability, which support conflict handling between services in a state of network saturation. In spite of this concept and function definitions, their relation to the main functional entities in IMS layered architecture is still an ongoing process.

The main objective in this work is to define an enhanced IMS QoS architecture, in order to support QoS providing for flexible services with dynamic requirements in an efficient way. Then, we defined an architecture that supports service relocation between different QoS levels, based on information about priority, pre-emption and the service capability to be flexible. To achieve this, we defined a new QoS parameter called the Service Flexibility Bit (SFB) and a new entity named the QoS Level Relocation Function (QoS-LRF)in the PCC architecture.

The remainder of this paper is organized as follows. In Section 2, we describe some related work. In Section 3, we present the PCC architecture. In Section 4, we propose an enhanced QoS architecture and a heuristic algorithm to validate the architecture. In Section 5, we present the architecture and performance evaluation. The discussion of the results is presented in Section 6. Finally, Section 7 contains our conclusions and directions for further study.

2 Related Work

Related work about QoS in IMS has been presented prior the standardization of the PCC architecture in IMS Release 7. The main focus is on the heterogeneity introduced by different access networks and discrepancies between QoS classes in all of them. This problem is analyzed in [8], where authors present the work developed by 3GPP and ETSI TISPAN in QoS provisioning for IMS. With regard to the session control layer from the IMS architecture, authors emphasize on the importance of the Policy Decision Function (PDF) for 3GPP specifications, a function that is later performed by the PCC architecture. The transport layer is also considered, presenting the benefits and weaknesses' in DiffServ core networks. In the end, a practical implementation on a real network is stated and given for further study. After the PCC architecture specifications where given, several works have been presented focusing on enhancements for charging and QoS functions. In IMS, QoS may be studied according to the different architectural layers, starting with the session control layer and their effects on the application and service layers. In [9], authors propose an approach to IMS policy control based on session policies. In this work, they present service integration using common functions provided by IMS, and horizontal integration as the methodology applied for multimedia service development. With this methodology, they

are allowed to combine service functions together in order to provide a specific functionality, in contrast to the traditional vertical service integration, which basically provides all the functionality with one service module. There are more studies concerning different problems in QoS on IMS, like [10], [11], and [12]; however, the problem introduced by dynamic QoS requirements, service level relocation, and their effect in the transport network, has not been considered.

3 Quality of Service in IMS

The IMS PCC architecture specified for Release 9 in [7] comprises high-level functions for both Charging and QoS. This architecture associates functions previously carried by the Flow Based Charging (FBC) and the Service-Based Local Policy (SBLP) mechanisms, which were separated in previous releases. The evolution process that leads to the PCC architecture starts in Release 5, with a policy framework specification based on the IETF's Policy Management Architecture standardized in [13], and the Common Open Policy (COPS) protocol defined in [14]. Then, in Release 6, 3GPP specifies the Service-Based Local Policy (SBLP) mechanism to differentiate QoS parameters in the service level. Later, in Release 7, the PCC architecture was first introduced, including charging functions related to the QoS decisions and the allocated resources. Finally, in Release 9 the PCC architecture includes some new specifications. The functions included in the PCC architecture to control the QoS are the following: resource allocation, event triggering, media flow establishment, and gating control.

The PCC architecture includes the specification of four service-level QoS parameters: QoS Class Identifier (QCI), Allocation and Retention Priority (ARP), Guaranteed Bit Rate (GBR), and Maximum Bit Rate (MBR). These parameters define QoS features that will be taken into account for further implementations of functions performed by PCC entities [7].

QoS Class Identifier (QCI) The QCI is a scalar number associated to a network element and it is used to describe the packet forwarding treatment in terms of performance characteristics. This value needs to be pre-configured by the operator directly into the element. Since there may be many characteristics associated to the QCI values, 3GPP standardized four characteristics: resource type, priority, packetdelaybudget, and packeterrorlossrate.

Allocation and Retention Priority (ARP) The ARP parameter incorporates information about the priority level, pre-emption capability (PEC) and pre-emption vulnerability (PEV). The priority level has a range of values from 1 to 15, in which 1 is the highest possible value. In the same way, values from 1 to 8 should be assigned to services with priority treatment in the network, and values from 9 to 15 should be used for roaming services. In the case of PEC and PEV, they are defined as the capability of a session to get resources that are already assigned to another session with lower priority lever, and as the vulnerability of a session to allow the loss of resources that are already assigned from another session with higher priority level, respectively. The values of the PEC and PEV parameters are set as "yes" or "no".

Guaranteed Bit Rate (GBR)/Non-Guaranteed Bit Rate (non-GBR) This parameter indicates whether a session has reserved bit rate resources or not. It is associated to the resource type characteristic of the QCI.

Maximum Bit Rate (MBR) The MBR parameter indicates the maximum bit rate authorized for a session.

Up to this point, we have presented the specifications given by 3GPP for QoS provisioning at a service level involving the IMS session control and multimedia services layers. As mentioned

earlier, DiffServ is the QoS model defined for the IMS media transport layer, therefore an association is needed between DiffServ's parameters and the service-level QoS parameters discussed in the previous subsection. To define that association, 3GPP includes QoS classes for UMTS networks in the QoS concept and architecture specification given in [6]. There are four UMTS QoS classes: conversational, streaming, interactive, and background. The principal characteristic that differentiates between these classes is delay sensitivity, going from the most sensitive (conversational class), to the less sensitive (background class). Having a characteristic to differentiate between classes, many services could be classified according to their specific requirements.The relation between UMTS QoS classes and DiffServ parameters is presented in [2], based on the GSMA specification for the GPRS Roaming eXchange (GRX). This relation includes additional distinguishing factors in addition to delay sensitivity, such as jitter, packet loss, and Service Data Unit (SDU) error ratio.

4 Proposed Architecture

In the previous section we presented the QoS specifications in IMS on a service level and how they are associated toDiffServ parameters in the media transport layers. We focus on congested networks that need diverse mechanisms to solve conflicts between the different sessions trying to access the network. In current IMS specifications, these mechanisms are based on information contained in the ARP QoS parameter: priority, PEC, and PEV. Nevertheless, it is not completely specified how these parameters are used to solve conflicts, and because of this, configurations may be applied according to each carrier on its own convenience. The problem when this information is not specified, is that each carrier may apply its own configuration following 3GPP indications about service priority levels, but missing to have congruent configurations will lead to increase the probability of rejecting incoming and active user sessions.

DiffServ assigns a percentage of the network capacity to each Per-Hop Behavior (PHB), based on previous information the carrier knows about their users demands [15]. Despite having accurate information about their users demands, the dynamism introduced by IMS services, makes it very difficult to collect that information for one operator, and when relations between different operators are also introduced, there may be several scenarios in which many sessions will be rejected. At the same time that IMS introduces dynamic services, those services allow some flexibility in their QoSrequirements. Flexibility could be used to define mechanisms that not necessarily resolve session conflicts by *blocking* or *canceling* sessions when there are not enough resources. We use the concepts blocking and canceling to differentiate the time when a session is rejected from the network; when a new session is trying to enter the network and that request is denied, we name it blocking the session, and when the session is already activated by the time it is removed from the network, we name it canceling the session.

We define an enhanced IMS QoS architecture that supports flexible services and their relocation in the QoS level assigned at the IP media transport layer. First, relying on the service-level QoS parameters standardized for the PCC architecture [7], we specified a new parameter named the Service Flexibility Bit (SFB) that reflects the service capability of being relocated in a different QoS level. The SFB can be set to "1" or "0", when a session accepts being relocated or not, respectively. The enhanced PCC architecture that we propose is depicted in Figure 1. This architecture introduces a new entity called QoS Level Relocation Function (QoS-LRF), which is in charge of making decisions about session relocation in the QoS levels.

The *QoS Level Relocation Function* (QoS-LRF) uses the information given by the SFB, priority level, PEC, and PEV, in addition to parameters about the transport network state, to decide whether a session is going to be relocated and where. In order to define how the QoS-LRF uses the information to make the decision, we define the mapping of these parameters

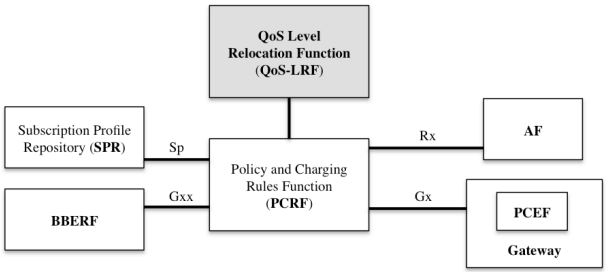

Figure 1: The enhanced PCC architecture

according to the standardized QCI characteristics [7] and UMTS QoS classes and their relation to DiffServ parameters [2]. First, we take the QoS transport levels defined in DiffServ by each PHB and we assign them a priority level between 1 and 9, which is the specified range of values. To assign these values, we joined the corresponding services, starting with IMS signaling that has the highest priority value, and then the different services according to their QoS level. After that, we defined the information required from each service andthat is considered by the QoS-LRF to make the relocation decisions. At this point, we divided QoS parameters in two classes: parameters associated to the QoS level and parameters associated to the session. Finally, we reduced the QoS level parameters to the Bandwidth (BW) requirement in order to reduce the problem complexity, maintaining the relation between UMTS QoS classes and DiffServ parameters, as described in the previous section.

According to the QoS level classification and the services that would be using each of these levels, we define the session relocation as the possibility of reserving the required network resources on a different QoS level, and transferring the session to a different level in order to provide the service according to the QoS parameters specified for the new level. The main objective of this feature included in the QoS-LRF is to benefit the session with higher priority in each QoS level, and also to optimize network resources offering the possibility to use other QoS level resources,

We use the pre-emption functions specified with the PCC architecture, the PEC and PEV parameters, which give us the possibility to use other session's resources and reserve them for a different session with higher priority level. The introduction of the SFB gives us the possibility of using the pre-emption functions in the other QoS levels before blocking the activation of a new session, or before canceling an active session with lower priority level. The heuristic algorithm used by the QoS-LRF is given in Algorithm 1.

As seen in Algorithm 1, when a new session is going to be relocated, the PEC, PEV and SFB values are saved as historical values in order to recover them when resources become available at the original QoS level. In addition, when those values are saved, the new values assigned depends on how the relocation is being done; for example, if a new AF session finds enough resources at the EF level, its PEV and SFB parameters are set to "1", so that if a new EF session enters the networks, the AF session could be relocated in a different level or rejected, but just until the EF level resources are required. On the other hand, when EF and AF sessions are relocated, they go to a lower QoS level, then the PEC parameter is set to "1" and the SFB is set to "0", so that the session that is being relocated can use resources from sessions with lower priority and with the PEV parameter activated. In addition, when the session is relocated it cannot be relocated again. This means that a session cannot be transferred two levels below its initial QoS level and we will not find EF sessions in the BE level. The relocation algorithms for EF and AF sessions are given in Algorithm 4. Finally, when users leave the network and finish their sessions, if they forced other sessions relocation and those sessions are still active, they can be relocated at their

Algorithm 1 New sessions entering the network

```
A new session enters the network
if qos-level = EF then
  if availability in EF then
    resources are reserved in EF/ the new EF session is activated in EF
  else if PEC is activated and enough resources from EF users with lower priority and PEV activated then
    resources are released from the selected EF users/ EF sessions are relocated in AF (*)/ released resources
    in EF are reserved for the new EF session/ the new EF session is activated in EF
  else if SFB is activated then
    the PEC, PEV and SFB values from the new EF session are saved as historical values/ PEC = 1 /
    PEV = 0/ SFB = 0
    if availability in AF then
      resources are reserved in AF for the new EF session/ the new EF session is activated in AF
    else if PEC is activated and enough resources from AF users with lower priority and PEV activated
    then
      resources are released from the selected AF users/ AF sessions are relocated in BE (*)/ released resources
      in AF are reserved for the new EF session/ the new EF session is activated in AF
    else
      the new EF session entering the network is rejected
    end if
  else
    the new EF session entering the network is rejected
  end if
else if qos-level = AF then
  if availability in AF then
    resources are reserved in AF/ the new AF session is activated in AF
  else if availability in EF then
    the PEC, PEV and SFB values from the new EF session are saved as historical values/ PEC = 0/
    PEV = 1/ SFB = 1/ resources are reserved in EF/ the new AF session is activated in EF
  else if PEC is activated and enough resources from AF users with lower priority and PEV activated then
    resources are released from the selected AF users/ AF sessions are relocated in BE (*)/ released resources
    in AF are reserved for the new AF session/ the new AF session is activated in AF
  else if SFB is activated then
    the PEC, PEV and SFB values from the new EF session are saved as historical values/ PEC = 1/
    PEV = 0/ SFB = 0
    if availability in BE then
      resources are reserved in BE for the new AF session/ the new AF session is activated in BE
    else if PEC is activated and enough resources from BE users with lower priority and PEV activated
    then
      resources are released from the selected BE users/ the sessions from the selected BE users are rejected/
      released resources in BE are reserved for the new AF session/ the new AF session is activated in BE
    else
      the new AF session entering the network is rejected
    end if
  else
    the new AF session entering the network is rejected
  end if
else if qos-level = BE then
  if availability in BE then
    resources are reserved in BE/ the new BE session is activated in BE
  else if availability in AF then
    the PEC, PEV and SFB values from the new EF session are saved as historical values/ PEC = 0/
    PEV = 1/ SFB = 1/ resources are reserved in AF/ the new BE session is activated in AF
  else if the new BE session priority level is 8 (highest priority in the BE level) and enough resources from
  BE users with lower priority and PEV activated then
    resources are released from the selected BE users/ the sessions from the selected BE users are rejected/
    released resources in BE are reserved for the new BE session/ the new BE session is activated in BE
  else
    the new EF session entering the network is rejected
  end if
end if
```

initial QoS level with the historic PEC, PEV and SFB values.

Algorithm 2 EF and AF session relocation algorithms

EF session relocation
the PEC, PEV and SFB values from the EF session are saved as historical values
PEC = 1 / PEV = 0 / SFB = 0
if availability in AF **then**
  resources are reserved in AF for the EF session
  the EF session is activated in AF
else if PEC is activated **and** enough resources from AF users with lower priority and PEV activated **then**
  resources are released from the selected AF users
  AF sessions are relocated in BE (*)
  released resources in AF are reserved for the EF session / *the EF session is activated in AF*
else
  the EF session rejected
end if

AF session relocation
the PEC, PEV and SFB values from the EF session are saved as historical values
/ PEC = 1 / PEV = 0 / SFB = 0
if availability in BE **then**
  resources are reserved in BE for the AF session
  the AF session is activated in BE
else if PEC is activated **and** enough resources from AF users with lower priority and PEV activated **then**
  resources are released from the selected BE users
  the sessions from the selected BE users are rejected
  released resources in BE are reserved for the AF session / *the AF session is activated in BE*
else
  the AF session is rejected
end if

5 Architecture and Performance Evaluation

The evaluation presented in this section is based on simulations of architectural models in different scenarios. We define three architectural models in order to have different values to compare results and to have the opportunity to observe improvements given by the session relocation feature and the SFB. Then, the scenarios present different network states, varying times and service requirements for sessions entering the network.

5.1 Architectural models

The first architectural (M1) model is the reference point that gives standard values to compare results obtained with models 2 (M2) and 3 (M3). This model implements neither the session relocation feature, nor the SFB functionality, and for this reason its behavior under congestion conditions is similar to current 3G networks. It looks if there are enough resources and if there are not, the new session is rejected. This reference to current networks is based on the analysis presented on [8] regarding DiffServ networks and QoS resource management. The second architectural model, M2, implements the session relocation feature in case there are resources available in a higher level, and it also implements the pre-emption functions for using resources in the same QoS level. The sessions, which resources are released to be used by a higher priority session, are rejected. In this model, a session can only be upgraded to a higher level, so that the QoS provided is not reduced from the original requirements. The third architectural model, M3, comprises all the functionality that we propose for the QoS-LRF. Besides implementing the second model's functionality, it implements the SFB that allows using the pre-emption functions in a lower level before rejecting the session. In this model before rejecting any session, even sessions with lower priority and the PEV parameter activated, if the SFB is activated there is a possibility to use resources from a lower QoS level. The relevant information we want to obtain from simulations is the number of rejected and active sessions; with this information we are able to analyze the benefits of the proposed architecture. The first architectural model gives standard values to calculate a percentage error for other models using (1).

(a) Deterministic Parameters

Variable	Description
N	Number of Monte Carlo simulations
λ[users/time]	Process rate
T	Simulation time
even_num = $\lambda * T$[sessions]	Number of sessions
Cap_EF	Level EF capacity
Cap_AF	Level AF capacity
Cap_BE	Level BE capacity

(b) Services Priority Level and Bandwidth Requirements

Priority Level	QoS Level	Service	Bandwidth
2	EF	VoIP	32 Kbps
3	EF	Video conference	1 Mbps
4	AF	Streaming	512 Mbps
5	AF	Transactional services	1 Mbps
6	AF	Web browsing	64 Kbps
7	AF	Telnet	8 Kbps
8	BE	E-mail	1 Mbps
9	BE	Web browsing	1 Mbps

(c) Ranges and Distributions for Random Parameters

Parameter	Distribution	Ranges
Arrival time	Uniform	$[1, T]$
Session lengh	Normal	$N(\mu, \sigma)$ according to the scenario
QoS level (type of service)	According to the scenario	EF, AF, BE
Priority level	Uniform	According to the QoS level
Bandwidth	Uniform	According to the QoS level and the priority level
PEV/PEC	Uniform	$0, 1$
SFB	Uniform	$0, 1$

Table 1: Simulation Parameters

$$\delta = \frac{100\,(V_{exp} - V_{std})}{V_{std}} \tag{1}$$

We simulate implementations of the three architectural models and the network behavior. Arrival of network users is simulated as a Poisson Stochastic Process with a rate parameter λ, using Monte Carlo simulations, and we define the simulation deterministic parameters as shown in Table 1(a). Table 1(b) shows the bandwidth requirements defined for services in the different priority levels. Afterwards, we specify the random parameters of the simulation, such as arrival time, length of the session, QoS level, priority levels, session requirements, PEC/PEV, and SFB; Table 1(c) shows the ranges and distributions for the random parameters.

5.2 Simulation scenarios

Simulation parameters were fixed for all scenarios. They were selected to achieve the objective of simulating the architecture in a saturated network and therefore, having the opportunity of studying the model's behavior in that state. The process rate λ was set to 0.95 simulations per period. Then, the simulation time was set to *2000 sec*; it can also be interpreted as any other consistent unit of time. With this values, for each simulation *1900 users* try to access the network with a random service, and a service duration time following a normal distribution with μ=*300 sec* and σ=*200 sec*. Afterwards, levels capacities are set to 20 Mbps and according to the bandwidth requirements from Table 0(b), the state of network saturation may be achieved with at least *60 sessions* in a worst-case scenario. Finally, type of service is selected as the parameter that changes for each scenario and all the other parameters are defined as random with equal probability for every value in its range. Figure 2 presents a basic description of each simulation scenario, and the results obtained for the number of rejected users and the percentage of usage for each QoS level.

6 Discussion

Previous simulations give information about the number of rejected and active sessions for three models in the four scenarios we selected. The four scenarios were chosen to test the models varying the type of sessions entering the network, a parameter that we selected as the most sensitive to the algorithm proposal because inthe simulation it determines how the QoS level resources are used, and it also gives information about the type of carrier. That allows us to analyze the results according to the behavior a carrier would expect.

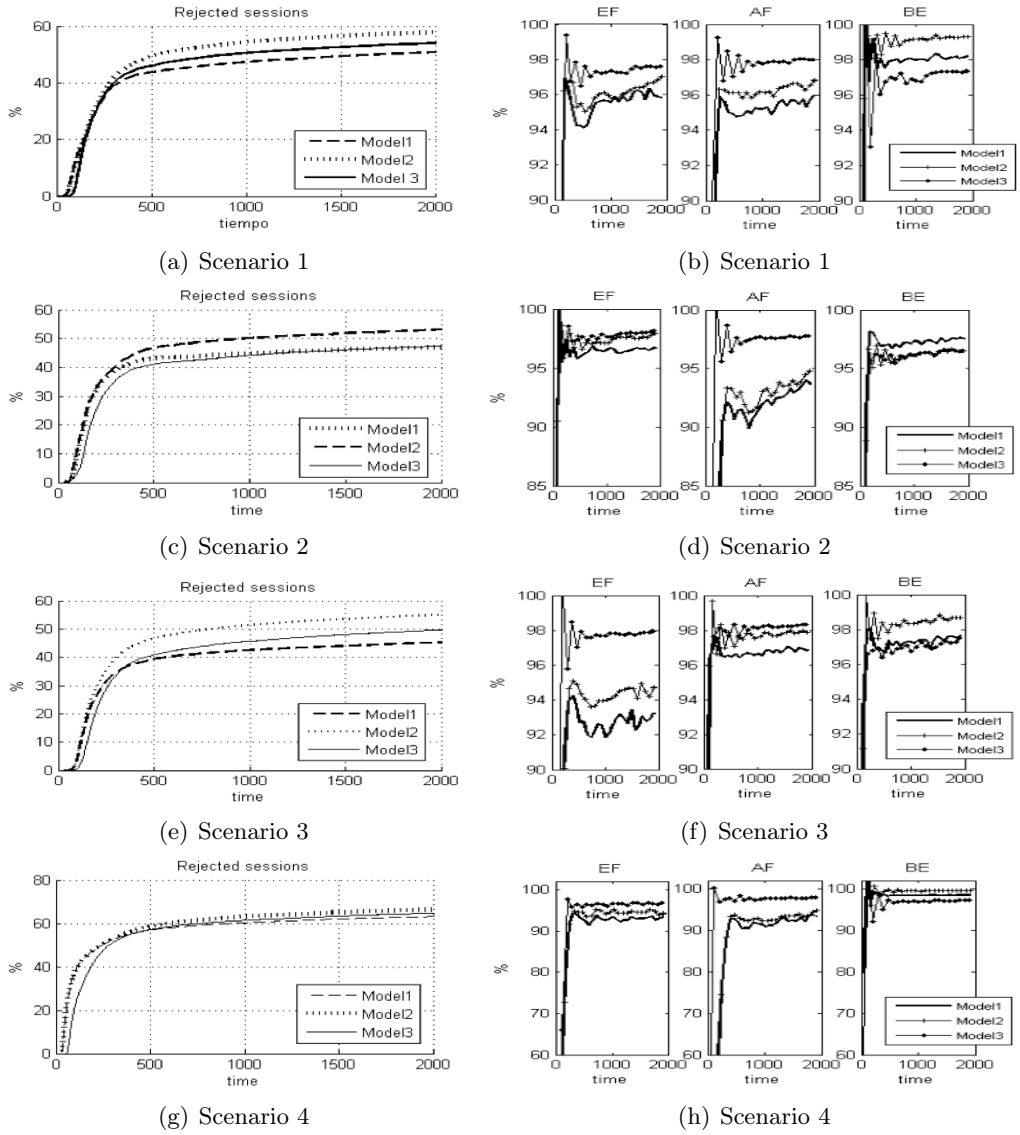

(a) Scenario 1 (b) Scenario 1

(c) Scenario 2 (d) Scenario 2

(e) Scenario 3 (f) Scenario 3

(g) Scenario 4 (h) Scenario 4

Figure 2: Simulation scenarios. Scenario 1: Basic scenario, sessions generated with the same probability. Scenario 2: Sessions generated with 60% probability for EF, 20% for AF, 20% for BE. Scenario 3: Sessions generated with 60% probability for AF, 20% for EF, 20% for BE. Scenario 4: Sessions generated with 60% probability for BE, 20% for EF, 20% for AF. (a), (c) (e) and (g) show the accumulated percentage of rejected sessions, and (b),(d), (f) and (h) show the Percentage of usage of each QoS-level in the network.

The first graphics presented, for each scenario, depict the behavior of rejected sessions. As we defined it previously, a blocked session refers to a session that could not be activated in the network due to the lack of resources. A canceled session is counted when a session that was already active in the network is removed from it at because a new session, with the PEC parameter activated and with a higher priority, is going to use the resources from the canceled session. Then, rejected sessions refer to the total number of sessions that leave the network, adding the blocked and canceled values. Comparing results from the different scenarios in the previous section, we can see that M3 reduces the number of blocked sessions in all scenarios compared to M2 and M1. This results presented in Figure 3(a), indicates a benefit from implementing M3 over

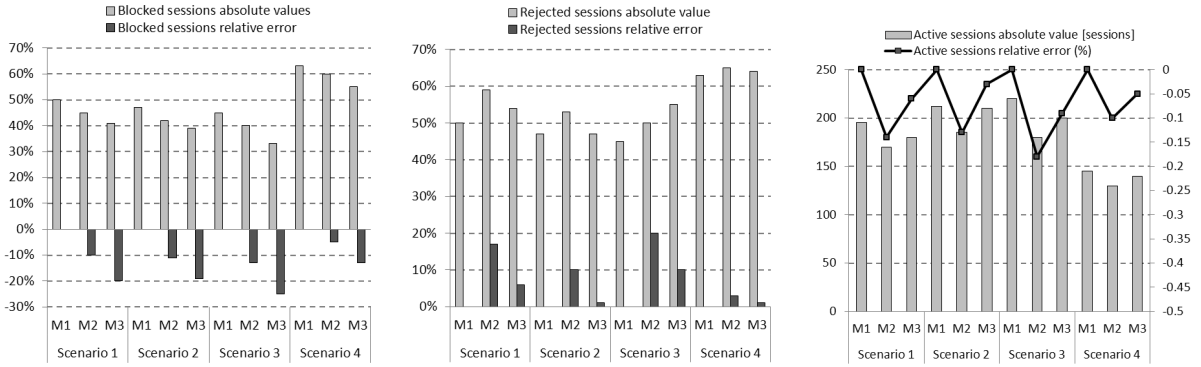

(a) (b) (c)

Figure 3: Simulation results. Part (a) shows the blocked sessions relative error comparison and, it shows the blocked sessions absolute values comparison at *t=2000sec*. Part (b) shows the rejected sessions relative error comparison, and the rejected sessions absolute values comparison at *t=2000sec*. Part (c) shows the active sessions relative errors to Model 1 at *t=2000sec*, and the number of active sessions at *t=2000sec*.

M1 and M2. Despite having this result for the number of blocked sessions, it is very important for the algorithm not to increment abruptly the canceled session percentage because M1 does not cancel any session. According the definition of M1, once a session reserves resources they cannot be released until the user finishes the session. The small effect of canceled sessions may be confirmed with the percentage of rejected sessions, as depicted in Figure 3(b). Looking at the results in all scenarios, the number of canceled sessions in M3 may be considered to have an effect that we may consider as small if we take into account that M2 always ends having a mayor percentage of canceled sessions than M3. The small effect of canceled sessions may be confirmed with the percentage of rejected sessions form Figure 2. In scenarios 2 and 4 there is no significant difference for the percentage of rejected sessions between M1 and M3; however, in scenarios 1 and 3 there are relative errors of 6% and 10%, respectively. As expected, M2 increases the total percentage of rejected sessions compared to M1 and M3, and it is also very important to remark that the behavior of M3 may maintain the percentage of rejected sessions obtained in M1, the reference model.

It is not enough to demonstrate that our proposal maintains the percentage of rejected sessions to validate it, because there would be no reason to select M3 over M1. The value added given by this work comes from the number of active sessions and how they are distributed among the QoS levels. In this point, M3 algorithm's behavior is better for scenarios 2 and 4 than for scenarios 1 and 3, but it still has a negative relative error, which means that M3 may reduce the number of active sessions. Unlike blocked session data, the information in Figure 3(c) about active sessions is considered instantaneous and in absolute values, not accumulated percentages as before. Then, taking into account the final values is not enough. If we consider the results for the number of active sessions in each QoS level presented in the previous section, we can observe there is a consistent behavior for M3 increasing the number of EF active sessions. Therefore, results obtained with M3 are according to the objectives, increasing the number of active sessions that have the highest priority level, and M2 does not increase the number of active EF session compared to M1 in any scenario. Under saturation conditions, the number of EF active sessions in M1 is higher than M2, validating the importance of the SFB implementation in M3.

Bringing previous observations together, the simulations results show that our proposal, implemented in M3, may be a feasible implementation for the four considered scenarios, although

it has a better behavior in scenarios 2 and 4. In scenario 2, it is very important to see that M3 maintains the same values as M1 for both rejected and active sessions. There is significant reduction of the number of active AF users, but since EF sessions are arriving with three times AF session's probability, it may be considered as an accepted tradeoff. Then, Scenario 4 gives important results because M3 also maintains very small differences with M1 in rejected and active sessions. In this scenario, the number of BE sessions entering the network is higher compared to the other QoS level sessions. Finally, scenarios 1 and 3 present higher differences between M1 and M3; nevertheless, we consider them feasible scenarios because they maintain the model's objective and increase the number of high priority sessions with a higher tradeoff in the number of sessions rejected from the network. Analyzing the complexity of the algorithms in a worst case basis, it is evident that for every incoming session, the running time will be $O(n)$, where n is the number of active sessions in the network. Considering concurrent sessions entering the network, the running time will be $O(mn)$, where m is the number of sessions entering the network.

7 Conclusions

In this work we present an efficient and enhanced IMS QoS architecture to support QoS providing for flexible services with dynamic requirements. Our approach follows the 3GPP QoS specifications and is based on the PCC architecture. We propose an architecture including new features in the PCRF entity given by the concept of session relocation and the introduction of the QoS-LRF and SFB. The proposed heuristic algorithms for the QoS-LRF use information already available at the PCRF according to the PCC architecture specifications. According to the three model simulations, our proposal overcomes the first two models, which offer a valid implementation of current 3GPP PCC architecture specifications. The results obtained for the number of rejected and active sessions validates it, and for this reason, our proposal would have a good performance for carriers with customers requesting more EF and BE services. Furthermore, for carriers with customers requesting all types or services at the same rate, or requesting more AF services, the algorithm achieve the objectives but with some tradeoffs for its implementation that would need to be evaluated. The architecture proposal achieves the objectives of efficiency and flexibility. Efficiency may be analyzed according to how network resources are used. The objective validation is given by the simulations showing that implementing our proposal, the number of rejected and active sessions is maintained and at the same time, the number of high priority sessions is increased, then network resources are properly assigned according to the priority level. Flexibility is achieved with the definition of the SFB and the algorithms implementations. They offer the possibility of relocating a session in a lower QoS level, before it is rejected from the network. Other important contributions of this work is that carriers would have the possibility of assigning different priorities to the same service within the same QoS level, and offer the service at different rates controlled by the PCC architecture charging mechanisms. Finally, the worst case running time of the algorithms is $O(n)$, where n is the number of active sessions in the network, and if the possibility of having m concurrent sessions entering the network is considered, the worst case running time is $O(mn)$. For further study, we will continue with the message flow analysis required to implement our proposal and a prototype implementation. We will also study scenarios involving different carriers and roaming services, which could be implemented in the prototype.

Bibliography

[1] 3GPP, "IP Multimedia Subsystem (IMS); Stage 2", Release 5, TS 23.228 V5.15.0, June 2006. http://www.3gpp.org/ftp/Specs/html-info/23228.htm

[2] R. Copeland, Converging NGN wire line and Mobile 3G Networks, CRC Press, USA, 2009.

[3] G. Camarillo and M. A. García-Martín, The 3G IP Multimedia Subsystem (IMS): Merging the Internet and the Cellular Worlds, 2nd Edition, John Wiley & Sons Ltd., England, 2006.

[4] M. Sauter, Beyond 3G - Bringing Networks, Terminals and the Web Together. John Wiley & Sons Ltd., United Kingdom, 2009.

[5] T. Magedanz, A. Diez, M. Corici, and D. Vingarzan, "Understanding NGMN and Related Technologies - LTE, EPC and IMS", IMS Workshop 2009, Tutorial 4, Fraunhofer FOKUS. Berlin, Germany, November 2009.

[6] 3GPP, "Quality of Service (QoS) concept and architecture", Release 9, TS 23.107 V9.0.0, December 2009. http://www.3gpp.org/ftp/Specs/html-info/23107.htm

[7] 3GPP, "Policy and charging control architecture", Release 9, TS 23.203 V9.0.0, March 2009. http://www.3gpp.org/ftp/Specs/html-info/23203.htm

[8] S. Tompros, and S. Denazis. "Interworking of heterogeneous access networks and QoS provisioning via IP multimedia core networks", Computer Networks, Volume 52, Issue 1, pp. 215-227, January 2008.

[9] G. Camarillo, T. Kauppinen, M. Kuparinen, and I. M. Ivars, "Towards an innovation oriented IP multimedia subsystem", Communications Magazine, IEEE, volume 45, issue 3, pp. 130-136, March 2007.

[10] R. Good and N. Ventura, "End to end session based bearer control for IP multimedia subsystems", IFIP/IEEE International Symposium on Integrated Network Management IM '09, pp. 497-504. June 2009.

[11] M. Ageal, R. Good, A. Elmangosh, M. Ashibani, N. Ventura, and F. Ben-Shatwan, "Centralized policy provisioning for inter-domain IMS QOS", EUROCON '09, pp. 1793-1797. May 2009.

[12] S. Tompros, C. Kavadias, D. Vergados, and N. Mouratidis, "A Strategy for Harmonised QoS Manipulation in Heterogeneous IMS Networks", Wireless Personal Communications, vololume 49, number 2, pp. 197-212. Springer Netherlands, August 2008.

[13] R. Yavatkar, D. Pendarakis, and R. Guerin, "RFC2753 - A Framework for Policy-based Admission Control", Network Working Group, January 2000. http://www.rfc-editor.org/rfc/rfc2753.txt

[14] D. Durham, J. Boyle, R. Cohen, S. Herzog, R. Rajan, and A. Sastry, "RFC 2748 - The COPS (Common Open Policy Service) Protocol", Network Working Group, January 2000. http://www.rfc-editor.org/rfc/rfc2748.txt

[15] C. Filsfils and J. Evans, Deploying Diffserv in Backbone Networks for Tight SLA Control, IEEE Internet Computing, volume 9, issue 1, pp. 66-74. January 2005

Int. J. of Computers, Communications & Control, ISSN 1841-9836, E-ISSN 1841-9844
Vol. VII (2012), No. 1 (March), pp. 135-146

Adaptive Neuro-Fuzzy Controler With Genetic Training For Mobile Robot Control

O. Obe, I. Dumitrache

Olumide Obe
"Politehnica" University of Bucharest, Romania
E-mail: oluobes@gmail.com

Ioan Dumitrache
"Politehnica" University of Bucharest, Romania
E-mail: ioan.dumitrache@cncsis.ro,
idumitrache@ics.pub.ro

Abstract:
In this paper, we investigate the use of adaptive techniques in the optimization of navigation of Khepera mobile robot in an unstructured and dynamic environment. We optimize the performance of our simplified fuzzy controller using neural network that utilizes genetic algorithm learning. The adaptation of the system involves the tuning of the control rules thereby trimming the control actions, and adjusting the fuzzy controller output gain. We realised an improved performance in our adaptive neuro-fuzzy controller with genetic training for various implemented behaviours on the robot.
Keywords: Khepera, fuzzy controller, neuro-fuzzy controller, navigation, genetic algorithm.

1 Introduction

Navigation and obstacle avoidance are very important issues for the successful use of an autonomous mobile robot in a dynamic and unstructured environment. Mobile robot researchers aim to build an autonomous and intelligent robot which can plan its motion in a dynamic environment. A successful use of an autonomous mobile robot depends on its controller. Mobile robot control is difficult as they are subjected to non-holonomic (non-integrable) kinematic constraints involving the time derivates of configuration variables [12] and dynamic constraints. Both analytical like potential field method as well as graph-based techniques have been used to solve the navigation problems of robot involving both static and dynamic obstacles. But, all such methods may not be suitable for on-line implementations due to their inherent computational complexity and limitations. Mobile robot researchers have carried out various researches in this direction using various intelligent techniques methods such as fuzzy logic, neural network and genetic algorithm and their different hybrids. Because of the non-linear kinematics of the robot, the uncertainty in sensors readings, and unstructured environmental constrains in the control of mobile robot navigation; researchers have found fuzzy logic as one of the best intelligent technique for handling the constraints. However, fuzzy logic needs tuning for optimal performance. Hand tuning is very difficult and time consuming therefore there is need for automation of the tuning process. The process of tuning requires learning brought about by training or adaptation of the robot to adapt to its dynamic environment. The poor learning capability of fuzzy logic is compensated for by hybridizing fuzzy logic with other soft computing techniques with excellent learning features such as neural network. In this paper, we present an adaptive neuro-fuzzy controller with genetic algorithm learning for the navigation of Khepera mobile robot.

2 State-of-the-art of Control of Mobile Robots

A mobile robot is a situated and embodied agent endowed with mobility; and operates autonomously, communicating with, and exploring its environment. Mobile robots are complex systems functioning in real world environments thus, making it uneasy to design an adaptive control system that can control robots to act as desired. Task based decomposition of robot control by Brooks' [8] subsumption architecture that makes easy design of robots to realize multiple behaviours, respond to multiple sensors and incrementally extension has been successfully applied in mobile robot [9].Researchers in robotics use theories and concepts from intelligent control theory described as behaviour-based control as an alternative to conventional robot control since real world cannot be accurately modeled. Because of the need to operate in unknown environments, mobile robots demand much higher level of intelligence in order to learn to adapt successfully to its ever changing environment. Intelligence in a mobile robot is considered as an adaptive behaviour that makes a robot adapt to and acts intelligently in its environment.

Intelligent control is an act of directing a complex system to a goal [1].The intelligence is the property of a system that emerges when procedures of focusing attention, combinatorial search and generalization are applied to the input information so as to receive the output results [2].Consequently, Murphy [3]defines an intelligent mobile robot as a situated agent with a mechanical structure that operates autonomously.

Intelligent systems strategies like fuzzy logic, neural network, and genetic algorithms have been used to endow robot with intelligent capability to navigate its environment autonomously. Various hybrids of these strategies have also been implemented successfully on mobile robots. In this work, we employ hybrid geno-neuro-fuzzy intelligent strategies to control Khepera mobile robot.

3 Fuzzy Control of Mobile Robot

Fuzzy control is one of the intelligent control techniques that pertain to the realization of intelligent control systems. Fuzzy control provides a mechanism for incorporating human-like reasoning capabilities and computation in control systems. The linguistic variables are used to mimic the human action into a system more closely than traditional control. Fuzzy logic is a logical system that aims at a formalization of approximate reasoning [10].These can be represented as the concept of a linguistic variable, canonical from, fuzzy if-then rule, fuzzy quantifiers, and modes of reasoning.

3.1 Fuzzy Controller Design

In this paper, we design a simple fuzzy logic controller for Khepera mobile robot for obstacle avoidance and wall following behaviours.

Our Fuzzy logic controller architecture is as shown in figure 1:

Where, r = sensors input from the robot and $U_{ext} = [5000, 5000]$ i.e. the maximum robot's motor speed for stability (for our design), which is equal to $35mms^{-1}$ real speed.U_{fc} is the Fuzzy Controller output; U = the resultant speed for the robot; and Y = the robot output control signal.

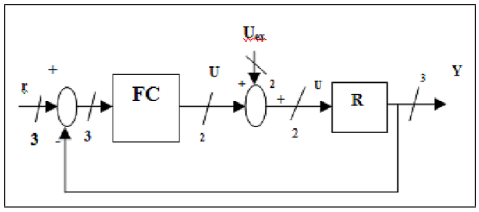

Figure 1: Architecture of our Fuzzy Logic Controller for the Mobile robot showing the number of inputs and outputs parameters at each processing stage.

Obstacle Avoidance Fuzzy Controller

We design the obstacle avoidance controller to allow the robot to avoid colliding with any object along its path to its target. The controller will empower the robot to maneuver its way around any obstacles without colliding with them. By using Mamdani fuzzy logic approach, we define three sensor input variables representing relative distance between the robot and any object in its environment. These include: Left Distance (LD), Right Distance (RD), and Front Distance (FD). Since the robot rarely uses the back sensors because, the robot usually moves forward, we exclude back sensor readings in our design. The physical domains over which these input variables are defined are determined as:

$LD = Max(S2, S3)$;
$FD = Max(S4, S5)$;
$RD = Max(S6, S7)$.

Where $Si(i = 2, 3...7)$ are the sensor values normalized within the interval [0,1]. All these input variables have the same base variable length.

Figure 2.1 shows our defined membership function distributions of the input variables. For simplicity, we use two types of shapes for our membership function. These include the z-shaped and s-shaped membership functions shape types. Two linguistics variables (or grades of distance) from the robots' sensors are considered: Not Detected (ND), and Detected (D). We use z-shaped membership function type for the ND grade and s-shaped membership function type for the D membership function. These membership function types are the variant of Gaussian membership functions that have been proved experimentally by [11] to be of better performance for the same robot navigation problems.

The output fuzzy variables are the motor speed of the robot's wheels, represented by Left Velocity, LV and Right Velocity, RV. For the output fuzzy variables, we use three linguistic variables (S-Slow, Z-Zero, and F-Fast) for each of the fuzzy output variables. We use Gaussian membership function type for each of the linguistic variables. The simplicity in the design is to reduce complexity. This is at the cost of granularity which we belief would be compensated for by the optimization of fuzzy controller using neural network with genetic training. This design invariably reduces the number of fuzzy rules as expected, to 8 rules. Some of the 8 rules are shown in Table 1.

4 Neural Network Design

A layer network is used for our Neural Network as shown in figure 2.
Where,
Xi = sensors input (the context and the last two history inputs each of three pair)

$Y = f(W * \begin{bmatrix} 1 \\ X \end{bmatrix}) + bias)$, bias=1

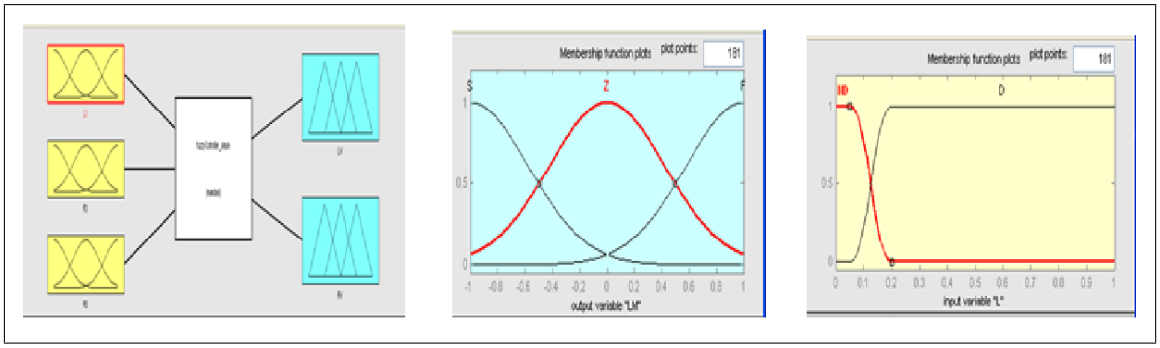

Figure 2: Fig.2.1 Fuzzy Controller design Fig.2.2: Input MFs Plot Fig.2.3: Output MFs Plot.

Rule No.	INPUT SENSORS IF LD	FD	RD	OUTPUT MOTOR WHEELS THEN LV	RV
1	ND	ND	ND	Z	Z
2	ND	ND	D	Z	F
3	D	ND	ND	F	Z
4	ND	D	–	S	F
5	D	D	–	F	S

Table 1: Fuzzy Rule Table for Khepera III Fuzzy Controller

$f(s) = \frac{1}{1+e^{-s}}$
$S = W_{01} + W_{11} * X_1 + \cdots + W_{19} * X_9$
$W \in U_{5,10}(R)$ (5 neurons for fuzzy weights with 9 sensors inputs and a bias).

We design a network of 5 neurons representing the 5 fuzzy rules weight to be optimized. The inputs are the sensor readings from the 3 fuzzy input variables (LD, FD, and RD). In other to ensure that our robot collides not with the obstacles considering the simplicity in our fuzzy design, we decided to keep history of the last two sensors readings with the context readings of the robot as the input to our NN. This allows the robot to keep history of the last two previous inputs values from the sensors thereby increasing accuracy of decision of eliciting obstacle avoidance bahaviour.

The input of our NN is the sensor values from the robot and the output is the 5 optimized rule weights to optimize fuzzy logic controller performance for obstacles and wall following behaviours.

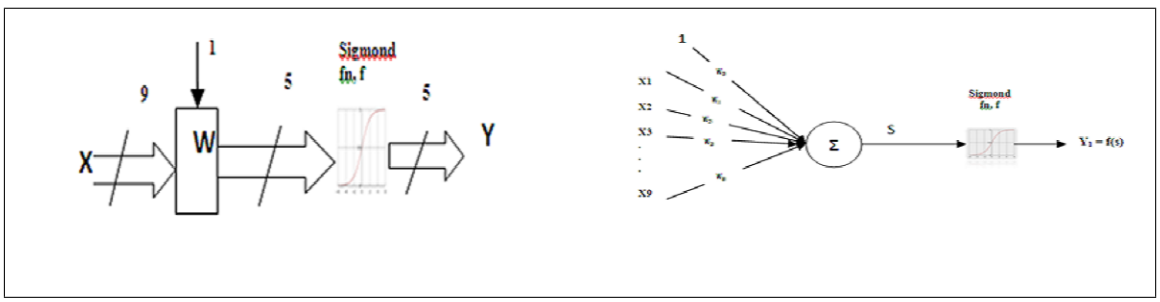

Figure 3: A layer Neural Network Architecture for our Network design

Genetic Algorithm for Training

We employ GA as the learning algorithm of Neural network weight which invariably optimize NN performance resulting in NN optimizing fuzzy Logic rules weights and thereby optimizing the Robot navigation in terms of wall following and obstacle avoidance behaviours.

Initially, 50 random weight matrix of 20 population size for each individual are generated and made to evolve for 100 generations. This was tested on the robot to get new 50 different weights. For each generation, a performance index, ϵ to evaluate the fitness of each chromosome is computed in terms of the number obstacles avoidance performed successfully. We set a fixed path to be traversed by the robot for each generation. Each chromosome is evaluated based on this performance measure. The evaluation of the chromosome fitness determines either to accept the chromosome as potential part of the new population for reproduction in the next generation. The fit chromosomes are set as part of the new population. For the next generation, 20 new populations are generated by using genetic operators like crossover and mutation. Two point crossovers were used and the mutation factor was set at 0.05. With the best 10 chromosome and 10 new chromosomes, the robot is tested. In this way the algorithm continues till the optimum obstacle performance is obtained.

Figure 4 below shows the flow chart for our genetic algorithm implementation for the optimization of NN weights.

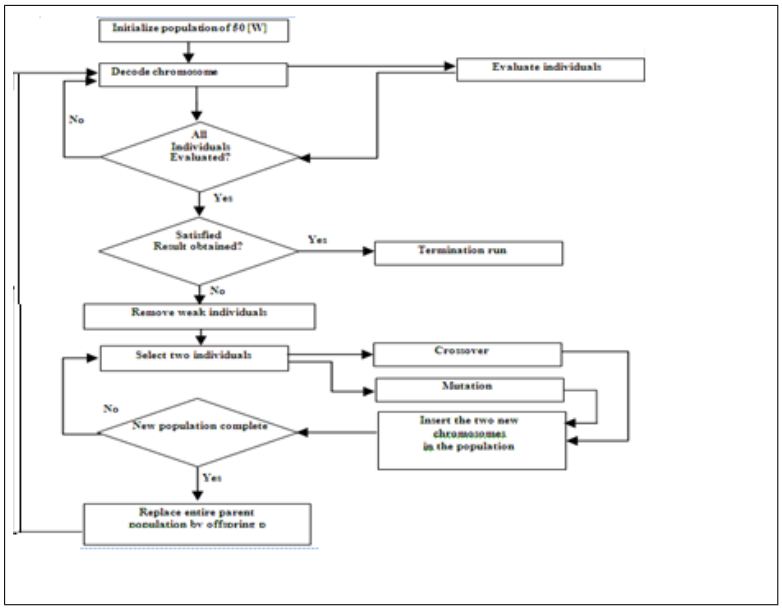

Figure 4: Flow chart for our genetic algorithm implementation for the purpose of optimization of NN weights.

5 Neuro-Fuzzy Control of Mobile Robot with Genetic training Design

We design a Neuro-Fuzzy controller for our mobile robot control using genetic training(figure 5).

The overall design of our Neuro-Fuzzy controller with genetic algorithm learning is as illustrated in figure 9 above.

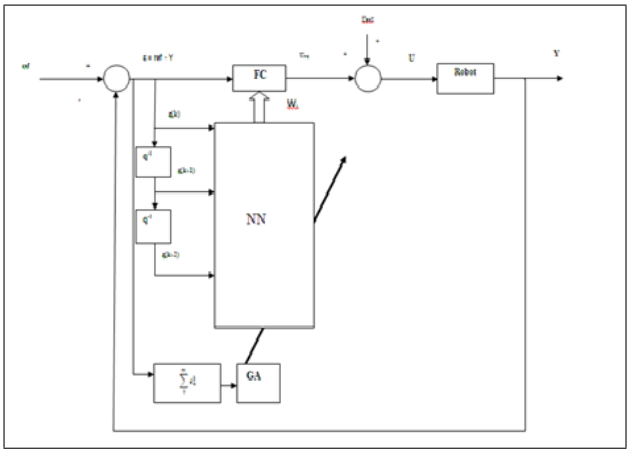

Figure 5: Geno-Neuro-Fuzzy Controller for Khepera Mobile Robot

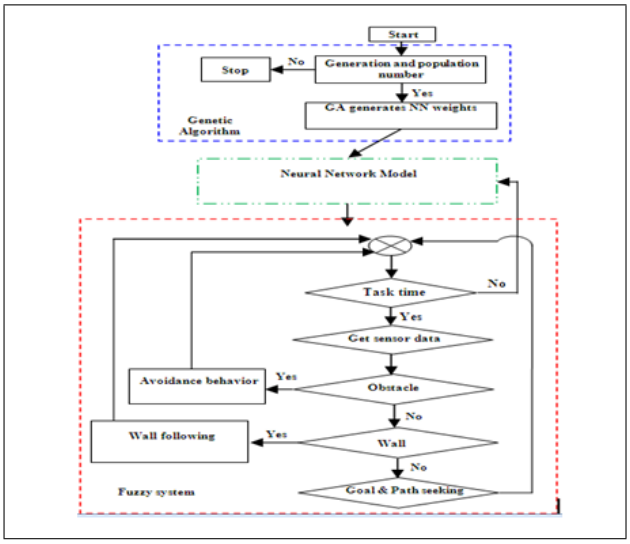

Figure 6: A schematic diagram showing flowchart of the the Khepera Mobile Robot motion planning scheme of our robot control using geno-neuro-fuzzy controller.

The overall Neuro-Fuzzy controller with genetic training has the sensors values of the robot from the fuzzy variable parameters as the reference input, all initialized to zero. The sensor readings from the robot are the inputs to the fuzzy controller and the neural network. The outputs of the fuzzy controller are the speed values for the left and right motors of the robot. The external speed input, U_{ext} represents the possible maximum set hardware speed for the Khepera robot in other to obtain stable performance. The resultant output speed, U is used for the navigation control of the robot. The difference in the robot output speed Y and input speed is computed and feed back as error, ϵ. This error serves as the fitness function to measure the fitness of each individual chromosome in the GA.

6 Result and Discussion

In the developed neuro-fuzzy approach, training is done off-line with the help of Genetic algorithm. The computer simulation is carried out by considering an arena (KiKS arena) with number of obstacles. Apart from smoothness in path traced by the robot, we have decided to use other index of performance measures to evaluate the performance of the optimization results. These include the error measure implemented in our program to monitor the difficulties in obstacles avoidance. Each experiment is run in the same environment with equal number of obstacles along the robot's path. Hence, we can measure performance in terms of difficulties in circumventing obstacles by the robot by penalizing or rewarding the actions. This measure is what we call error penalty (EP) in this work. The objective function is to minimize this error. Hence, the smaller the error, the better the performance output.

Fuzzy Controller Obstacle avoidance simulation results

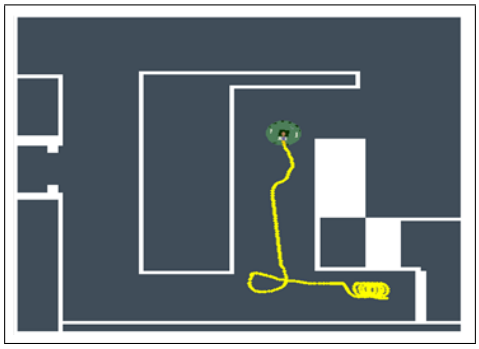

Figure 7: FL controller output (EP = 57.99)

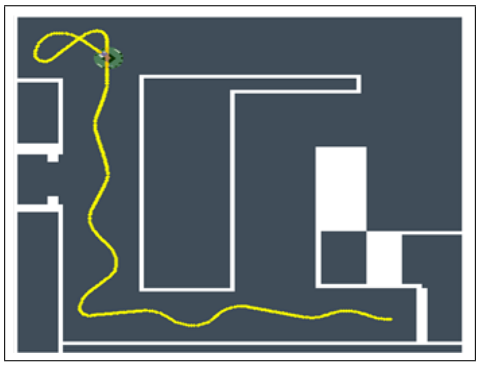

Figure 8: FL controller output after manual tuning of rule base (EP =12.58)

From figure 7, it is obvious that even though our fuzzy controller succeeds in avoiding obstacles, the robot was trapped initially and could not move forward until after several loops. In other to improve the robot's performance, we decided to manually tune our fuzzy controller by adjusting some rules consequences of the rule base. The result of the manual tuning is made obvious by the improved performance observed in figure 11 below. The robot can now move forward to the target without being caught in a loop. We equally observed reduced error measured from 57.99 to 12.58.We further improve on the fuzzy controller by manually adjusting the membership sets of the fuzzy controller. We notice improved performance in the path traced by the robot and the number of error encountered in obstacle avoidance behaviour (from 57.99 errors to 12.58 errors). This result is shown in figure 9 below.

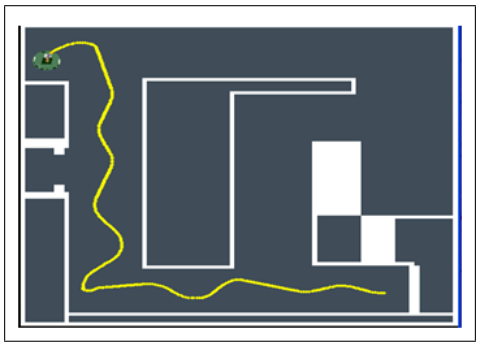

Figure 9: Fuzzy controller after hand tuning of rule base and membership function sets (EP = 12.58)

From the fuzzy controller performance results presented above, we could not reach better performance in terms smoothness of path traced by the robot by manual tuning. The lack in granularity is responsible for the zig-zag movement of the robot along its path. Therefore, we decided to employ neural network with genetic training to fine tune the navigation performance. Because of the simplicity in the fuzzy design, in terms of number of rules in the rule base, we observed that the optimal result would be better realized by deciding on what rules to be executed at an instant of time instead of further tuning of rule base and membership function parameters. Hence, we focus on the automatic tuning of the rule weights. The idea is based on the fact that we can train an NN model using a genetic training to evolve an optimal rule weights for the navigation control, wall following, and obstacle avoidance behaviours for our robot. The neuro-fuzzy controller with genetic training designed in this paper was put to test and we have realized the results below.

Neuro-fuzzy with genetic training for obstacle avoidance result

In this section, we present the implementation result of our neuro-fuzzy controller with genetic training.

The first weights set generated by our neuro-fuzzy with genetic training were used in the neuro-fuzzy controller. The simulated output result of this implementation is shown in figure 13. Apart from smoothness in path traced by the robot and error penalty (EP), we equally utilize the readings as observed by the simulation trace output report window of the KiKS simulator as shown in figure 14.

The report gives information on the number of Forward, Backward, and Straight moves of

the robot. With this information, we can easily measure the performance based on number of straight moves made by the robots and also find the ratio of straight moves to forward moves (called performance ratio in this work) in other to compare the performance of each set of weights set generated in each generation. This performance ratio helps to further justify path smoothness traced by the robot.

Hence, our overall desire is to obtain performance output result with the smoothest path traced by the robot; minimum error penalty (EP); and maximum performance ratio (PR).

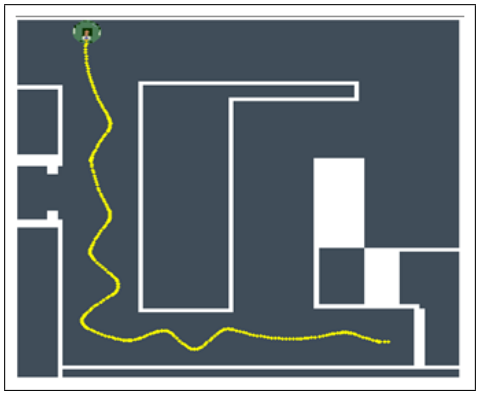

Figure 10: Geno-Neuro-Fuzzy Controller output after first evolution of rule base weights. Error penalty: 64.89; Forward: 181cm; Straight: 84.6cm; Performance ratio: 0.46

The result of implementation of the first weight set output of the neuro-fuzzy controller with genetic training on the robot navigation is shown in figure 10. By comparing figure 9 of manual tuned fuzzy controller with figure 10, there is no much difference in terms of path traced smoothness of the robot.

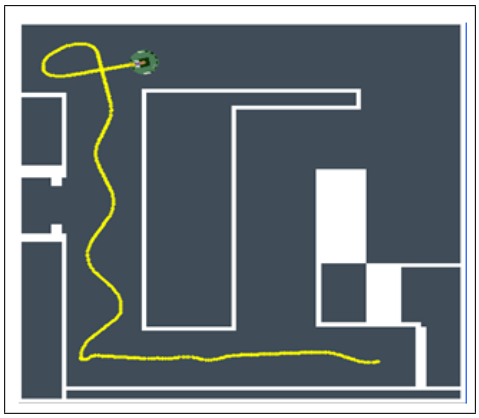

Figure 11: Geno-Neuro-Fuzzy Controller output after 50 evolutions.Error penalty: 12.79; Forward: 181.0cm;Straight: 84.6cm; Performance ratio: 0.46

After several evolutions, we tested the best rule weight output on the robot and observed the performance output in figure 14. We noticed a greater improved performance in terms of path traced by the robot and error penalty (from 64.89 to 12.79).

The performance output after further evolutions of rule weights by the genetic algorithm for the NN learning results in greater improved performance measures in terms of error penalty (from 12.79 to 9.7390), and performance ratio (0.46 to 0.66) as indicated in figure 15.

Further evolution results show a little drop in performance as shown in the figure 16. After several generations by the GA, we could not get a rule weights set of better performance than

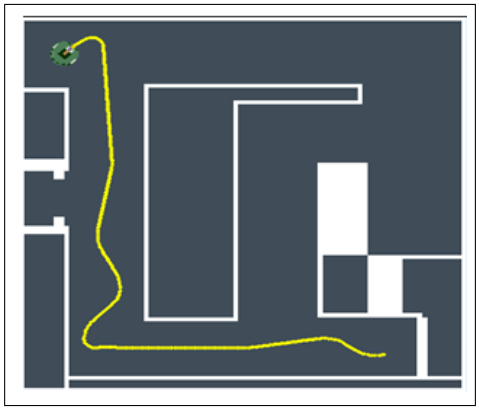

Figure 12: Geno-Neuro-Fuzzy Controller at 95^{th} evolutions. Error penalty: 9.7390; Forwards: 146.7cm; Straight: 96.6cm; Performance Ratio = 0.66

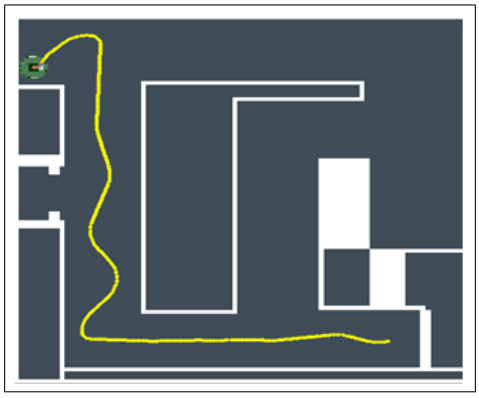

Figure 13: Geno-Neuro-Fuzzy controller output after 100 evolutions of rule weights.Error penalty: 12.20; Forward: 154.3cm;Straights: 96.8cm; Performance ratio = 0.63

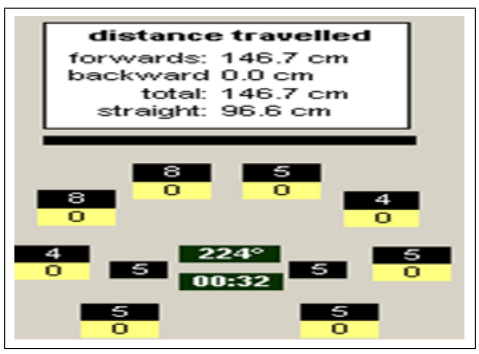

Figure 14: KiKS Window to monitor Simulation details

the one shown in figure 15 (95^{th} generation). This shows that we have reach the optimum performance for the rule weight generation for our experiment. Hence, we can use the NN model for this optimal rule weight set to obtain an optimal performance in terms of obstacle avoidance behaviour and navigation of our Khepera robot. The NN model with this optimal netweight values for rule weights is judged as the best NN model for our research result.

7 Conclusion

In this paper, a simple neuro-fuzzy strategy with genetic training has been proposed to drive a Khepera mobile robot. With this approach, we have been able to tune the rule weights of our fuzzy controller in order to guide our robot. The proposed neuro-fuzzy controller is a layer neural network along with an evolutionary (genetic) learning algorithm. This system has been successfully implemented in simulation obtaining satisfactory results which is better than fuzzy controller output. The lack of granularity in the membership functions has been to a large extent compensated for by the adaptive hybrid neuro-fuzzy with genetic training controller. This is obvious from the smoothness of path traced by the hybrid system compared to the path traced by the fuzzy controller outputs. We have equally adapted the neuro-fuzzy controller with genetic training to work on real Khepera III robot. The result was satisfactory. The simulation and real implementation on the Khepera III robot have shown the efficacy of using hybrid systems in improving mobile robot navigational performances in terms of obstacles, wall following and path tracking behaviours.

Bibliography

[1] I. Dumitrache, 1996, Intelligent Control of industrial Robots, Mediamira Press, Cluj, 1996.

[2] I. Dumitrache, 2000, Intelligent Autonomous Systems, Revue Roumaine des Sciences techiniques - Electrotechique et Energetique, Vol. 45, No.3, Pp. 439-453, Bucharest.

[3] R.R. Murphy, 2000, Introduction to AI Robotics,MIT Press.

[4] I. Dumitrache and M. Dragocea, 2006, Some problems of advanced mobile robot control,CEAI, Vol. 7, No. 4, pp. 11-30

[5] G. Campion , G. Bastin, 1996, Structural Properties and classification of Kinematics and Dynamic Model of wheeled Mobile Robots, IEEE Transaction on Robotics and Automation, Vol. 12,No. 1.

[6] H.R. Everett, 1995, Sensors for Mobile Robots,A.K. Peters, Ltd.

[7] X.Q. Chen, Y.Q. Chen, and J.G. Chase, Mobiles Robots-Past Present and Future, Intech.

[8] R. A. Brooks, 1986, A robust layered control system for a mobile robot. IEEE Journal of Robotics and Automation, RA-2(1):14-23.

[9] R. A. Brooks, 1999, Cambrian Intelligence: The Early History of the New AI, The MIT Press, Cambridge, Massachusetts.

[10] L.A. Zadeh, 1994, Fuzzy logic, Neural networks, and soft computing, Communications of the ACM, 37(3):77-84.

[11] O.O.Obe and I. Dumitrache, Fuzzy Control of Autonomous Mobile Robot, U.P.B. Sci. Bull., Series C, Vol. 72,Iss. 3, 2010

[12] M.Jackson Phinni et. al, Obstacle Avoidance of a wheel mobile Robot: A Genetic-neuro-fuzzy approach, IISc Centary-International Conference on Advances in Mechanical Engineering (IC-ICAME),Bangalore, India, July, 2008

Int. J. of Computers, Communications & Control, ISSN 1841-9836, E-ISSN 1841-9844
Vol. VII (2012), No. 1 (March), pp. 147-162

Analyzing the Impact of Using Interactive Animations in Teaching

R. Pinter, D. Radosav, S.M. Cisar

Robert Pinter
Subotica Tech-College of Applied Sciences
Serbia, 24000 Subotica, Marka Oreškovića 16
E-mail: probi@vts.su.ac.rs

Dragica Radosav
University of Novi Sad, Technical faculty "Mihajlo Pupin" Zrenjanin
Serbia, 23000 Zrenjanin, Djure Djakovica bb
E-mail: radosav@tfzr.uns.ac.rs

Sanja Maravić Čisar
Subotica Tech-College of Applied Sciences
Serbia, 24000 Subotica, Marka Oreškovića 16
E-mail: sanjam@vts.su.ac.rs

Abstract: This study intends to measure the impact of interactive animations on the students' performance. Two courses from Subotica Tech were included, the subjects "Analog and Digital Electronics" and "Microcontrollers". The experiment lasted over a period of tree years, and it involved the formation of two groups in every academic. Both groups' members participated in traditional frontal teaching, but the experimental group could use interactive Flash animations built from selected parts of those courses as supplementary tool. At the end of the semester, the exam marks were analyzed with a Two-Sample T-Test. The results show that learning with properly created interactive animations could have positive effects on most students' academic performance.
Keywords: distance education and telelearning, improving classroom teaching, interactive learning environments, simulations, media in education.

1 Introduction

In the era of modernization in the teaching process, when the use of novel information technologies aims to achieve easier, faster and more efficient knowledge transfer in education, the application of interactive animations has become more and more important. The questions arises as to what the reasons are which have made interactive animations a vital part of modern e-curricula, and whether there is empirical evidence to support claims that using multimedia and interactivity in e-curriculum has positive impact to cognitive development and academic achievement at students. In the first part of this paper, authors analyze characteristics of the interactive animations. The second part presents some research done with interactive animations developed at Subotica Tech. The e-contents are compiled from selected parts of the course "Analog and Digital Electronics" and "Microcontrollers" at Subotica Tech.

The thorough investigation by Sekular and Blake [1] into how students take in information, how they learn pointed out that the learning process takes place primarily by way of sight, and since it is the most vital of our senses, it is also the most highly-developed one. It enables a person to gather information from one's surroundings, analyze these and then decide how to process based on the deduced data. In terms of teaching, it is by seeing that students will best grasp a complicated string of steps as it helps transform a vague idea into an image in their brains.

Kraidy [2] started that, if the aim is to increase the amount of information to be processed by students within a set time frame, then giving them visual information to work with will help them reach this goal.

Graphical representations are defined as visual aids that act as supplement to any other textual information and will concentrate learners' attention [3]. Such representations will have maximum effect when accompanying some learning material that is (relatively) new to the learner [4]. This is especially the case with computer animation that is designed to aid long-term learning in the form of focusing learners on certain objects in the beginning.

The research of Rieber [5] portrayed that abstractions connected with time transitions in a process can be decreased by implementing animations to convey ideas and processes that change over time. Dual-coding theory by Paivio, [6] [7] offers an explanation as to why graphics are so effective: retaining memory over a long time is made easier if a combination of verbal and visual cues is used. This makes animations a distinctively significant support of visualizing material for long-term memorization. Animation and narration further support dual-coding [8].

What makes animations stand out is movement, as opposed to static, still images, and this demonstrates the various relationships within and along a certain process. By Goldstein, Chance, Hoisington and Buescher [9] movement will be remembered longer than static images. According to Gordin and Pea [10] and also Brodie, Carpenter, Earnshaw, Gallop, Hubbold, Mumford, Osland, Quarendon [11] visualization is a vital part in the acquisition of scientific topics, since important relationships between concepts will be pointed out for learners.

It was demonstrated by research results that animations are more effective learning tools that static images, and this was further supported by lesson plans incorporating lectures as well as different learning inputs [12]. Based on the dual-coding theory [7] it may be asserted that learning will be the most effective if there are lectures alongside animations, since they together form a base of reference that will help learners fully understand the knowledge that was conveyed through the animations. Lectures will cue the students, but actual studying happens through the animations [13].

2 Interactive Animations

One of the tendencies in education is the continually growing amount of learning content which must be acquired by the student. Almost every generation's curricula are extended by a certain amount of new, updated or revised material. With this swelling of learning contents, another issue arises, namely that the time which is intended for learning these amount of contents is growing ever shorter for each subsequent generation. Besides that, students are no longer interested in the foundations of some complex system, and how it is compiled, but rather, they want to know how the system works and how it can be managed. In accordance with these tendencies the educators have been searching for learning tools which can help the students acquire knowledge.

As animation are able to unambiguously portray changes over time (temporal changes), they are extremely suitable for using them in process and procedure teaching. Animations are applied to show dynamic content, and they reflect alterations in position (translation), as well as form (transformation) which form the basis of learning this kind of topic [14].

Unlike static pictures, temporal changes are shown in animations directly (instead of indirectly by some awkward auxiliary markings including arrows and motion lines). The application of animations, as opposed to static graphics, makes these extra markings unnecessary, thus stripping down the displays and making them attractive, lively and easily understandable [15]. Furthermore, there is no need for the learner to process these auxiliary markings and what changes they try indicate. Interpreting the markings and the inferences may actually surpass the level

of graphical skills that the learner possesses. Yet with animations, these displays immediately show all information concerning the changes, thus no extra mental depiction is required.

Learning can be facilitated by animations in two ways. On the one hand, their function is to affect the learner, raise their interest and keep up motivation. The entertainment industry implements this same function in their animations. On the other hand, though, animations also have the function to facilitate comprehension and memorization of a given content. The knowledge-building process is thus supported and this cognitive function is essential to effective learning.

Superficially, it may seem that animations are the perfect candidates to be applied in presenting dynamic content. Nevertheless, there is no unambiguous research evidence supporting this. Some researchers have conducted comparisons of how effective static and animated displays are in education by using a number of content domains. Although there have been positive results where animations have proven to be rather effective, these results have been countered by other investigations that have found no positive, and even negative effects of using animations. On the whole it is safe to say that animations are not by definition more effective than static graphics. Instead, the specific features of certain animations and their method of application is crucial in what kind of effect they will have on knowledge acquisition.

2.1 Do Animations Make Learning Faster?

Animations play an important role in computer-based learning environments. So far, however, it has not been sufficiently resolved under which conditions and in which respect animations do actually lead to better learning outcome. Well-designed animations are likely to be a real asset to the teacher. They will speed up the learning process and make it easier to grasp and memorize the material. It especially comes in handy when the teacher is trying to explain a difficult subject. The question arises: Why is a subject perceived as difficult? It may either be because it requires a certain amount of imagination. For example, in our animations we visualized a clock signals, a values and shapes of the input and output voltage signals, a states and changes of the microcontroller internal registers etc. With the help of computer animations both the teaching and learning process will be made less difficult, it will take less time and it will be livelier.

However, what then explains the fact that sometimes animations are not educationally effective as one would expect them to be? A possible answer would be that students are unable to "compute" the information seen in the animation adequately. If a complex subject is to be presented with animation, it may result in an equally complex animation, thus leaving students feeling overwhelmed. This is supported by the role of visual perception and cognition in human information processing. The perceptual and cognitive systems of humans have their limits for information processing. Once the presented animation reaches or oversteps the learners' information processing limits, the learning process may no longer be effective. Also negative effects come forward if the new information being presented in animations is faster than the speed of how fast the learner is capable of processing that effectively.

Replacing current static graphics with animations without careful consideration is not likely to result in improved learning; instead animations should be accompanied by textual explanations, and let the learner have control over the speed of the animation. Such user-controllable animations will enable learners to "customize" the animations by varying the playing speed and direction, labels and audio commentary to suit their own personality. The controllable animation can be realized with interactive animation. The interactivity within the animation could mean the own playing speed and walk-through, different amount of auxiliary explanations etc.

Besides the visualization of the curriculum, this kind of animation offers another advantage: the possibility of modeling and simulating systems. This means that knowledge acquisition can

take place also by changing the model's parameters, or otherwise experimenting with the system. So, when using interactive simulations besides the previously mentioned advantages, some new ones can be defined:

- The model offers the possibility for analyzing and doing experiments with those systems, which cannot be done in real life.
- The models enables studying of certain fast occurrences in a much slower mode, or time-consuming events in a much shorter time span than in reality.
- The model makes it possible to focus on the vital characteristics of the learning content being taught.
- The model offers the users the freedom of experimentation without any consequences.

2.2 The Advantages of Flash Animations

The developing environment provided by the packet Adobe Flash CS3 (and its prior versions) was used by the authors as the tool of choice for creating these interactive animations. In a simplified form, this software tool is an application for creating vector sketches and animation, with the option of adding this interactive feature. Naturally, the Flash developing environment offers many more options, but it also includes very straight-forward ways of creating animations. The fact that it is rather easy to create interactive animations is a crucial aspect, as in such a case it is not a pre-requisite for the subject teacher to be highly educated in information technologies. This type of animation can be used for presenting the material in theoretical classes, but also for creating a fully electronic curriculum for consolidating the material previously taught in practices, as well as for independent work outside the classes.

Practice shows that creating effective interactive animations still requires the close cooperation of the teacher and the expert for Flash technologies. Successful acceptance of the animations by the students primarily depends on the course teacher. It is their task to determine the following:

- Goals that are to be achieved with this animation,
- The content that is to be shown,
- Which elements of the learning material are to be represented statically (with an image), and which will take the forms of animation or interactive animation (simulation),
- Guidelines (design of the outlook, which controls are to be used, the user's options within the system, etc.) based on which the application will be developed.

The task of the "Flash expert" is to realize the requirements of the teacher as best as possible. The programmability of the animation thus comes in really handy for the expert. When developing the Flash application of the programs that may be used is Action Script (the current version is 4), an object-oriented programming language. With the help of this language every element of the animation (lines, colors, sound, etc.) can be controlled, calculations can be made using the entered parameters, and finally, the results can be presented, and actually used to draw new objects or their trajectories, as well as communicate with the server, among others.

It is safe to say there is no such task in creating an animation that an experienced Flash programmer cannot solve. In fact, this is the real advantage of this tool, as it can meet all the requirements irrespective of school age or learning material. Besides the listed advantages

of a Flash animation, it is also rather easy to distribute this application. There are two most commonly used formats for saving this animations: the executive (*.EXE) format, which starts in its in-built player; and the standard (*.SWF) format for playing in a web browser or in the FlashPlayer player (it can be downloaded easily from the Internet). What is characteristic of these two formats is the small file size, which is a vital factor when distributing the application via the Internet. Another benefit of the Flash animation is that it is a single file, there are no separate sound files, and the images do not comprise a separate module. All this ensures that there is no special installation procedure, only the file to be saved and started, which makes it an accessible program for even the somewhat computer-wary users.

Besides the so-called technical advantages, with the use of adequate design techniques, the Flash-type animation could gain further benefits. One of those benefits is the result of how a Flash animation is developed: most often the parts of a Flash animation are drawn, and there is little use of images from the real world. The advantage of drawing, i.e. of creating vector objects for animation is that the drawn objects are represented in a simpler form, with less detail than, for example, if they were shown in a bitmap format. This means once the educator has abstracted the material for the students there is yet another simplification of the learning material. But there are other design techniques which could lead to more effective learning process, for example:

- Using the "Inserting and removing fragments" technique. The complexity and information load of the animation interface can be regulated by inserting or removing objects or pieces of information form it.
- Using the "Dimming fragments" technique. With this technique one can differentiate between important parts of the animation and those which serve as additional information. The dimmed elements look like as if they are melting into the background.
- Using background (blurred) animation to attract and keep user's attention on the interface.

Also, in these projects the following design aspects were used:

- Minimize the number of visual elements, thus making it easy to follow the presented process.
- Minimal amount of lateral information used solely for presenting the essence as simply as possible.
- " Data entry by keyboard was not incorporated. The reason for this is that the data entry option does not always mean an advantage in the learning process: they may cause the user to be preoccupied with trying to crash the application by entering invalid formats and values.

As a result of these design techniques, the system will show a straight-forward form, using only the vital details, leading directly to a better and easier understanding of the model, and the user cognitive load is kept on adequate (i.e. low) level.

Are these the only reasons why the animation should be used in teaching? No, they are not. There are problems which occur in educational communication called information barriers, and the Flash animation will yield some solutions to this problem. Some of these barriers can be classified in the following way:

- perceptual barriers – each subject in the communication process feels and interprets events occurring to them differently, depending on their psychological, cultural and social status,

- psychological barriers – the same word or event will have a different meaning for different persons,
- social barriers – these barriers become apparent by the different social statuses of the subjects in the educational communication,
- cultural barriers – these arise in communication due to the different cultural backgrounds of the subjects participating in the communication process,
- semantic barriers – barriers of this type appear when interpreting written contents, speeches, images, and other, thus the way the message is read will change the content itself,
- media barriers – this information barrier occurs when the there are different communication media used on educational communication. It is well-known fact that each carrier has their own markings, which may be helpful as well as distracting in communication,
- physical barriers - informational barriers come up in educational communication when transferring the message, i.e. in the channels of connection.

How and where do information barriers occur when there are PCs used in the teaching process? Some of possible sources of problems are described below:

- experience shows that old programs which exclusively use the keyboard for interaction will be accepted to a lesser extent due to the fact that using the keyboard is more complicated than using the mouse,
- programs (simulations) designed using too much detail will be harder to accept because first the users have to make out what is on the screen and only then move on to the explanation of the modeling system,
- if there are too many options for simulation set up, result saving, parameter input, etc, where the users might 'become disoriented', then, according to Murphy 's Law, they probably will.

3 Practical Applications

The following section describes interactive animations which have been successfully in use as an auxiliary teaching tool at Subotica Tech - College of Applied Sciences [16]. Unfortunately, the advantages of the animations as described before are difficult to transfer to paper only with the help of images. The applications have been designed as interactive tutorials for presenting the functioning of some of the basic systems of analogue and digital electronics (Figure 1.) and microcontrollers (Figure 9. and 10.). For the Microcontrollers course two e-contents (interactive Flash simulation) were developed. They presents exercises for three out of fourteen lessons, but these three lessons count as "difficult", for example they cover the following themes: using the microcontrollers built in timer/counter in different modes, setting and using interrupts, communication through serial port, controlling analog to digital signal (and vice versa) conversion etc. The e-content for the Analogue and Digital Electronics there are altogether 19 simulations classified into 5 groups/exercises. Through these simulations the students can practice approximately about 40% of curriculum's theory. For example, "Exercise 1" contains simulations on the topics: Sources of alternating signals, Voltage splitter, Passive voltage adder, RC low-pass filter, RC high-pass filter. Figure 1. shows the screenshot of Exercise 3 and the accompanying simulation entitled "Pojačavač sa zajedničkim" (Common emitter amplifier). The design of the

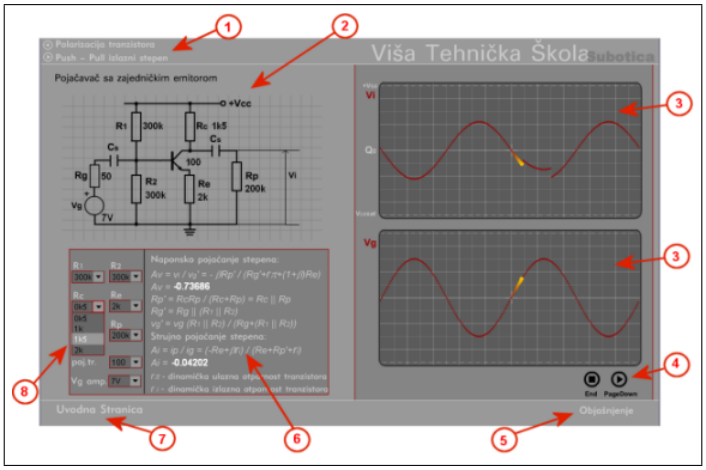

Figure 1: Representation of the exercise "Common emitter amplifier"

application shown in this image is followed through in the rest of the simulations, as well: the upper left corner contains the sketch of the system, below are the system parameters which can be altered in the simulation, while the "oscilloscope" is situated in the right side of the screen, showing the change of the signal over time. In this part of the application, by clicking on the link labeled "Objašnjenje" (Explanation) the theoretical background comes up in text form.

Below is a detailed description of the content and functions of the elements on the screen:

1. Links for transition to the next/other simulation within this exercise.
2. Sketch to be simulated. The parameters listed next to the components are changing depending on values of the checkboxes under the sketch.
3. Representation of the shape of voltage signal at the input and output. Part of the image marked with the arrow 3 shows the shape of output voltage, while the one marked 4 shows the input voltage. These shapes of signals are constantly redrawn. The lighter point on the line shows the current voltage value. The break in the line is the consequence of the change in RC components on the sketch during the simulation.
4. Buttons for starting and stopping the simulation.
5. The button for calling up the background explanation for how the sketch functions.
6. The list of equations used for calculating the necessary parameters of the sketch and the results of the calculation/estimation.
7. The return button leading to the introductory page where the exercises can be chosen.
8. Values of the sketch components. These parameters can be changed by choosing values from the checkboxes. Each change has affects the listing of calculated values based on the new parameters and the change of signal shape at the output ("upper canal of the oscilloscope").

The following image (Figure 2) shows the simulation "Decade counter" with the help of which students can learn the logic of the synchronous counter.

All simulations in this application are entirely controlled by mouse. Changing the parameters is done with the help of combo boxes and the predefined values they contain. In this way the

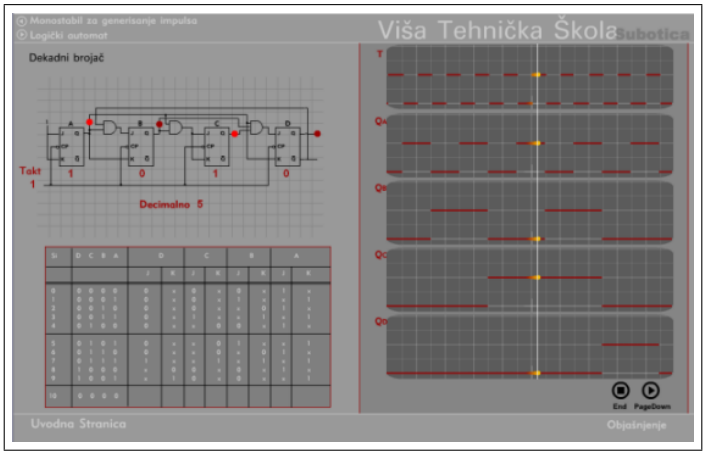

Figure 2: Representation of the exercise “Decade counter”

application is protected from irregular data. It is important to mention the following advantages of these simulations:

- it is not necessary to really ‘create’ an electric circuit in order to see how it works,
- changing the components in the system only takes a few clicks in the checkbox,
- it is possible to show the state of important values in continuity, as done by an oscilloscope.

The following few paragraphs present some ActionScript (version 2) programming code, which shows how one can input data from the combo box, calculate the output voltage, and draw the form of voltage signal like it is done on a real oscilloscope. The combo box is presented as an object on the main animation scene. The next figure shows a combo box, which is used for input of predefined resistor values:

Figure 3: Input option via combo box

The following code was attached to the combo box:

```
_root.shema.r1l = r1.getSelectedItem().label;
_root.shema.r1 = r1.getSelectedItem().data;
```

Figure 4: Source code for combo box’s onClipEvent event

When the user selects a value from the "r" combo box’s list, the code is executed . The first line of the code assigns the currently selected item’s label (currently it is a "50k" string) to the ’r1’ variable. The ’r1’ variable is the label in the scheme (see Figure 5, dashed line rectangle, right from the R resistor). So changes in the values in the combo box are displayed also on the scheme. The second line of the code assigns the value (numerical value: 50000) associated with the item currently selected ("50k" string) to the "r" variable. The scheme has its own action script code, which uses the "r" variable for calculating the new output value of the voltage. Because this code changes several global variables, other movie clips on the scene which also use those variables are affected with it. In this way, for example the changes in the resistor value

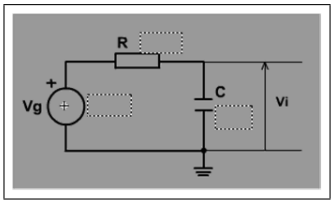

Figure 5: Scheme of the RC low–pass filter

```
_root.bode.lin1._y = 105;
_root.bode.lin1._x = 40*Math.LOG10E*Math.log ((1/r) * (1/c));
_root.bode.w0._y = 100;
_root.bode.w0._x = 40*Math.LOG10E*Math.log(_root.shema.vg);
tacX = 40*Math.LOG10E*Math.log(_root.shema.vg);
tacX1 = 40*Math.LOG10E*Math.log ((1/r) * (1/c));
razlika = (tacX1 - tacX);
if (razlika > 0) slabljenje = Math.exp(razlika/40);
else    slabljenje = 1;
if (_root.shema.vg == 1000)     f = 400;
if (_root.shema.vg == 10000)    f = 40;
s = 90/slabljenje;
w = (Math.PI/2)-(f/(4*Math.PI)*Math.atan(1/(2*Math.PI*f*r*c)));
y1 = 100-_root.sinus(s,f,-w,i);
struja = 100 - _root.sinus(90,f,0,i);
i = i+2;
if (i >= 400) i = 0;
```

Figure 6: Source code attached to the RC low–pass filter schema

affects the movie clip which represents the oscilloscope function, and the new form of the output signal is displayed. Drawing the form of voltage signal on the oscilloscope is done by moving a special movie clip on the coordinates which are determined in the code above. In the movie clip which presents the current output value one yellow circle changes to a smaller and orange colored circle. This animation of the movie clip with 4 picture out of 10 is presented in Figure 7. When drawing the output signal this movie clip is moving on the screen, and with its own

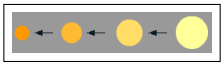

Figure 7: Movie clip of the oscilloscope drawing beam

animation the effect preented on the Figure 8 is achieved. Figure 9 shows one of a series of seven interactive simulations that are part of the e-curriculum which had been developed for the Microcontrollers course. The simulations present the i8051 microcontroller's timer/counter hardware, the setting and use of interrupts, and the application of the special forms of the ADD and MOV instructions.

Figure 10 presents one of the four interactive simulations created specifically for the Microcontrollers course. The simulations refer to the practical use of the i8051 microcontroller.

4 Experiments and Analysis

For the purpose of this study the following research questions were specified: what is the impact of interactivity of the animations on learning? The null hypothesis is defined as follows:

Interactive animations have no significant positive impacts on studying "Microcontroller" and "Analog and Digital Electronics" courses.

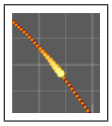

Figure 8: Appearance of the drawing beam in the oscilloscope movie clip

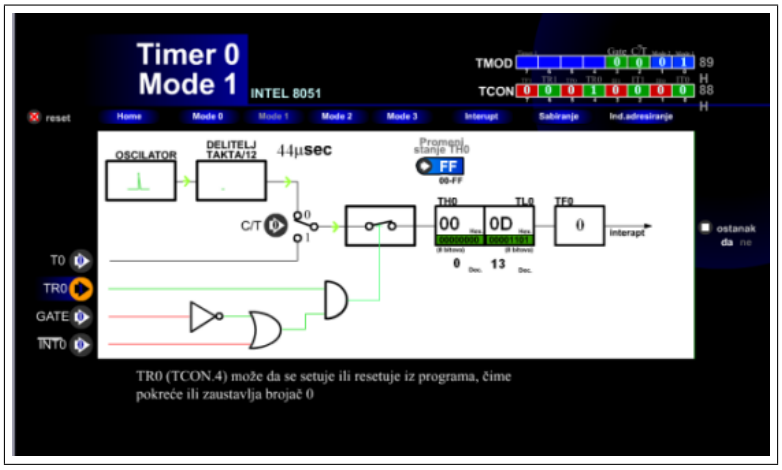

Figure 9: Representation of the exercise “Timer0 in mode 1”

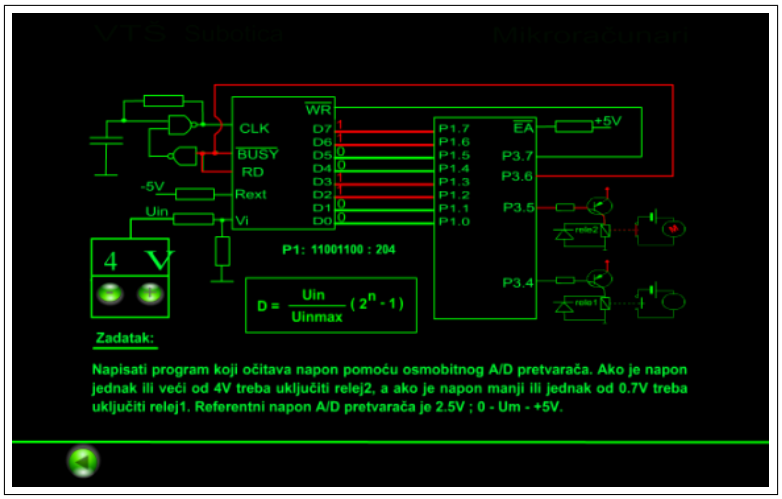

Figure 10: Representation of the exercise “Microcontroller with A/D”

In order to obtain answers to the research questions, the authors compared the final exam score standard deviation at "Analog and Digital Electronics" and "Microcontrollers" courses independently, where the animations were used as supplementary tools for learning and practicing after class.

4.1 Participants and Data Collecting Method

The data acquisition was done at Subotica Tech - College of Applied Sciences over a three-year period. It involved the second year students from two undergraduate programs the Electro-technical Engineering major (EE) where these two courses were obligatory and the Computer Science major (CS) where these courses were optional. The number of participants for the first course (Analog and Digital Electronics) over the period of 3 years is 441 students, 56 female (12.7%) and 385 male (87.3%) students. The second course's participants (Microcontrollers) were the same students from EE major, and from the CS major there were some old students and some new ones (those who did not select the first course). The composition of this group was: 464 participants, 58 females (12.5%) and 406 males (87.5%) See Table 1. Most participants, 98.5%, were between 18 and 20 years old; the remaining percentage is represented by a few students whose age were between 20 and 30. In these 3 years at the beginning of the semesters (the first course was in the fall and the second in the spring semester), the students were divided in two equal-sized groups, the control and the experimental group. The group members were chosen randomly, and only one condition had to be satisfied for the experimental group members: to have possibility of accessing the web application and the simulations from home. If this condition was not satisfied, that student automatically becomes the member of control group.

After forming the groups accessing the web application was enabled only for the experimental group. There was no additional motivation for the students. All participants visited face to face (f2f) classes of these two courses, which were taught by the same lecturer presenting identical material. This further strengthens the consistency of comparisons.

The web application collected the following data from the users:

1. How many time did he/she logged on to the system to use the e-content,

2. How many time did he/she spent using the particular simulation.

Students who logged on only few times and spent less time that the authors foresaw are assumed to be not using the system in an adequate mode, and they are not taken as members of the experimental group, so they were transferred to the control group (for details see Table 1). Ineligibility meant that the number of loggings is less than half of the available exercises, and the time spent in the system is less than 2 minutes per exercise

The authors took as null hypothesis that the two groups would have the same mark average at both courses. The alternative hypothesis claims that the control group will achieve better result at both courses. The data was analyzed with one-sided, t-test, assuming that the variances of the two samples are different. Because one course was in the fall semester and the second one in the spring semester, the analysis was done twice a year at the end of the semesters and independently for both courses.

Courses	2007 school year		2008 school year		2009 school year	
	Experiment. group	Control group	Experiment. group	Control group	Experiment. group	Control group
Analog&Digital Electronics	61	83	72	80	69	76
Microelectronics	75	86	74	81	73	75

Table 1 –The number of participants in the groups

4.2 Student Survey

At the end of each semester and before the final exam, the control group members were asked to fill out a questionnaire with 5 questions. From the answers (marks from 1 to 5 and comments) the authors received feedback about generally how students were satisfied with simulation, how did it help or not in the learning process and what would they like to see done in a different way. These data were collected in order to perform further improvement of the teaching materials in the way that would lead to a widely accepted e-curriculum.

5 Results and Discussion

The t-test applied to our two sample groups (main and control group) allows us to compare the means of the final exam marks of both groups. The following table presents these values.

	2007 Microcontrollers course					
	n	SS	Mean	MeanE-MeanC	df	t_{obs}
Experimental group	75	121.9467	7.973	0.438	159	2.16
Controll group	86	139.3953	7.534			

	2008 Microcontrollers course					
	n	SS	Mean	MeanE-MeanC	df	t_{obs}
Experimental group	71	105.098	7.887	0.420	144	2.06
Controll group	75	110.666	7.466			

	2009 Microcontrollers course					
	n	SS	Mean	MeanE-MeanC	df	t_{obs}
Experimental group	73	99.780	8.054	0.375	146	1.93
Controll group	75	104.32	7.680			

	2007 Analog and Digital Electronics course					
	n	SS	Mean	MeanE-MeanC	df	t_{obs}
Experimental group	61	57.147	8.540	0.457	142	2.48
Controll group	83	124.409	8.084			

	2008 Analog and Digital Electronics course					
	n	SS	Mean	MeanE-MeanC	df	t_{obs}
Experimental group	72	110.611	8.139	0.451	150	2.18
Controll group	80	135.187	7.687			

	2009 Analog and Digital Electronics course					
	n	SS	Mean	MeanE-MeanC	df	t_{obs}
Experimental group	69	104.289	8.232	0.403	143	1.97
Controll group	76	110.776	7.829			

Table 2 – Students' score distribution

Where the notations in the table are:

- n - number of participants,
- SS - sum of squared deviates,
- MeanE/MeanC - mean for of experimental/controll group,
- df - degrees of freedom,
- t_{obs}- observed values of t-distribution.

6 Conclusions and Future Works

The authors compared the observed value of t with the t from the table of critical values that pertain to $df > 140$, and the results are shown in Table 3:

Courses	Significance of the Difference between the Variances of the Two Samples	
M2007	$t_{95\%} < t_{obs} < t_{99\%}$	1.98<2.16<2.61
M2008	$t_{95\%} < t_{obs} < t_{99\%}$	1.98<2.06<2.61
M2009	$t_{obs} < t_{95\%}$	1.93<1.98
AD2007	$t_{95\%} < t_{obs} < t_{99\%}$	1.98<2.48<2.61
AD2008	$t_{95\%} < t_{obs} < t_{99\%}$	1.98<2.18<2.61
AD2009	$t_{obs} < t_{99\%}$	1.97<1.98

Table 3 – Significance differences between two groups

From the presented data, the following conclusions can be drawn:

- In 4 cases out of 6 we can reject the null hypothesis, and we can say with probability of 95%, that those experimental groups achieved better results on exam than the control groups.
- In two cases there are no reasons to reject the null hypothesis.

The results show evidence that interactive simulation contents can be very effective tools in the learning process. It can deliver information in a very attractive way, which also can be advantageous in assembling curricula for the students who have different skill levels and learning styles. Besides that, it can help learners to understand scientific topics, with presenting important conceptual relationships. It is also important that simulations enable students to become acquainted with the shown system and make changes in the parameters with no additional costs or risks.

But only well-designed animations may help to ease and shorten the learning process, and only with them, through play and experimentation can the learning process become more interesting [17] [18]. The students' answers from the questionnaires show that not every simulation is accepted in the same manner. For example, the third e-content (Figure 10) was given lower grades/worse comments than the other two. The reasons for this could be the themes which were presented with the simulation, because it does not contain spectacular and experimenting options. The design/the look of the animation also received worse marks from the students. Some future researches should also investigate how effective the interactive animations are when the users have different learning styles

Various researches focusing on the effectiveness of learning with the help of visualization point out that in order for the animation to be well accepted, by the [19] [20] [21] the following have to be kept in mind :

- positive effects in learning can only be achieved in topics that are dynamic in character,
- an exaggerated multitude of colors in the animation will have the exact opposite effect,
- it is important for the application to contain an optimal amount of information.

Due to the lack of a standard in creating successful visual applications [22], experiences gained from well-accepted electronic materials may serve as guidelines for defining a methodology, which, if applied in the design of animations and simulations, will lead to greater effect and efficiency in the learning process [23].

However, results also show that there is a tendency of decreasing the difference between those learners who had used the animation and those who had not. Is this because there is an increasing number of such and similar e-curricula available to students, and this kind of

attractive multimedia presentations are no longer motivate students as they used to before; or was is simply the case of students of the control group getting hold of the animations and using them in their learning process. Unfortunately, the questionnaire filled in by the students at the end of the semester failed to provide definitive answers to this question. The questionnaires show that students were on the whole satisfied with the applications.

A number of studies indicate that the user's performance is much better if the teaching methods are matched to the user's learning style [24]. Designing the animation's interface and contents to match the students' preferred learning style could lead to a more effective learning process. For example, according to the Felder–Silverman [25] learning style model, the animations containing a lot of visual elements, such as pictures, diagrams, flow charts etc. are preferred for the visual learning profile, while written and auditory explanations are effective with the verbal type of student. And to mention another example: students with an active profile prefer the simulation (interactive animation) which allows experimenting with the system parameters.

Bibliography

[1] Sekular, R., and Blake, R., *Perception, Second Ed.*, New York, McGraw-Hill, 1990

[2] Kraidy, U., *Digital Media and Education: cognitive impact of information visualization.* Journal of Educational Media, 27(3),95-106., 2002

[3] Richard E. Mayer, *Systematic Thinking Fostered by Illustrations in Scientific Text*, Journal of Educational Psychology, 1989, Vol. 81, NTo. 2, 240-246

[4] Mayer, R.E., Gallini, J.K., *When is an illustration worth ten thousand words?*, Journal of Educational Psychology, 1990, Vol. 82, No. 4,715-726

[5] Rieber, L.P., *Computers, graphics, and learning.* Madison, Wisconsin: Brown & Benchmark, 1994

[6] Allan Paivio, *Imagery and Verbal Processes*, Lawrence erlbaum associates, publishers, Hillsdale, New Jersey, 1979

[7] Paivio, A. *Dual coding theory: retrospect and current status.* Can. J. Psychol. 45,255 -287.

[8] Mayer, R.E., and Anderson, R.B., *Animations need narrations: an experimental test of a dual-coding hypothesis.* J. Educ. Psychol. 83,484-490

[9] Goldstein, A., Chance, J., Hoisington, M., and Buescher, K., *Recognition memory for pictures: dynamic vs. static stimuli.* Bull. Psychonomic Soc. 20,37 -40

[10] Gordin, D.N., and Pea, R.D., *Prospects for scientific visualization as an educational technology.* J. Learn. Sci. 4,249 -279.

[11] Brodie, K.W., Carpenter, L.A., Earnshaw, R.A., Gallop, J.R., Hubbold,R.J., Mumford, A.M., Osland, C.D., and Quarendon, P.*Scientific Visualization*, Berlin: Springer-Verlag, 1992.

[12] Rieber, L.P. *Using animation in science instruction with young children.* J. Ed. Psychol. 82,135 -140, 1990.

[13] Phillip McClean, Christina Johnson, Roxanne Rogers, Lisa Daniels: *Molecular and Cellular Biology Animations: Development and Impact on Student Learning*, Cell Biol Educ 4(2): 169-179 2005, DOI: 10.1187/cbe.04-07-047.

[14] Gabriela Moise, *A Formal Description of the Systemic Theory based e-Learning*, International Journal of Computers, Communications & Control, Vol. III (2008), No. 1, pp. 90-102

[15] R. Pinter, D. Radosav, S. Maravic Cisar,*Interactive Animation in Developing e-Learning Contents*, 33rd International Convention on Information and Communication Technology, Electronics and Microelectronics - MIPRO 2010, May 24 - 28, 2010, Opatija, Croatia, ISSN 1847-3938, ISBN 978-953-233-054-0, pp. 251-254

[16] Pinter Robert, Sanja Maravic Cisar, *The Application Of Flash Animation In The Developmnet Of E-Learning* , Simpozijum o racunarskim naukama i tehnologijama, Kopaonik, 10-14.03.2003, Serbia and Montenegro

[17] Jan L. Plass, Bruce D., Homer, Elizabeth O. Hayward: *Design factors for educationally effective animations and simulations*, Journal of Computing in Higher Education, (2009) 21:31-61, DOI 10.1007/s12528-009-9011-x

[18] Moreno, R., & Mayer, R., *Interactive multimodal learning environments: Special issue on interactive learning environments: Contemporary issues and trends*, Educational Psychology Review. Special Issue: Interactive Learning Environments: Contemporary Issues and Trends, 19(3), 309–326, 2007

[19] Moreno, R., *Optimising learning from animations by minimising cognitive load: Cognitive and affective consequences of signaling and segmentation methods*, Applied Cognitive Psychology, 21,765–781, 2007.

[20] Weiss, R. E., Knowlton, D. S., & Morrison, G. R., *Principles for using animation in computerbased instruction: Theoretical heuristics for effective design*, Computers in Human Behavior, 18, 465–477, 2002.

[21] Um, E., Song, H., & Plass, J. L., *The effect of positive emotions on multimedia learning*, Paper presented at the World Conference on Educational Multimedia, Hypermedia & Telecommunications(D-MEDIA 2007) in Vancouver, Canada, June 25–29, 2007.

[22] Maria D. A. Suarez, Cayetano G. Artal, Francisco M. T. Hernandez *E-learning multimedia applications: Towards an engineering of content creation* Int. J. of Computers, Communications & Control, ISSN 1841-9836, E-ISSN 1841-9844, Vol. III (2008), No. 2, pp. 116-124

[23] Rieber, L. P., *Effects of visual grouping strategies of computer-animated presentations on selective attention in science*, Educational Technology Research and Development, 39, 5–15, 1991.

[24] Chen S., Macredie R.,*Cognitive Styles and Hypermedia Navigation: Development of a Learning Model*, Journal of the American Society for Information Science and Technology, 53(1):3 15, (2002)

[25] Richar F., Rebeca B.,*Understanding Student Differences*, Journal of Engineering Education, 94 (1), 57-72 (2005)

Int. J. of Computers, Communications & Control, ISSN 1841-9836, E-ISSN 1841-9844
Vol. VII (2012), No. 1 (March), pp. 163-172

Load-aware and Position-aided Routing in Satellite IP Networks

L. Wang, L. Liu, X. Hu

Wang Lu
1. Graduate University of Chinese Academy of Sciences
Beijing, China, 100049, and
2. Institute of Software, Chinese Academy of Sciences
Beijing, China, 100190
E-mail: wlu810@gmail.com

Liu Lixiang, Hu Xiaohui
Institute of Software, Chinese Academy of Sciences
Beijing, China, 100190

Abstract: Satellite communication is regarded as a promising way to achieve seamless global coverage with an array of advantages over the traditional terrestrial network. However, the non-uniform distribution of users and the highly topological dynamics have been a matter of facts. The traditional load balancing technique is able to guarantee a better traffic distribution around the Inter Satellite Links with heavy loads after considering the non-uniform distribution of users, but it transmits load information passively and fails to provide a fair traffic distribution over the entire constellation. Given the highly topological dynamics, traditional routing protocols may experience the convergence processes frequently or use a large amount of storage to keep the snapshots. This paper proposes a novel routing protocol named LPR for the Satellite IP Networks, which transmits the bottleneck link load information to upstream satellites in a Hop-by-Hop manner actively, to guarantee a better distribution of traffic among satellites. In response, upstream satellites select less congested paths and communicate a portion of data according to the priority of different classes of traffic. In addition, LPR applies the geographical position when selecting the routing path to eliminate the convergence process which may cause the routing tables invalid. Finally, various aspects of performance of LPR have compared with other mechanisms. Our evaluations show that a routing protocol with load-aware and position-aided leads to higher throughput and better traffic distribution compared to the traditional routing protocol and load balancing technique.
Keywords: satellite networks, load balancing, position, routing.

1 Introduction

Satellite networks exhibit unique features and offer an array of advantages over traditional terrestrial networks. They are able to provide coverage to extensive geographic areas and to interconnect among remote terrestrial networks. A satellite communicates with other satellites via inter-satellite links(ISLs). The links between satellites in the same plane are called intra-plane ISLs. The links between satellites in different planes are called inter-plane ISLs. Satellites communicate with the ground stations over user data links(UDL).

LEO satellites provide short round-trip delays and have been the focus of several researches for a period of time [1], [2]. Given recent advancements in satellite communications, researchers find that a combination of different layers of satellites would yield a better performance than

these layers individually. Researchers have proposed severals routing protocols for multi-layered satellite networks, such as MLSR [3], SGRP [4], SOS [5] et. al. MLSR is a link state routing protocol for multi-layered satellite networks. SGRP is a multi-layered satellite network routing protocol based on snapshots. In these multi-layered satellite network routing protocols, LEO satellites transmit data, and MEO/GEO satellites are managers and compute the routing paths. Another type of satellite network routing protocol is based on geographical location, such as LPDB [6]. LPDB utilizes satellites' inherent broadcast capabilities, and predict transmission direction according to the geographical location.

The majority of the routing protocols have convergence processes to collect information and update routing tables when the topology changes, however satellites move rapidly relative to the surface of the Earth and to the ground stations(LEO satellites speed at over 2500km/hour [7]) and a lot of packets may be lost during the convergence process, due to routing tables becoming invalid. Furthermore, satellites' rapid movements cause frequent convergence processes, which increases the algorithms' overhead. When satellites use routing protocols based on snapshots, it takes a large amount of storage. If satellites' links interrupted, routing tables of the current snapshot and the following snapshots would be invalid, and in turn it takes a long interval for the central control nodes, such as ground stations, GEO/MEO, to calculate new routing tables and update routing tables for the satellites.

In addition, an important missing point in the previous designs consists in their focus on searching for the paths without any consideration of the total traffic distribution over the entire constellation, which leads to unfair distribution of traffic. Recently, researchers propose some load balance mechanisms, such as CEMR [8], ELB [9] et. al. CEMR is based on a cost metric that involves both propagation and queuing delays, however it does not reflect the congestion state of the next hop, nor does it estimate the queuing delay a packet may experience there. ELB is an explicit load balancing mechanism that classifies users into three classes. Neighboring satellites exchange load information and reduce data forwarding rates when the queue occupancies exceed a pre-determined threshold. However, ELB only exchanges information among neighboring satellites actively and it takes a long interval to notify sources of the congestion state. Furthermore, although ELB applies a routing metric that instantly reflects both the one-way propagation delay and the instant queuing delay to avoid loops, the traffic forwarding may still cause loops.

The objective of this paper is to design a novel satellite network routing protocol named LPR (Load-aware and Position-aided Routing), which is able to guarantee fair distribution of traffic among the entire constellation and eliminate the convergence process. LPR calculates every link's load information and transmits it to the upstream satellites actively. LPR calculates the next hop set based on geographical position, and the next hop set includes a main path and several alternative paths. LPR transmits traffic on the main path when the load on the main path is low, and begins to communicate a portion of traffic on the alternative paths when the load on the main path becomes high. The main path is the routing path with the shortest distance.

2 Dissemination and Estimation of Load Information

2.1 Load Transmission

In traditional load balancing technique, the load information is exchanged among neighboring satellites. It is able to achieve better traffic distribution than the routing protocols which do not take traffic distribution into account, but the ISLs are expected to be heavily loaded around the overload region and others remain underutilized, and in turn it fails to achieve fair traffic

distribution over the entire constellation, as in Figure 1.

In LPR, each satellite calculates the load information and compares its own link load with the received link load , and updates the link load, if the local link load is larger than the received link load. Then satellites transmit the load information in a Hop-by-Hop manner. In other words, each satellite transmits the bottleneck link load information to upstream satellites actively. The upstream satellites receive the bottleneck link load, and begin to detour traffic when the bottleneck link load is larger than the threshold, resulting that all upstream satellites on the transmission path are able to communicate a portion of data when there is a link congested. In turn, the traffic is distributed fairly over the entire constellation and satellites are able to return back to free state quickly, as in Figure 2.

In addition to the fair traffic distribution, LPR is able to disseminate the load information instantly to all upstream satellites. In traditional load balancing technique, it takes a relatively long interval to transmit the overload information to upstream satellites, for the traditional load balancing technique only transmits load information actively to neighboring satellites, and load information is transmitted passively to the upstream satellites. Let I and O denote the total input and output traffic at a given satellite. A satellite is considered to be overloaded if the load exceeds the *threshold*. Let t_n denote the time for satellite n becomes overloaded when I is larger than O. Let d_n denote the transmission delay between satellite n and satellite $n+1$. In traditional load balancing technique, it takes $\sum_{n=i}^{j-1}(t_n + d_n)$ for satellite i to know the overload sate originated from satellite j. But in LPR, it only takes $\sum_{n=i}^{j-1} d_n$ for satellite i to know the load information of satellite j, due to the active transmission of load information in a Hop-by-Hop manner.

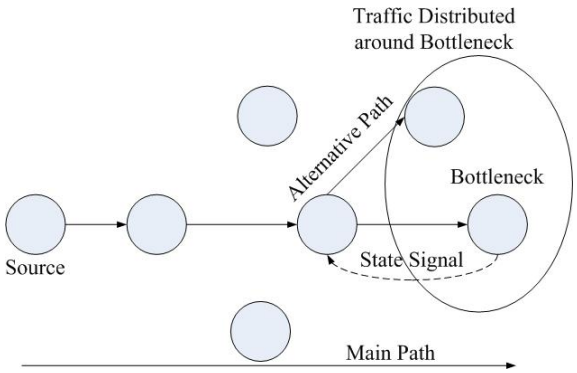

Figure 1: Traditional Load Balancing

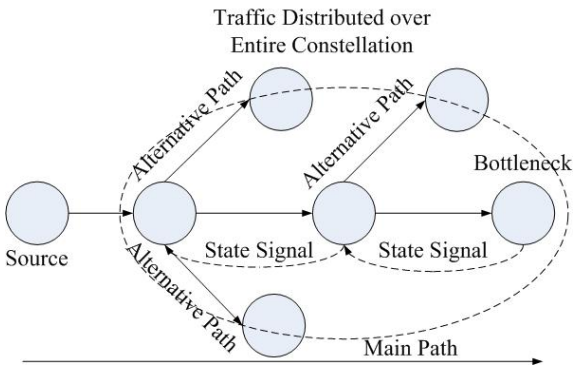

Figure 2: LPR's Load Balancing

2.2 Load Estimation and Setting of Thresholds

In LPR, satellites keep a virtual queue for every link and estimate link load R_l over an appropriate interval time t_R, and t_R is estimated according to RTT in one hop. R_l is computed similar to [10]:

$$R_l = \frac{\lambda_l + k_q \cdot \overline{q}_l}{\gamma_l \cdot C_l \cdot t_R} \tag{1}$$

Here the definitions of λ_l and $\overline{q}_l$ are different from [10]. λ_l is the total amount of input data in a virtual queue for one link during t_R, and $\overline{q}_l$ is the persistent queue length of a virtual queue for one link during t_R . k_q controls how fast the persistent queue drains, γ_l is the target utilization that sets close to 1, and C_l is the link capacity. The input traffic λ_l and the persistent queue length $\overline{q}_l$ are measured using bytes [10]. LPR sets k_q to 0.8 to make full use of the limited memory space. The persistent queue length $\overline{q}_l$ is measured by using a low-pass filter that samples the instantaneous queue size, $q(t)$, every $t_R/20$.

2.3 Setting of Detouring Ratio

The objective of setting the detouring ratio is to allow the satellites' overloaded links to return back to light load state and keep this state for at least a period of θ.

Let I_t denote the total rate of traffic coming from terminals to the bottleneck link within the coverage area of a satellite, I_n denote the total rate of traffic coming from neighboring satellites to the bottleneck link, O denote the total rate of output traffic of the bottleneck link, and l_d denote the ISL delay. A satellite receives link load $R_l(t)$ from neighboring satellites at time $(t + l_d)$. $R_l(t)$ is the neighboring satellite's link load at time t, and the satellite's link load at time $(t + l_d)$ is $R_l(t + l_d)$:

$$R_l(t + l_d) = \frac{\gamma_l + k_q \cdot (\overline{q}_l + (I_t + I_n - O) \cdot I_d)}{\gamma_l \cdot C_l \cdot t_R} \tag{2}$$

In order to ensure a prompt recovery and a residual time in the light load for at least θ, the new rate of traffic coming from neighboring satellites I_n^{new} should satisfy:

$$R_l(t + I_d + \theta) = \frac{\gamma_l + k_q \cdot (\overline{q}_l + (I_t + I_n - O) \cdot I_d + (I_t + I_n^{new} - O) \cdot \theta)}{\gamma_l \cdot C_l \cdot t_R} < threshold \tag{3}$$

threshold is the link load's threshold. If the link load is larger than *threshold*, the link is overloaded and satellites begin to detour a portion of traffic according to the detouring ratio on the alternative paths. The traffic detouring ratio φ can be computed as:

$$\varphi = 1 - min(max(0, \frac{I_n^{new}}{I_n}), 1) \tag{4}$$

3 Load-aware and Position-aided Routing

3.1 Path Selectioin

The key technologies required to support positioning over satellite systems have been developed, such as GPS, Galileo and GLONASS. With these advancements, satellites are able to get the high precision orbit determination. In LPR, path selection is performed by using the position. LPR calculates the routing path for every arriving packet, instead of maintaining routing tables to avoid the convergence process, however, it takes a large amount of computing resources. So

satellites cache the routing results until the topology state changes, to reduce the computation overhead.

Step 1: Predicting transmission direction-The polar constellation networks have orbital seams, and LPR assumes that there are no cross-seam links, for the regular hand over as satellites pass. Satellites would transmit receiving packets cross seam, if the destination and current satellites located on different side of the orbital seam. The orbital seams are located between the fixed planes of ascending and descending satellites in the same layer and in turn LPR is able to utilize the longitude difference between the orbital plane of current satellites and the orbital seam to judge whether packets should cross the seams or not. Assuming that satellite A's geographical position is $(long_a, latitude_a)$.The points of the intersections of the orbital seams and the equator are $Left(long_{left\_seam}, 0)$ and $Right$ $(long_{right\_seam}, 0)$. The point of the intersection of the plane of satellite A and the equator is $A'(plong, 0)$:

$$plong = long_a + \arcsin(\tan(latitude_a)/\tan(inclination)) \tag{5}$$

where $inclination$ is the constellation's inclination angle, and the constellation is composed of satellites in one layer. Let $left\_seam\_diff$ denote the longitude difference between A' and $Left$ and $right\_seam\_diff$ denote the longitude difference between A' and $Right$.

$$left\_seam\_diff = plong - long_{left\_seam} \tag{6}$$

$$right\_seam\_diff = long_{right\_seam} - plong \tag{7}$$

$left\_seam\_diff$ and $right\_seam\_diff$ are fixed in the same layer. Assuming that the point of intersection of the destination and the equator is $(long_{dest}, 0)$. If the difference between $plong$ and $long_{dest}$ is less than $left\_seam\_diff$ or $right\_seam\_diff$, packets will not be transmitted across the orbital seams and A's neighboring satellites set $Nei(A)$ includes all satellites having ISLs with A, otherwise packets will be transmitted across the orbital seams and $Nei(A)$ only includes satellites which are able to transmit packets across the seams by means of passing through the poles or another satellites layer. After estimating neighboring satellites set $Nei(A)$, satellite A calculates the distance from x , where $x \in Nei(A)$, to the destination to get next hop set $N(x)$:

$$N(x) = \{x | D(x, dest) < D(A, dest), x \in Nei(A)\} \tag{8}$$

In multi-layered satellite networks, all satellites are projected to the surface of the Earth when calculating the distance. If several satellites in different layers are projected in one point on the surface of the Earth, the satellite in the same layer with the sender has the highest priority.

Step 2: Selecting next hop-After predicting transmission direction, satellite A will choose next hop from $N(x)$ depending on the load information collecting from the transmission paths. LPR transmits traffic on the main path when the load is low, and begin to detour traffic when the load of the main path becomes high. LPR classifies traffic into three types, similar to [11], to guarantee the QoS requirements. Class A is delay-sensitive traffic, Class B is through-put sensitive traffic, and Class C is best effort traffic. When the load increases, LPR starts detouring traffic of Class C. If the requested detouring ratio of traffic is larger than the traffic percentage of Class C, the traffic of Class B is detoured as well. If the requested detouring ratio of traffic φ is larger than the traffic percentage of Class C and Class B, the traffic of A begins to detour. Let a, b and c denote the predicted traffic ratio of class A, B and C, the traffic detouring ratio is shown in Table 1.

3.2 Loop Avoidance

In LPR, forwarding traffic depending on the geographical position and the load information may cause loops. To cope with this issue, LPR adds the routing path into the packet header

Table 1: Traffic Detouring Ratio

	Class A	Class B	Class C
$\varphi < c$	0	0	$\frac{\varphi}{c}$
$c \leq \varphi < (b+c)$	0	$\frac{\varphi - c}{b}$	1
$\varphi \geq (b+c)$	$\frac{\varphi - b - c}{a}$	1	1

after selecting the next hop, to form the traversed link set LS. Consider satellite A sending the set of traversed link LS to satellite B, and satellite B will not select links in the LS. However it would take a lot of bandwidth to transmit the traversed link set information. LPR proposes a mechanism to reduce this overhead at the expense of local mapping. Considering that satellite A associates a traversed link set LS to $label_{LS}$, and sends the traversed link set LS and the mapping label $label_{LS}$ to satellite B. Satellite B will establish a mapping $label_{LS} \rightarrow LS$ and send an acknowledgement to Satellite A. After satellite A receives the acknowledgement of the mapping from satellite B, satellite A only includes $label_{LS}$ rather than the entire traversed link set LS in the packet header. Labels exchange among neighboring satellites do not have global meaning. Furthermore, a time-to-live value T is associated with a mapping at the receiver and the mapping is deleted, if no packet with the label associated with this mapping is received for T. Then the receiver notify the sender of deleting the timeout mapping $label_{LS} \rightarrow LS$. Considering that satellite B finds that $label_{LS} \rightarrow LS$ is timeout, satellite B will delete the mapping and notify satellite A that the mapping is timeout. Satellite A will delete the mapping after receiving the notification.

4 Simulation Setup

In this section, we describe the simulation topology and parameters that have been used to compare the performance of LPR, Dijkstra, ELB on Dijkstra and Snapshot [12]. We have used OMNeT++ simulator [13] and developed a constellation of Iridium satellites and the main parameters are shown in Table 2.

Table 2: Main Parameters of Satellite Topology

Parameters	Values
Satellite Number	66
Orbit Altitude	780km
Inclination Angle	84.4degrees
ISLs	2 Intra-SLs, 2Inter-SLs
Polar Area Border	70degrees
Plane Number	6
Seam Links	no
Constellation Type	Polar

It is assumed that each satellite maintains four ISLs with its neighboring satellites. Uplinks, downlinks and ISLs are each given a capacity equal to 25Mbps. The average packet size is set to 1KB. Lengths of drop-Tail based buffers equal to 200 KB. Simulations are all run for 2 hours, for

LEO satellite constellation operates at the altitude of 780 km with the system period of about 100 minutes.

In the simulation, we consider 100 data flows. The source and destination end-terminals are dispersed all over the world and the distribution of end-terminals is shown in Table 3. The traffic distribution is identical to [14]. The sources send data at constant rates from 0.8 Mbps to 1.5 Mbps. The traffic percentages of delay-sensitive traffic, throughput-sensitive traffic and best effort traffic are set to 20%,30% and 50%.

Table 3: Distribution of End Users

	North America	South America	Europe	Africa	Asia	Oceania
End Users Number	35	10	25	5	20	5

5 Simulation Results

In this section, we will show the performance results of LPR in the presence of different traffic classes in terms of average transmission delay and average throughput, and will compare the load balancing index among LPR, ELB on Dijkstra, Snapshot and Dijkstra.

5.1 Multiple Traffic Classes

The performance of LPR with multiple traffic classes is compared with Dijkstra algorithm. Figure 3 shows the average packet transmission delay. The delay of packets belonging to the delay-sensitive traffic is smaller compared to other types of traffic This is because the delay-sensitive data is always sent via the paths with the shortest distance. When the traffic load gets higher (the individual transmission rate is larger than 1.3Mbps), Dijkstra exhibits the minimum transmission delay, but at the expense of significant packet drops, as shown in Figure 4. LPR's transmission delay increases higher, due to the traffic detouring which increases the communication delay.

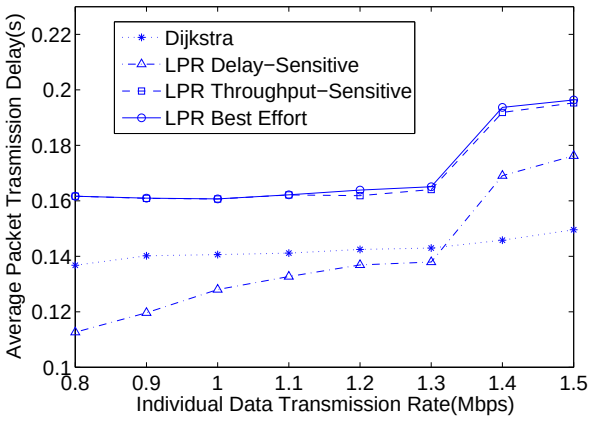

Figure 3: Packets Transmission Delay

As shown in Figure 5, the average throughput of Dijkstra is always lower than other schemes, due to the overflow of the drop-tail buffers, as shown in Figure 4. Throughput of the delay-sensitive traffic outperforms the other two types of traffic, because of the detouring priority.

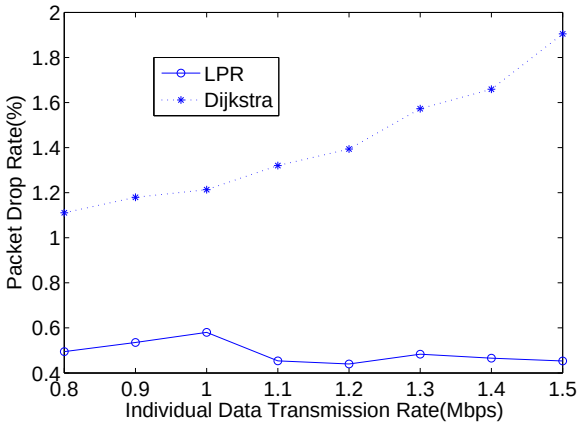

Figure 4: Packets Drop Rate

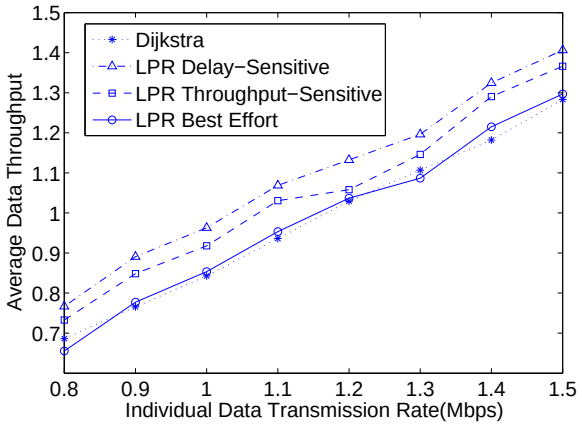

Figure 5: Throughput

These results demonstrate that LPR is able to guarantee QoS requirements by the effective load balance mechanism and a routing method without the convergence process.

5.2 Load Balancing Index

To evaluate the traffic distribution of LPR, this paper compares LPR with Dijkstra, Snapshot and ELB with the following traffic distribution index:

$$f = \frac{(\sum_{i=1}^{n} x_i)^2}{n \cdot \sum_{i=1}^{n} x_i^2} \tag{9}$$

Where n is the total number of ISLs and UDLs, x_i denotes the actual number of packets that traversed the ith link. The index ranges from zero to one and high value of this traffic distribution index represents good distribution of traffic over the entire constellation. In the simulation, LPR's threshold ranges from 0.85 to 0.95 and the interval is 0.5, and LPR's distribution index is the average of the results of these different thresholds, in order to evaluate the performance of LPR under different thresholds.

In Dijkstra scheme, the traffic distribution index is low (Figure 6), for packets always traverse through paths with the smallest number of hops without taking the traffic distribution into account. LPR scheme always try to distribute the traffic on the transmission paths when the link

is overloaded, so the traffic distribution is higher than the plots of Dijkstra and Snapshot. ELB on Dijkstra is higher than the plots of Dijkstra, Snapshot, for ELB searches for less congested paths, after receiving a Busy Signal Advertisement from neighboring satellites. However, in LPR scheme, not only neighboring satellites are able to communicate a portion of data via less congested paths, but also the upstream satellites. Furthermore the load estimation of LPR is more accurate than ELB, in that LPR's granularity of load estimation is the link, but ELB is the node. In turn, the distribution index of LPR is much higher than ELB on Dijkstra.

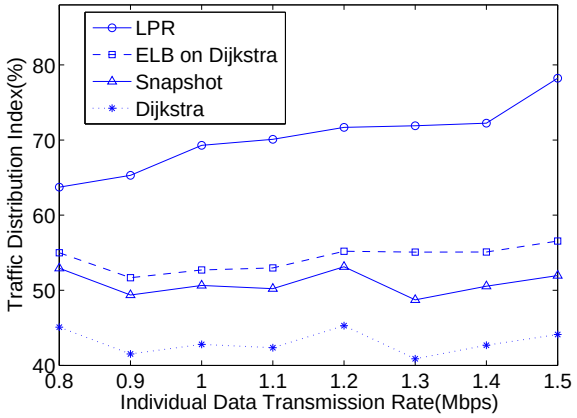

Figure 6: Traditional Load Balancing

6 Conclusions

In this paper, we propose a Load-aware and Position-aided Routing protocol named LPR, which transmits load information in a Hop-by-Hop manner and enables all the upstream satellites to know the load information instantly and to communicate a portion of traffic on the less congested paths when the load becomes high. Furthermore, LPR utilizes the geographical positions of satellites and select the routing path to eliminate the convergence process. Finally, we evaluate the performance of LPR in the Iridium constellation. The simulation results indicates that LPR is capable of guaranteeing a good distribution of traffic among satellites and supporting different QoS requirements. As future work, we intend to improve the ability of providing different QoS by differentiating traffic, and analyze LPR's impacts on packets reordering. Finally, we will implement LPR in Linux kernel to assess its strengths and limitations in practice.

Bibliography

[1] E. Ekici, I.F. Akyildiz, M.D. Bender, A Distributed Routing Algorithm for Datagram Traffic in LEO Satellite Network, *IEEE/ACM Transactions on Networking*, 9(2):137-147, 2001.

[2] T. Henderson, R.H. Katz, On Distributed, Geograhpic-based Packet Routing for LEO Satellite Networks, *Proceedings of IEEE GLOBECOM*, 2000.

[3] I.F. Akyildiz, E. Ekici, M.D. Bender, MLSR:A Novel Routing Algorithm for Multilayered Satellite IP Networks, *IEEE/ACM Transactions on Networking*, 10(3):411-424,2002.

[4] C. Chen, E. Ekici, A routing protocol for hierarchical LEO/MEO satellite IP networks, *Wireless Networks*, 11(4):507-521, 2005.

[5] J. Lee, S. Kang, Satellite over Satellite (SOS) Networks: A Novel Architecture for Satellite Network, *Proceeding of IEEE INFOCOM*, 2000.

[6] C. Chen, C. ZeSheng, Towards a routing framework in ad hoc space network, *Internation Journal of Ad Hoc and Ubiquitour Computing*, 5(1):44-55, 2010.

[7] L. Wood, Internetworking with Satellite Constellations, School of Electronics, Computing and Mathematics, University of Surrey, Guildford, 2001.

[8] B. Jianjun, L. Xicheng, L. Zexin, Compact Explicit Multipath Routing for LEO Satellite Networks, *Proceedings of IEEE Workshop on High Performance Switching and Routing*, HongKong, China, 2005.

[9] T. Taleb, D. Mashimo, A. Jamalipour, et. al., Explicit Load Balancing Technique for NGEO Satellite Networks with On-Board Processing Capabilities, *IEEE/ACM Transactions on Networking*, 17(1):281-291,2009.

[10] Y. Xia, L. Subramanian, I. Stoica, One more bit is enough, *IEEE/ACM Transactions on Networking*, 16(6):1281-1294, 2008.

[11] A. Svigelj, M. Mohorcic, G. Kandus, et. al., Routing in ISL networks considering empirical IP traffic, *IEEE Journal on Selective Areas Communication*, 22(2):261-272,2004.

[12] V. Gounder, R. Prakash, H. Abu-Amara, Routing in LEO-based satellite networks, *Emerging Technologies Symposium on Wireless Communications and Systems*,221-226,1999.

[13] A. Varga, OMNeT++ Discrete Event Simulation System, http://www.omnetpp.org.

[14] M. Mohorcic, M. Werner, A. Svigelj, et. al., Adaptive Routing for Packet-oriented intersatellite link networks: Performance in various traffic scenarios, *IEEE Transaction on Wireless Communications*, 1(4):808-818,2002.

Int. J. of Computers, Communications & Control, ISSN 1841-9836, E-ISSN 1841-9844
Vol. VII (2012), No. 1 (March), pp. 173-183

Small Universal Tissue P Systems with Symport/Antiport Rules

X. Zhang, B. Luo, L. Pan

Xingyi Zhang, Bin Luo
Key Lab of Intelligent Computing and
Signal Processing of Ministry of Education
School of Computer Science and Technology
Anhui University, Hefei 230039, China
E-mail: xyzhanghust@gmail.com,luobinahu@yahoo.com.cn

Linqiang Pan
Key Laboratory of Image Processing and Intelligent Control
Department of Control Science and Engineering
Huazhong University of Science and Technology
Wuhan 430074, China
E-mail: lqpan@mail.hust.edu.cn (corresponding author)

Abstract:
In this note, we consider the problem of looking for small universal one-symbol tissue P systems with symport/antiport rules. It is proved that six cells suffice to generate any recursively enumerable set of natural numbers by such a one-symbol tissue P system with symport/antiport rules, under the restriction that only one channel is allowed between two cells or between a cell and the environment. As for the case of allowing two channels between a cell and the environment, it is shown that the computational completeness can be obtained by one-symbol tissue P systems with symport/antiport rules having at most five cells. These results partially answer an open problem formulated by Artiom Alhazov, Rudolf Freund and Marion Oswald.
Keywords: membrane computing, tissue P system, symport/antiport rule, universality.

1 Introduction

Membrane computing is one of the recent branches of natural computing, which was initiated by Gh. Păun in 1998 [7]. The aim of membrane computing is to abstract novel computing ideas or models from the structure and the functioning of a living cell, as well as from the organization of cells in tissues, organs, and other higher order structures. The obtained models, called *P systems*, provide distributed parallel and non-deterministic computing models. The field of membrane computing has rapidly developed (already in 2003, ISI considered membrane computing as a "fast emerging research area in computer science", see http://esi-topics.com). Please refer to the handbook of membrane computing [9] for general information in this area, and to the membrane computing web site [11] for the up-to-date information.

Tissue P systems form a class of P systems, which were introduced in [6]. Tissue P systems were inspired by intercellular communication and cooperation between cells. Briefly, a tissue P system consists of a set of membranes (abstracted from cells) placed in the nodes of a graph. The net of membranes deals with symbols and communicates symbols along channels specified in advance. The communication among cells is based on symport/antiport rules [8]. Symport rules move objects across a membrane in one direction, whereas antiport rules move objects across a membrane in opposite directions. Between two cells or between a cell and the environment, it is

possible that there exists only one channel or more than one channel [2]. A tissue P system works in a synchronized mode (a global clock is assumed, marking the time for the whole system). In each time unit, if there are rules that can be applied in each channel, then one of the rules must be applied. At most one rule is applied in each channel, non-deterministically chosen among the rules that can be applied in the channel. So, the use of rules is sequential at the level of each channel, but it is parallel at the level of the system. In this note, we shall consider the following two restrictive versions of tissue P systems: (1) only one channel is allowed between two cells or between a cell and the environment, (2) two channels are allowed between a cell and the environment.

Table 1: The computational completeness results for tissue P systems with only one channel between two cells, or between a cell and the environment; where ? indicates an open problem, † indicates that the result is obtained in this note, the other results are from [1].

symbols/cells	1	2	3	4	5	6	7
1	NREG	?	?	?	?	NRE†	NRE
2	NREG	?	?	NRE	NRE	NRE	NRE
3	NREG	?	NRE	NRE	NRE	NRE	NRE
4	NREG	NRE	NRE	NRE	NRE	NRE	NRE

One of the central problems about tissue P systems is to investigate their computational power. This topic has been widely investigated for tissue P systems of various forms (e.g., see [4, 6, 10]). For the special case when tissue P systems use only a (very) small number of symbols and cells, please refer to [1, 3]. There seems to be a trade-off between the number of cells and the number of symbols needed for the computational power of tissue P systems. If only one channel is allowed between two cells or between a cell and the environment, it was shown that any recursively enumerable set of natural numbers can be generated by a tissue P system with at most seven cells and only one symbol [3]. The number of cells can decrease when two symbols are used; specifically, a tissue P system with two symbols and at most four cells can generate any recursively enumerable set of natural numbers [3]. The known results about the computational power of tissue P systems with only one channel between two cells or between a cell and the environment are listed in Table 1. If two channels are allowed between a cell and the environment, then one cell is enough to obtain computational completeness for tissue P systems with at most five symbols [1]. The number of symbols for computational completeness can decrease when the number of cells increases: for the case of tissue P systems with two channels between a cell and the environment, the computational completeness can be obtained by tissue P systems with two cells and three symbols, or three cells and two symbols. The known results about the computational power of tissue P systems with two channels between a cell and the environment are listed in Table 2.

Table 2: The computational completeness results for tissue P systems with two channels between a cell and the environment; where ? indicates an open problem, † indicates that the result is obtained in this note, the other results are from [1].

symbols/cells	1	2	3	4	5	6
1	NFIN	?	?	?	NRE†	NRE
2	?	?	NRE	NRE	NRE	NRE
3	?	NRE	NRE	NRE	NRE	NRE
4	?	NRE	NRE	NRE	NRE	NRE
5	NRE	NRE	NRE	NRE	NRE	NRE

In this note, we continue to investigate the computational power of tissue P systems with small numbers of symbols and cells. Specifically, we look for universal one-symbol tissue P systems with symport/antiport rules having a small number of cells. It is proved that six cells suffice to generate any recursively enumerable set of natural numbers for such a one-symbol tissue P system, under the restriction that only one channel is allowed between two cells or between a cell and the environment. The idea used in the proof of the result can also be extended to the case of allowing two channels between a cell and the environment, then one cell can be saved. The results obtained in this note partially answer open problems formulated in [1] (see Tables 1 and 2).

This note is organized as follows. In Section 2, the formal language theory preliminaries are recalled, including the formal definition of register machine. The formal definition of tissue P systems is introduced in Section 3. Two universal one-symbol tissue P systems are presented in Section 4, with an overview of the computation. Conclusions and comments are presented in Section 5.

2 Formal language theory preliminaries

For an alphabet V, V^* denotes the set of all finite strings over V, with the empty string denoted by λ. The set of all nonempty strings over V is denoted by V^+.

A *register machine* is a construct $M = (m, H, l_0, l_h, I)$, where m is the number of registers (each holds a natural number), H is the set of instruction labels, l_0 is the start label (labeling an ADD instruction), l_h is the halt label (assigned to instruction HALT), and I is the set of instructions. Each label from H labels only one instruction from I, thus precisely identifying it. The instructions are of the following forms:

- $l_i : (\texttt{ADD}(r), l_j, l_k)$ (add 1 to register r and then go to one of the instructions with labels l_j, l_k),
- $l_i : (\texttt{SUB}(r), l_j, l_k)$ (if register r is non-zero, then subtract 1 from it, and go to the instruction with label l_j; otherwise, go to the instruction with label l_k),
- $l_h : \texttt{HALT}$ (the halt instruction).

A register machine M computes (generates) a number n in the following way. The register machine starts with all registers empty (i.e., storing the number zero). It applies the instruction with label l_0 and proceeds to apply instructions as indicated by labels (and, in the case of SUB instructions, by the content of registers). If the register machine reaches the halt instruction, then the number n stored at that time in the first register is said to be computed by M. It is known that register machines compute all sets of numbers which are Turing computable, hence they characterize NRE [5] (NRE is the family of length sets of recursively enumerable languages; that is, those recognized by Turing machines). Especially, it is known that three registers are enough to generate any recursively enumerable set of natural numbers.

Without loss of generality, it can be assumed that l_0 labels an ADD instruction and that in the halting configuration all registers different from the first one are empty, and that the output register is never decremented during the computation (its content is only added to).

Without loss of generality, it can be assumed that in each ADD instruction $l_i : (\texttt{ADD}(r), l_j, l_k)$ and in each SUB instruction $l_i : (\texttt{SUB}(r), l_j, l_k)$ the labels l_i, l_j, l_k are mutually distinct (for a short proof, see [2]).

3 Tissue P systems with symport/antiport rules

Tissue P systems were introduced in [6], and tissue-like P systems with channel states were introduced in [2]. In this note, the following type of systems is considered, omitting the channel states.

A *tissue P system* (of degree $m \geq 1$) with symport/antiport rules is a construct

$$\Pi = (O, T, E, w_1, \ldots, w_m, ch, (R(i,j))_{(i,j)\in ch}), \text{ where:}$$

- O is the alphabet of *objects*;
- $T \subseteq O$ is the alphabet of *terminal* objects;
- $E \subseteq O$ is the set of objects present in the environment in arbitrarily copies each;
- $w_1, \ldots, w_m$ are strings over O, representing the multisets of objects placed in the cells of the system at the beginning of the computation (it is assumed that the system contains m cells, labelled with $1, 2, \ldots, m$);
- $ch \subseteq \{(i,j) \mid i,j \in \{0,1,2,\ldots,m\}, (i,j) \neq (0,0)\}$ is the set of links (*channels*) between cells (they were also called *synapses* in [2]; 0 indicates the environment);
- $R(i,j)$ is a finite set of antiport rules of the form x/y, for some $x, y \in O^*$, associated with the channel $(i,j) \in ch$.

An *antiport rule* of the form $x/y \in R(i,j)$ for the ordered pair (i,j) of cells means moving the objects specified by x from cell i (from the environment, if $i = 0$) to cell j, and at the same time moving the objects specified by y from cell j to cell i. The rules with one of x, y being empty are, in fact, *symport rules*, but we do not always explicitly consider this distinction here, as it is not relevant for what follows.

Note that the objects from E are never exhausted, irrespective of how many copies of each of them are brought into the system, arbitrarily many copies remain available in the environment.

A *configuration* of a tissue P system is described by the multisets of objects over O associated with the cells of the system. The tuple $(w_1, w_2, \ldots, w_m)$ is the *initial* configuration. A *halting* configuration is a configuration such that there is no rule that can be applied. The *computation* starts from the initial configuration; in each time unit, a rule is used on each channel for which a rule can be used (if no rule is applicable for a channel, then no object passes over it). Therefore, the use of rules is sequential at the level of each channel, but it is parallel at the level of the system: all channels which can use a rule must do it (the system is synchronously evolving). The computation is successful if and only if it halts (reaching a configuration where no rule can be applied). The result of a halting computation is encoded by the multiset of objects over T appearing in a cell specified in advance in the halting configuration.

In this note, we deal with a restricted version of the systems introduced above. Only channels (i,j) with $i \neq j$ are allowed. If only one channel is allowed between two cells or between a cell and the environment, then for any i, j only one of (i,j) and (j,i) is allowed. If two channels are allowed between two cells or between a cell and the environment, then both (i,j) and (j,i) are allowed. Furthermore, only one-symbol tissue P systems are considered, hence we assume $O = T = E = \{a\}$. Then, for simplicity, a one-symbol tissue P system is written as $\Pi = (w_1, \ldots, w_m, ch, (R(i,j))_{(i,j)\in ch})$; the output cell is that with label 1. We also write x/y for an antiport rule a^x/a^y and x for multiset a^x.

4 Universality results

In [3], it was shown that one-symbol tissue P systems with symport/antiport rules having seven cells are Turing universal when only one channel is allowed between two cells or between a cell and the environment. This result is improved by showing that six cells are enough for Turing universality.

Theorem 1. *For any recursively enumerable set L of natural numbers, a one-symbol tissue P system with symport/antiport rules having at most 6 cells can be constructed to generate L, under the restriction that only one channel is allowed between two cells or between a cell and the environment.*

Proof: Let us consider a register machine $M = (m, H, l_0, l_h, I)$. As stated in Section 2, a register machine with three registers can generate any recursively enumerable set L of natural numbers, where the instructions that act on the first register are ADD instructions. This means that $m = 3$. In what follows, we shall construct a tissue P system Π with only one symbol a to simulate the register machine M.

The system Π consists of six cells labeled by $1, \ldots, 6$. The cell with label 1 represents register 1 (the output register); the cells with labels 2 and 3 represent registers 2 and 3, respectively; the cells with labels 4 and 5 are program cells (the cell with label 4 controls the simulation of the instructions that act on registers 1 and 2, the cell with label 5 controls the simulation of the instructions that act on register 3); the cell with label 6 is used as a trap that, whenever started, leads to a non-halting computation by using the antiport rule $2/2$ in channel $(6, 0)$. The number stored in each register r ($r = 1, 2, 3$) is represented by the number of copies of symbol a in the cell with label r in the following way. If register 1 contains number n ($n \geq 0$), then the cell with label 1 has $n + 5$ copies of symbol a; if register 2 (resp. 3) contains number n ($n \geq 0$), then the cell with label 2 (resp. 3) has $2n + 2$ copies of symbol a.

Without loss of generality, we assume that $l_i = 2i + 1$, $0 \leq i \leq t$, $t \geq 0$, are the labels of instructions of register machine M, and l_t is the label of halting instruction HALT. We define the function c:

$$c(0) = 12, \quad c(i+1) = \sum_{j=0}^{i} c(j) + c(0), \text{ for } i \geq 0.$$

It is easy to check that the function c has the following properties.

- For any $i < k, j < k$, $i \neq j$, we have $c(k) > c(i) + c(j) + 12$.
- For any i, $0 \leq i \leq t$, we have $c(l_i) > 12$.
- For any $i \neq j$, $0 \leq i, j \leq t$, we have $c(l_i) \neq c(l_j)$.
- For any $i < j$, $0 \leq i, j \leq t$, the value $c(l_i + 1)$ is between $c(l_i)$ and $c(l_j)$.

In the initial configuration of Π, the cell with label 1 contains five copies of symbol a, and the cells with labels 2 and 3 contain two copies of symbol a, which represents the fact that registers 1, 2 and 3 initially have number 0; the cell with label 4 contains $c(l_0)$ copies of symbol a; the cells with labels 5 and 6 contain 0 copy of symbol a. In general, when the cell with label 4 contains $c(l_i)$ copies of symbol a, system Π starts to simulate the instruction l_i.

Formally, the tissue P system Π is a construct of the form

$$\Pi = (5, 2, 2, c(l_0), 0, 0, ch, (R(i,j))_{(i,j)\in ch}), \text{ where:}$$

- $ch = \{(4, i) \mid i \in \{0, 1, 2, 5, 6\}\} \cup \{(5, 0), (5, 3), (5, 6), (6, 0)\}$;

- the sets of rules $R(i,j)$, $(i,j) \in ch$, are as follows:

$$\begin{aligned}
R(4,0) &= \{(c(l_i)-6)/(c(l_j)-5), (c(l_i)-6)/(c(l_k)-5) \mid l_i : (\texttt{ADD}(1), l_j, l_k) \in R\} \\
&\cup \{(c(l_i)-3)/(c(l_j)-1), (c(l_i)-3)/(c(l_k)-1) \mid l_i : (\texttt{ADD}(2), l_j, l_k) \in R\} \\
&\cup \{(c(l_i)-1)/(c(l_i+1)-3), (c(l_i+1))/(c(l_j)), \\
&\quad (c(l_i+1)-2)/c(l_k) \mid l_i : (\texttt{SUB}(2), l_j, l_k) \in R\}, \\
R(4,1) &= \{6/5\}, R(4,2) = \{3/1, 1/3\}, R(4,6) = \{2/0\}, R(5,3) = \{3/1, 1/3\}, \\
R(4,5) &= \{c(l_i)/0, 0/c(l_j), 0/c(l_k) \mid l_i : (\texttt{ADD}(3), l_j, l_k)\} \\
&\cup \{c(l_i)/0, 0/c(l_j), 0/c(l_k) \mid l_i : (\texttt{SUB}(3), l_j, l_k)\}, \\
R(5,0) &= \{(c(l_i)-3)/(c(l_j)-1), (c(l_i)-3)/(c(l_k)-1) \mid l_i : (\texttt{ADD}(3), l_j, l_k) \in R\} \\
&\cup \{(c(l_i)-1)/(c(l_i+1)-3), (c(l_i+1))/(c(l_j)), \\
&\quad (c(l_i+1)-2)/c(l_k) \mid l_i : (\texttt{SUB}(3), l_j, l_k)\}, \\
R(5,6) &= \{2/0\}, \quad R(6,0) = \{2/2\}.
\end{aligned}$$

In order to show that tissue P system Π can correctly simulate register machine M, we only need to show how the following six kinds of rules of register machine M are simulated by tissue P system Π.

(1) Simulating ADD instructions that act on register 1.

Let $l_i : (\texttt{ADD}(1), l_j, l_k)$ be an ADD instruction that acts on register 1, and the cell with label 4 contains $c(l_i)$ copies of symbol a (in the initial configuration, the cell with label 4 contains $c(l_0)$ copies of symbol a). The simulation uses the rules:

$$6/5 \in R(4,1), \quad (c(l_i)-6)/(c(l_k)-5) \in R(4,0), \quad (c(l_i)-6)/(c(l_j)-5) \in R(4,0).$$

The simulation takes one step. At this step, six copies of symbol a from the cell with label 4 are sent to the cell with label 1 by the rule $6/5 \in R(4,1)$ (the number n stored in register 1 is encoded by $n+5$ copies of symbol a in the cell with label 1, so the cell with label 1 contains at least five copies of symbol a, and thus the rule $6/5 \in R(4,1)$ can be applied), exchanging with five copies of symbol a. The number of copies of symbol a in the cell with label 1 increases by one, which simulates that the number stored in register 1 is increased by one. At the same time, the other copies of symbol a from the cell with label 4 can be used by the rule $(c(l_i)-6)/(c(l_j)-5) \in R(4,0)$ or $(c(l_i)-6)/(c(l_k)-5) \in R(4,0)$, non-deterministically chosen. Note that the cell with label 4 also gets five copies of symbol a at this step by the rule $6/5 \in R(4,1)$. The cell with label 4 accumulates $c(l_j)$ or $c(l_k)$ copies of symbol a in total after this step. In this way, system Π starts to simulate instruction l_j or l_k.

All objects in cell 4 are simultaneously used by communications along the channels (4,0) and (4,1). If the system does not use at the same time the rule $6/5 \in R(4,1)$ and one of the rules $(c(l_i)-6)/(c(l_j)-5) \in R(4,0)$ or $(c(l_i)-6)/(c(l_k)-5) \in R(4,0)$, then the system will enter an infinite loop and then the computation gives no result.

For instance, the rule $(c(l_i)-6)/(c(l_j)-5) \in R(4,0)$ or $(c(l_i)-6)/(c(l_k)-5) \in R(4,0)$ consumes $c(l_i)-6$ copies of symbol a in the cell with label 4, and there are 6 copies of symbol a that are subject to other possible rules. Because for $0 \leq i\prime, j\prime, k\prime \leq t$, the encoding $c(l_{i\prime})$ of each instruction $l_{i\prime}$ of register machine M is larger than 6, these 6 copies of symbol a cannot be used by the rules $(c(l_{i\prime})-6)/(c(l_{j\prime})-5)$, $(c(l_{i\prime})-6)/(c(l_{k\prime})-5)$, $(c(l_{i\prime})-3)/(c(l_{j\prime})-1)$, $(c(l_{i\prime})-3)/(c(l_{k\prime})-1)$, $(c(l_{i\prime})-1)/(c(l_{i\prime}+1)-3)$, $c(l_{i\prime}+1)/c(l_{j\prime})$, $(c(l_{i\prime}+1)-2)/c(l_{k\prime})$, $c(l_t)/0$ from $R(4,0)$ and the rule $c(l_{i\prime})/0$ from $R(4,5)$. These 6 copies of symbol a can be used by the rule $3/1$ or $1/3$ from $R(4,2)$, but not both, since at most one rule is allowed to be used in each channel at one step. So there are at least 3 copies of symbol a that are subject to other possible

rules. By the maximal parallel manner of application of rules, the rule $2/0 \in R(4,6)$ must be applied at this step, hence two copies of symbol a are sent to the cell with label 6.

Conversely, the rule $6/5 \in R(4,1)$ consumes 6 copies of symbol a in the cell with label 4, and there are $c(l_i) - 6$ copies of symbol a that are subject to other possible rules. For $0 \leq i, i\prime, i\prime\prime, j\prime, k\prime \leq t$, $i\prime \neq i\prime\prime$, $i\prime < i$ and $i\prime\prime < i$, these $c(l_i) - 6$ copies of symbol a can be used by the rule $c(l_{i\prime\prime})/0$ from $R(4,5)$, and one of the rules $(c(l_{i\prime}) - 6)/(c(l_{j\prime}) - 5)$, $(c(l_{i\prime}) - 6)/(c(l_{k\prime}) - 5)$, $(c(l_{i\prime}) - 3)/(c(l_{j\prime}) - 1)$, $(c(l_{i\prime}) - 3)/(c(l_{k\prime}) - 1)$, $(c(l_{i\prime}) - 1)/(c(l_{i\prime} + 1) - 3)$, $c(l_{i\prime} + 1)/c(l_{j\prime})$, $(c(l_{i\prime} + 1) - 2)/c(l_{k\prime})$ from $R(4,0)$. By the first property of the function c, $c(i) > c(i\prime) + c(i\prime\prime) + 12$, there are at least 6 copies of symbol a that are subject to other rules at this moment. These 6 copies of symbol a can be used by the rule $3/1$ or $1/3$ from $R(4,2)$, but not both. Therefore, there are at least 3 copies of symbol a that are subject to the rule $2/0 \in R(4,6)$; the rule $2/0 \in R(4,6)$ must be applied, and two copies of symbol a are sent to the cell with label 6.

In each of these two cases, the cell with label 6 receives two copies of symbol a, and the rule $(2,2) \in R(6,0)$ would be applied forever. Consequently, the rule $6/5 \in R(4,1)$ and one of the rules $(c(l_i) - 6)/(c(l_j) - 5) \in R(4,0)$ or $(c(l_i) - 6)/(c(l_k) - 5) \in R(4,0)$ must be used, hence the instruction $l_i : (\texttt{ADD}(1), l_j, l_k)$ is correctly simulated by system Π (otherwise, the computation cannot halt).

(2) Simulating ADD instructions that act on register 2.

Let $l_i : (\texttt{ADD}(2), l_j, l_k)$ be an ADD instruction that acts on register 2, and the cell with label 4 contains $c(l_i)$ copies of symbol a. The following rules are used to simulate the instruction $l_i : (\texttt{ADD}(2), l_j, l_k)$:

$$3/1 \in R(4,2), \quad (c(l_i) - 3)/(c(l_j) - 1) \in R(4,0), \quad (c(l_i) - 3)/(c(l_k) - 1) \in R(4,0).$$

The simulation takes one step. The content of the cell with label 4 is split into two parts, with one part containing $c(l_i) - 3$ copies of symbol a and the other part containing 3 copies of symbol a. The $c(l_i) - 3$ copies of symbol a in the cell with label 4 are exchanged with $c(l_j) - 1$ copies of symbol a from the environment by the rule $(c(l_i) - 3)/(c(l_j) - 1) \in R(4,0)$, or exchanged with $c(l_k) - 1$ copies of symbol a by the rule $(c(l_i) - 3)/(c(l_k) - 1) \in R(4,0)$, non-deterministically chosen. The 3 copies of symbol a in the cell with label 4 are exchanged with one copy of symbol a from the cell with label 2 by the rule $3/1 \in R(4,2)$. In this way, the number of copies of symbol a in the cell with label 2 increases by two, which simulates that the number stored in register 2 is increased by one. The number of copies of symbol a in the cell with label 4 becomes $c(l_j)$ or $c(l_k)$, which means that system Π starts to simulate instruction l_j or l_k.

Similar to the case of simulating ADD instructions that act on register 1, if system Π does not use the above rules, then the rule $2/2 \in R(6,0)$ can be applied and would be applied forever. The computation is not a successful one and gives no result. Therefore, the ADD instruction $l_i : (\texttt{ADD}(2), l_j, l_k)$ is correctly simulated by system Π.

(3) Simulating SUB instructions that act on register 2.

Let $l_i : (\texttt{SUB}(2), l_j, l_k)$ be an SUB instruction that acts on register 2, and the cell with label 4 contains $c(l_i)$ copies of symbol a. The following rules are used to simulate $l_i : (\texttt{SUB}(2), l_j, l_k)$:

$$(c(l_i) - 1)/(c(l_i + 1) - 3) \in R(4,0), \qquad 1/3 \in R(4,2),$$
$$c(l_i + 1)/c(l_j) \in R(4,0), \qquad (c(l_i + 1) - 2)/c(l_k) \in R(4,0).$$

The simulation takes two steps. Note that one of the main issues in the process of simulating $l_i : (\texttt{SUB}(2), l_j, l_k)$ is to check whether the number stored in register 2 is non-zero. The number n in register 2 is represented by $2n+2$ copies of symbol a in the cell with label 2, so the system should check whether the cell with label 2 contains more than two copies of symbol a. The checking is done as follows. At the first step, the $c(l_i)$ copies of symbol a are split into two parts, with one

part containing $c(l_i) - 1$ copies of symbol a and the other part containing one copy of symbol a. The $c(l_i) - 1$ copies of symbol a can be used by the rule $(c(l_i) - 1)/(c(l_i + 1) - 3) \in R(4, 0)$, exchanging with $c(l_i + 1) - 3$ copies of symbol a. For the remaining copy of symbol a, there are two cases. If the number stored in register 2 is non-zero and thus the cell with label 2 contains at least 4 copies of symbol a, then the only rule which can be used is $1/3 \in R(4, 2)$. If the number stored in register 2 is zero and thus the cell with label 2 contains only 2 copies of symbol a, then no rule can be used and the symbol stays in the cell with label 4. In the case of the number stored in register 2 being non-zero, the number of copies of symbol a in the cell with label 2 decreases by two (this simulates that the number stored in register 2 is subtracted by one), and the number of copies of symbol a in the cell with label 4 becomes $c(l_i + 1)$. For the case of the number stored in register 2 being zero, the number of copies of symbol a in the cell with label 2 keeps unchanged (this simulates that the number stored in register 2 is still zero), and the cell with label 4 accumulates $c(l_i + 1) - 2$ copies of symbol a. At the second step, by using the rules $c(l_i + 1)/c(l_j) \in R(4, 0)$ or $c(l_i + 1) - 2/c(l_k) \in R(4, 0)$, the cell with label 4 eventually obtains $c(l_j)$ or $c(l_k)$ copies of symbol a, respectively. Note that system Π should simulate $l_i : (\mathtt{SUB}(2), l_j, l_k)$ by using the above rules; otherwise, the rule $2/0 \in R(4, 6)$ must be used, which actives a trap in the sense of the rule $2/2 \in R(6, 0)$ being used forever.

(4) Simulating ADD instructions that act on register 3.

Let $l_i : (\mathtt{ADD}(3), l_j, l_k)$ be an ADD instruction that acts on register 3, and the cell with label 4 contains $c(l_i)$ copies of symbol a. The simulation uses the rules:

$$c(l_i)/0 \in R(4, 5), \quad (c(l_i) - 3)/(c(l_j) - 1) \in R(5, 0), \quad (c(l_i) - 3)/(c(l_k) - 1) \in R(5, 0),$$
$$3/1 \in (5, 3), \quad 0/c(l_j) \in R(4, 5), \quad 0/c(l_k) \in R(4, 5).$$

The simulations of instructions that act on register 3 are controlled by the cell with label 5. The simulation of the instruction $l_i : (\mathtt{ADD}(3), l_j, l_k)$ takes three steps. At the first step, the $c(l_i)$ copies of symbol a in the cell with label 4 are sent to cell with label 5 by the rule $c(l_i)/0 \in R(4, 5)$. In the cell with label 5, the $c(l_i)$ copies of symbol a are split into two parts at the second step, with one part containing $c(l_i) - 3$ copies of symbol a and the other part containing 3 copies of symbol a. The $c(l_i) - 3$ copies of symbol a are exchanged with $c(l_j) - 1$ copies of symbol a from the environment by the rule $(c(l_i) - 3)/(c(l_j) - 1) \in R(5, 0)$ or exchanged with $c(l_k) - 1$ copies of symbol a from the environment by the rule $(c(l_i) - 3)/(c(l_k) - 1) \in R(5, 0)$, non-deterministically chosen. The 3 copies of symbol a in cell with label 5 are exchanged with one copy of symbol a from the cell with label 3. In this way, the number of copies of symbol a in the cell with label 3 increase by two, which simulates that the number stored in register 3 is increased by one. The cell with label 5 accumulates $c(l_j)$ or $c(l_k)$ copies of symbol a, these copies of symbol a are sent to the cell with label 4 by the rules $0/c(l_j) \in R(4, 5)$ or $0/c(l_k) \in R(4, 5)$ at the third step. In this way, the system can continue to simulate the next instruction l_j or l_k. Note that system Π should simulate $l_i : (\mathtt{ADD}(3), l_j, l_k)$ by using the above rules; otherwise, the rule $2/0 \in R(5, 6)$ must be used, which actives a trap in the sense of the rule $2/2 \in R(6, 0)$ being used forever. Therefore, the ADD instruction $l_i : (\mathtt{ADD}(3), l_j, l_k)$ is correctly simulated by system Π.

(5) Simulating SUB instructions that act on register 3.

Let $l_i : (\mathtt{SUB}(3), l_j, l_k)$ be an SUB instruction that acts on register 3, and the cell with label 4 contains $c(l_i)$ copies of symbol a. The following rules are used to simulate the instruction $l_i : (\mathtt{SUB}(3), l_j, l_k)$:

$$c(l_i)/0 \in R(4, 5), \quad (c(l_i) - 1)/(c(l_i + 1) - 3) \in R(5, 0), \quad c(l_i + 1)/c(l_j) \in R(5, 0),$$
$$1/3 \in R(5, 3), \quad (c(l_i + 1) - 2)/c(l_k) \in R(5, 0), \quad 0/c(l_j) \in R(4, 5), \quad 0/c(l_k) \in R(4, 5).$$

The simulation takes four steps. Similar to the simulation of ADD instructions that act on register 3, the $c(l_i)$ copies of symbol a in the cell with label 4 are first sent to the cell with label

5 and then the cell with label 5 takes care of the simulation of SUB instructions that act on register 3. At the second step, system Π starts to check whether the number stored in register 3 is non-zero. Note that the number n in register 3 is represented by $2n+2$ copies of symbol a, thus the system should check whether the cell with label 3 contains more than two copies of symbol a. The checking is done as follows. The $c(l_i)$ copies of symbol a in the cell with label 5 are split into two parts, with one part containing one copy of symbol a and the other one containing $c(l_i)-1$ copies of symbol a. The $c(l_i)-1$ copies of symbol a are exchanged with $c(l_i+1)-3$ copies of symbol a from the environment by the rule $(c(l_i)-1)/(c(l_i+1)-3) \in R(5,0)$. For the one copy of symbol a, there are two cases. If the cell with label 3 contains at least 3 copies of symbol a (this corresponds to the fact that the number stored in register 3 is non-zero), then the only rule which can be applied is $1/3 \in R(5,3)$ and thus the number stored in register 3 is decreased by one. If the number of copies of symbol a in the cell with label 3 is less than 3 (this corresponds to the fact that the number stored in register 3 is zero), then no rule can be applied and thus the number in register 3 keeps unchanged; furthermore, the one copy of symbol a stays in the cell with label 5. In this way, the cell with label 5 accumulates either $c(l_i+1)$ copies of symbol a or $c(l_i+1)-2$ copies of symbol a. By using the rules $c(l_i+1)/c(l_j) \in R(5,0)$ or $(c(l_i+1)-2)/c(l_k) \in R(5,0)$, the $c(l_i+1)$ copies of symbol a are exchanged with $c(l_j)$ copies of symbol a or the $c(l_i+1)-2$ copies of symbol a are exchanged with $c(l_k)$ copies of symbol a at the third step. At the fourth step, the $c(l_j)$ or $c(l_k)$ copies of symbol a in the cell with label 5 are sent to the cell with label 4 by the rules $0/c(l_j) \in R(4,5)$ or $0/(l_k) \in R(4,5)$, and system Π starts to simulate the next instruction l_j or l_k. Note that the rules $2/0 \in R(5,6)$ and $2/2 \in R(6,0)$ guarantee that system Π should use the above rules to simulate $l_i : (\mathtt{SUB}(3), l_j, l_k)$; otherwise, system Π would enter into a computation that cannot halt.

(6) Simulating the halting instruction.

The halting instruction l_h is simulated by the rule $c(l_t)/0$ from $R(4,0)$.

When the register machine M reaches the halting instruction l_h, the cell with label 4 accumulates $c(l_t)$ copies of symbol a. At that moment, the rule $c(l_t)/0 \in R(4,0)$ can be used, by which all the copies of symbol a in the cell with label 4 are moved into the environment, and thus the computation halts.

From the above explanation, we can find that the register machine M can be correctly simulated by tissue P system Π. From the formal definition of tissue P system Π, we see that system Π has at most one channel between two cells or between a cell and the environment. Therefore, Theorem 1 holds. □

Corollary 2. *For any recursively enumerable set L of natural numbers, a one-symbol tissue P system with symport/antiport rules having at most 5 cells can be constructed to generate L, when two channels are allowed between a cell and the environment.*

Proof: Let us first recall that the cell with label 6 in system Π constructed in the proof of Theorem 1 is used as a trap. If two channels are allowed between a cell and the environment, then the "trap" cell can be saved by introducing two antiport rules $2/2c(l_t) \in R(4,0)$ and $2/2c(l_t) \in R(5,0)$, where the function c is defined as in the proof of Theorem 1. These two rules are used as a "trap" in the sense that, once one of the rules is used, then the rule will be used forever. Note that the number $2c(l_t)$ is so large that even in the case of all possible rules which can be used being used, there remain enough copies of symbol a to repeat the "trap" rule $2/2c(l_t) \in R(4,0)$ or $2/2c(l_t) \in R(5,0)$. In this way, the computation enters an infinite loop. The changes in the construction from the proof of Theorem 1 are left to the reader. □

5 Conclusions and Comments

In this note, a one-symbol universal tissue P system with symport/antiport rules having six cells is obtained, under the restriction that one channel is allowed between two cells or between a cell and the environment. As a corollary of the above result, a one-symbol universal tissue P system with symport/antiport rules having five cells is also constructed, under the restriction that two channel are allowed between a cell and the environment. These results partially answer open problems formulated in [1] (see Tables 1 and 2).

Some improvement of the number of cells used in the universal tissue P systems given in this work may be still possible (thus answering more open problems in Tables 1 and 2). A natural idea is to consider removing the trap cell, just as done in the case of allowing two channels between the cell and the environment.

In the universal tissue P systems given in this work, two cells have been used to control the simulation of the SUB instructions of register machine: the cell with label 4 is responsible for the simulation of the SUB instructions that act on register 2; the cell with label 5 takes care of the simulation of the SUB instructions that act on register 3. We conjecture that one cell is enough to take care of the simulation of the SUB instructions that act on registers 2 and 3.

Acknowledgements

This work was supported by the National Natural Science Foundation of China (Grant Nos. 61033003, 30870826, 61003131 and 61003038), the Fundamental Research Funds for the Central Universities (2010ZD001), Ph.D. Programs Foundation of Ministry of Education of China (20100142110072), the Opening Foundation of Key Laboratory of University of Science and Technology of China for High-Performance Computing and Applications (Grant No. NHPCC-KF-1102), and Scientific Research Foundation for Doctor of Anhui University (Grant No. 02203104).

Bibliography

[1] A. Alhazov, R. Freund, M. Oswald, Tissue P Systems with Symport/Antiport Rules and Small Numbers of Symbols and Cells, *Lecture Notes in Computer Science*, 3572:100–111, 2005.

[2] R. Freund, Gh. Păun, M.J. Pérez-Jiménez, Tissue-Like P Systems with Channel States, *Theoretical Computer Science*, 296:295–326, 2003.

[3] R. Freund, M. Oswald, Tissue P Systems with Symport/Antiport Rules of One Symbol Are Computational Complete, in: M.A. Gutiérrez-Naranjo, Gh. Păun, M.J. Pérez-Jiménez (eds.), *Proceedings of the European Science Foundation PESC Exploratory Workshop Cellular Computing (Complexity Aspects)*, Sevilla, pp.178–187, 2005.

[4] S.N. Krishna, K. Lakshmanan, R. Rama, Tissue P Systems with Contextual and Rewriting Rules, *Lecture Notes in Computer Science*, 2597:339–351, 2003.

[5] M. Minsky (eds.), *Computation: Finite and Infinite Machines*, Prentice Hall, 1967.

[6] C. Martín Vide, J. Pazos, Gh. Păun, A. Rodríguez Patón, Tissue P Systems, *Theoretical Computer Science*, 296:295–326, 2003.

[7] Gh. Păun, Computing with Membranes, *Journal of Computer and System Sciences*, 61(1):108–143, 2000.

[8] A. Păun, Gh. Păun, The Power of Communication: P Systems with Symport/Antiport, *New Generation Computing*, 20(3):295–305, 2002.

[9] Gh. Păun, G. Rozenberg, A. Salomaa (eds.), *Handbook of Membrane Computing*, Oxford University Press, 2010.

[10] Y. Rogozhin, S. Verlan, On the Rule Complexity of Universal Tissue P Systems, *Lecture Notes in Computer Science*, 3850:356–362, 2006.

[11] The P systems web page: http://ppage.psystems.eu

Int. J. of Computers, Communications & Control, ISSN 1841-9836, E-ISSN 1841-9844
Vol. VII (2012), No. 1 (March), pp. 184-195

Maintaining Communication Links Using a Team of Mobile Robots

W. Zhuang, X. Chen, J. Tan

Wei Zhuang
Nanjing University of Information
Science & Technology
Nanjing,210044,P.R.China
E-mail: zw@nuist.edu.cn

Xi Chen, Jindong Tan
Michigan Technological University
Houghton,MI 49931,USA
E-mail: xchen@mtu.edu, jitan@mtu.edu

Abstract:
This paper presents a comprehensive metric to evaluate the link quality and the corresponding control schemes for the distributed control of a team of robots to maintain the communication links. The mobile robots dynamically reconfigure themselves to maintain reliable end-to-end communication links. Such applications require online measurements of communication quality in real time and require a mapping between link quality and robot positions. In this paper, we present the empirical results and analysis of a link variability study for an indoor and outdoor environments including received signal strength indicator (RSSI), throughput and packet loss rate. The distributed control algorithms consider the environmental constrains and obstacles. Moreover, the self-deployment algorithms allow a team of robots to recognize the coverage gap by monitoring link qualities, and deploy the mobile robots for a variety of applications including self-healing, tethering, intelligent relaying. The assessment of link quality acts as the feedback for cooperative control of mobile robots. The experimental results have shown the effectiveness of evaluation for communication links and the related control schemes.
Keywords: Communication Link, Networked Robots, Decentralized Control, RSSI.

1 Introduction

With the advancement in wireless sensor technologies, a communication network can be rapidly setup by densely deploying sensor nodes in an area of interests. These intelligent wireless sensors will self-organize themselves to form a communication and sensor grid. The quality of communication links are subject to many factors including the distance between neighboring nodes, the topology of the network, the environment attenuation, and the use of battery. The wireless sensors, once deployed, can not be reconfigured to maximize the network performance nor to guarantee end-to-end data transmission. The failure of a few wireless nodes on a critical path may lead to the failure of the entire network. There are many advantages to use mobile robots to setup a temporary communication network whose link qualities can be dynamically maintained by the motion control of mobile robots.

Fig. 1 shows a scenario where a team of mobile robots can be used to setup a self-organizable communication network in battlefield. These robots can be equipped many sensors for monitoring and reconnaissance of battlefields. Military personnel relies on these sensors for situation

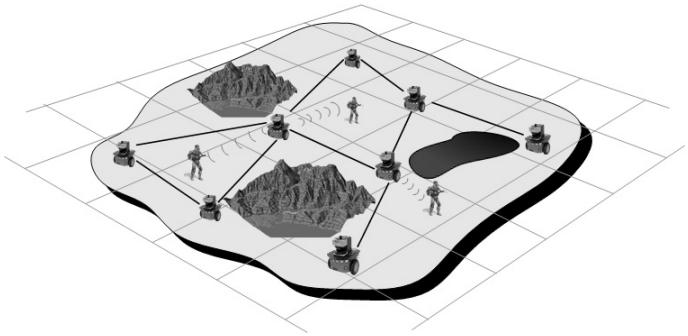

Figure 1: A large scale battlefield cooperation using networked robotic team

awareness. In many circumstances, communication connections could be lost due to many reasons, such as ubiquitous wireless signal noise, angle of signal arrival, natural obstacles, and even a slight movement of pedestrian. The natural settings such as mountains and lakes shown in Fig. 1 represents some of the barriers for smooth communication traffic within the network. In these situations, neighboring mobile robots can monitor their link quality and re-position themselves accordingly to the measurement of link quality. A rapidly deployable mobile network with a team of mobile robots has many potential applications in military and disaster relief.

The self-deployment and maintaining a team of mobile robots face challenges in both link quality measurement and distributed control a multi-robot system. The quality of an end-end communication link are affected by both many factors including the ambient noise, environment attenuation, battery level, motion of the robots, direction of the antenna, etc. Many evaluation metrics such as signal to noise ratio, received signal strength, packet loss, etc. None of these evaluation metrics are easily quantified for control purposes. The second challenge is the distributed control of mobile robots for dynamic link quality improvements. Though distributed control of multiple mobile robots have been intensively discussed, the cooperative control of mobile robots for communication links faces new challenges in the coupling of environment and communication factors.

The monitoring of communication links has long been a research topic in the communication society, and many approaches for evaluating link quality have been proposed. It is shown that that distance cannot be directly adopted as an assessment for link quality [1]. Base on the celebrated Shannon-Hartley theory, the capacity of communication link is proportional to SNR (signal-to-noise ratio). Souryal *et al.* validated that SNR can reliably predict the link quality. However, it is difficult to improve the SNR measurements with this model due to consideration of external interference in the model [2]. Dixon and Frew employed SNR of the communication links to define an optimal communication chain [3]. Apart from using SNR to evaluate link quality, researchers adopted wireless signal strength to assess the quality of connectivity in multi-robot system. Luthy and Grant *et al.* used RSSI measurements to repair disconnected wireless sensor networks [4]. Stump *et al* adopted Fielder value (the second-smallest eigenvalue) to describe the degree of connectivity in a communication grid [1]. Packet loss rate can also serve as a metric to reflect the performance of communication links. In this work, we analyze a set of comprehensive metrics ,RSSI, throughput, packet loss rate and velocity,to explore the possibility of controlling mobile robots for reliable end-to-end communication links. RSSI measurement may serve as an main metric to assess the link quality. However, from the results of our experiments, some other metrics such as speed, angle of arrival, can also reflect the link quality.

Many control algorithms for a large distributed robotic cooperation are presented before. These approaches could be divided into two categories, the centralized and decentralized algo-

rithms. Generally, the question of whether to have centralized or decentralized control comes down to resources [5]. If one of the robots is defined as a central unit which is in charge of the data fusion and decision, the entire system could be brittle when such the manager did not work [6]. Additionally, communication overhead and response time are limiting factors for centralized control. In our previous work, a scalable graph model for decentralized control of mobile robots was discussed. The combination of Delaunay triangulation and potential field make it possible to adjust the robot positions in a distributed way while a global objective is achieved [7]. Similarly, a decentralized mobility control scheme using Extremum Seeking method was presented to form a linked chain of mobile relays [8]. They focused on maximizing the total link bandwidth. Simulation results and movement data from different platforms performing different applications verified the above approaches [9]. In this work, we discuss the control of multiple mobile robots to guarantee reliable end-to-end communication links using a distributed control method.

2 Impact of Comprehensive Metrics

In this section, we introduce the analysis of three metrics and related effects on communication links, RSSI (Received Signal Strength Indicator), throughput and packet loss rate respectively. The Shannon-Hartley theory stated that the channel capacity $C = B\log_2(1 + S/N)$. Where, C is the channel capacity, and B is the bandwidth of the channel. S is the total signal power over the bandwidth, and N represents the total noise power over the bandwidth. With a fixed noise distribution and bandwidth, the metric S is proportional to channel capacity which denoted RSSI should be adopted as a metric to evaluate the links. Throughput as a conventional metric to define quality of end-end communication link is also taken into account. Moreover, packet loss rate, a real-time traffic steam detector, is accepted as a threshold to estimate network health status. We take these metrics into account so that the quality of link could be evaluated qualitatively and quantitatively.

2.1 Received Signal Strength Indicator (RSSI)

RSSI VS. Distance

In wireless communication area, Received Signal Strength Indicator (RSSI) is a measurement of the power present in a received radio signal. RSSI measurements from mobile sensor networks could be directly acquired using simple light-weight processing, especially in IEEE 802.11 protocol family. Generally, RSSI is not a stable measurement owning to the multi-path fading and shadowing [10]. It is not linearly proportional to corresponding physical distance. However, it could be considered as a threshold to evaluate the quality of link. Fig. 2(a) shows the ubiquitous fluctuation of RSSI measurement when the robot is deployed in static. We set the distance between a sender and a receiver as 2 meters in a noisy corridor. Two sets of experiments have been done in a noisy corridor and open space outside respectively. It is obvious that the measurements sampled in outdoor are larger than that in a constrained indoor environment. The figure shows the measurements fluctuating all the time. The largest amplitude of measurements reaches -5dBm. Another set of experiments aims to test feasibility of RSSI as a metric for evaluating links in the same two scenarios. Fig. 2(b) shows RSSI value varies with the movement of mobile robots. One is set to move forward along a straight line. The results illustrates RSSI values varies synchronously with corresponding distance. In a large scale area, if the noise distribution is fixed, we can adopt RSSI value as a metric to reflect the link quality inferred from the Shannon-Hartley theory.

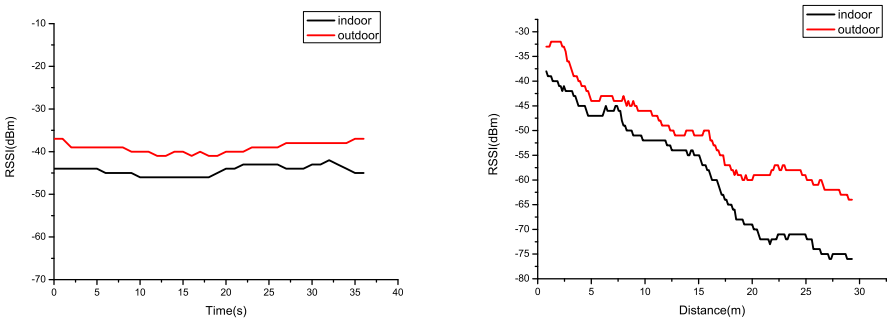

(a) Fluctuation of RSSI in static(indoor and outdoor)

(b) RSSI VS. distance during the movement of robot

Figure 2: RSSI performance with and without mobility

Angle of Arrival

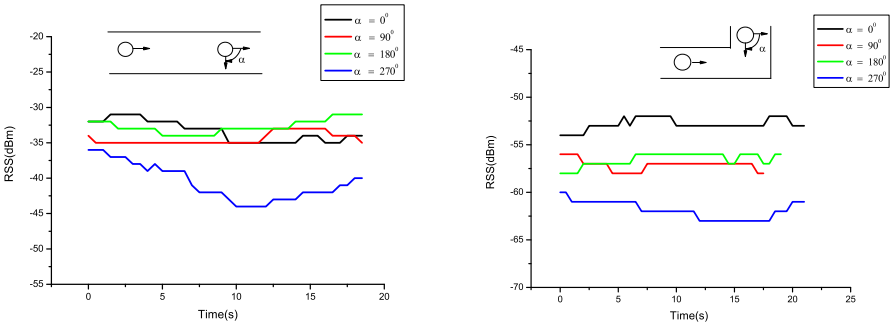

(a) RSSI performance with robots being deployed in a line

(b) RSSI performance with robots being deployed in a diagonal

Figure 3: Impact of angle of arrival

It have been testified that the angle of arrival could affect the performance of RSSI measurements [11]. In this section, we also illuminate this phenomenon during the movement of robots. Theoretically, the antenna of 802.11b/g compatible network device is omni-directional, that is, no matter what direction it receives from the signal, the RSSI measurers should be the same. But, these off-the-shelf devices do not show the symmetric feature in different orientation. Fig. 3(a) and Fig. 3(b) shows the variety in different signal received directions when being deployed in a line and diagonal respectively. Two robots are deployed in a long corridor, where one is in static and the other is moving. The robot changes its orientation clockwise in turn at the same spot. Both of the results show that RSSI value has the minimum when the angle turns to 270 degree. The difference of measurements is up to -10dBm. Moreover, the RSSI difference between 0 degree and the other degrees is larger than that in a line. The results can be useful for the reliable sampling of RSSI since the angle between neighbor robots could varied during the task.

Speed

Speed is also concerned both in RSSI and throughput performance. Note the speed we mentioned here is the velocity of mobile robot rather than signal modulation rate. In order

to obtain the real influence on the performance in mobile sensor network, we set up a series of outdoor experiments to testify it. Two mobile robots equipped with 802.11b/g compatible network devices are deployed on a long road. We selected the maximum translate velocity of the robots as 700mm/s and the minimum speed as 100mm/s. To avoid the interference of other metrics like angle of arrival, etc., one of the robots is requested to move straightly, the other was stationary. The final trajectory is a straight line.

Fig. 4(a) shows the connection between RSSI and related distance. The black curve (upper line) and the red curve(lower line) denoted the relationship with the speed of 100mm/s and 700mm/s respectively. It was obvious that the RSSI measurements with lower speed is always larger than that with higher speed at the same distance except for the startup period. Note that the convex curve of the red line was shown in Fig. 4(a). Theoretically, the curve is proportional to λ^{-n} where λ is distance, and presents monotonic decreasing. However, with higher speed, the RSSI measurements could be affected seriously by multi-path fading and reflection of constructions. Here, the convex part locates at a special zone in which RSSI could be disturbed acutely. Meanwhile, the difference between fixed RSSI value with two speed modes fluctuated rather than increasing continuously which is shown in Fig. 4(b). These could be also explained by the special zones the robot passed in and out. Here, the results illuminate that at a higher speed the robot moved, the much more possibility of interference and instability of RSSI occurred.

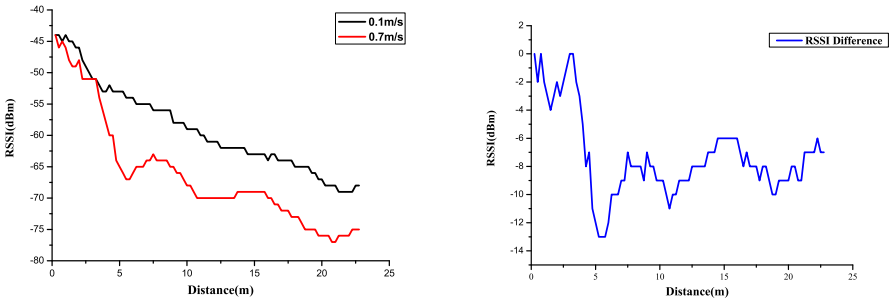

(a) Impact of translate velocity on RSSI (b) RSSI difference of two speed modes

Figure 4: RSSI vs. distance with different speeds

2.2 Throughput performance

In this section, we introduce the performance of throughput in our proposed environment. Mobility, transmission rate and speed of robots were concerned. Throughput as a conventional metric in communication network reflects the performance of communication capacity [12]. As we mentioned before, if the robot moved into a "gray zone" [13] or extremely noisy area, the measurements of RSSI could decayed by a small value (dBm) but the link is broken possibly. So, throughput and related parameters like response time or latency are prone to be accepted as compliments for the entire evaluation.

Mobility

Compared with computer networks, mobility is one of emphasis in mobile sensor network which can have effects on the throughput of neighbor robots. We deployed two mobile robots (Pioneer-3AT) in a walled indoor environment. One is set in static, the other moves along the corridor. IxChariot, a Tcp/Udp packets generator and analyzer is used to obtain real time

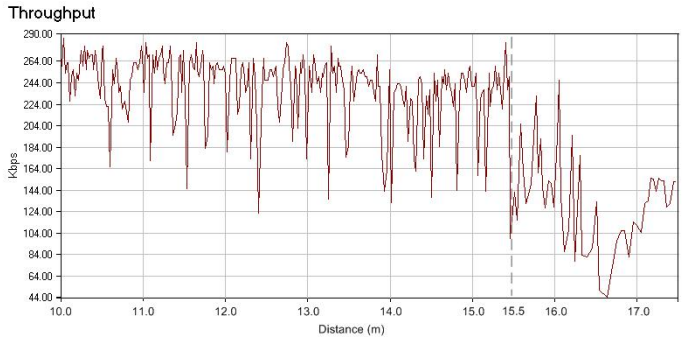

Figure 5: Results of active measurements during the movement

Table 1: Ixchariot parameters of mobility

Console Protocol	TCP
Scripts	Credits
number of timing records	50
size of record to send	100
send buffer size	Default

throughput in our experiments. All the network parameters are listed in Table 1. Fig. 5 shows the fading of the throughput with movement. The obvious decreasing of throughput occurred at 15.5 meters approximately. Based on the theory mentioned above, as long as the mobile robot stays in a circle with the radius less than a value the communication link can retain connection status. If the robot moves out of the circle, it still has ability to exchange data with neighbors but the throughput presents sharply fading. Note that deploying in different scenarios (indoor and outdoor) or using different sending packets size, the metric could vary due to the multi-path fading and MAC overhead.

Speed VS. Throughput

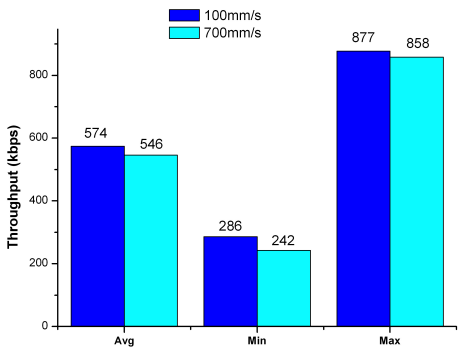

Figure 6: Comparison of throughput performance with different speeds

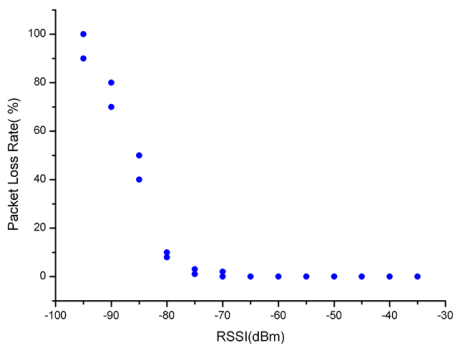

Figure 7: Packet loss rate VS. Received signal strength

Another relationship should be concerned is the speed influence on throughput. Fig.6 shows the impact of speed on throughput. The upper line and the lower line denote transformation of

throughput as time elapsing with the speed of 100mm/s and 700mm/s respectively. IxChariot is adopted to sample the throughput using the parameters in Table 1. There is no obvious difference between the two lines. Since the mobile robot always keep connecting with neighbors, as long as the transmission rate stays lower than bandwidth, the traffic could be smooth and stable. The average throughput 546kbps at speed of 700mm/s is adequate for message and low-resolution low FPS video transmission.

2.3 Packet Loss Rate

Packet loss rate can also reflect quality of communication links in wireless network. However, [2] confirm that the low correlation between packet loss rate and distance and show the extent of variation in an indoor office environment. So, we select RSSI instead of distance as X domain and corresponding packet loss rate as Y domain shown in Fig.7. One robot is set to move along the corridor while the other is stationary. 100 packets (522 byte per packet) were transmitted from the base to mobile robot every second continuously. The RSSI interval is set as -5dBm, and the range is set from -35dBm to -95dBm. The result indicated the critical area of related RSSI lay in $-85dBm \pm -5dBm$. We assumed the point A where the observed RSSI value is -80dBm and point B where the sampled RSSI value is -90dBm. We define d as the distance between A and B. The mobile robot is arranged to move from A to B repeatedly. The average distance $\tilde{d}$ is less than 1 meter which denoted that it took less than 3.3 seconds at the speed of 300mm/s. Generally, the interval is so short that fast responding action such as stop, turn, reverse, etc. could not be achieved in our assumed scenario. So, the packet loss rate can be fit for evaluation of data traffic integrality but not suitable for a feedback for controlling the robotic team.

3 Decentralized Control Algorithms

In this section, we introduce a decentralized control scheme adaptive to unconstrained and constrained scenarios. The improved RSSI measurement is adopted to be feedback input into control system. Base on the Delaunay graphic model, We define two different chained form networks describing self-healing and tethering respectively. Virtual forces composed of abstractive forces and repulsive forces are exploited to drive the robot to a stable status.

3.1 Delaunay Triangulation and Network Model

First, we define the graph model for the multi-robot system. The configuration and control input of the whole system could be defined as:

$$q = \{q_1, q_2, ..., q_n\}^T \tag{1}$$

The overall system can be denoted by $\dot{q} = f(q, u)$, where f is the vector of system dynamics. In a unified inertial coordinate system, $\tilde{p_i} = \{x_i(t), y_i(t)\}^T$ is defined as the position of the robot R_i. We define $p_i = \{x_i(t), y_i(t)\}^T$ as the position of the robot R_i in its local coordinate frame.

The Delaunay triangulation with a set of nodes is defined such that any additional edge between any two nodes intersected one of the existing edges. The Delaunay triangulation define the link properties between one-hop neighbors, which are described by a set of edges.

Here, we can adopt adjacency matrix to specify the connectivity of the Delaunay tessellation using these edges. Motivated by the connectivity in multi-robot team [3], we define the quality of communication link between R_i and R_j which connected with each other through one-hop link as a continuous value. This value is denoted by improved RSSI measurement. The quality is set to be:

$$\Psi_{ij} \triangleq \begin{cases} \Delta_{ij}, & \|p_{ij}\| < \rho \\ 0, & \|p_{ij}| > R \\ exp[\frac{-5(\|p_{ij}\|-\rho)}{R-\rho}], & \text{otherwise} \end{cases} \tag{2}$$

Where, R means the cut-off RSSI measurement which is able to guarantee the link connection and ρ means a saturation RSSI measurement where the communication status between robots does not change as they get closer together. The two parameters can be estimated by results of packet loss rate and active throughput respectively. Unlike the idea in [1],we define Δ as a variant which describes the degree of the connectivity of neighbors. All the analysis of the Δ has been demonstrated in [14],which shows the impact of comprehensive metrics including RSSI, active throughput and packet loss rate. We define an Adjacency Matrix $A(t)$ to specify the connectivity of the Delaunay triangulation. Here, $A_{ij} = \Psi_{ij}$ if R_i and R_j are one-hop neighbors, otherwise $A_{ij} = 0$. So, the link properties of R_i and its one-hop neighbors are denoted by i^{th} column of $A(t)$, that is $A_i(t) = \{a_{i1}, a_{i2}, ..., a_{in}\}^T$.

3.2 Graphic Model Based Control Algorithm

General model

For a multi-robot system, the computation of Delaunay triangulation is time consuming. A decentralized control method is presented to calculate individually and cooperate to repair the communication link. In this paper, a distributed control method is proposed based on both the potential field method and the Delaunay triangulation. For a mobile robot R_i, a performance index (candidate lyapunov function) is defined as follows:

$$V_i = \frac{1}{2}\sum_{j=1}^{N_i} k_{ip}(\|p_{ij}\| - c_{ij})^2 + \frac{1}{2}k_{iv}\|v_i\|^2 \tag{3}$$

Where p_{ij} states the improved RSSI value between robot R_i and robot R_j. $\|p_{ij}\|$ equals to a_{ij} which is an entry in adjacency matrix A_{ij}, and c_{ij} is the actual and desired RSSI value between the two neighboring robots. N_{ij} is the total number of the one-hop neighbors of R_{ij}. k_{ip} and k_{iv} are the parameters for the virtual potential energy and kinetic energy of the robot. The control input is derived by:

$$\begin{aligned} u_i &= -\frac{\partial V_i}{\partial a_i} - \frac{\partial V_i}{\partial v_i} \\ &= -\sum_{j=1}^{N_i} k_{ip}(a_{ij} - c_{ij})\frac{p_{ij}}{a_{ij}} - k_{iv}v_i \\ &= -F_i - k_{iv}v_i \end{aligned} \tag{4}$$

Here, we have obtained the necessary conditions for controlling R_i to keep the connection. When one node is lost in communication chain, the whole system can repair the network connection using neighboring robots to fill the position automatically. If all the other robots but R_i are static, it is easy to prove that the above controller is globally convergent [7].

Self-configuration and Self-healing

Self-healing is based on the same theory of self-configuration. In our works before, [7] proposed an control algorithm for self-configuration both in constrained and unconstrained environment.

Fig. 8(a) shows the simulation result of self-configuration after 10 random robots implemented the cooperation scheme. Fig. 8(b) shows the result of self-healing using the general model when two nodes are disconnected with neighbors. The objective is to fill the coverage gaps the disconnected robots generated before.

Tethering and Intelligent Relays

Tethering is the reverse processing of intelligent relaying which stretches the network to be a chain as long as possible. Different with self-healing, the objective is to keep connection with neighbors so as to maximize the end-end distance. Theoretically, if the communication range is larger than double of sensing range, the chain should transform into a line in an unconstrained situation while not possible in real environment.

An control algorithm named $Minimum - Follow$ for stretching the network is proposed in this section. The Delaunay triangulation could be broken into a chained form network. Every robot in this network just have two one-hop links at last. The nearest neighbor with respect to ready-to-move robot could be chosen to take a movement every round in the iterative loop. The offset is determined by the virtual force generated by foregoing robot. Each robot is considered to follow its foregoing moving robot. Fig. 9 shows the simulation results of tethering algorithm. We set v_i as 1m/s and c_{ij} as 40. The total processing time was 100 seconds. The start-up scenario was from the stable status after self-healing shown in Fig. 8(b). As long as the space is wide enough, finally the chained form network will transform into a line. It is obvious that the cooperation using our algorithm is not optimal for stretching the network using this decentralized algorithm. However, each robot just needs to connect with neighbor robots while a powerful processing unit is able to manage the robots in centralized control.

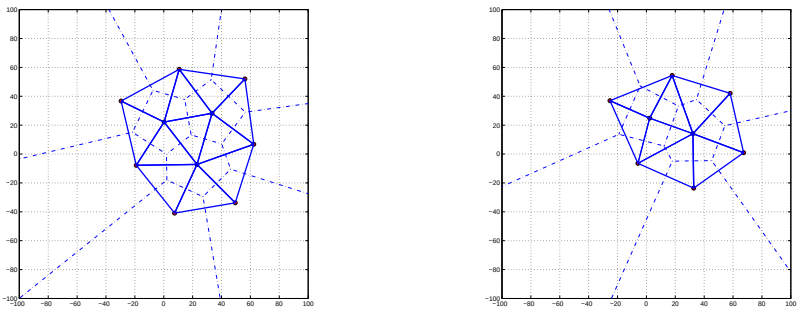

(a) Stable status of the Delaunay triangulation with 10 robots

(b) Stable status with 8 robots after self-healing

Figure 8: The simulation results of self-healing

4 Experiments

In this section, we introduce related experiments of indoor and outdoor to test our algorithms. We used Pioneer 3-AT as our mobile robot which is equipped with one laser detector upper the board and 8 arrays of sonar mounted in front and back flank. A Dell-D430 laptop is chosen to be the data processing unit. The real time RSSI measurements are collected through $WirelessMon$. In order to minimize impact of speed, the linear velocity of mobile robot is defined as 110mm/s and the wireless channel is set in 1Mbps/s. All the processing and control command codes are implemented in Matlab.

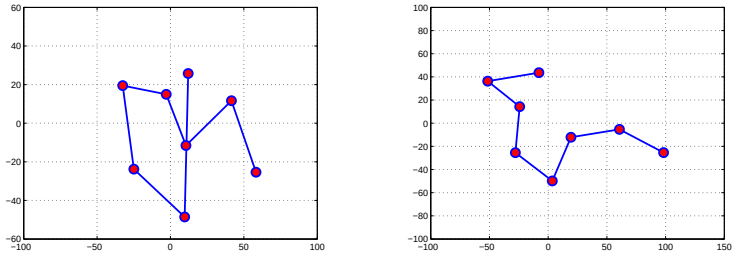

(a) The snapshot after 10s

(b) The snapshot after 50s

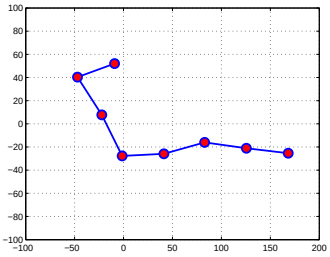

(c) The snapshot after 150s

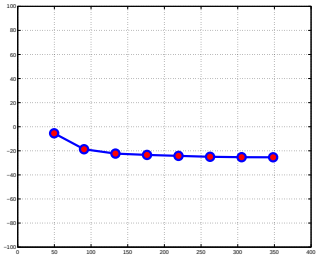

(d) The snapshot after 300s

Figure 9: The snapshots of tethering simulation results. The lead robot is demanded to keep moving at 1m/s, while optional neighbor robots respond. Speeds of these ready-to-move robots are determined by virtual forces. Finally, every robot only has two one-hop neighbors in the chained form network.

Table 2: Environmental parameters of indoor and outdoor

Environment	ρ	R	c_{ij}	γ
Indoor	-65dBm	-90dBm	-40dBm	20mm
Outdoor	-70dBm	-95dBm	-50dBm	50mm

4.1 Indoor and outdoor

The environmental parameters has been listed in Table 3. Here, ρ means the RSSI threshold of smooth traffic without obvious decaying while R means the link cutoff RSSI of current environment. c_{ij} is the optimal desired RSSI value in our system. For obstacles avoidance, γ is designed to denote the safe distance between robots and barriers. When the distance acquired from laser or sonar is larger than γ, the virtual repulsive force would resist the robot as a result of turning.

4.2 Link and motion test

In order to testify the effectiveness of the proposed metric for our control algorithm, a test of robotic cooperation is implemented using real-time sampled link metric. Six robots are deployed in the end of U corridor. First, the team transforms into a chained form network. Then, the team leader is demanded to take exploring along the wall. The speed of leader is set at 110mm/s. The desired RSSI value c_{ij} is set as -40dBm. The parameter K_p is set as 25. The objective is to extend the team of robots so as to maintain the end-end communication link during team leader's

exploration. The sonar sensors are used to detect the range with wall in order to avoid colliding. Fig. 10 shows the RSSI measurements from every mobile robot. The relationship between RSSI and related distance exhibited the RSSI variety which could act as a feedback for robotic motion. When the RSSI measurement is lager than -40dBm, which means a repulsive force rather than an abstractive force could be loaded, it could result in speed descending sharply or moving back. For example, five sharp spikes in Fig. 10(a) reflect the robot 2 keep moving forth and back. Note that the speed of each robot varies with respect to the dispersion of desired measurement. This PI control method could guarantee the smooth of robotic motion and cooperative stability.

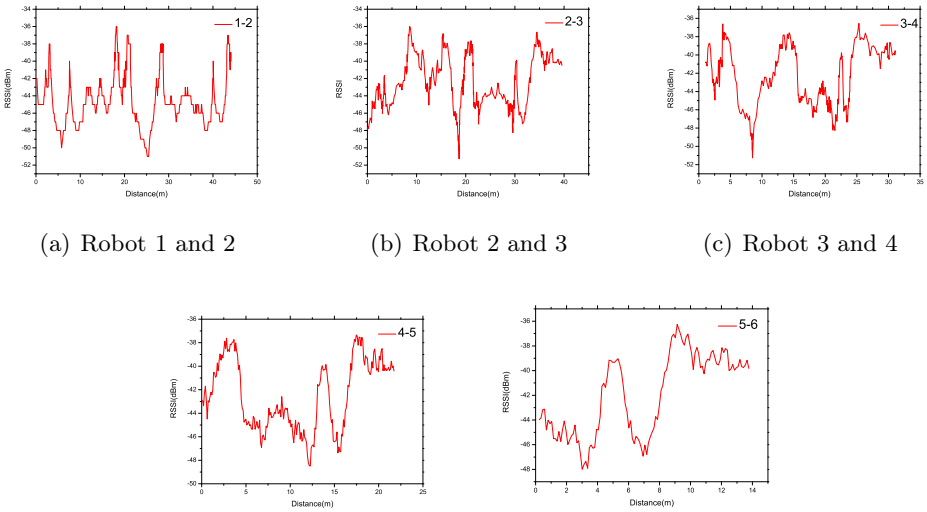

(a) Robot 1 and 2 (b) Robot 2 and 3 (c) Robot 3 and 4

(d) Robot 4 and 5 (e) Robot 5 and 6

Figure 10: Experimental results in an U corridor

5 Conclusions

A comprehensive metric for evaluating communication link quality and the robotic cooperation algorithms are proposed in this paper. Received signal strength indicator has been testified to be an assessment for link quality by a series of empirical experiments. Throughput and packet loss rate are the complements for the control system by generating critical point and cutoff point respectively. Virtual forces are produced to drive the robot composed of repulsive forces and abstractive forces. Two graphic models including self-healing and tethering are proposed to illustrated the kinematic modes of the team of robots. Experimental results showed the feasibility of our comprehensive metric for link quality and stability of our control schemes.

Bibliography

[1] E. Stump, A. Jadbabaie, and V. Kumar. Connectivity management in mobile robot teams. *Robotics and Automation, 2008. ICRA 2008. IEEE International Conference on*, pages 1525–1530, May 2008.

[2] M.R. Souryal, L. Klein-Berndt, L.E. Miller, and N. Moayeri. Link assessment in an indoor 802.11 network. *Wireless Communications and Networking Conference, 2006. WCNC 2006. IEEE*, 3:1402–1407, 2006.

[3] Cory Dixon and Eric W. Frew. Maintaining optimal communication chains in robotic sensor networks using mobility control. In *Mobile Networks and Applications*, volume 14, Issue 3, June 2009.

[4] K.A. Luthy, E. Grant, and T.C. Henderson. Leveraging rssi for robotic repair of disconnected wireless sensor networks. *Robotics and Automation, 2007 IEEE International Conference on*, pages 3659–3664, April 2007.

[5] Yongguo Mei, Yung-Hsiang Lu, Y.C. Hu, and C.S.G. Lee. Deployment of mobile robots with energy and timing constraints. *Robotics, IEEE Transactions on*, 22(3):507–522, June 2006.

[6] P. Ogren, E. Fiorelli, and N.E. Leonard. Cooperative control of mobile sensor networks:adaptive gradient climbing in a distributed environment. *Automatic Control, IEEE Transactions on*, 49(8):1292–1302, Aug. 2004.

[7] Jindong Tan. A scalable graph model and coordination algorithms for multi-robot systems. *Advanced Intelligent Mechatronics. Proceedings, 2005 IEEE/ASME International Conference on*, pages 1529–1534, July 2005.

[8] C. Dixon and E.W. Frew. Controlling the mobility of network nodes using decentralized extremum seeking. *Decision and Control, 2006 45th IEEE Conference on*, pages 1291–1296, Dec. 2006.

[9] E.W. Frew, D.A. Lawrence, C. Dixon, J. Elston, and W.J. Pisano. Lyapunov guidance vector fields for unmanned aircraft applications. *American Control Conference,. ACC '07*, pages 371–376, July 2007.

[10] M.R. Souryal and N. Moayeri. Channel-adaptive relaying in mobile ad hoc networks with fading. *Sensor and Ad Hoc Communications and Networks, IEEE SECON 2005. Second Annual IEEE Communications Society Conference on*, pages 142–152, Sept., 2005.

[11] Michael R. Souryal, Johannes Geissbuehler, Leonard E. Miller, and Nader Moayeri. Real-time deployment of multihop relays for range extension. In *MobiSys '07: Proceedings of the 5th international conference on Mobile systems, applications and services*, pages 85–98, New York, NY, USA, 2007. ACM.

[12] Arzad Kherani Sorav Bansal, Rajeev Shoreyý. Performance of tcp and udp protocols in multi-hop multi-rate wireless networks. In *IEEE Wireless Communications and Networking Conference*, volume Vol.1, pages 231 – 236, 2004.

[13] Henrik Lundgren, Erik Nordströ, and Christian Tschudin. Coping with communication gray zones in ieee 802.11b based ad hoc networks. In *WOWMOM '02: Proceedings of the 5th ACM international workshop on Wireless mobile multimedia*, pages 49–55, New York, NY, USA, 2002. ACM.

[14] Wei Zhuang, Xi Chen, Jindong Tan, and Aiguo Song. An empirical analysis for evaluating the link quality of robotic sensor networks. In *IEEE international conference on wireless communication and signal processing, Nanjing, China, November 13-15, 2009.*, 2009.

Author index